



Provided by the author(s) and University of Galway in accordance with publisher policies. Please cite the published version when available.

Title	Theoretical, experimental and modelling studies of the reactions of hydrogen atoms with C2 – C5 alkenes and cyclisation reactions of hydroperoxyl-alkyl radicals forming cyclic ethers and hydroxyl radicals
Author(s)	Power, Jennifer
Publication Date	2021-06-22
Publisher	NUI Galway
Item record	<a href="http://hdl.handle.net/10379/16824">http://hdl.handle.net/10379/16824</a>

Downloaded 2024-04-27T10:40:05Z

Some rights reserved. For more information, please see the item record link above.



**Theoretical, experimental and modelling studies of the reactions  
of hydrogen atoms with C<sub>2</sub>–C<sub>5</sub> alkenes and cyclisation reactions  
of hydroperoxyl-alkyl radicals forming cyclic ethers and hydroxyl  
radicals**

Jennifer Power

(BSc)

Submitted in fulfilment of the requirements for the  
degree of

Doctor of Philosophy

School of Chemistry

National University of Ireland, Galway



Supervisor: Prof. Henry J. Curran

Head of School: Prof. Olivier Thomas

Submitted April 2021



## Abstract

*This thesis* presents a hierarchical study of the reactions of  $\dot{\text{H}}$  atom addition to and abstraction from both linear and branched  $\text{C}_2 - \text{C}_5$  alkenes. The subsequent C–C and C–H  $\beta$ -scission reactions and H-atom transfer reactions are also considered. As mentioned throughout *this thesis*, alkyl radicals are prominent in combustion chemistry as they are formed by hydrogen abstraction from a stable molecule or from radical attack on hydrocarbons. The addition of  $\dot{\text{H}}$  atoms to the carbon-carbon double bond (C=C) plays a significant role in controlling experimental high-temperature ignition delay times, flame speeds, and species profiles measured as a function of temperature and/or time in reactors including jet-stirred (JSR) and flow reactors. Therefore, accurate determinations of the thermochemistry and kinetics of their unimolecular isomerisation and decomposition reactions and related addition reactions to alkenes are important in simulating the combustion chemistry of virtually all hydrocarbon fuels. Despite their importance, alkenes have not been as extensively studied as alkanes, especially the larger alkenes such as pentene. By having a consistent set of rate constants for  $\text{C}_2 - \text{C}_5$  alkenes +  $\dot{\text{H}}$  using the same level of theory, the calculation results help constrain available models and the development of recommended rules for rate constants associated with certain reaction types. This will provide a tool in developing mechanisms describing the pyrolysis and oxidation of larger alkenes for which calculations do not exist in the literature.

Thermochemical values for species on the  $\dot{\text{C}}_2\text{H}_5$ ,  $\dot{\text{C}}_3\text{H}_7$ ,  $\dot{\text{C}}_4\text{H}_9$  and  $\dot{\text{C}}_5\text{H}_{11}$  potential energy surfaces (PESs) are calculated as a function of temperature (298–2000 K), with enthalpies of formation determined using a network of isodesmic reactions. High-pressure limiting and pressure-dependent rate constants are calculated using Rice-Ramsperger-Kassel-Marcus (RRKM) theory coupled with a one-dimensional (1-D) master equation (ME). Geometries are optimised using the density functional theory (DFT)  $\omega\text{B97XD}$  method coupled with the aug-cc-pVTZ basis set. Harmonic frequency analysis is simultaneously carried out at the same level of theory to verify the nature of each stationary point. Low-frequency torsional modes are treated via relaxed PES scans in 10-degree increments with the  $\omega\text{B97XD} / 6-311++\text{G}(\text{d},\text{p})$  method, with the potential energies as a function of dihedral angle used as input for a one-dimensional (1-D) hindered rotor approximation as implemented in the Master Equation System Solver (MESS). To compute barrier heights, single point energies for minima and transition states are calculated with coupled cluster theory, specifically (CCSD(T)), and Møller-Plesset perturbation theory (MP2), with cc-pVXZ basis sets, where X = D, T and Q

levels of theory. As a validation of the theoretical results calculated in *this thesis*, the results are implemented into kinetic models (AramcoMech3.0, NUIGMech1.0 and NUIGMech1.2) and simulations are compared to new hydrogen atomic resonance absorption spectrometry ( $\dot{\text{H}}$ -ARAS) experimental measurements taken as part of a collaboration with Dr. Sebastian Peukert at Duisburg-Essen University. The  $\dot{\text{H}}$ -ARAS experiments measured for 1- and 2-pentene +  $\dot{\text{H}}$  provide the first measurements of the global rates of reaction of  $\dot{\text{H}}$  atoms with 1- and 2-pentene, with the theoretical results predicting the experiments well. Satisfactory agreement is also observed for the theoretical results compared to the single-pulse shock tube pyrolysis experiments of linear and branched 1-alkenes recorded at NUIG, both of which serve as direct and in-direct validation targets for the current calculations.

Additionally, as part of *this thesis*, rate constants for the low-temperature reaction class: cyclisation of hydroperoxyl-alkyl ( $\dot{\text{QOOH}}$ ) radicals to form cyclic ethers and hydroxyl radicals ( $\dot{\text{QOOH}} \leftrightarrow \text{cyclic ether} + \dot{\text{OH}}$ ) are calculated, involving species ranging in size from  $\text{C}_2\text{H}_5\dot{\text{O}}_2$  to  $\text{C}_5\text{H}_{11}\dot{\text{O}}_2$ . These rate constants are determined using density functional theory (DFT) and ab initio approaches. Geometry optimisations are conducted using the M06-2X method, coupled with the 6-311++G(d,p) basis set. Single point energies are calculated using coupled cluster (CCSD), specifically CCSD(T) and second-order Møller-Plesset perturbation theory (MP2) methods, with relatively large basis sets (cc-pVXZ, where X = D,T,Q). Standard statistical thermodynamics and canonical transition state theory are employed to derive the kinetic data of interest. The use of these new rate coefficients in the NUIG pentane oxidation model produces favourable agreement with  $\text{C}_5$  cyclic ether concentration measurements in JSRs at Nancy and Orléans. These had previously been over-predicted by the model utilising literature rate constant values.

## **Declaration**

This is to certify that:

- (1) This thesis is my original work which is in partial fulfilment for the degree of Doctor of Philosophy. Work that is not my original work is indicated appropriately.
- (2) All other literature material used has been appropriately cited.



*To Mam and Dad*





"You are braver than you believe, stronger than you seem, and smarter than you think." — Christopher Robin



## Acknowledgements

First and foremost, I would like to thank my supervisor Prof. Henry Curran for giving me the opportunity to carry out my PhD, as well as all the opportunities to present my research at conferences, both in Ireland and internationally and to study in Chicago. These experiences have taught me a lot both professionally and personally. Thank you also for giving me the opportunity to carry out a placement during my undergraduate studies, where this journey all began! You took the chance on me to undertake the PhD when I didn't believe I could, so thank you for your support and encouragement in achieving this goal.

A special thank you to Kieran. Your support, mentorship and patience have made this journey a lot easier. No question was ever too silly to ask, and I have learned so much from you. We may have debated over a few pints on a Friday, but I will always be grateful for your encouragement and friendship.

A big thank you to past and present members of the group Chong-Wen, Yang, Yingjia, Ultan, Manik, Amrit, Snehasish, Zhaohong, Mohammadreza, Pat, Morad, Shijun, Ahmed, Haitao, Shashank, Vaibhav, Nitin, Gavin, and Sergio as well as other postgrads in the school of chemistry (especially Fiona who was always up for a cuppa or had the wine chilling in the fridge when it was needed.) Thank you also to Yanjin. I will always value our friendship and memories of conferences and our time in Chicago! Thank you to John B. for your support during my placement and introducing me to theoretical chemistry. Thank you to Colin for being such a good host when we were in Chicago. You made us feel at home! Thank you to Dr. Stephen Klippenstein for your support and guidance during our time at Argonne National Laboratory. Thank you also to John Simmie. Even though we didn't have many encounters, you were always very friendly and helpful.

Mam, Dad and Patrick – the past two years have been particularly tough ones for us, but I could not have done this without you. Mam, seeing your strength and resilience through all that has been thrown your way encouraged me to keep going even at times when I wanted to give up. Dad, you kept us all going, and you and Mam have given Patrick and I all we have ever needed to achieve our goals so thank you. I will be forever grateful. This is for you!

Thank you to my best friends who are both in different countries – Claire and Carol. Claire, you were my first year lab partner from day one of first year and have been best friends ever since. Carol, we have been friends from day one and are now both finishing up PhDs – who would have thought! Shauna, Brona and Amy. Thank you for your friendship

and support over the past few years, especially over the last few months. We are now housemates and I am looking forward to see what our Dublin adventure brings!

## Lead Author Publications

- (1) **J. Power**, K.P. Somers\*, C.W. Zhou, S. Peukert, H.J. Curran, “Theoretical, Experimental, and Modelling Study of the Reaction of Hydrogen Atoms with 1- and 2-Pentene”, *J. Phys. Chem. A* 123(40) (2019) 8506–8526.
- (2) **J. Power**, K.P. Somers, S.S. Nagaraja, W. Wyrebak, H.J. Curran\*, “A Theoretical Study of the Reaction of Hydrogen atoms with three pentene isomers; 2-methyl-1-butene, 2-methyl-2-butene, and 3-methyl-1-butene”, *J. Phys. Chem. A* 124(51) (2020) 10649–10666.
- (3) **J. Power**, K.P. Somers, S.S. Nagaraja, H.J. Curran\*, “A hierarchical study of the reactions of hydrogen atoms to alkenes: A theoretical study of the reactions of hydrogen atoms with C<sub>2</sub>–C<sub>4</sub> alkenes”, *J. Phys. Chem. A* 125(23) (2021) 5124–5145.

## Other Publications

- (1) S. Nagaraja, **J. Power**, G. Kukkadapu, S. Dong, S. W. Wagnon, W. J. Pitz, H. J. Curran, “A single pulse shock tube study of pentene isomer pyrolysis”, *Proc. Combust. Inst.* 38(1) (2021) 881–889.
- (2) J. Bugler, **J. Power**, H.J. Curran, “A Theoretical Study of Cyclic Ether Formation Reactions” *Proc. Combust. Inst.* 36(1) (2017) 161–167.

## Conferences Attended

- (1) **J. Power**, K.P. Somers\*, C.W. Zhou, S. Peukert, H.J. Curran, “Theoretical, Experimental, and Modelling Study of the Reaction of Hydrogen Atoms with 1- and 2-Pentene”, 37<sup>th</sup> International Symposium on Combustion, Dublin, 29<sup>th</sup> July–3<sup>rd</sup> August, 2018.
- (2) **J. Power**, K.P. Somers\*, C.W. Zhou, S. Peukert, H.J. Curran, “Theoretical, Experimental, and Modelling Study of the Reaction of Hydrogen Atoms with 1- and 2-Pentene”, Proceedings of the 3<sup>rd</sup> General Meeting and Workshop on SECs in Industry of SMARTCATs Action, Czech Academy of Sciences, Prague, Czech Republic. 25<sup>th</sup>–27<sup>th</sup> October, 2017.
- (3) **J. Power**, K.P. Somers\*, C.W. Zhou, S. Peukert, H.J. Curran, “Theoretical, Experimental, and Modelling Study of the Reaction of Hydrogen Atoms with 1- and 2-Pentene”, Proceedings of the European Combustion Meeting, University of Zagreb, Croatia, 18<sup>th</sup>–21<sup>st</sup> April, 2017.

## **Other Presentations**

- (1) Science Foundation Ireland (SFI) project work to SFI board committee, 3<sup>rd</sup> December, 2019.
- (2) Chemistry Research Day, NCBES Building, NUI Galway, 9<sup>th</sup> January, 2019.

## **Research Visits**

Location: Argonne National Laboratory, Chicago Illinois, USA

Host: Dr. Stephen Klippenstein

Duration: April 4<sup>th</sup> – May 6<sup>th</sup>, 2019

## Contents

<b>Chapter 1 : General Introduction</b> .....	1
1. Combustion.....	1
2. Quantum chemistry .....	3
2.1. Quantum chemistry calculations .....	5
3. Kinetic/thermodynamic properties.....	7
3.1. Pressure-dependent rate constants.....	7
3.2. Transition state theory.....	7
3.3. Chemical kinetics .....	8
3.4. Thermodynamics.....	8
4. Detailed kinetic mechanism development .....	9
5. Model validation.....	12
5.1. $\dot{H}$ -ARAS experimental measurements .....	12
5.2. Pyrolysis experiments .....	13
5.3. Cyclic ether validation .....	14
References.....	15
<b>Chapter 2 : A Theoretical, Experimental and Modelling Study of the Reaction of Hydrogen Atoms with 1- and 2-Pentene</b> .....	18
Abstract.....	20
1. Introduction.....	20
2. Computational Details .....	26
2.1. Electronic Structure Calculations .....	26
2.2. Thermochemistry .....	28
2.3. Transition State Theory (TST), Rice Ramsperger-Kassel-Marcus (RRKM) and Master Equation (ME) Calculations .....	31
2.4. Experimental Section.....	32
2.5. Chemical Kinetic Modelling.....	33
3. Theoretical Results.....	37
3.1. Thermochemistry .....	37



3.2.	Reactions of $\dot{\text{H}}$ with 1-pentene and 2-pentene .....	43
3.3.	Reactions of pentyl radicals .....	46
4.	Detailed Kinetic Modelling.....	50
4.1.	$\dot{\text{H}}$ -ARAS Experiments.....	50
4.2.	Literature Experiments .....	56
5.	Conclusions.....	58
	References .....	60
	<b>Chapter 3 : A Theoretical Study of the Reaction of Hydrogen Atoms with Three Pentene Isomers; 2-Methyl-1-Butene, 2-Methyl-2-Butene, and 3-Methyl-1-Butene. ....</b>	<b>65</b>
	Abstract.....	67
1.	Introduction.....	67
2.	Computational Details .....	71
2.1.	Electronic Structure Calculations .....	71
2.2.	Naming scheme for C5 species on the $\dot{\text{C}}_5\text{H}_{11}$ PES .....	72
2.3.	Thermochemistry .....	75
2.4.	Transition State Theory (TST), Rice Ramsperger–Kassel Marcus (RRKM) and Master Equation.....	76
3.	Theoretical Results.....	76
3.1.	Thermochemistry .....	76
3.2.	Potential energy surface (PES) .....	79
3.2.1.	Reactions of $\dot{\text{H}}$ with the $\text{C}_5\text{H}_{10}$ isomers.....	79
3.2.1.1.	Rate Constant Comparisons .....	85
3.2.2.	Reactions of Pentyl Radicals .....	92
3.2.2.1.	Rate Constant Comparisons .....	95
4.	Detailed Kinetic Modelling.....	101
5.	Conclusions.....	106
	References .....	108
	<b>Chapter 4 : A hierarchical study of the reactions of hydrogen atoms with alkenes: A theoretical study of the reactions of hydrogen atoms with <math>\text{C}_2 - \text{C}_4</math> alkenes .....</b>	<b>112</b>

Abstract.....	114
1. Introduction .....	114
2. Computational Details .....	121
2.1. Electronic structure calculations.....	121
2.2. Thermochemistry.....	122
2.3. Transition-State Theory (TST), Rice-Ramsperger-Kassel-Marcus (RRKM), and Master Equation (ME) Calculations.....	122
3. Theoretical Results.....	122
3.1. Thermochemistry.....	122
3.2. Reactions of $\dot{\text{H}}$ atoms with $\text{C}_2\text{H}_4$ , $\text{C}_3\text{H}_6$ , $\text{C}_4\text{H}_8\text{-1}$ , $\text{C}_4\text{H}_8\text{-2}$ , and $\text{iC}_4\text{H}_8$ .....	128
3.2.1. Branching ratios of terminal/internal $\dot{\text{H}}$ atom addition to linear and branched alkenes.....	139
3.3. Reactions of alkyl radicals .....	144
3.3.1. Ethyl ( $\dot{\text{C}}_2\text{H}_5$ ) radical.....	144
3.3.2. Propyl ( $\text{n}\dot{\text{C}}_3\text{H}_7$ and $\text{i}\dot{\text{C}}_3\text{H}_7$ ) radicals.....	144
3.3.3. Butyl ( $\dot{\text{C}}_4\text{H}_9\text{-1}$ and $\dot{\text{C}}_4\text{H}_9\text{-2}$ ) radicals .....	145
3.3.4. Branched butyl ( $\text{i}\dot{\text{C}}_4\text{H}_9$ and $\text{t}\dot{\text{C}}_4\text{H}_9$ ) radicals.....	145
4. Detailed kinetic modelling .....	148
4.1. Ethylene pyrolysis.....	149
4.2. Propene pyrolysis.....	150
4.3. 1-Butene pyrolysis.....	151
4.4. Trans 2-butene pyrolysis.....	152
4.5. Isobutene pyrolysis .....	153
5. Chemically activated pathways.....	154
5.1. Effect of pressure .....	154
5.2. Effect of molecular size .....	156
6. Conclusions .....	157
References .....	159

<b>Chapter 5 : A Theoretical Study of Cyclic Ether Formation Reactions .....</b>	<b>163</b>
<b>Abstract .....</b>	<b>165</b>
<b>1. Introduction .....</b>	<b>165</b>
<b>2. Computational methods .....</b>	<b>167</b>
<b>2.1. Rate coefficient determination .....</b>	<b>167</b>
<b>2.2. Uncertainty .....</b>	<b>168</b>
<b>3. Results and Discussion.....</b>	<b>169</b>
<b>3.1. Validity of CBS limit extrapolation approach.....</b>	<b>169</b>
<b>3.2. Comparisons with the literature .....</b>	<b>170</b>
<b>3.3. Implications for combustion modelling.....</b>	<b>172</b>
<b>4. Conclusions.....</b>	<b>174</b>
<b>References .....</b>	<b>175</b>
<b>Chapter 6 : A single pulse shock tube study of pentene isomer pyrolysis .....</b>	<b>177</b>
<b>Abstract.....</b>	<b>179</b>
<b>1. Introduction .....</b>	<b>179</b>
<b>2. Experiments .....</b>	<b>180</b>
<b>3. Kinetic Modelling.....</b>	<b>181</b>
<b>3.1. Computational Methods .....</b>	<b>181</b>
<b>4. Results and discussions.....</b>	<b>182</b>
<b>4.1. 1-Pentene.....</b>	<b>182</b>
<b>4.2. trans-2-Pentene.....</b>	<b>183</b>
<b>4.3. 2-methyl-1-butene .....</b>	<b>184</b>
<b>4.4. 2-methyl-2-butene .....</b>	<b>185</b>
<b>4.5. 3-methyl-1-butene .....</b>	<b>186</b>
<b>5. Discussion.....</b>	<b>186</b>
<b>5.1. Fuel reactivities and ethylene formation.....</b>	<b>186</b>
<b>5.2. Formation of benzene and aromatic precursors .....</b>	<b>187</b>
<b>6. Conclusions.....</b>	<b>189</b>
<b>References .....</b>	<b>190</b>

<b>Chapter 7 : General conclusions and future work</b> .....	193
<b>1. Conclusions</b> .....	193
<b>2. Future Work</b> .....	194
<b>Appendix A</b> .....	195
<b>A.1 Experimental Conditions</b> .....	195
<b>A.2 Theoretical Energies</b> .....	196
<b>A.3 Comparison of Energies and Rate Constants Computed in This Work with Literature Data</b> .....	203
<b>A.4 Thermochemical Data</b> .....	209
<b>A.5 Comparison Entropies and Heat Capacities from This Work and Literature Data</b>	217
<b>A.6 Comparison of Gibbs Free Energies and Boltzmann Factors computed in This work with Literature Data</b> .....	220
<b>A.7 Kinetic Modeling of <math>\dot{H}</math>-ARAS Experiments</b> .....	223
<b>Appendix B</b> .....	226
<b>B.1 Approximate Variational Transition State Theory</b> .....	232
<b>References</b> .....	234

## List of Figures

<b>Figure 1.1.</b> Overview of energy use in Ireland broken down by fuel [2].....	1
<b>Figure 1.2.</b> Schematic diagram (courtesy of Dr. Kieran Somers) showing the steps in the development of the understanding of combustion from the molecular level to its application at the device level. ....	3
<b>Figure 1.3.</b> General schematic mechanism for fuel oxidation [40, 42].....	10
<b>Figure 1.4.</b> Experimental (black) and simulated (red) $\dot{H}$ -atom profiles for $C_2H_5I/1$ -pentene/Ar mixtures at (a) 985 K, (b) 1031 K and (c) 1046 K [19].....	13
<b>Figure 2.1.</b> (Top) high-pressure limit rate constants for the reactions of (a) 1-pentene + $\dot{H}$ and (b) 2-pentene + $\dot{H}$ .....	45
<b>Figure 2.2.</b> Temperature and pressure-dependent branching ratios for (a) 1-pentene + $\dot{H}$ and (b) 2-pentene + $\dot{H}$ via hydrogen atom addition reactions at 0.1 atm (dotted lines), 1 (dashed lines) and 10 (solid lines) atm. ....	46
<b>Figure 2.3.</b> Axial (left) and equatorial (right) transition states for the 1,4-hydrogen atom transfer reaction of 1-pentyl to 2-pentyl. Figures can be viewed in colour through the online version. ....	47
<b>Figure 2.4.</b> Branching ratio at 0.1, 1 and 10 atm for (a) 1-pentyl, (b) 2-pentyl and (c) 3-pentyl radicals. Dotted line (0.1 atm), dashed (1 atm) and solid (10 atm). ....	48
<b>Figure 2.5.</b> Experimental (black) and simulated (red) $\dot{H}$ -atom profiles for $C_2H_5I/1$ -pentene/Ar mixtures at (a) 985 K, (b) 1031 K and (c) 1046 K. ....	50
<b>Figure 2.6.</b> Sensitivity analysis to $\dot{H}$ atom concentrations for $C_2H_5I/1$ -pentene/Ar mixtures at 985 K and 1046 K and at times of 300, 600 and 1200 $\mu$ s. ....	51
<b>Figure 2.7.</b> Rate of production analysis for $\dot{H}$ atoms for the $C_2H_5I/1$ -pentene/Ar experiments at 985 K (bold) and 1046 K (italics). at 300 $\mu$ s (black), 600 $\mu$ s (red) and 1200 $\mu$ s (blue). Solid blue arrows represent $\dot{H}$ -atom producing pathways, while red arrows represent $\dot{H}$ atom consumption pathways. ....	52
<b>Figure 2.8.</b> Experimental (black) and simulated (red) $\dot{H}$ atom concentrations for $C_2H_5I/2$ -pentene/Ar mixtures at (a) 980 K (b) 1032 K and (c) 1044 K and (d) 1055 K. ....	53
<b>Figure 2.9.</b> Sensitivity analysis to $\dot{H}$ atom concentrations for $C_2H_5I/1$ -pentene/Ar mixtures at 980 and 1055 K and times of 300, 600 and 1200 $\mu$ s. ....	54
<b>Figure 2.10.</b> Rate of production analysis for $\dot{H}$ atoms for $C_2H_5I/2$ -pentene/Ar mixtures at 980 K (bold) and 1055 K (italics), at 300 $\mu$ s (black), 600 $\mu$ s (red) and 1200 $\mu$ s (blue). Solid	

blue arrows represent $\dot{\text{H}}$ -atom producing pathways, while red arrows represent $\dot{\text{H}}$ -atom consumption pathways. ....	54
<b>Figure 2.11.</b> Model predictions (colour) of measured (black) $\dot{\text{H}}$ atom profiles upon factor of two perturbations to the most promoting and inhibiting reactions for 2-pentene (top) and 1-pentene (bottom). Solid lines illustrate the result of increasing a rate constant by a factor of two, and vice versa for dashed lines. ....	55
<b>Figure 2.12.</b> Comparison of the experimentally measured and theoretically predicted ratios ( $\Phi$ ) of ethylene to propene from the studies of Awan et al.[6] (■) and Comandini et al.[7] (UIC: ▲, NIST: ▼). $\Phi = X_{\text{ethylene}}/X_{\text{propene}}$ , where X is the mole fraction. ....	56
<b>Figure 2.13.</b> Comparison of the experimentally measured and theoretically predicted ratios ( $\Phi$ ) of (a) ethylene to butene and (b) propene to butene from the study of Manion et al.[5]. $\Phi = X_{\text{species}}/X_{\text{butene}}$ where X = mole fraction. ....	57
<b>Figure 3.1.</b> (a) Schematic of aC <sub>5</sub> H <sub>10</sub> , (b) aC <sub>5</sub> H <sub>11</sub> , and (c) aC <sub>5</sub> H <sub>9</sub> -a1. ....	72
<b>Figure 3.2.</b> Potential energy surface for $\dot{\text{H}}$ atom addition reactions of aC <sub>5</sub> H <sub>10</sub> , bC <sub>5</sub> H <sub>10</sub> and cC <sub>5</sub> H <sub>10</sub> . Black lines represent $\dot{\text{H}}$ atom addition reactions. C–C $\beta$ -scission reactions are presented in blue and $\dot{\text{H}}$ atom shift isomerisation reactions in red. Energies in kJ mol <sup>-1</sup> . ....	79
<b>Figure 3.3.</b> PES for H-atom abstraction reactions. (a) aC <sub>5</sub> H <sub>10</sub> , (b) bC <sub>5</sub> H <sub>10</sub> and (c) cC <sub>5</sub> H <sub>10</sub> . Red lines represent the reactions which lead to resonantly stabilised radicals. Energies in kJ mol <sup>-1</sup> . ....	81
<b>Figure 3.4.</b> Evans–Polanyi correlation for (a) $\dot{\text{H}}$ atom addition to C <sub>5</sub> alkenes, and (b) H-atom abstraction from C <sub>5</sub> alkenes. In Fig. 3.4 (a), solid symbols represent external addition reactions of $\dot{\text{H}}$ atom and open symbols represent internal addition. Different colours correspond to different reactions classes, which are further divided into different symbols to represent different reactants. (1) 1-alkenes, black ■ 1-pentene, black ● 2-methyl-1-butene, black ▲ 3-methyl-1-butene. (2) 2-alkenes, red ▼ 2-pentene, red ★ 2-methyl-2-butene. In Fig.3.4 (b), different colours represent different reactants while different symbols correspond to the different abstraction sites. Black(1-pentene), red (2-pentene), magenta (2-methyl-1-butene), orange (2-methyl-2-butene) and blue (3-methyl-1-butene). ■ (primary), ● (secondary), ▲ (primary allylic), ▼ (primary vinylic), ★ (secondary allylic), ◆ (secondary vinylic) and ◆ (tertiary allylic). ....	82
<b>Figure 3.5.</b> High-pressure limit rate constants of (a) aC <sub>5</sub> H <sub>10</sub> + $\dot{\text{H}}$ , (b) bC <sub>5</sub> H <sub>10</sub> + $\dot{\text{H}}$ and (c) cC <sub>5</sub> H <sub>10</sub> + $\dot{\text{H}}$ . ....	83

- Figure 3.6.** Temperature- and pressure- dependent branching ratios for (a)  $aC_5H_{10} + \dot{H}$ , (b)  $bC_5H_{10} + \dot{H}$  and (c)  $cC_5H_{10} + \dot{H}$  via hydrogen atom addition reactions at 0.1 atm (dotted lines), 1 atm (dashed lines) and 10 atm (solid lines). .....84
- Figure 3.7.** High-pressure limiting rate constants for  $\dot{H}$  atom addition to (a)  $aC_5H_{10}$ , (b)  $bC_5H_{10}$  and  $cC_5H_{10}$ . External addition is represented in black, while red represents internal addition. For  $bC_5H_{10}$ , black lines represent the formation of the tertiary  $bC_5H_{11}$  radical, while red represents the formation of the  $cC_5H_{11}$  radical. Solid lines represent the current work and dotted lines represent rate constants by Leon et al. [8] Rate constants used in the models of Westbrook et al. [11] are shown as dashed lines. ....86
- Figure 3.8.** Rate constants for terminal and internal  $\dot{H}$  atom addition to (a) linear and (b) branched  $C_5$  alkenes from previous[2] and current work. Solid and dashed lines represent terminal and internal addition, respectively. Different colours represent different radical types formed. Black (primary), red (secondary) and blue (tertiary). Different symbols correspond to the different reactants. ■ (1-pentene), ● (2-pentene), ▲ (2-methyl-1-butene), ▼ (2-methyl-2-butene), ◆ (3-methyl-1-butene), ◆ (1-butene), ◀ (2-butene) and ★ (iso-butene). ....87
- Figure 3.9.** High-pressure limiting rate constants for H-atom abstraction from (a) primary, (b) primary allylic, and (c) primary vinylic carbon sites. (on a per H-atom basis) .....90
- Figure 3.10.** High-pressure limiting rate constants (on a per H-atom basis) for H-atom abstraction from (a) secondary allylic and (b) secondary vinylic carbon sites. ....91
- Figure 3.11.** Evans–Polanyi correlation for (a) H-atom isomerisation, and (b) C–C scission of pentyl radicals. ....93
- Figure 3.12.** Branching ratio at 0.1, 1, and 10 atm for (a)  $a\dot{C}_5H_{11}$ , (b)  $b\dot{C}_5H_{11}$ , (c)  $c\dot{C}_5H_{11}$  and (d)  $d\dot{C}_5H_{11}$ . 0.1 atm (dotted lines), 1 atm (dashed lines) and 10 atm (solid lines). ....94
- Figure 3.13.** High-pressure limit rate constant comparisons for pentyl radical decomposition reactions. Rate constants are expressed as a ratio of  $k_{\text{literature}} / k_{\text{this work}}$ . Different literature studies are represented as follows; Power [2] (black), Awan [44] (red), Comandini [45] (blue), Jitariu [52] (cyan), Curran [29] (magenta), and Leon [8] (orange). ....95
- Figure 3.14.** High-pressure limit rate constant comparisons for alkyl radical additions to olefins. Rate constants are expressed as a ratio of  $k_{\text{literature}} / k_{\text{this work}}$ . Different literature studies are represented as follows; Power [2] (black), Curran [29] (magenta) and Westbrook [11] (wine). ....98

- Figure 3.15.** High-pressure limit rate constant comparisons for H-atom shift isomerisation reactions. Rate constants are expressed as a ratio of  $k_{\text{literature}} / k_{\text{this work}}$ . Different literature studies are represented as follows; Power [2] (black), Comandini [45] (blue), Matheu [53] (orange), Yu [54] (green), and Westbrook [11] (wine). P→P, P→S, and P→T represent hydrogen atom shift from primary carbon to primary, secondary and tertiary carbons, respectively. .... 100
- Figure 3.16.** Species profiles for 2M1B pyrolysis. Dotted lines are model simulations with the current model, dashed lines represent approximate variational effects predictions, dashed-dot lines represent these approximate variational effects along with changes to  $\dot{\text{C}}\text{H}_3$  abstraction reactions in the current model and solid lines represent all these changes in addition to altering  $\dot{\text{C}}\text{H}_3$  abstraction from isobutene by a factor of two..... 102
- Figure 3.17.** Species profiles for 2M2B pyrolysis. Dotted lines are model simulations with the current model, dashed lines represent approximate variational effects predictions, dashed-dot lines represent these approximate variational effects along with changes to  $\dot{\text{C}}\text{H}_3$  abstraction reactions in the current model and solid lines represent all these changes in addition to altering  $\dot{\text{C}}\text{H}_3$  abstraction from isobutene by a factor of two..... 103
- Figure 3.18.** Species profiles for 3M1B pyrolysis. Dotted lines are model simulations with the current model, dashed lines represent approximate variational effects predictions, dashed-dot lines represent these approximate variational effects along with changes to  $\dot{\text{C}}\text{H}_3$  abstraction reactions in the current model and solid lines represent all these changes in addition to altering  $\dot{\text{C}}\text{H}_3$  abstraction from isobutene by a factor of two..... 104
- Figure 4.1.** High pressure limit rate constants for the reactions of (a) ethylene +  $\dot{\text{H}}$ , (b) propene +  $\dot{\text{H}}$ , (c) isobutene +  $\dot{\text{H}}$ , and (d) 1- and 2-butene +  $\dot{\text{H}}$ ..... 129
- Figure 4.2.** High-pressure limiting rate constant comparisons for the reactions of  $\dot{\text{H}}$  atom addition with ethylene. Solid lines represent the current work (ROCCSD(T)/aug-cc-pVXZ), dotted (Curran [58]), dashed (Miller and Klippenstein [17]), dashed-dotted (Feng et al. [7]), ● (Lee et al. [9]), ▲ (Hanning et al. [8]), ■ (Lightfoot et al. [10]), and △ (Sugawara et al. [14]). .... 130
- Figure 4.3.** High-pressure limiting rate constant comparisons for the reactions of  $\dot{\text{H}}$  atom addition to propene. Solid lines represent the current work (ROCCSD(T)/aug-cc-pVXZ), dotted (Curran [58]), dashed (Miller and Klippenstein [18]), dashed-dotted (Chen [20]), ■ (Seakins et al. [23]), △ (Watanabe et al.[27]), ○ (Kurylo et al. [26]), ◀ (Harris et al. [31]), and ◻ (Kerr et al. [24]). .... 131



<b>Figure 4.4.</b> Temperature- and pressure-dependent branching ratios for propene + $\dot{\text{H}}$ via hydrogen atom addition reactions at 0.1 (short-dotted lines), 1 (short-dashed lines), 10 (dotted lines), 100 (dashed lines), and 1000 (solid lines) atm. ....	132
<b>Figure 4.5.</b> High-pressure limiting rate constant comparisons for the reactions of $\dot{\text{H}}$ atom addition to the butene isomers. Solid lines represent the current work (ROCCSD(T)/aug-cc-pVXZ) dotted (Curran [58]), dash-dotted (Manion et al.[19]), ● (Harris et al. [31]), and ◻ (Kyogotu et al. [59]). ....	133
<b>Figure 4.6.</b> Temperature- and pressure-dependent branching ratios for (a) 1-butene, (b) 2-butene and (c) isobutene via hydrogen atom addition reactions at 0.1 (short-dotted lines), 1 (short-dashed lines), 10 (dotted lines), 100 (dashed lines), and 1000 (solid lines) atm. ....	134
<b>Figure 4.7.</b> Rate constants (symmetry uncorrected) for terminal and internal $\dot{\text{H}}$ atom addition to (a) linear and (b) branched $\text{C}_2 - \text{C}_5$ alkenes from previous [4, 5] and current work. Solid and dashed lines represent terminal and internal addition, respectively. Different colours represent different radical types formed. Black (tertiary), red (secondary) and blue (primary). Different symbols correspond to the different reactants. ■ (ethylene), ● (propene), ▲ (1-butene), ▼ (2-butene), ◆ (isobutene), ◀ (1-pentene), ▶ (2-pentene), ◆ (2-methyl-1-butene), ★ (2-methyl-2-butene), and ◆ (3-methyl-1-butene). ....	135
<b>Figure 4.8.</b> Rate constant recommendations (symmetry uncorrected) for $\dot{\text{H}}$ atom addition to linear (▲) and branched (■) $\text{C}_2 - \text{C}_5$ alkenes. Solid, dashed and dotted lines represent the formation of tertiary, secondary and primary radicals, respectively. Open symbols are internal C-atom additions, solid symbols are external C-atom additions. ....	137
<b>Figure 4.9.</b> Examples of the application of the proposed rules for $\dot{\text{H}}$ atom addition to alkenes. ....	138
<b>Figure 4.10.</b> Branching ratio for terminal to internal $\dot{\text{H}}$ atom addition to (a) linear and (b) branched 1-alkenes. ....	139
<b>Figure 4.11.</b> Branching ratio for terminal to internal $\dot{\text{H}}$ atom addition to branched 1-alkenes. ....	140
<b>Figure 4.12.</b> High-pressure limiting rate constants for H-atom abstraction from alkylic (primary) carbon sites on a per H-atom basis. ....	141
<b>Figure 4.13.</b> High-pressure limiting rate constants for H-atom abstraction from allylic carbon sites on a per H-atom basis. ....	142

<b>Figure 4.14.</b> High-pressure limiting rate constants for H-atom abstraction from vinylic carbon sites on a per H-atom basis. ....	142
<b>Figure 4.15.</b> Rate constant recommendations for H-atom abstraction from C <sub>2</sub> – C <sub>5</sub> alkenes. Solid (allylic), dashed (alkyl) and dotted (vinylic). ....	143
<b>Figure 4.16.</b> High-pressure limiting rate constants for alkyl radical decomposition, forming (a) olefin + $\dot{\text{C}}\text{H}_3$ . Solid (current work), dashed (Curran), dotted (Awan) and short-dotted (Comandini). ....	145
<b>Figure 4.17.</b> High-pressure limiting rate constants for alkyl radical decomposition, forming an olefin + $\dot{\text{C}}_2\text{H}_5$ . Solid (current work), dashed (Curran), dotted (Awan), short-dotted (Comandini), and dashed-dotted (Jitariu). ....	146
<b>Figure 4.18.</b> High-pressure limiting rate constants for alkyl radical decomposition, forming an olefin + $\dot{\text{C}}_3\text{H}_7$ . Solid (current work), dotted (Awan), short-dotted (Comandini), and dashed-dotted (Jitariu). ....	147
<b>Figure 4.19.</b> Rate constant recommendations for alkyl radical decomposition to olefin + radical. ....	148
<b>Figure 4.20.</b> Species profiles for ethylene pyrolysis at 2 bar. Dashed lines represent NUIGMech1.1 and solid lines represent NUIGMech1.2. ....	150
<b>Figure 4.21.</b> Species profiles for propene pyrolysis at 2 bar. Dashed lines represent NUIGMech1.1 and solid lines represent NUIGMech1.2. ....	151
<b>Figure 4.22.</b> Species profiles for 1-butene pyrolysis at 2 bar. Dashed lines represent NUIGMech1.1 and solid lines represent NUIGMech1.2. ....	152
<b>Figure 4.23.</b> Species profiles for 2-butene pyrolysis at 2 bar. Dashed lines represent NUIGMech1.1 and solid lines represent NUIGMech1.2. ....	153
<b>Figure 4.24.</b> Species profiles for isobutene pyrolysis at 2 bar. Dashed lines represent NUIGMech1.1 and solid lines represent NUIGMech1.2. ....	154
<b>Figure 4.25.</b> Potential energy surface for $\dot{\text{H}}$ atom addition reactions of propene. Energies in $\text{kJ mol}^{-1}$ . ....	155
<b>Figure 4.26.</b> Potential energy surface for $\dot{\text{H}}$ -atom addition reactions of 1- and 2-butene. Energies in $\text{kJ mol}^{-1}$ . ....	156
<b>Figure 4.27.</b> Potential energy surface for $\dot{\text{H}}$ -atom addition reactions of isobutene. Energies in $\text{kJ mol}^{-1}$ . ....	157
<b>Figure 5.1.</b> Comparison of literature values with this work for the cyclisation reaction of 3-hydroperoxyl-prop-2-yl radical forming methyloxirane and a hydroxyl radical. Black:	

This work, Red: Villano et al. [1], Blue: Miyoshi [2], Magenta: Wijaya et al. [3], Cyan: Cord et al. [4], Wine: Chan et al. [5], Orange: Goldsmith et al. [6]. ..... 172

**Figure 5.2.** Model-simulated effects of rate coefficients presented in this study on n-pentane (a) ignition delay times at 10 (black) and 20 atm (red), and perfectly-stirred reactor profiles of (b) n-pentane, (c) 2-methyltetrahydrofuran (black), and 2,4-dimethyloxetane (red). Symbols represent experimental data, dashed lines represent Model A, and solid lines Model B (see Section 3.3 for details). The thicker lines in (a) represent simulations accounting for facility effects. .... 173

**Figure 6.1.** Schematic of the NUIG SPST. .... 180

**Figure 6.2.** Species profiles for 1-pentene pyrolysis. Solid lines: model simulations. .... 182

**Figure 6.3.** RFD for 1-pentene pyrolysis at ~50% fuel consumption, 2.13 bar, 1243 K. .... 182

**Figure 6.4.** Species profiles for t-2-pentene pyrolysis. Solid lines: model simulations. .... 183

**Figure 6.5.** RFD for t-2-pentene pyrolysis at ~50% fuel consumption, 2.01 bar, 1205.4 K. .... 183

**Figure 6.6.** Species profiles for 2M1B pyrolysis. Solid lines: model simulations. .... 184

**Figure 6.7.** RFD for 2M1B pyrolysis at ~ 50% fuel consumption, 2.01 bar, 1254.2 K. .... 185

**Figure 6.8.** Species profile for 2M2B pyrolysis. Solid lines: model simulations. .... 185

**Figure 6.9.** RFD for 2M2B pyrolysis at ~50% fuel consumption, 2.13 bar, 1451.2 K. .... 185

**Figure 6.10.** Species profile for 3M1B pyrolysis. Solid lines: model simulations. .... 186

**Figure 6.11.** RFD for 3M1B pyrolysis at ~50% fuel consumption, 2.01 bar, 1205 K. .... 186

**Figure 6.12.** (a) Fuel reactivities for pentenes, (b) Ethylene formation. Solid lines: model simulations. .... 187

**Figure 6.13.** Benzene formation pathways. .... 187

**Figure 6.14.** Experiment results for (a) 1,3-butadiene concentration; (b) Cyclopentadiene concentration; (c) Allene and propyne total concentration; (d) Benzene concentration. Fuel consumed is calculated as (initial fuel concentration – final fuel concentration)/initial fuel concentration at a given temperature. This aids in offsetting the effect of fuel reactivity. .... 188

**Figure 6.15.** Relative ROP of Benzene at 1400 K and 2 bar. .... 189

## List of Tables

<b>Table 1.1:</b> Experimental Mixture Composition (ppm, the Balance is Ar) for $\dot{\text{H}}$ -ARAS Experiments Used to Study the Reactions of 1- and 2-Pentene + $\dot{\text{H}}$ . .....	12
<b>Table 2.1:</b> Summary of Experimental and Theoretical Studies Relevant to $\dot{\text{C}}_5\text{H}_{11}$ Species. ...	21
<b>Table 2.2:</b> List of Reaction Channels Considered in This Work. ....	25
<b>Table 2.3:</b> Formation Enthalpies and Uncertainties ( $2\sigma$ ) Computed via Isodesmic and Atomisation Methods, Together with ATcT, ANL0 and ANL1 Formation Enthalpies and Uncertainties. ....	28
<b>Table 2.4:</b> Illustrative Isodesmic Reactions Used To Calculate the Formation Enthalpy of 1-Pentene. ....	30
<b>Table 2.5:</b> Experimental Mixture Composition (ppm, the Balance is Ar) for $\dot{\text{H}}$ -ARAS Experiments Used To Study the Reactions of $\dot{\text{H}}$ + 1- and 2-Pentene. ....	32
<b>Table 2.6:</b> Estimated Rate Constants for Radical Recombination and Unimolecular Reactions Relevant to 1- and 2-Pentene Decompositions. <sup>a</sup> .....	34
<b>Table 2.7:</b> Comparisons of the Formation Enthalpies Computed in This Work with Literature Data <sup>a</sup> . ....	38
<b>Table 2.8:</b> Comparisons of Entropies Computed in This Work with Literature Data <sup>a</sup> . ....	40
<b>Table 2.9:</b> Comparisons of the Heat Capacities Computed in This Work with Literature Data. Units: ( $\text{J K}^{-1} \text{mol}^{-1}$ ) [a] This work, [b] Burcat [70], [c] Awan et al. [6]. ....	42
<b>Table 2.10:</b> Computed Energy Barriers, Heats of Reaction, and High-Pressure Limiting Rate Constant Fits for the Reactions of $\dot{\text{H}}$ with 1- and 2-Pentene. Units ( $AT^n = \text{cm}^3 \text{mol}^{-1} \text{s}^{-1}$ , energies = $\text{kJ mol}^{-1}$ ). R1 – R10 fit between 298 – 2000 K, R11 – R14 fit between 500 – 2000 K. ....	44
<b>Table 3.1:</b> List of Experimental and Theoretical Data of Related Studies. ....	68
<b>Table 3.2:</b> $\text{C}_5$ Species Considered in This Work. ....	73
<b>Table 3.3:</b> List of Reaction Channels Considered in This Work. ....	74
<b>Table 3.4:</b> Formation Enthalpies and Uncertainties ( $2\sigma$ ) via Isodesmic and Atomisation Methods. ....	75
<b>Table 3.5:</b> Enthalpy of Formation Comparisons of $\text{C}_5$ Species with Literature Data. ....	77
<b>Table 3.6:</b> Entropy Comparisons of $\text{C}_5$ Species with Literature Data (Units: $\text{J K}^{-1} \text{mol}^{-1}$ ). ...	77
<b>Table 3.7:</b> Computed Energy Barriers, Heats of Reaction, and High-Pressure Limiting Rate Constant Fits for the Reactions of $\dot{\text{H}}$ with $a\text{C}_5\text{H}_{10}$ , $b\text{C}_5\text{H}_{10}$ and $c\text{C}_5\text{H}_{10}$ . Units ( $AT^n = \text{cm}^3 \text{mol}^{-1} \text{s}^{-1}$ , energies = $\text{kJ mol}^{-1}$ ). R1 – R17 Fit Between 298 and 2000 K. ....	80

<b>Table 3.8:</b> Recommended Rate Constants for $\dot{\text{H}}$ atom Addition to Linear and Branched Alkenes (units: $\text{cm}^3/\text{mol}/\text{s}/\text{cal}$ ).....	88
<b>Table 3.9:</b> Recommended Rate Constants for H-atom Abstraction From Alkenes <sup>a</sup> .....	92
<b>Table 3.10:</b> Computed Energy Barriers, Heats of Reaction, and High-Pressure Limiting Rate Constant Fits for the Reactions of Pentyl Radicals. Units ( $\text{AT}^n = \text{s}^{-1}$ , Energies = $\text{kJ mol}^{-1}$ ). R18–R28 Fit between 298 and 2000 K.....	92
<b>Table 4.1:</b> Summary of Experimental and Theoretical Studies Relevant to $\text{C}_2 - \text{C}_4$ alkenes + $\dot{\text{H}}$ . .....	118
<b>Table 4.2:</b> Formation Enthalpies and Uncertainties ( $2\sigma$ ) Computed via Isodesmic and Atomisation Methods, Together with ATcT, ANL0, and ANL1 Formation Enthalpies and Uncertainties. ....	123
<b>Table 4.3:</b> Comparisons of the Formation Enthalpies Computed in This Work with Literature Data.....	124
<b>Table 4.4:</b> Comparisons of Entropies Computed in This Work with Literature Data. ....	125
<b>Table 4.5:</b> Comparisons of Heat Capacities Computed Here with Literature Data.....	126
<b>Table 4.6:</b> Computed Energy Barriers, Heats of Reaction, and High-Pressure Limiting Rate Constant (298 – 2000 K) for the Reactions of $\dot{\text{H}}$ Atoms with $\text{C}_2 - \text{C}_4$ Alkenes. Units ( $\text{AT}^n = \text{cm}^3 \text{mol}^{-1} \text{s}^{-1}$ , Energies $\text{kJ mol}^{-1}$ ). ....	128
<b>Table 4.7:</b> Rate Constant Recommendations (Symmetry Uncorrected) for $\dot{\text{H}}$ atom Addition to Linear and Branched Alkenes ( $\text{C}_2 - \text{C}_5$ ).....	137
<b>Table 4.8:</b> Symmetry Corrections to be Applied to Rate Constant Recommendations for $\dot{\text{H}}$ Atom Addition to Alkenes.....	138
<b>Table 4.9:</b> Recommended Rate Constants for H-atom Abstraction from Alkenes on a per H-atom basis. ( $\text{A.T}^n = \text{cm}^3 \text{mol}^{-1} \text{s}^{-1}$ , Energies = $\text{cal mol}^{-1}$ ). Fit between 300 and 2000 K. ....	144
<b>Table 4.10:</b> Computed Energy Barriers, Heats of Reaction, and High-Pressure Limiting Rate Constant Fits for the Reactions of $\text{C}_3 - \text{C}_4$ alkyl radicals. Units ( $\text{AT}^n = \text{s}^{-1}$ , Energies = $\text{kJ mol}^{-1}$ ). Fit Between 298 and 2000 K.....	144
<b>Table 4.11:</b> Recommended Rate Constants for Alkyl Radical Decomposition Forming an Olefin + Radical. ( $\text{AT}^n = \text{s}^{-1}$ , Energies = $\text{cal mol}^{-1}$ ). Fit between 300 K and 2000 K....	148
<b>Table 5.1:</b> Rate Coefficients Calculated in This Study. ....	170



# Chapter 1 : General Introduction

## 1. Combustion

Over 80% of the world's energy production is generated from the combustion of fossil fuels [1]. In Ireland alone, a similar situation prevails, with fossil fuels accounting for 89% of our energy production in 2018, as reported by the SEAI [2].

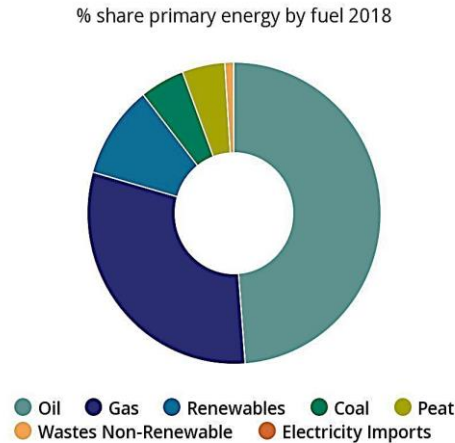


**Figure 1.1.** Overview of energy use in Ireland broken down by fuel [2].

On a fundamental level, the combustion of fossil fuels involves harnessing the chemical energy produced when organic molecules are oxidised to form carbon dioxide ( $\text{CO}_2$ ) and water ( $\text{H}_2\text{O}$ ). However, the process is much more complicated, with the combustion of a fuel occurring *via* hundreds to thousands of fundamental reactions. These reactions may form other secondary stable products in addition to the primary products  $\text{CO}_2$  and  $\text{H}_2\text{O}$ .

These secondary products can include carbon monoxide ( $\text{CO}$ ), and nitrogen oxides ( $\text{NO}_x$ ). Unburned hydrocarbons can also be released into the atmosphere. Carbon monoxide is a gas which is extremely toxic to humans, while nitrogen oxides are associated with acid rain. A large proportion of unburned hydrocarbons is carcinogenic and can lead to the formation of particulate matter (PM). Additionally, when nitrogen oxides are combined with unburned hydrocarbons, it leads to the formation of ground level ozone and smog. The primary products of combustion,  $\text{CO}_2$  and  $\text{H}_2\text{O}$  are also classified as pollutants, due to their contribution to the atmospheric greenhouse effect as greenhouse gases (GHGs). Several combustion exhaust gases have been demonstrated as GHGs including  $\text{CO}_2$ , methane ( $\text{CH}_4$ ), and  $\text{NO}_2$ , while the role of  $\text{H}_2\text{O}$  is still unclear [3].

The transportation sector in Ireland is responsible for the largest source of final energy demand, accounting for over 40%, with the residential sector coming in second accounting

for over 25%. The percentage of the transportation sector contributing to energy consumption tends to fluctuate with economic growth and contraction. In terms of transportation, private cars are the mode of transport with the highest energy use and accounted for 40% of transport fuel energy demand in 2018. In the past cars primarily ran on petrol, while commercial vehicles used diesel. In response to changes in car taxation and European Union (EU) obligations for manufacturers to mitigate fuel emissions, the amount of petrol consumed in Ireland fell by more than half between 2007 – 2018 as a result of the shift to diesel cars [2].

The Sustainable Energy Authority of Ireland (SEAI) states that for the average new car purchased, CO<sub>2</sub> emissions fell by 32% within this period [2]. There has been a slight increase in the use of renewable transport fuels, which is mostly from biofuels blended with petrol and diesel. This minor increase has grown from a very low base to 3% of the transport fuel energy use in 2018. Electrification remained at 0.1% of final energy demand in 2018 [2]. Light-duty ground vehicles powered by batteries are becoming popular due to advances made in battery technologies. These batteries can be charged from alternative stationary sources and have demonstrated themselves as alternatives to combustion engines. However, in terms of aviation and other heavy-duty ground and marine vehicles, batteries are not a viable option due to their low energy density [3]. As a result, the combustion of these energy dense fuels will be the primary means of energy for powering these heavy-duty vehicles for the foreseeable future. We cannot eliminate CO<sub>2</sub> entirely from the combustion of fossil fuels but we can aim to minimise the emissions they produce through increasing the efficiency of combustors.

Therefore, combustion science serves a great purpose in society today, as it facilitates the study and analysis of the problems associated with the generation of air pollutants. Here in the Combustion Chemistry Centre, through the application of combustion research to the design of energy-efficient engine and gas turbine combustion systems help address and mitigate the problems of air pollution and climate change [4].

The availability of high-speed supercomputers in tandem with cost-effective yet accurate computational methods has provided the combustion community with the tools needed to build kinetic models from ab-initio calculations. This data which is implemented into these kinetic models is often very difficult to obtain experimentally. These models provide an insight to the physical reality of the fuels combustion, but must be validated against experimental data, such as shock-tube and jet-stirred reactor data.

The first four steps, which are highlighted in blue in Figure 1.2 are the main focus of *this thesis*.



- Quantum chemistry calculations
- Kinetic/thermodynamic properties
- Detailed chemical kinetic model development
- Model validation

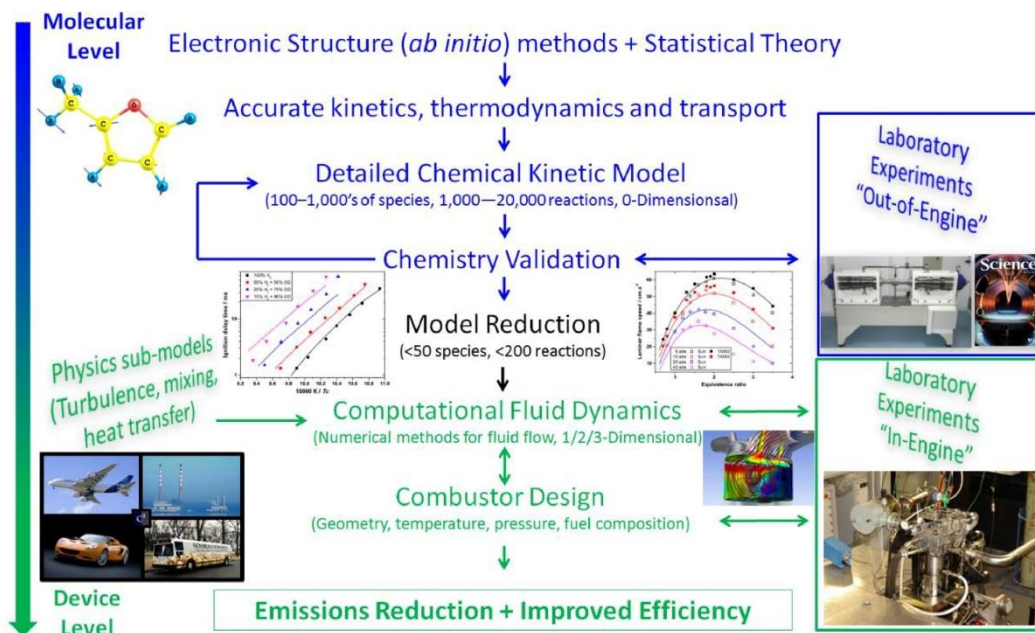


**Figure 1.2.** Schematic diagram (courtesy of Dr. Kieran Somers) showing the steps in the development of the understanding of combustion from the molecular level to its application at the device level.

The following sub-sections describe in part the methods employed in these four steps for the work carried out in *this thesis*, with further descriptions provided in detail in later sub-sections containing peer reviewed articles.

## 2. Quantum chemistry

Quantum chemistry applies quantum mechanics to problems in chemistry, and its application can be seen in all branches of chemistry. For physical chemists, quantum mechanics is generally used for a number of purposes; (1) theoretically calculate molecular properties, (2) calculate properties of transition states in chemical reactions, which are ultimately used for rate constant calculations, (3) calculate thermodynamic properties such as formation enthalpies, entropies and heat capacities of gases, through the aid of statistical mechanics, (4) interpret molecular spectra, thus allowing experimental determination of molecular properties such as molecular geometries, (5) understand intermolecular forces, and

(6) deal with bonding in solids. The rapid increase in computer speed and DFT methods have made quantum chemistry a practical tool in all areas of chemistry [5].

“Quantum mechanics...underlies nearly all of modern science and technology. It governs the behaviour of transistors and integrated circuits...and is...the basis of modern chemistry and biology”– Stephen Hawking 1988 (A Brief History of Time, 1988, Bantam, Chapter 4.)

Quantum mechanics states that the energy and other related properties may be obtained by solving the Schrödinger equation. However, for any but the smallest systems, the exact solution to the equation is not computationally practical, therefore the Born-Oppenheimer (BO) approximation is used [6, 7]. In this approximation, it is assumed that the nuclei are stationary, while the electrons move around them since nuclei are so much heavier. With the position of the nuclei fixed at arbitrary locations, the position of the electrons can be defined relative to them. By fixing the inter-nuclear separation the electronic Schrödinger equation can be solved for the electrons for that nuclear separation [7]. Electronic structure methods are classed into three main groups by their various mathematical approximations to its solution. (1) semi-empirical, (2) ab-initio and (3) density-functional theory (DFT). Semi-empirical and ab-initio differ in terms of the trade-off between computational expense and accuracy. Semi-empirical methods are relatively inexpensive and provide relatively good qualitative descriptions of molecular systems and quantitative predictions of energies and structures for systems where good parameter sets exist. The word “ab initio” is Latin for “from the beginning”. Ab initio calculations compute solutions to the Schrödinger equation, which is the fundamental equation of quantum mechanics [5, 6]. The Schrödinger equation is a differential equation, and the *time-independent* Schrödinger equation, for a single particle of mass  $m$  moving with energy  $E$  can be written as [7]:

$$-\frac{\hbar^2}{2m} \frac{d^2\psi}{dx^2} + V(x)\psi = E\psi \quad (1)$$

where  $\psi$  is known as the wavefunction or the state function.  $V$  is the potential energy function and  $\hbar$  is a convenient modification of Plank’s constant:

$$\hbar = \frac{h}{2\pi} = 1.055 \times 10^{-34} Js$$

Equation (1) is also widely written as:

$$\hat{H}\psi = E\psi \quad (2)$$

where  $\hat{H}$  is called the Hamiltonian of the system after the mathematician William Hamiltonian who had formulated a version of classical mechanics that used the concept.  $\hat{H}\psi$  represents everything to the left of equation (1).

The widely used interpretation of a wavefunction is that from a German physicist Max Born. The Born interpretation states that: The probability of finding a particle in a small region of space of volume  $\partial V$  is proportional to  $|\psi|^2\partial V$ , where  $\psi$  is the value of the wavefunction in the region [7]. The Born interpretation implies that for a small “inspection volume”  $\partial V$  of a given size that wherever  $\psi^2$  is large, there is a high probability of finding the particle and *vice versa* for a small  $\psi^2$ . It accepts that we can make predictions only about finding a particle somewhere, which is in contrast to classical physics, which claims to be able to predict precisely the location of a particle at a given point and time [7]. DFT methods are similar to ab-initio methods in many ways, however they are advantageous in the way they include the effects of electron correlation-they account for the instantaneous interactions of pairs of electrons with opposite spin. In *this thesis*, to study elementary gas-phase combustion reactions, ab initio and DFT methods are used, which are considered the current gold standard due to the accuracy they provide in the computation of molecular geometries, vibrational frequencies, and electronic energies [8, 9].

## 2.1. Quantum chemistry calculations

In *this thesis*, computational quantum chemical methods are used to determine a hierarchical set of high-pressure limiting and pressure-dependent rate constants for the reaction class of  $\dot{\text{H}}$  atom addition to, and abstraction from, both linear and branched  $\text{C}_2 - \text{C}_5$  alkenes. The subsequent C–C and C–H  $\beta$ -scission reactions and H-atom transfer reactions are also considered. These rate constants are then implemented into kinetic models (AramcoMech3.0 [10], NUIGMech1.0 [11-18] and NUIGMech1.2, in which calculation results from Chapter 4 are implemented into the base chemistry of NUIGMech1.1), and simulated against a range of shock-tube data, including new hydrogen atomic resonance absorption spectroscopy ( $\dot{\text{H}}$ -ARAS) experiments taken as part of this work [19] and literature pyrolysis experiments on linear and branched 1-alkenes using the single pulse shock tube at NUIG [12, 16], and serve as direct and in-direct validation targets for the current calculations, with good agreement being observed. Additionally, rate constant recommendations for  $\dot{\text{H}}$  atom addition to, and abstraction from, both linear and branched  $\text{C}_2 - \text{C}_5$  alkenes, as well as alkyl radical decompositions are proposed. Detailed descriptions of the methodologies employed in the derivation of these rate constants and rate constant recommendations are

provided in published peer-reviewed articles or articles under review presented later in *this thesis* [16, 19-22], with a brief description of the methods provided here. Density functional theory (DFT) and ab initio methods are employed in this study in order to derive rate coefficients of high enough accuracy to warrant their direct use in chemical kinetic models describing combustion processes.

Geometries are optimised using the density functional theory (DFT)  $\omega$ B97XD [23] method coupled with the aug-cc-pVTZ [24] basis set. Harmonic frequency analysis is simultaneously carried out at the same level of theory to verify the nature of each stationary point. Low-frequency torsional modes are treated via relaxed PES scans in 10-degree increments with the  $\omega$ B97XD / 6-311++G(d,p) method, with the potential energies as a function of dihedral angle used as input for a one-dimensional (1-D) hindered rotor approximation as implemented in the Master Equation System Solver (MESS) [25]. To compute barrier heights, single point energies for minima and transition states are calculated at the coupled cluster level, (CCSD(T)) and Møller-Plesset perturbation theory (MP2), with cc-pVXZ basis sets, where X = D, T and Q levels of theory.

Moreover, as part of *this thesis*, rate constants for the low-temperature reaction class: the cyclisation of hydroperoxyl-alkyl ( $\dot{\text{Q}}\text{OOH}$ ) radicals to form cyclic ethers and hydroxyl radicals ( $\dot{\text{Q}}\text{OOH} \leftrightarrow \text{cyclic ether} + \dot{\text{O}}\text{H}$ ) are calculated involving species ranging in size from  $\text{C}_2\text{H}_5\text{O}_2$  to  $\text{C}_5\text{H}_{11}\text{O}_2$  [20]. These rate constants are determined using density functional theory (DFT) and ab initio approaches. Geometry optimisations are conducted using the M06-2X method coupled with the 6-311++G(d,p) basis set. Single point energies are calculated using coupled cluster (CCSD), specifically CCSD(T), and second-order Møller-Plesset perturbation theory (MP2) methods, with relatively large basis sets (cc-pVXZ, where X = D,T,Q). Standard statistical thermodynamics and canonical transition state theory are employed to derive the kinetic data of interest. The methods used in deriving the rate coefficients represent the highest level of theory employed for a large set of reactions of this type. The values tend to be lower than those present in the literature and provide better modelling results than ones used previously in the literature, which is described in Section 3.3 of Chapter 5.

All calculations were performed using the supercomputer, Fionn and Kay, run by the Irish Centre for High-End Computing (ICHEC). All electronic structure calculations were carried out using Gaussian software packages, Gaussian 09 [26] and Gaussian 16 [27]. The application Chemcraft [28] was used to visualise the output structures and frequencies, and also to generate the input geometries.

### 3. Kinetic/thermodynamic properties

#### 3.1. Pressure-dependent rate constants

Unlike high-pressure limiting rate constants, where the rate constant is independent of pressure, pressure dependent rate constants vary with pressure [9]. The pressure dependence is as a result of the competition between thermal equilibration via collisional excitation/de-excitation and the dissociation process. The distribution of reacting energy states, and ultimately the thermal rate constant, depends on the rate of collisions between both the bath gas and the excited molecule. At very high pressures, thermal equilibration is complete, and this distribution is simply Boltzmann. However, at lower pressures, higher energy states are depleted by reaction and collisions. Every molecule that gets excited above the dissociation threshold ultimately dissociates, and the rate of dissociation is thus determined by the rate of collisional activation. This rate is linearly dependent on the number of collisions and thus the pressure. The collisions are not fast enough to maintain a Boltzmann distribution. Ab initio kinetics which involves the combination of ab-initio electronic structure theory, transition state theory (TST) and the master equation (ME) is an effective way of determining unknown rate coefficients [9]. The master equation system solver (MESS) [25], which is adopted in *this thesis*, works by first constructing the global relaxation matrix that describes both chemical transformations and collisional energy relaxation. It then finds the eigenstates of the relaxation matrix, and extracts from those the full set of phenomenological chemical rate coefficients [25].

#### 3.2. Transition state theory

The expression for the temperature-dependence of the rate constant for pressure-independent reactions is generally written as [9]:

$$k^{\text{TST}}(T) = \kappa \frac{k_B T}{h} \frac{Q^\ddagger(T)}{Q_{\text{react}}(T)} \exp\left(-\frac{\Delta E^\ddagger}{k_B T}\right) \quad (3)$$

where  $\kappa$  is a correction factor to account for tunnelling and non-classical reflection,  $k_B$  and  $h$  are the Boltzmann and Planck constants, respectively. The Boltzmann factor accounts for the probability of having sufficient energy ( $\Delta E^\ddagger$ ) to cross the barrier.  $Q_{\text{react}}$  and  $Q^\ddagger$  are the partition functions for the reactants and the TS, respectively. These quantities can be readily obtained from ab initio electronic structure theory described in *this thesis*. The relationship between the reaction rate constant and temperature was experimentally elucidated by Svante Arrhenius [29] in 1889 based on earlier work by Van't Hoff in 1884 [30]. Arrhenius deduced

that a plot of  $\ln(k)$  vs  $1/T$  showed a linear dependence, with the slope equal to  $-Ea/R$ . If the activation energy is high, this corresponds to a reaction rate that is very sensitive to temperature, while a small activation energy indicates a reaction rate that is not sensitive to temperature. Finally, a reaction with zero activation energy has a rate that is independent of temperature, for example some radical recombination reactions in the gas phase. This correlation was further improved to a modified form, which is shown as follows:

$$k = AT^n \exp(-Ea/RT) \quad (4)$$

where  $A$  is the pre-exponential factor,  $n$  is a factor which accounts for curvature in the rate constant as a function of temperature,  $R$  is the gas constant and  $Ea$  is the activation energy. These three parameters are termed the Arrhenius parameters and are fundamental to chemical kinetic modelling. The equation offers a concise way to represent a rate constant over a wide temperature range and is thus widely adopted in chemical kinetic modelling.

### 3.3. Chemical kinetics

For the studies of  $\dot{H} +$  alkenes [19, 21, 22], high-pressure limiting and pressure-dependent rate constants are calculated using Rice-Ramsperger-Kassel-Marcus (RRKM) theory with a one-dimensional (1-D) master equation (ME) analysis using the Master Equation System Solver, (MESS). Tunnelling is accounted for via an un-symmetric Eckart model, as implemented in MESS, where parameters include the imaginary frequency, and the forward and reverse barrier heights. To model collisional energy transfer, the single-exponential down model is used, with appropriate estimations for the average energy transferred in a downward collision discussed within the articles.

In the case of the cyclic ether study [20], the thermo application of MultiWell [31] is used to compute high-pressure limit rate coefficients as a function of temperature (298.15–2000 K) from canonical transition state theory. Quantum mechanical tunnelling is accounted for via inclusion of 1-D tunnelling through an unsymmetrical Eckart energy barrier, with further details discussed in Section 2.1 of Chapter 5.

### 3.4. Thermodynamics

Thermodynamics and kinetics go hand in hand in developing detailed combustion models. The fundamental thermodynamic properties of interest in kinetic model development are the formation enthalpy, entropy and heat capacity as a function of temperature, which are used during the modelling simulations to determine species thermodynamic properties,

thermal transport properties, and reaction equilibrium constants. The equilibrium constant may be expressed in terms of the standard reaction Gibbs energy.

$$\Delta_r G^\theta = -RT \ln K_p \quad (5)$$

One use of equation 5 is to determine  $\Delta_r G^\theta$  by measuring the equilibrium constant of a reaction. A reaction is thermodynamically feasible in the sense ( $K_p > 1$ ) if  $\Delta_r G^\theta < 0$ . Conversely, if  $\Delta_r G^\theta > 0$ , a reaction is not thermodynamically feasible.

$$\Delta_r G^\theta = \Delta_r H^\theta - T\Delta_r S^\theta \quad (6)$$

the standard reaction Gibbs energy is negative if both  $\Delta_r H^\theta < 0$  and  $\Delta_r S^\theta > 0$ . It is also negative if the reaction is endothermic ( $\Delta_r H^\theta > 0$ ) and  $T\Delta_r S^\theta$  is sufficiently large and positive. For an endothermic reaction to have  $\Delta_r G^\theta < 0$ , its standard reaction entropy must be positive. Moreover, the temperature must be high enough for  $T\Delta_r S^\theta$  to be greater than  $\Delta_r H^\theta$ .

Thermochemical values for species on the  $\dot{C}_2H_5$ ,  $\dot{C}_3H_7$ ,  $\dot{C}_4H_9$  and  $\dot{C}_5H_{11}$  potential energy surfaces (PESs) are calculated as a function of temperature (298–2000 K), with enthalpies of formation determined using a network of isodesmic reactions. For species where ATcT, [32, 33] ANL0, [34] and ANL1 [34] formation enthalpy values do not exist, quantum chemical composite methods (CBS–QB3, CBS–APNO, G3, and G4) [35–37] are used to calculate formation enthalpies at 0 K via a network of isodesmic reactions suitable for each species, using ATcT values for the molecular and radical chaperones. Comparisons between atomisation and isodesmic values obtained in these studies are made, with excellent agreement observed. However, as mentioned, although isodesmic and atomisation methods give similar nominal 0 K enthalpy of formation values, the isodesmic approach is often used to approach “chemical accuracy”. The uncertainties in the enthalpies of formation are calculated using the methods employed by Simmie et al. [38] and are described in detail in Section 2.2 of in Chapter 2.

Temperature-dependent enthalpies, entropies, and heat capacities are calculated using traditional statistical thermodynamics methods, as implemented in MESSPF [25], with Chemkin format NASA polynomials fitted using PAC99 [39].

#### 4. Detailed kinetic mechanism development

In Fig. 1.3, Curran describes the history of chemical kinetic modelling development. The major classes of elementary reactions considered in most of the mechanisms include 25 reaction classes, which were described in detail in his earlier work [40]. The number of reaction classes has been extended to 31 by Bugler et al. [41], through an evaluation of recent

quantum-chemically derived rate coefficients with associated rate constants to describe the low temperature oxidation of the pentane isomers.

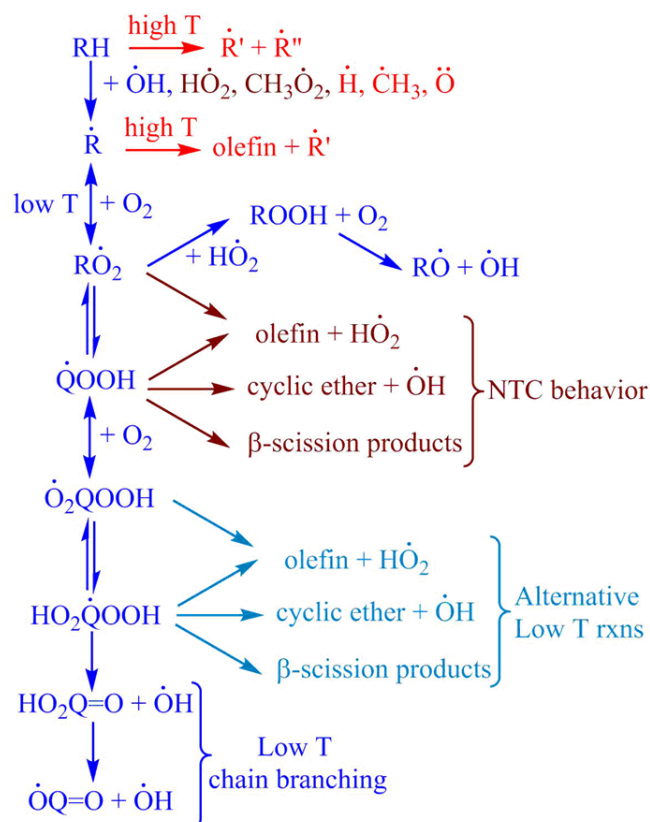


**Figure 1.3.** General schematic mechanism for fuel oxidation [40, 42].

Detailed mechanism development is a key focus of the Combustion Chemistry Centre, C<sup>3</sup>. A detailed chemical kinetic mechanism consists of tens, through hundreds to thousands of elementary chemical reactions with associated rate constants, thermodynamic, and transport properties for each species. For example, hydrogen requires eight species and approximately 22 elementary reactions to describe its oxidation over a wide range of pressure and temperature, while methane requires approximately 30 species and 200 elementary reactions. The development of such chemical kinetic model requires modelers to adopt the best measured and/or calculated rate constant and thermochemistry for target reactions from the literature. The performance of a mechanism is generally compared to experimental results and, in practice, some optimizations of the mechanism maybe needed by adjusting the rate constants to fit a wide range of experimental targets. The oxidation of any fuel at high temperatures depends largely on C<sub>0</sub> – C<sub>4</sub> chemistry. It is now commonly accepted that it is possible to manually or automatically generate mechanisms by first generating a core C<sub>0</sub> – C<sub>4</sub>



mechanism and then building the chemistry for larger components upon this, in a “ground up” approach [42]. Our earlier kinetic mechanism AramcoMech3.0 [10], which mainly focuses on  $C_0 - C_4$  kinetics, has been widely recognized and used in the combustion community. This has recently been built upon and adapted, with the  $C_0 - C_7$  chemistry being comprehensively validated, and is named NUIGMech1.0 [11-18].

As part of this work on 1- and 2-pentene +  $\dot{H}$  [19], which is described in Section 2.4 of Chapter 2, hydrogen atomic resonance absorption spectroscopy ( $\dot{H}$ -ARAS) experiments were performed on the  $\dot{H}$  atom addition and abstraction reactions of 1- and 2-pentene by Dr. Sebastian Peukert at the University of Duisburg-Essen, Germany. These represent direct validation targets for our theoretical results. The a priori model is found to reproduce important absolute species concentrations and product ratios. An initial chemical kinetic model was built by implementing the computed rate constants and thermochemistry into AramcoMech3.0 [10], including higher-level RO-aug-cc-pVXZ single point energies (SPEs) for reactions which were found to be important in predicting the available experimental data, which are again explained in further detail in a peer reviewed article herein [19]. A series of secondary reactions are also added to the mechanism, which are found to be important to accurately model the experiments. Preliminary simulations showed that the  $\dot{H}$  atom yields were sensitive to pentene isomer unimolecular decomposition reactions. Therefore, high-pressure limiting rate constants are estimated for the recombination of the radical products, with the forward decomposition rate constants calculated using the species thermochemistry. Thermochemistry and kinetics for radical initiators and scavengers are also incorporated to appropriately model these literature experiments by Awan et al. [43] and Manion et al. [44].

## 5. Model validation

As mentioned above, one of the most important components in developing chemical kinetic models is having reliable data with which to validate the model [42]. In *this thesis*, ( $\dot{\text{H}}$ -ARAS) experiments were performed on the  $\dot{\text{H}}$  atom addition and abstraction reactions of 1- and 2-pentene by Dr. Sebastian Peukert in the University of Duisburg-Essen, Germany. These represent direct validation targets for our theoretical results. Additionally, the theoretical results presented in *this thesis* are simulated against other literature experimental results and are described in detail Section 4.2 of Chapter 2 [20].

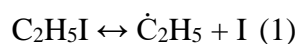
### 5.1. $\dot{\text{H}}$ -ARAS experimental measurements

Temporal  $\dot{\text{H}}$ -atom profiles have been measured for  $\dot{\text{H}}$ -atom reaction with 1- and 2-pentene and have been simulated with a detailed kinetic model described in further detail in a later sub-section.  $\dot{\text{H}}$ -atom concentrations were monitored behind reflected shock waves by applying the sensitive hydrogen atomic resonance absorption spectrometry ( $\dot{\text{H}}$  ARAS) technique.

**Table 1.1:** Experimental Mixture Composition (ppm, the Balance is Ar) for  $\dot{\text{H}}$ -ARAS Experiments Used to Study the Reactions of 1- and 2-Pentene +  $\dot{\text{H}}$ .

$\text{C}_2\text{H}_5\text{I}$	$\text{C}_5\text{H}_{10-1}$	$\text{C}_5\text{H}_{10-2}$	p (atm)	T / K
0.34	0.00	8.49	$\sim 1.5$	980 – 1055
0.35	8.90	0.00	$\sim 1.5$	985 – 1046

These experiments were taken by Dr. Sebastian Peukert as part of this work at the University of Duisburg-Essen, Germany and provide direct validation targets for the calculation results. The shock-tube apparatus currently used and the method for gas mixture preparation were described previously [45, 46]. Dilute gas mixtures containing small amounts of ethyl iodide ( $\text{C}_2\text{H}_5\text{I}$ ) as the  $\dot{\text{H}}$ -atom precursor and excess 1-pentene and 2-pentene were prepared, using argon as the diluent. The rise of  $\dot{\text{H}}$  -atom concentration is based on the thermal decomposition of  $\text{C}_2\text{H}_5\text{I}$ , which is a well-characterized two channel process.



The  $\dot{\text{H}}$  atoms then react with the excess 1-pentene or 2-pentene through addition and abstraction reactions. The experiments cover a narrow temperature range as at temperatures around 1100 K, the thermal decomposition of 1- and 2-pentene starts to contribute to  $\dot{\text{H}}$  -atom

formation, and at lower temperatures, there is a limit due to the slow decomposition of  $C_2H_5I$  ( $<1000$  K). By incorporating the calculations into a detailed kinetic model (AramcoMech 3.0) as described herein, excellent agreement with these experiments is observed. Further validation of the results for 1- and 2-pentene +  $\dot{H}$  reaction systems are validated against a comprehensive series of simulations of literature data [43, 47, 48], with the a priori model reproducing important absolute species concentrations and product ratios.

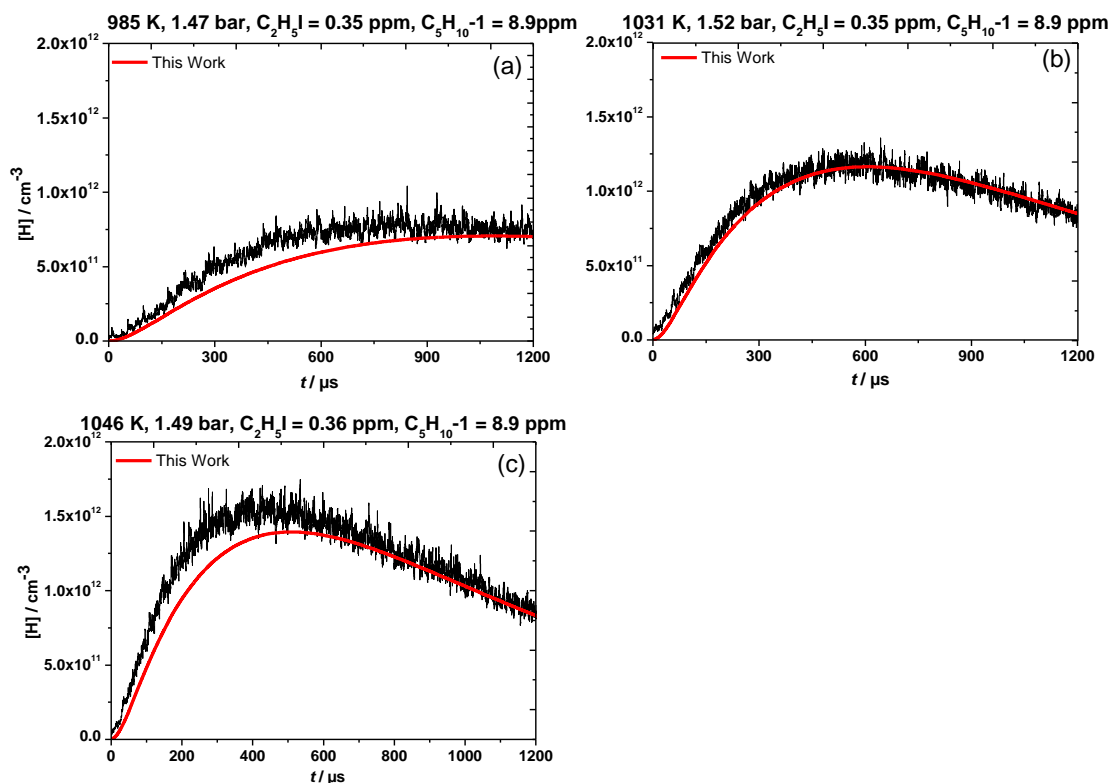


**Figure 1.4.** Experimental (black) and simulated (red)  $\dot{H}$ -atom profiles for  $C_2H_5I$ /1-pentene/Ar mixtures at (a) 985 K, (b) 1031 K and (c) 1046 K [19].

## 5.2. Pyrolysis experiments

Theoretical results for  $C_2 - C_4$  alkenes and the branched pentene isomers +  $\dot{H}$  reaction systems calculated in *this thesis* are validated against a series of literature pyrolysis experiments taken by Nagaraja et al. using the NUIG single-pulse shock-tube, with satisfactory agreement being observed. In the study of pentene isomer pyrolysis [16], calculations from work in *this thesis* on the branched pentene isomers +  $\dot{H}$  [21] are used in their model (NUIGMech1.0), with detailed discussions of the modelling results discussed within the article. This model also includes the published results on the 1- and 2-pentene +  $\dot{H}$

systems [19]. As previously mentioned, good agreement against species mole fractions is observed.

### 5.3. Cyclic ether validation

The calculated rate coefficients are implemented into the NUIG pentane oxidation model and it is shown that the model now produces favourable agreement with C<sub>5</sub> cyclic ether concentration measurements in the JSRs at Nancy and Orléans. These had previously been over-predicted by the model utilising literature rate coefficient values. Detailed descriptions of the modelling results are presented in the published article [20].

Theoretical and kinetic modelling approaches are performed to provide a comprehensive hierarchical set of rate constants for the reactions of  $\dot{\text{H}}$  atoms with linear and branched alkenes, ranging in size from C<sub>2</sub> – C<sub>5</sub>.  $\dot{\text{H}}$ -ARAS experiments were taken as part of this work and provided direct validation targets for the 1- and 2-pentene +  $\dot{\text{H}}$  calculations. Further validation of these results are made with literature studies and discussed herein. Also, rate constants for the low-temperature reaction class: cyclisation of hydroperoxyl-alkyl radical to form a cyclic ether and a hydroxyl radical ( $\dot{\text{Q}}\text{OOH} \leftrightarrow \text{cyclic ether} + \dot{\text{O}}\text{H}$ ) are calculated, involving species ranging in size from C<sub>2</sub>H<sub>5</sub> $\dot{\text{O}}_2$  to C<sub>5</sub>H<sub>11</sub> $\dot{\text{O}}_2$ . This work is available to the scientific community in five peer reviewed articles, either published or “in review”, and are produced in full in the remaining sections of *this thesis*.

## References

- [1] IEA world energy balance 2019.
- [2] SEAI statistics.
- [3] C.Banyon, The combustion of fuel reference compounds in laboratory scale reactors and flames, Department of Chemistry, National University of Ireland, Galway, 2018.
- [4] Combustion Chemistry Centre, NUI Galway. <https://www.nuigalway.ie/combustionchemistrycentre/> (accessed 03/12/20).
- [5] I.N. Levine, Quantum chemistry, 7th ed., Pearson, Pearson Education, Inc., Permissions Department, 1 LakeStreet, Department 1G, Upper Saddle River, NJ 07458., 2014.
- [6] J.B. Foresman, A.E. Frisch, Exploring chemistry with electronic structure methods, 2nd ed.
- [7] P. Atkins, J. dePaula, Elements of physical chemistry, 6th ed., Oxford 2013.
- [8] K.P. Somers, On the Pyrolysis and Combustion of Furans: Quantum Chemical, Statistical Rate Theory, and Chemical Kinetic Modelling Studies, Department of chemistry, National University of Ireland, Galway, 2014.
- [9] S.J. Klippenstein, C. Cavallotti, Ab initio kinetics for pyrolysis and combustion systems, Computer Aided Chemical Engineering, Elsevier 2019, pp. 115-167.
- [10] C.-W. Zhou, Y. Li, U. Burke, C. Banyon, K.P. Somers, S. Ding, S. Khan, J.W. Hargis, T. Sikes, O. Mathieu, et al, An experimental and chemical kinetic modeling study of 1,3-butadiene combustion: Ignition delay time and laminar flame speed measurements, Combust. Flame 197 (2018) 423-438.
- [11] M. Baigmohammadi, V. Patel, S. Martinez, S. Panigrahy, A. Ramalingam, U. Burke, K.P. Somers, K.A. Heufer, A. Pekalski, H.J. Curran, A comprehensive experimental and simulation study of ignition delay time characteristics of single fuel C<sub>1</sub>–C<sub>2</sub> hydrocarbons over a wide range of temperatures, pressures, equivalence ratios, and dilutions, Energy Fuels 34 (2020) 3755-3771.
- [12] S.S. Nagaraja, J. Liang, S. Dong, S. Panigrahy, A. Sahu, G. Kukkadapu, S.W. Wagnon, W.J. Pitz, H.J. Curran, A hierarchical single-pulse shock tube pyrolysis study of C<sub>2</sub>–C<sub>6</sub> 1-alkenes, Combust. Flame 219 (2020) 456-466.
- [13] N. Lokachari, S. Panigrahy, G. Kukkadapu, G. Kim, S.S. Vasu, W.J. Pitz, H.J. Curran, The influence of iso-butene kinetics on the reactivity of di-isobutylene and iso-octane, Combustion and Flame 222 (2020) 186-195.
- [14] S. Panigrahy, J. Liang, S.S. Nagaraja, Z. Zuo, G. Kim, T. MacDougall, S.S. Vasu, H.J. Curran, A comprehensive experimental and improved kinetic modeling study on the pyrolysis and oxidation of propyne, Proc. Combust. Inst. 38 (2021).
- [15] A.A.E.-S. Mohamed, S. Panigrahy, A.B. Sahu, G. Bourque, H. Curran, An experimental and kinetic modeling study of the auto-ignition of natural gas blends containing C<sub>1</sub>–C<sub>7</sub> alkanes, Proceedings of the Combustion Institute, (2020).
- [16] S.S. Nagaraja, J. Power, G. Kukkadapu, S. Dong, S.W. Wagnon, W.J. Pitz, H.J. Curran, A single pulse shock tube study of pentene isomer pyrolysis, Proc. Combust. Inst. 38 (2021).
- [17] S. Dong, K. Zhang, P.K. Senecal, G. Kukkadapu, S.W. Wagnon, S. Barrett, N. Lokachari, S. Panigrahy, P. W. J, H.J. Curran, A comparative reactivity study of 1-alkene fuels from ethylene to 1-heptene, Proc. Combust. Inst. 38 (2021).
- [18] S. Dong, K. Zhang, E.M. Ninnemann, A. Najjar, G. Kukkadapu, J. Baker, F. Arafin, Z. Wang, W.J. Pitz, S.S. Vasu, A comprehensive experimental and kinetic modeling study of 1- and 2-pentene, Combustion and Flame 223 (2021) 166-180.
- [19] J. Power, K.P. Somers, C.-W. Zhou, S. Peukert, H.J. Curran, Theoretical, experimental, and modeling study of the reaction of hydrogen atoms with 1- and 2-pentene, J. Phys. Chem. A 123 (2019) 8506-8526.
- [20] J. Bugler, J. Power, H.J. Curran, A theoretical study of cyclic ether formation reactions, Proceedings of the Combustion Institute 36 (2017) 161-167.

- [21] J. Power, K.P. Somers, S.S. Nagaraja, W. Wyrebak, H.J. Curran, Theoretical study of the reaction of hydrogen atoms with three pentene isomers: 2-methyl-1-butene, 2-methyl-2-butene, and 3-methyl-1-butene, *J. Phys. Chem. A* 124 (2020) 10649-10666.
- [22] J. Power, K.P. Somers, S.S. Nagaraja, H.J. Curran, A hierarchical study of the reactions of hydrogen atoms to alkenes: A theoretical study of the reactions of hydrogen atoms with C2 – C4 alkenes, *J. Phys. Chem. A* (2021).
- [23] J.-D. Chai, M. Head-Gordon, Long-range corrected hybrid density functionals with damped atom-atom dispersion corrections, *Phys. Chem. Chem. Phys.* 10 (2008) 6615-6620.
- [24] T.H. Dunning, Gaussian-basis sets for use in correlated molecular calculations .1. The atoms boron through neon and hydrogen, *J. Chem. Phys.* 90 (1989) 1007-1023.
- [25] Y. Georgievskii, J.A. Miller, M.P. Burke, S.J. Klippenstein, Reformulation and solution of the master equation for multiple-well chemical reactions, *J. Phys. Chem. A* 117 (2013) 12146-12154.
- [26] M.J. Frisch, G.W. Trucks, H.B. Schlegel, G.E. Scuseria, M.A. Robb, J.R. Cheeseman, G. Scalmani, V. Barone, G.A. Petersson, H. Nakatsuji, e. al., *Gaussian 09*, 2009.
- [27] M.J. Frisch, G.W. Trucks, H.B. Schlegel, G.E. Scuseria, M.A. Robb, J.R. Cheeseman, G. Scalmani, V. Barone, G.A. Petersson, H. Nakatsuji, e. al., *Gaussian 16 Rev. B.01*, Wallingford, CT, 2016.
- [28] Chemcraft version 1.8 [www.chemcraftprog.com](http://www.chemcraftprog.com).
- [29] S. Arrhenius, On the reaction rate of the inversion of non-refined sugar upon souring, *Zeitschrift fur Physikalische Chemie*, (1889) 226-248.
- [30] J.H.V.t. Hoff, *Etudes de dynamique chimique*, Muller (1884).
- [31] MultiWell-2014.1 Software, 2014, designed and maintained by J. R. Barker with contributors N. F. Ortiz, J. M. Preses, L. L. Lohr, A. Maranzana, P. J. Stimac, T. L. Nguyen, and T. J. D. Kumar, University of Michigan, Ann Arbor, MI, .
- [32] B. Ruscic, R.E. Pinzon, M.L. Morton, G. von Laszewski, S.J. Bittner, S.G. Nijsure, K.A. Amin, M. Minkoff, A.F. Wagner, Introduction to active thermochemical tables: several “key” enthalpies of formation revisited, *J. Phys. Chem. A* 108 (2004) 9979-9997.
- [33] B. Ruscic, R.E. Pinzon, G.v. Laszewski, D. Kodeboyina, A. Burcat, D. Leahy, D. Montoy, A.F. Wagner, Active thermochemical tables: thermochemistry for the 21st century, *J. Phys.* 16 (2005) 561-570.
- [34] S.J. Klippenstein, L.B. Harding, B. Ruscic, Ab initio computations and active thermochemical tables hand in hand: heats of formation of core combustion species, *J. Phys. Chem. A* 121 (2017) 6580-6602.
- [35] J.M. Simmie, K.P. Somers, Benchmarking compound methods (CBS-QB3, CBS-APNO, G3, G4, W1BD) against the active thermochemical tables: a litmus test for cost-effective molecular formation enthalpies, *J. Phys. Chem. A* 119 (2015) 7235-7246.
- [36] J.M. Simmie, K.P. Somers, W.K. Metcalfe, H.J. Curran, Substituent effects in the thermochemistry of furans: A theoretical (CBS-QB3, CBS-APNO and G3) study, *J. Chem. Thermodyn.* 58 (2013) 117-128.
- [37] K.P. Somers, J.M. Simmie, Benchmarking compound methods (CBS-QB3, CBS-APNO, G3, G4, W1BD) against the active thermochemical tables: formation enthalpies of radicals, *J. Phys. Chem. A* 119 (2015) 8922-8933.
- [38] J.M. Simmie, G. Black, H.J. Curran, J.P. Hinde, Enthalpies of formation and bond dissociation energies of lower alkyl hydroperoxides and related hydroperoxy and alkoxy radicals, *J. Phys. Chem. A* 112 (2008) 5010-5016.
- [39] B.J. McBride, S. Gordon, Computer program for calculating and fitting thermodynamic functions, (1992).
- [40] H.J. Curran, P. Gaffuri, W.J. Pitz, C.K. Westbrook, A comprehensive modeling study of iso-octane oxidation, *Combustion and flame* 129 (2002) 253-280.

- [41] J. Bugler, K.P. Somers, E.J. Silke, H.J. Curran, Revisiting the kinetics and thermodynamics of the low-temperature oxidation pathways of alkanes: a case study of the three pentane isomers, *The Journal of Physical Chemistry A* 119 (2015) 7510-7527.
- [42] H.J. Curran, Developing detailed chemical kinetic mechanisms for fuel combustion, *Proceedings of the Combustion Institute* 37 (2019) 57-81.
- [43] I.A. Awan, D.R. Burgess, Jr., J.A. Manion, Pressure dependence and branching ratios in the decomposition of 1-pentyl radicals: shock tube experiments and master equation modeling, *J. Phys Chem. A* 116 (2012) 2895-2910.
- [44] J.A. Manion, I.A. Awan, Evaluated kinetics of terminal and non-terminal addition of hydrogen atoms to 1-alkenes: a shock tube study of H+ 1-butene, *J.Phys.Chem.A* 119 (2015) 429-441.
- [45] S. Peukert, P. Sela, D. Nativel, J. Herzler, M. Fikri, C. Schulz, Direct Measurement of High-Temperature Rate Constants of the Thermal Decomposition of Dimethoxymethane, a Shock Tube and Modeling Study, *J. Phys. Chem. A* 122 (2018) 7559-7571.
- [46] S. Peukert, P. Yatsenko, M. Fikri, C. Schulz, High-Temperature Rate Constants for the Reaction of Hydrogen Atoms with Tetramethoxysilane and Reactivity Analogies between Silanes and Oxygenated Hydrocarbons, *J. Phys. Chem. A* 122 (2018) 5289-5298.
- [47] A. Comandini, I.A. Awan, J.A. Manion, Thermal decomposition of 1-pentyl radicals at high pressures and temperatures, *Chem. Phys. Lett.* 552 (2012) 20-26.
- [48] J.A. Manion, I.A. Awan, The decomposition of 2-pentyl and 3-pentyl radicals, *Proc. Combust. Inst.* 34 (2013) 537-545.

# Chapter 2 : A Theoretical, Experimental and Modelling Study of the Reaction of Hydrogen Atoms with 1- and 2- Pentene

Published in: *J. Phys. Chem. A* 123(40) (2019) 8506–8526

Publication Date: September 10, 2019

DOI: <https://doi.org/10.1021/acs.jpca.9b06378>

## Author Contributions

- (1) Jennifer Power: Performed electronic structure calculations, modelling work and wrote the manuscript
- (2) Kieran P. Somers: Provided input for theoretical and modelling work. Reviewed the manuscript prior and post review process.
- (3) Chong-Wen Zhou: Reviewed the manuscript prior and post review process.
- (4) Sebastian Peukert: Performed hydrogen atomic resonance absorption spectroscopy experiments and reviewed the manuscript prior and post review process.
- (5) Henry J. Curran: Managed the project throughout and reviewed the manuscript prior and post review process.





## Abstract

Alkyl radicals are prominent in combustion chemistry as they are formed by hydrocarbon decomposition or from radical attack on hydrocarbons. Accurate determinations of the thermochemistry and kinetics of their unimolecular isomerisation and decomposition reactions and related addition reactions of alkenes are therefore important in simulating the combustion chemistry of virtually all hydrocarbon fuels. In this work, a comprehensive potential energy surface (PES) for  $\dot{\text{H}}$  atom addition to, and abstraction from 1- and 2-pentene, and the subsequent C–C and C–H  $\beta$ -scission reactions, and H-atom transfer reactions have been considered. Thermochemical values for the species on the  $\dot{\text{C}}_5\text{H}_{11}$  PES were calculated as a function of temperature (298 – 2000 K), with enthalpies of formation determined using a network of isodesmic reactions. High-pressure limiting and pressure-dependent rate constants were calculated using Rice-Ramsperger-Kassel-Marcus theory coupled with a one-dimensional master equation. As a validation of our theoretical results, hydrogen atomic resonance absorption spectrometry experiments were performed on the  $\dot{\text{H}}$  atom addition and abstraction reactions of 1- and 2-pentene. By incorporating our calculations into a detailed chemical kinetic model (AramcoMech 3.0), excellent agreement with these experiments is observed. The theoretical results are further validated via a comprehensive series of simulations of literature data. Our *a priori* model is found to reproduce important absolute species concentrations and product ratios reported therein.

## 1. Introduction

Alkenes are key components of hydrocarbon fuels and are formed as intermediates during the pyrolysis and oxidation of alkanes. Therefore, understanding their combustion chemistry will help in our understanding of hydrocarbon fuel combustion. Despite their importance, alkenes have not been as extensively studied as alkanes, in particular larger alkene species such as pentene, which is an important component of gasoline [1].

Based on previous studies of propene [2] and the butene isomers [3, 4] (1- and 2-butene and iso-butene), it was found that the reactions of  $\dot{\text{H}}$  atom addition to carbon–carbon double (C=C) bonds plays a significant role in controlling experimental high-temperature ignition delay times, flame speeds and species profiles measured as a function of temperature and/or time in jet-stirred and flow reactors.

**Table 2.1:** Summary of Experimental and Theoretical Studies Relevant to  $\dot{C}_5H_{11}$  Species.

Year	Author	Reactions	$T / K$	$p / kPa$	Method
2013	Manion et al.[5]	$\dot{H} + 2$ -pentene; decomposition of 2-pentyl and 3-pentyl radicals.	973–1121	120–800	Experiment/Theory SPST/(G3MP2B3, G3B3)
2012	Awan et al.[6]	decomposition of a 1-pentyl radical	880–1055	80–680	Experiment/Theory SPST/(G3MP2B3, G3B3)
2012	Comandini et al.[7]	decomposition of a 1-pentyl radical	833–1130	100–5000	Experiment/Theory SPST/(G3MP2B3, G3B3)
2012	Sirjean et al.[8]	H-atom transfer reactions for species ranging in size from pentyl to octyl radicals	500–2000	high pressure limit	Theory CBS-QB3
2011	Davis et al.[9]	H-atom migration across $n$ -alkyl radicals	200–2500	high pressure limit	Theory G2, G4,CBS-Q
2011	Yu et al.[10]	1–4 isomerization of a 1-pentyl radical	200–2400	high-pressure limit	Theory MS-VTST
2009	Zheng et al.[11]	H-atom transfer isomerisation of 1-pentyl and 1-hexyl radical.	200–2400	high pressure limit	Theory MCG3-MPW//M06-2X/MG3
2003	Jitariu et al.[12]	1,2, 1,3, 1,4, and 1,5 isomerisation, $\beta$ -scission and H-atom elimination reactions of pentyl radicals	400–2000	high pressure limit	Theory PUMP-SAC2/6-311G**//AM1
2002	Miyoshi et al.[13]	1-4 isomerisation of 1-pentyl radical	440–520	0.13–0.93	Experiment Laser photolysis-photoionisation mass spectrometry
1999	Yamauchi et al.[14]	unimolecular reactions of $C_3$ – $C_6$ alkyl radicals	900–1400	$\approx 101$	Experiment ST/ $\dot{H}$ -ARAS

Alkyl radicals are important intermediates in alkane pyrolysis/oxidation and can undergo unimolecular decomposition and isomerisation reactions. Unimolecular decomposition of the radical species results in the formation of lower molecular weight alkyl radicals and alkenes. For larger alkyl radicals, including pentyl radicals, H-atom isomerisation reactions are important, leading to many different branching possibilities in the reaction pathway [9]. These unimolecular decomposition reactions compete with bimolecular oxidation steps which lead to chain branching and are also responsible for endothermicity under some conditions [15]. However, at high temperatures alkyl radical lifetimes are so short that bimolecular reactions cannot compete, and unimolecular decomposition reactions dominate [6]. The fragmentation pattern of the parent radical determines both the way in which the species oxidises and also the formation of the product species [5]. Therefore, a knowledge of these decomposition mechanisms and quantitative predictions of the rate constants is essential in developing accurate combustion models.

There have been quite a number of experimental and theoretical studies on the unimolecular reactions of pentyl radicals, which are summarised in Table 2.1. Perhaps the most significant for the construction and validation of detailed chemical kinetic combustion models are a trio of studies from Manion et al. [5], Awan et al. [6], and Comandini et al. [7] which provide valuable data for the development and validation of theoretical combustion models.

The first study by Awan et al. [6] used 1-iodopentane as a source of pentyl radicals. Dilute mixtures of 1-iodopentane were thermally decomposed, with an excess of radical scavenger [1,3,5-trimethylbenzene (135TMB) and *m*-xylene]. Decomposition and H-atom transfer reactions of 1-pentyl radical were characterised in a single-pulse shock tube over temperature and pressure ranges of 880–1055 K and 80–680 kPa, respectively.

Gas chromatographic analysis with mass spectrometric and flame ionisation techniques were used to quantify the reaction products, with ethylene and propene identified as the dominant olefinic products, with secondary products such as (*E*)-2-pentene, (*Z*)-2-pentene and 1-butene accounting for less than 1% of olefin yield. A mechanism was postulated based on the measured products, with the ethylene/propene ratio determined largely by the kinetics of 1-pentyl  $\leftrightarrow$  ethylene + *n*-propyl relative to 1-pentyl  $\rightleftharpoons$  2-pentyl *via* a 5-member ring transition state.

As part of their work, an initial kinetic model was developed based on the G3MP2B3 determinations of the reactants and transition state properties. Partition functions and thermochemical values were derived using a rigid-rotor harmonic oscillator (RRHO) model

with the widely used modification for internal rotors. Statistical thermodynamics and Rice-Ramsperger-Kassel-Marcus RRKM / master equation (ME) analyses [16] were employed to compute the thermochemistry of minima, and to compute rate constants as a function of temperature and pressure. These theoretical results were then validated directly against their experimental results [6], via construction of a detailed chemical kinetic model.

To improve agreement with experimental results, Awan et al. [6] made alterations to their G3MP2B3-derived molecular properties. To derive rate constants, a combined analysis of their data and data from the literature was carried out [6]. The rate constant for the reaction 1-pentyl  $\leftrightarrow$  ethylene + *n*-propyl was determined based on three criteria, (i) on their G3MP2B3 calculations [6], (ii) the evaluation of direct experiments by Knyazev and Slagle [17] on the decomposition of butyl radicals, and (iii) existing theoretical and experimental data on alkyl radical addition reactions [18, 19]. For 2-pentyl  $\leftrightarrow$  propene + ethyl, their G3MP2B3 calculations were used together with (i) evaluated data from Knyazev and Slagle [17], (ii) data on the decomposition of secondary butyl radical by Knyazev and Tsang [20] and (iii) theoretical and experimental results on alkyl radical addition reactions [18, 19].

For 3-pentyl  $\leftrightarrow$  1-butene + methyl, their G3MP2B3 calculations were used in tandem with experimental data on 2-butyl decomposition [20, 21] and theoretical and experimental data on alkyl radical addition reactions [18, 19]. For 1-pentyl  $\rightleftharpoons$  2-pentyl, a combination of their G3MP2B3 calculations with a number of experimental and theoretical studies of the isomerisation of the 1-pentyl  $\rightleftharpoons$  2-pentyl reaction were used [8, 11-14, 22-27]. No experimental data was available for the 1-pentyl  $\rightleftharpoons$  3-pentyl reaction; thus, to derive a rate constant, their G3MP2B3 calculations were used in tandem with the work of Hayes et al. [28], who calculated barriers for H-atom transfer reactions for a range of alkyl, allylic and oxo-allylic radicals.

Other changes to the potential energy surface (PES) were made by altering the energies of the transition states (TSs) by adjusting the lowest vibrational frequency in the TSs to alter the pre-exponential parameters, with some changes made to enthalpies of formation for key species as described in Table AS8 of Appendix A. Energy barriers were kept within 6 kJ mol<sup>-1</sup> of the original unadjusted values and pre-exponential factors were kept within a factor of 2.5 of the original values, which is in line with the uncertainties of the G3MP2B3 method. This best-fit model optimised against their shock-tube data was then used to calculate rate constants over temperature and pressure ranges of 700 – 1900 K and 10<sup>1</sup> – 10<sup>5</sup> kPa, respectively.

A companion study by Comandini et al. [7] on the thermal decomposition of 1-pentyl radicals provided new experimental data from pressures of 80 – 5000 kPa, and temperatures of 833 – 1130 K. This work also used 1-iodopentane to generate the radicals of interest but removed all inhibitors from the initial mixtures, to ensure that all olefinic products were derived from the starting substrate, and the results confirm that there is no significant alteration of the ethylene/propene ratio due to the absence of an inhibitor. The theoretically derived model of Awan et al. [6] gave good agreement with the new experimental data [7].

Manion et al. [5] subsequently studied the isomerisation and decomposition reactions of 2-pentyl and 3-pentyl radicals in a single-pulse shock tube over the temperature and pressure ranges of 973 – 1121 K and 120 – 800 kPa, respectively. This was the first direct study of the olefin branching ratio resulting from the competitive kinetics of isomerisation and C–C  $\beta$ -scission for secondary straight chain alkyl radicals at high temperatures. A small amount of precursor, hexamethylethane (HME) was used to thermally generate  $\dot{\text{H}}$ -atoms in the presence of excess (*E*)-2-pentene, resulting in the formation of the radicals of interest by the addition of a  $\dot{\text{H}}$ -atom to the double bond. The stable products, ethylene, propene and 1-butene were detected using the same procedure as Awan et al. [6], and predictions made by the best-fit model [6] were found to be in good agreement with experiment [5].

Other recent experimental studies of note include the works of Yamauchi et al. [14] and Miyoshi et al. [13]. Yamauchi et al. [14] studied the thermal decomposition of a range of  $\dot{\text{C}}_3$  –  $\dot{\text{C}}_6$  alkyl radicals using a shock-tube coupled to a hydrogen atomic resonance absorption spectrometry ( $\dot{\text{H}}$ -ARAS) detection system. A series of alkyl iodides were used to generate the alkyl radical of interest, and the hydrogen atoms generated from the thermal decomposition of these alkyl radicals were quantified as a function of time for temperatures of 900 – 1400 K. High-pressure limiting rate constants for the unimolecular decomposition and isomerisation of 1-pentyl and 2-pentyl radical were derived via RRKM/ME modelling of their experiments and literature data.

Miyoshi et al. [13] studied the unimolecular isomerisation reaction of 1-pentyl to 2-pentyl radical using laser photolysis photoionisation mass spectrometry over the temperature and pressure ranges of 440 – 520 K and 1 – 7 Torr, respectively, in He bath gas. The photolysis of 1-chloropentane was used to produce the 1-pentyl radical, which then isomerised to 2-pentyl radical. The 2-pentyl radical was then photo-ionised and detected based on its lower ionisation potential relative to 1-pentyl radical. The experimental rate constants were found to be both temperature and pressure-dependent and an RRKM/ME

analysis fitted to the experimental data allowed a high-pressure limiting rate constant to be derived.

Other than the above experimental works, there have been many purely theoretical works [8-12, 29], which have studied the unimolecular decomposition and isomerisation reactions of pentyl radicals. Unlike the work of Manion et al. [5], Awan et al.[6], and Comandini and co-workers [5-7], the provision of a validated and comprehensive set of temperature- and pressure-dependent rate constants for use in combustion modelling was not the aim of any of these studies. Rather, these studies [8-12, 29] tend to focus on the influence of various theoretical approximations on computed high-pressure limiting rate constants, such as the influence of electronic structure method, tunnelling models, multi-structural torsional anharmonicity, and variational effects. A full series of comparisons of our computed rate constants with relevant literature studies [8-12, 29] are provided in Figure AS2 of Appendix A.

**Table 2.2:** List of Reaction Channels Considered in This Work.

Reaction number	Reaction channel
R1	$1\text{-C}_5\text{H}_{10} + \dot{\text{H}} \leftrightarrow \dot{\text{C}}_5\text{H}_9\text{1-1} + \text{H}_2$
R2	$1\text{-C}_5\text{H}_{10} + \dot{\text{H}} \leftrightarrow \dot{\text{C}}_5\text{H}_9\text{1-2} + \text{H}_2$
R3	$1\text{-C}_5\text{H}_{10} + \dot{\text{H}} \leftrightarrow \dot{\text{C}}_5\text{H}_9\text{1-3} + \text{H}_2$
R4	$1\text{-C}_5\text{H}_{10} + \dot{\text{H}} \leftrightarrow \dot{\text{C}}_5\text{H}_9\text{1-4} + \text{H}_2$
R5	$1\text{-C}_5\text{H}_{10} + \dot{\text{H}} \leftrightarrow \dot{\text{C}}_5\text{H}_9\text{1-5} + \text{H}_2$
R6	$(E)\text{-2-C}_5\text{H}_{10} + \dot{\text{H}} \leftrightarrow \dot{\text{C}}_5\text{H}_9\text{2-1} + \text{H}_2$
R7	$(E)\text{-2-C}_5\text{H}_{10} + \dot{\text{H}} \leftrightarrow \dot{\text{C}}_5\text{H}_9\text{2-2} + \text{H}_2$
R8	$(E)\text{-2-C}_5\text{H}_{10} + \dot{\text{H}} \leftrightarrow \dot{\text{C}}_5\text{H}_9\text{2-3} + \text{H}_2$
R9	$(E)\text{-2-C}_5\text{H}_{10} + \dot{\text{H}} \leftrightarrow \dot{\text{C}}_5\text{H}_9\text{2-4} + \text{H}_2$
R10	$(E)\text{-2-C}_5\text{H}_{10} + \dot{\text{H}} \leftrightarrow \dot{\text{C}}_5\text{H}_9\text{2-5} + \text{H}_2$
R11	$1\text{-C}_5\text{H}_{10} + \dot{\text{H}} \leftrightarrow \dot{\text{C}}_5\text{H}_{11}\text{-1}$
R12	$1\text{-C}_5\text{H}_{10} + \dot{\text{H}} \leftrightarrow \dot{\text{C}}_5\text{H}_{11}\text{-2}$
R13	$\dot{\text{C}}_5\text{H}_{11}\text{-2} \leftrightarrow (E)\text{-2-C}_5\text{H}_{10} + \dot{\text{H}}$
R14	$\dot{\text{C}}_5\text{H}_{11}\text{-3} \leftrightarrow (E)\text{-2-C}_5\text{H}_{10} + \dot{\text{H}}$
R15	$\dot{\text{C}}_5\text{H}_{11}\text{-1} \leftrightarrow \text{C}_2\text{H}_4 + \dot{\text{C}}_3\text{H}_7$
R16	$\dot{\text{C}}_5\text{H}_{11}\text{-2} \leftrightarrow \text{C}_3\text{H}_6 + \dot{\text{C}}_2\text{H}_5$
R17	$\dot{\text{C}}_5\text{H}_{11}\text{-3} \leftrightarrow \dot{\text{C}}_4\text{H}_8\text{-1} + \dot{\text{C}}\text{H}_3$
R18	$\dot{\text{C}}_5\text{H}_{11}\text{-1} \rightleftharpoons \dot{\text{C}}_5\text{H}_{11}\text{-2}$

R19	$\dot{\text{C}}_5\text{H}_{11-1} \rightleftharpoons \dot{\text{C}}_5\text{H}_{11-3}$
R20	$\dot{\text{C}}_5\text{H}_{11-2} \rightleftharpoons \dot{\text{C}}_5\text{H}_{11-3}$

The aims of the current work parallel those of Manion et al., Awan et al., and Comandini et al. [5-7]. The first is to revisit the kinetics and thermodynamics of the pentyl radical decompositions to construct an RRKM/ME model for the complete list of relevant reactions (Table 2.2) within a single theoretical framework. Despite the large number of studies in the literature of relevance to pentyl radicals, this work is the first to provide a complete set of temperature- and pressure-dependent rate constants for all well-to-well, bimolecular product-to-well, and bimolecular-to-bimolecular reactions, including formally direct well-skipping reactions. The second aim of this work is to study the abstraction reactions of hydrogen atom with 1- and 2-pentene, which have not been considered in past works. Here, we show through a combination of theory and experiment that they are non-negligible in the high-temperature pyrolysis of 1- and 2-pentene. Our results are subsequently incorporated into a detailed chemical kinetic model [30] and validated against experimental data by Manion, Awan, Comandini and co-workers [5-7], Yamauchi et al. [14], and Miyoshi et al. [13], together with new hydrogen atomic resonance absorption spectrometry experiments from this work.

## 2. Computational Details

### 2.1. Electronic Structure Calculations

All electronic structure calculations were performed using Gaussian 09 [31] and Gaussian 16 [32]. As many of the species have multiple equilibrium geometries, conformational searches were carried out to obtain the minimum energy structure of all PES minima and saddle points. Each stationary point was initially optimised using  $\omega\text{B97X-D}$  [33]/aug-cc-pVTZ [34] level of theory to ensure the entire PES could be studied using a single method. These were then used as input for a conformer sampling routine, where the dihedral angles of each non-methyl internal rotational group were assigned a value between  $-180^\circ$  and  $+180^\circ$ .

For each well, a minimum of 23 samples were generated for species with one non-methyl rotor, a minimum of 29 samples for species with two non-methyl rotors, and a minimum of 50 samples for species with three non-methyl rotors. For transition states, a minimum of 60 samples were generated for each structure. In total, approximately 1600 geometries were generated for the  $\text{C}_5$  PES of interest, which were then used as input for a geometry optimisation and frequency analysis with modest basis sets ( $\omega\text{B97X-D}$  [33]/6-31+G(D) for



wells,  $\omega$ B97X-D [33]/6-31G(D) for transition states). The zero-point-vibrational-energy-corrected electronic energy was computed for each conformer, and the conformer with the lowest zero-point-vibrational-energy-corrected electronic energy was taken as being the global minimum. The resulting lowest energy conformer were optimised using the  $\omega$ B97X-D [33]/aug-cc-pVTZ method [34], with harmonic frequency analyses simultaneously carried out to verify the nature of each stationary point, with a single imaginary frequency indicative of a transition state structure.

Low frequency torsional modes were treated separately from vibrational modes, via relaxed PES scans carried out with a ten degree increment with the  $\omega$ B97X-D [33]/6-311++G(d,p) method. The potential energies as a function of dihedral angle were then used as input for a one-dimensional (1-D) hindered rotor approximation as implemented in the Master Equation System Solver (MESS solver) [35].

To refine the computed barrier heights, single point energies for minima and transition states were calculated at the CCSD(T)/cc-pVXZ (where X = D and T) and MP2/cc-pVXZ (where X = D, T and Q) levels of theory. The resulting energies were extrapolated to the complete basis set limit using the following formula [36]

$$E_{\text{CCSD(T)/CBS}} = E_{\text{CCSD(T)/cc-pVTZ}} + (E_{\text{CCSD(T)/cc-pVTZ}} - E_{\text{CCSD(T)/cc-pVDZ}}) (3^4 / 4^4 - 3^4) + E_{\text{MP2/cc-pVQZ}} + (E_{\text{MP2/cc-pVQZ}} - E_{\text{MP2/cc-pVTZ}}) (4^4 / 5^4 - 4^4) - E_{\text{MP2/cc-pVTZ}} - (E_{\text{MP2/cc-pVTZ}} - E_{\text{MP2/cc-pVDZ}}) (3^4 / 4^4 - 3^4). \quad (1)$$

An initial model was constructed based on these results, and higher level RO-aug-cc-pVXZ SPEs were carried out for reactions which were found to be important on the  $\dot{\text{C}}_5\text{H}_{11}$  PES. These reactions included; R3, R6, R9, R11–20. The energies were extrapolated using the formula:

$$E_{\text{ROCCSD(T)/CBS}} = E_{\text{ROCCSD(T)/aug-cc-pVTZ}} + (E_{\text{ROCCSD(T)/aug-cc-pVTZ}} - E_{\text{ROCCSD(T)/aug-cc-pVDZ}}) (3^4 / 4^4 - 3^4) + E_{\text{ROMP2/aug-cc-pVQZ}} + (E_{\text{ROMP2/aug-cc-pVQZ}} - E_{\text{ROMP2/aug-cc-pVTZ}}) (4^4 / 5^4 - 4^4) - E_{\text{ROMP2/aug-cc-pVTZ}} - (E_{\text{ROMP2/aug-cc-pVTZ}} - E_{\text{ROMP2/aug-cc-pVDZ}}) (3^4 / 4^4 - 3^4). \quad (2)$$

The T1 diagnostic [37] for all minima and transition state species is  $\leq 0.025$ , indicating that single reference methods to describe the wave function are appropriate [36].

## 2.2. Thermochemistry

**Table 2.3:** Formation Enthalpies and Uncertainties ( $2\sigma$ ) Computed via Isodesmic and Atomisation Methods, Together with ATcT, ANL0 and ANL1 Formation Enthalpies and Uncertainties.

Species	Isodesmic (0K, kJ/mol)	Isodesmic ( $2\sigma$ )	Atomisation (0K, kJ/mol)	Atomisation ( $2\sigma$ )	ATcT (0K, kJ/mol)	ATcT (298.15K, kJ/mol)	ATcT ( $2\sigma$ )	ANL0	ANL1
C <sub>2</sub> H <sub>6</sub>	-69.48	2.65	-69.44	7.67	-68.33	-83.96	0.13	-68.90	-69.00
C <sub>2</sub> H <sub>4</sub>	60.54	0.45	61.36	3.85	60.91	52.39	0.12	60.20	60.20
$\dot{C}_2H_5$	131.66	0.76	131.40	6.65	130.94	119.87	0.28	131.30	131.00
$\dot{C}_2H_3$	303.37	0.97	301.26	5.41	301.14	296.94	0.34	300.90	300.50
C <sub>3</sub> H <sub>8</sub>	-82.75	0.18	-83.53	11.12	-82.74	-105.03	0.19	-83.20	-
C <sub>3</sub> H <sub>6</sub>	35.02	0.36	35.85	7.33	34.98	19.98	0.21	34.50	-
$\dot{C}_3H_7-1$	117.68	0.65	118.15	9.75	118.27	100.87	0.60	118.20	-
$\dot{C}_3H_7-2$	105.17	0.92	105.71	9.63	105.05	88.18	0.56	105.10	-
$\dot{C}_3H_5-1(\text{Cis})$	277.79	0.87	278.38	7.53	277.99	267.20	0.79	278.40	-
$\dot{C}_3H_5-1(\text{Trans})$	279.72	0.68	280.30	7.20	280.03	269.22	0.81	-	-
$\dot{C}_3H_5-2$	262.22	0.95	262.80	6.86	262.81	252.46	0.78	263.00	-
$\dot{C}_3H_5-3$	178.15	1.32	179.03	6.69	179.54	167.82	0.55	179.60	-
C <sub>4</sub> H <sub>10</sub>	-98.24	0.24	-98.68	14.36	-98.65	-125.96	0.26	-98.80	-
C <sub>4</sub> H <sub>8</sub> -1	21.14	0.20	22.40	10.66	20.86	-0.09	0.38	21.30	-
C <sub>4</sub> H <sub>8</sub> -2-E	9.40	0.25	10.63	10.86	9.24	-11.32	0.41	9.60	-
C <sub>4</sub> H <sub>8</sub> -2-Z	14.68	0.40	15.91	11.07	13.93	-7.34	0.42	-	-
$\dot{C}_4H_9-1$	102.04	0.78	102.04	13.08	102.52	80.02	0.72	103.20	-
$\dot{C}_4H_9-2$	90.43	0.74	91.55	12.82	90.19	65.42	0.98	90.90	-
$\dot{C}_4H_7-1$	263.30	0.90	263.97	10.27	-	-	-	-	-
$\dot{C}_4H_7-2$	248.39	0.94	249.16	9.84	-	-	-	-	-
$\dot{C}_4H_7-3$	152.21	0.82	152.04	9.48	-	-	-	-	-
$\dot{C}_4H_7-4$	222.68	0.78	224.34	12.26	-	-	-	-	-
C <sub>5</sub> H <sub>10</sub> -1	5.29	0.25	7.08	14.01	-	-	-	-	-
C <sub>5</sub> H <sub>10</sub> -2	-5.07	0.29	-3.43	14.31	-	-	-	-	-
$\dot{C}_5H_{11}-1$	86.45	0.76	86.95	16.40	-	-	-	-	-
$\dot{C}_5H_{11}-2$	73.99	0.77	75.86	16.21	-	-	-	-	-
$\dot{C}_5H_{11}-3$	75.40	0.71	77.27	16.04	-	-	-	-	-
$\dot{C}_5H_9-1-1$	247.57	0.76	248.19	13.53	-	-	-	-	-
$\dot{C}_5H_9-1-2$	231.91	0.77	233.06	13.02	-	-	-	-	-
$\dot{C}_5H_9-1-3$	137.77	0.81	138.02	12.77	-	-	-	-	-
$\dot{C}_5H_9-1-4$	193.95	0.59	196.13	14.78	-	-	-	-	-
$\dot{C}_5H_9-1-5$	205.46	0.83	207.68	14.83	-	-	-	-	-
$\dot{C}_5H_9-2-1$	137.60	1.18	138.02	12.77	-	-	-	-	-
$\dot{C}_5H_9-2-2$	224.62	1.28	225.54	13.24	-	-	-	-	-
$\dot{C}_5H_9-2-3$	225.18	1.33	226.39	13.29	-	-	-	-	-
$\dot{C}_5H_9-2-4$	125.86	0.83	126.10	12.75	-	-	-	-	-
$\dot{C}_5H_9-2-5$	194.40	2.39	196.70	15.69	-	-	-	-	-

Table 2.3 presents formation enthalpies and uncertainties ( $2\sigma$ ) computed *via* isodesmic and atomisation methods, together with ATcT [38, 39], ANL0 [40] and ANL1 [40] formation enthalpies and uncertainties ( $2\sigma$ ). For the species  $\dot{C}_4H_7$ -1,  $\dot{C}_4H_7$ -2,  $\dot{C}_4H_7$ -3,  $\dot{C}_4H_7$ -4 and all  $C_5$  species, ATcT, ANL0 and ANL1 formation enthalpy values do not exist. Quantum chemical composite methods (CBS–QB3, CBS–APNO, G3 and G4) [41-43] were therefore used to calculate formation enthalpies at 0 K via a network of isodesmic reactions suitable for each species, using ATcT values for the molecular and radical chaperones.

Formation enthalpies at 0 K for the 18  $C_2$ – $C_4$  species, for which ATcT values exist were calculated initially via the isodesmic approach in order to verify our method and confirm the ATcT results. A systematic and hierarchical approach was taken, where  $C_2$  species were used as chaperones for  $C_3$  species, and  $C_2$  and  $C_3$  species for  $C_4$  species, etc. These calculated values were then compared with ATcT, ANL0 and ANL1.

Excellent agreement is observed, with differences, defined as the mean absolute error (MAE), between ATcT and this work being on average  $0.56 \pm 1.08$  kJ mol<sup>-1</sup>. Differences between this work and ANL0 are on average  $0.67 \pm 1.12$  kJ mol<sup>-1</sup>. The remaining 20 species were then calculated using ATcT values for the chaperones. In the case of the  $C_5$  radical species, formation enthalpies at 0 K for the four  $\dot{C}_4H_7$  radicals were first calculated using the isodesmic approach, and these were then used as chaperones in conjunction with ATcT values, to derive the  $C_5$  radical species isodesmic networks.

Comparisons between atomisation and isodesmic values obtained in this work were made and excellent agreement is observed, with a MAE of  $0.97 \pm 1.30$  kJ mol<sup>-1</sup>. However, although isodesmic and atomisation methods give similar nominal 0 K heats of formation, the isodesmic approach is often used to approach “chemical accuracy”, and our computed final heat of formation uncertainties for the isodesmic reactions are between 0.18–2.65 kJ mol<sup>-1</sup>.

Uncertainties in the enthalpies of formation of each species *via* the isodesmic approach were calculated using the methods described by Simmie et al. [44] The formation enthalpy of the target species  $x_j$ , for the isodesmic reaction  $j$  is computed with an associated uncertainty  $u_j$ . In this work  $u_j$  is given by,

$$u_j = \sqrt{\sum u_c^2 + u_r^2} \quad (3)$$

where  $u_c$  and  $u_r$  are the uncertainties in the heat of formation of the chaperone species and in the heat of reaction of the isodesmic reaction, respectively, and  $u_r$  is computed with  $2\sigma$  uncertainties of the four compound methods employed.

The final enthalpy [44] is calculated *via* a weighted grand mean,

$$\bar{x} = \sum (x_j/u_j^2)/\sum(1/u_j^2) \quad (4),$$

and the final uncertainty is given by

$$\bar{u} = 1/[\sum(1/u_j^2)]^{1/2} \quad (5)$$

Table 2.4 provides an example of how the enthalpy of formation at 0 K in  $\text{kJ mol}^{-1}$  was determined for  $\text{C}_5\text{H}_{10-1}$  using the isodesmic approach. Values in bold represent  $\Delta_f H_{0\text{K}}$  along with its  $2\sigma$  uncertainty for each isodesmic reaction and the final  $\Delta_f H_{0\text{K}}$  is given at the end of the isodesmic reaction list. Section A.4 of Appendix A provides a complete list of isodesmic reactions.

**Table 2.4:** Illustrative Isodesmic Reactions Used To Calculate the Formation Enthalpy of 1-Pentene.

(1)	Method	$\text{C}_5\text{H}_{10-1}$	+	$\text{CH}_4$	=	$\text{C}_2\text{H}_4$	+	$\text{C}_4\text{H}_{10}$	$\Delta_f H$
	CBS-QB3	14.95		-66.34		64.16		-92.45	23.09
	CBS-APNO	-2.08		-70.85		59.79		-108.94	23.78
	G3	7.19		-67.73		60.61		-97.76	23.39
	G4	8.24		-66.62		60.86		-95.58	23.67
	$\Delta_f H$	<b>5.33</b>		-66.56		60.91		-98.65	23.48
	$\pm 2\sigma$	<b>0.61</b>		0.06		0.12		0.26	0.53

(2)	Method	$\text{C}_5\text{H}_{10-1}$	+	$\text{CH}_4$	=	$\text{C}_3\text{H}_6$	+	$\text{C}_3\text{H}_8$	$\Delta_f H$
	CBS-QB3	14.95		-66.34		40.38		-78.90	12.87
	CBS-APNO	-2.08		-70.85		31.41		-91.50	12.84
	G3	7.19		-67.73		35.61		-82.89	13.27
	G4	8.24		-66.62		35.99		-80.84	13.53
	$\Delta_f H$	<b>5.66</b>		-66.56		34.98		-82.74	13.13
	$\pm 2\sigma$	<b>0.64</b>		0.06		0.21		0.19	0.58

(3)	Method	$\text{C}_5\text{H}_{10-1}$	+	$\text{CH}_4$	=	$\text{C}_4\text{H}_8-1$	+	$\text{C}_2\text{H}_6$	$\Delta_f H$
	CBS-QB3	14.95		-66.34		28.57		-66.40	13.56
	CBS-APNO	-2.08		-70.85		15.58		-74.94	13.57
	G3	7.19		-67.73		22.35		-69.08	13.81
	G4	8.24		-66.62		23.11		-67.32	14.17
	$\Delta_f H$	<b>5.31</b>		-66.56		20.86		-68.33	13.78
	$\pm 2\sigma$	<b>0.64</b>		0.06		0.38		0.13	0.50

(4)	Method	$\text{C}_5\text{H}_{10-1}$	+	$\text{C}_2\text{H}_6$	=	$\text{C}_3\text{H}_6$	+	$\text{C}_4\text{H}_{10}$	$\Delta_f H$
	CBS-QB3	14.95		-66.40		40.38		-92.45	-0.62
	CBS-APNO	-2.08		-74.94		31.41		-108.94	-0.51
	G3	7.19		-69.08		35.61		-97.76	-0.25
	G4	8.24		-67.32		35.99		-95.58	-0.51
	$\Delta_f H$	<b>5.14</b>		-68.33		34.98		-98.65	-0.48
	$\pm 2\sigma$	<b>0.45</b>		0.13		0.21		0.26	0.27

(5)	Method	C <sub>5</sub> H <sub>10</sub> -1	+	C <sub>2</sub> H <sub>6</sub>	=	C <sub>4</sub> H <sub>8</sub> -1	+	C <sub>3</sub> H <sub>8</sub>	$\Delta_f H$
	CBS-QB3	14.95		-66.40		28.57		-78.90	1.13
	CBS-APNO	-2.08		-74.94		15.58		-91.50	1.09
	G3	7.19		-69.08		22.35		-82.89	1.36
	G4	8.24		-67.32		23.11		-80.84	1.36
	$\Delta_f H$	<b>5.21</b>		-68.33		20.86		-82.74	1.23
	$\pm 2\sigma$	<b>0.50</b>		0.13		0.38		0.19	0.25
$\Delta_f H_{0K} = 5.29 \pm 0.25$									

As these isodesmic reactions are based on ATcT values for the heat of formation of each chaperone, the final value is dependent on the uncertainties of these chaperones and on the enthalpy of reactions, both of which are less than 2 kJ mol<sup>-1</sup> for the reactions we utilise. Temperature-dependent enthalpies, entropies and heat capacities were then calculated using traditional statistical thermodynamics methods as implemented in MESSPF [35], with Chemkin format NASA polynomials fitted using PAC99 [45]. The fitted polynomials are provided in the Supporting Information.

### 2.3. Transition State Theory (TST), Rice Ramsperger-Kassel-Marcus (RRKM) and Master Equation (ME) Calculations

High-pressure limiting and pressure-dependent rate constants were calculated using RRKM theory with master equation (ME) analysis using the Master Equation System Solver program, MESS [35].

Tunnelling was accounted for via an asymmetric Eckart model [46], as implemented in MESS [35], where parameters include the imaginary frequency, and the forward and reverse barrier heights. To model collisional energy transfer, the single-exponential down model was used, with the average energy transferred in a downward collision at a given temperature estimated as  $\langle \Delta E_{\text{down}}(T) \rangle = 202.5 \times (T/300)^{1.0} \text{ cm}^{-1}$  based on previously optimised values employed in studies of *sec*-butyl [20] and pentyl [5-7] radical decompositions.

Predictions of hydrogen atom profiles from this work were found to be insensitive to this parameter, with factor of two perturbations changing predictions by 1–3%. SI contains a comprehensive comparison of the effect of this parameter on the predictions of literature data, where factor of two perturbations were found to change predictions of absolute mole fractions by up to  $\approx 20\%$  for experiments where 1-pentyl radical decomposition controls product yields [6, 7]. For experiments where 2-pentene and hydrogen atom were the effective reactants [5], this parameter was again found to be insensitive. Lennard Jones parameters of  $\sigma = 4.04 \text{ \AA}$  and  $\varepsilon = 235 \text{ cm}^{-1}$  were estimated for the  $\dot{\text{C}}_5\text{H}_{11}$  radicals by analogy to C<sub>5</sub>H<sub>12</sub> [47], while  $\sigma = 3.462 \text{ \AA}$  and  $\varepsilon = 89 \text{ cm}^{-1}$  were used for Ar. Rate constants for all thermally and

chemically activated reactions were calculated over the temperature and pressure ranges 500 – 1500 K and 0.01 – 1000 atm for use in general modelling work, and 750 – 1150 K and 0.5 – 60 atm to specifically model current experiments and literature experiments [5-7]. These rate constants are fitted in PLOG format and are provided as Supporting Information.

## 2.4. Experimental Section

Temporal  $\dot{\text{H}}$ -atom profiles have been measured for  $\dot{\text{H}}$ -atom reaction with 1- and 2-pentene and have been simulated with a detailed kinetic model described subsequently.  $\dot{\text{H}}$ -atom concentrations were monitored behind reflected shock waves by applying the sensitive hydrogen atomic resonance absorption spectrometry ( $\dot{\text{H}}$ -ARAS) technique. The shock tube apparatus currently used and the method for gas mixture preparation were described previously [48, 49]. Dilute gas mixtures containing small amounts of ethyl iodide ( $\text{C}_2\text{H}_5\text{I}$ ) as the  $\dot{\text{H}}$  atom precursor, and excess 1-pentene and 2-pentene were prepared, using argon as the diluent.

**Table 2.5:** Experimental Mixture Composition (ppm, the Balance is Ar) for  $\dot{\text{H}}$ -ARAS Experiments Used To Study the Reactions of  $\dot{\text{H}}$  + 1- and 2-Pentene.

$\text{C}_2\text{H}_5\text{I}$	$\text{C}_5\text{H}_{10-1}$	$\text{C}_5\text{H}_{10-2}$	$p$ (atm)	$T / \text{K}$
0.34	0.00	8.49	~1.5	980 – 1055
0.35	8.90	0.00	~1.5	985 – 1046

Due to the high sensitivity of the  $\dot{\text{H}}$ -ARAS detection technique, even small uncertainties in the initial mole fractions of  $\text{C}_2\text{H}_5\text{I}$  can affect the simulated temporal  $\dot{\text{H}}$  atom concentration profiles. With reactant mole fractions below 0.5 ppm, previous  $\dot{\text{H}}$ -ARAS studies indicated mole fraction uncertainties to be within  $\pm 0.02$  ppm. The rise in  $\dot{\text{H}}$  atom concentration is based on the thermal decomposition of  $\text{C}_2\text{H}_5\text{I}$ , which is a well-characterised two channel process [50].

- $\text{C}_2\text{H}_5\text{I} \rightleftharpoons \dot{\text{C}}_2\text{H}_5 + \dot{\text{I}}$
- $\text{C}_2\text{H}_5\text{I} \rightleftharpoons \text{C}_2\text{H}_4 + \text{HI}$

The  $\dot{\text{H}}$ -atoms then react with the excess 1-pentene or 2-pentene through addition and abstraction reactions. The experiments cover a narrow temperature range as at temperatures around 1100 K, the thermal decomposition of 1- and 2-pentene starts to contribute to  $\dot{\text{H}}$  atom formation, and at lower temperatures there is a limit due to the slow decomposition of  $\text{C}_2\text{H}_5\text{I}$  ( $< 1000$  K). Table 2.5 outlines the mixture compositions studied in the experiments, with detailed conditions provided in Table AS1 of Appendix A.

## 2.5. Chemical Kinetic Modelling

An initial model was built by implementing our computed thermochemistry and rate constants into AramcoMech 3.0 [30], including higher level RO-aug-cc-pVXZ SPEs calculations for the reactions, R3, R6, R9, and R11–20, which were found to be important in predicting the available experimental data. In order to accurately model experiment, rate constants for a series of secondary reactions were also added to the mechanism.

Preliminary simulations showed that the  $\dot{\text{H}}$  atom yields were somewhat sensitive to pentene isomer unimolecular decomposition reactions, in particular, the reaction  $\text{C}_5\text{H}_{10-2} \leftrightarrow \text{C}_4\text{H}_7-13 + \dot{\text{C}}\text{H}_3$ . High pressure limiting rate constants were estimated for the recombination of the radical products, with the forward decomposition rate constants computed using the species thermochemistry, Table 2.6.

For  $\dot{\text{H}}$ -atom recombination reactions with alkyl, alkenyl and allylic radicals, rate constants of  $1 \times 10^{14} \text{ cm}^3 \text{ mol}^{-1} \text{ s}^{-1}$  were estimated by analogy to the recombination of  $\dot{\text{C}}\text{H}_3$  with  $\dot{\text{H}}$  atoms [30]. For the recombination of two carbon-centred radicals, a recombination rate constant of  $5 \times 10^{12} \text{ cm}^3 \text{ mol}^{-1} \text{ s}^{-1}$  was employed by analogy to the high pressure limiting self-recombination reaction of allyl radicals [51]. To estimate fall-off effects for the decomposition reactions, quantum Rice-Ramsperger-Kassel (QRRK) theory with a modified strong collision (MSC) approximation was implemented via the ChemDis code [52, 53]. To carry out the QRRK/MSC calculations, estimates of vibrational frequencies for each well were derived from molecular heat capacities through methods described by Bozzelli et al. [54]. These were then fitted using the THERM [55] package. Ultimately, fall-off effects were found to have only a modest influence on predictions of the measured  $\dot{\text{H}}$ -atom yields under the current conditions.

There are few direct measurements or high-level theoretical calculations of the unimolecular decomposition rate constants of the pentene isomers from which all channel-specific temperature and pressure-dependent rate constants can be derived.

There exist a few recommendations for the total decomposition rate constants of 1-pentene [56-60]. The pyrolysis study of Tsang [57] is perhaps of most relevance, with the formation of  $\dot{\text{C}}_3\text{H}_5\text{-a}$  and  $\dot{\text{C}}_2\text{H}_5$  found to be the dominant process, with a concerted pathway forming propene and ethylene of secondary importance. Our estimated high-pressure limiting rate constant of  $3.75 \times 10^{19} T^{-1.13} \exp(-38347.3/T) \text{ s}^{-1}$  for the radical formation pathway is approximately a factor of 6–10 lower than that of Tsang in the temperature range 900–1200 K, and the use of their rate constants would imply radical recombination rate constants of the order of  $5 \times 10^{13} \text{ cm}^3 \text{ mol}^{-1} \text{ s}^{-1}$  based on the thermochemistry employed in AramcoMech 3.0

[30], which appears to be an upper limit for such a process. If one employs the thermochemistry for ethyl and allyl radicals published by Goldsmith et al. [36] and our estimated recombination rate constant, a decomposition rate constant of  $4.96 \times 10^{19} T^{-1.15} \exp(-37655.7/T) \text{ s}^{-1}$  results, which is within a factor of 3 – 4 of the Tsang recommendation. Our estimated decomposition rate constants are therefore dependent not only on the estimated recombination rate constants, but also the species thermochemistry.

Figure AS8 of Appendix A illustrates predicted  $\dot{\text{H}}$ -atom yields if the rate constants of Tsang [57] are implemented in our mechanism, with a systematic increase in predicted yields observed. Inclusion of the molecular elimination pathway forming ethylene and propene has virtually no influence on predictions of the experimental data herein.

**Table 2.6:** Estimated Rate Constants for Radical Recombination and Unimolecular Reactions Relevant to 1- and 2-Pentene Decompositions.<sup>a</sup>

Reaction	$A_r$	$n_r$	$E_{a,r}$	$A_{uni}$	$n_{uni}$	$E_{a,uni}$
$\dot{\text{H}} + \dot{\text{C}}_5\text{H}_9\text{1-1} \rightleftharpoons \text{C}_5\text{H}_{10}\text{-1}$	$1 \times 10^{14}$	0.0	0.0	$2.55 \times 10^{15}$	0.13	461.9
$\dot{\text{H}} + \dot{\text{C}}_5\text{H}_9\text{1-2} \rightleftharpoons \text{C}_5\text{H}_{10}\text{-1}$	$1 \times 10^{14}$	0.0	0.0	$6.49 \times 10^{15}$	0.04	447.3
$\dot{\text{H}} + \dot{\text{C}}_5\text{H}_9\text{1-3} \rightleftharpoons \text{C}_5\text{H}_{10}\text{-1}$	$1 \times 10^{14}$	0.0	0.0	$2.19 \times 10^{14}$	0.24	350.5
$\dot{\text{H}} + \dot{\text{C}}_5\text{H}_9\text{1-4} \rightleftharpoons \text{C}_5\text{H}_{10}\text{-1}$	$1 \times 10^{14}$	0.0	0.0	$2.20 \times 10^{17}$	-0.31	411.1
$\dot{\text{H}} + \dot{\text{C}}_5\text{H}_9\text{1-5} \rightleftharpoons \text{C}_5\text{H}_{10}\text{-1}$	$1 \times 10^{14}$	0.0	0.0	$7.90 \times 10^{15}$	0.17	421.5
$\dot{\text{C}}\text{H}_3 + \dot{\text{C}}_4\text{H}_7\text{1-4} \rightleftharpoons \text{C}_5\text{H}_{10}\text{-1}$	$5 \times 10^{12}$	0.0	0.0	$3.05 \times 10^{20}$	-1.16	374.3
$\dot{\text{C}}_3\text{H}_5\text{-a} + \dot{\text{C}}_2\text{H}_5 \rightleftharpoons \text{C}_5\text{H}_{10}\text{-1}$	$5 \times 10^{12}$	0.0	0.0	$3.75 \times 10^{19}$	-1.13	318.8
$\dot{\text{C}}_2\text{H}_3 + n\text{-}\dot{\text{C}}_3\text{H}_7 \rightleftharpoons \text{C}_5\text{H}_{10}\text{-1}$	$5 \times 10^{12}$	0.0	0.0	$3.86 \times 10^{21}$	-1.41	425.4
$\dot{\text{H}} + \dot{\text{C}}_5\text{H}_9\text{1-3} \rightleftharpoons \text{C}_5\text{H}_{10}\text{-2}$	$1 \times 10^{14}$	0.0	0.0	$5.24 \times 10^{13}$	0.52	361.2
$\dot{\text{H}} + \dot{\text{C}}_5\text{H}_9\text{2-2} \rightleftharpoons \text{C}_5\text{H}_{10}\text{-2}$	$1 \times 10^{14}$	0.0	0.0	$5.02 \times 10^{15}$	0.02	450.6
$\dot{\text{H}} + \dot{\text{C}}_5\text{H}_9\text{2-3} \rightleftharpoons \text{C}_5\text{H}_{10}\text{-2}$	$1 \times 10^{14}$	0.0	0.0	$5.21 \times 10^{15}$	0.02	451.5
$\dot{\text{H}} + \dot{\text{C}}_5\text{H}_9\text{2-4} \rightleftharpoons \text{C}_5\text{H}_{10}\text{-2}$	$1 \times 10^{14}$	0.0	0.0	$2.07 \times 10^{14}$	0.23	350.3
$\dot{\text{H}} + \dot{\text{C}}_5\text{H}_9\text{2-5} \rightleftharpoons \text{C}_5\text{H}_{10}\text{-2}$	$1 \times 10^{14}$	0.0	0.0	$1.15 \times 10^{16}$	0.14	422.4
$\dot{\text{C}}\text{H}_3 + \dot{\text{C}}_4\text{H}_7\text{1-1} \rightleftharpoons \text{C}_5\text{H}_{10}\text{-2}$	$5 \times 10^{12}$	0.0	0.0	$5.32 \times 10^{18}$	-0.70	425.8
$\dot{\text{C}}_3\text{H}_5\text{-s} + \dot{\text{C}}_2\text{H}_5 \rightleftharpoons \text{C}_5\text{H}_{10}\text{-2}$	$5 \times 10^{12}$	0.0	0.0	$5.96 \times 10^{20}$	-1.22	419.7
$\dot{\text{C}}\text{H}_3 + \dot{\text{C}}_4\text{H}_7\text{1-3} \rightleftharpoons \text{C}_5\text{H}_{10}\text{-2}$	$5 \times 10^{12}$	0.0	0.0	$7.56 \times 10^{17}$	-0.61	311.8

<sup>a</sup>  $A_r, n_r$  ( $\text{cm}^3 \text{ mol}^{-1} \text{ s}^{-1}$ ),  $A_{uni}, n_{uni}$  ( $\text{s}^{-1}$ ). Activation energies are in  $\text{kJ mol}^{-1}$ .

The  $\dot{\text{C}}_4\text{H}_7$  radical isomers formed from pentene isomer decomposition can ultimately form  $\text{C}_4\text{H}_6$  isomers +  $\dot{\text{H}}$ , and theoretically-derived pressure-dependent rate constants for  $\dot{\text{C}}_4\text{H}_7$  radical decomposition from Li et al. [61] were added to the mechanism.

Following  $\dot{\text{H}}$ -atom abstraction from 1- and 2-pentene, a range of  $\dot{\text{C}}_5\text{H}_9$  radicals are formed, whose unimolecular reactions can lead to a variety of saturated and unsaturated radicals and stable species, some of which are important products in the Manion et al. [5]



study (e.g. 1,3-butadiene). As part of a separate work [62], we have carried out a systematic study of the thermochemistry and kinetics of relevance to the 1,3-pentadiene (13-C<sub>5</sub>H<sub>8</sub>) + H potential energy surface using a similar methodology to that of the current work. A set of high-pressure limiting rate constants which account for the unimolecular decomposition and isomerisation reactions of C<sub>5</sub>H<sub>9</sub> radicals were included based on preliminary results.

In terms of other important alkyl radical/alkene chemistry within the mechanism, rate constants for the unimolecular decomposition of C<sub>2</sub>H<sub>5</sub> and C<sub>3</sub>H<sub>7</sub> radicals are based on the theoretical results of Miller and Klippenstein [63]. The high-pressure limiting rate constant for the decomposition of C<sub>2</sub>H<sub>5</sub> was previously modified by 30% as part of the development of AramcoMech 3.0. This optimisation is removed as part of the current work, although it has only a minor effect on the current results.

Rate constants for abstraction reactions of hydrogen atoms from alkyl and allylic sites in C<sub>5</sub>H<sub>10-1</sub> and C<sub>5</sub>H<sub>10-2</sub> by C<sub>2</sub>H<sub>5</sub> radical are pre-existent in the mechanism [3, 4, 30], and are based on the work of Tsang for propane [64] and propene [65] and these are left unchanged.

Thermochemistry and kinetics for radical initiators and scavengers were incorporated to appropriately model literature experiments. In order to simulate both the literature and current H-ARAS shock tube experiments, rate constants for pentyl iodide decomposition from Awan et al. [6], and ethyl iodide decomposition from Bentz et al. [50] were added to the mechanism. The experiments of Manion et al. used hexamethylethane (HME) as an initial source of hydrogen atoms, the latter being produced via the reaction sequence HME ↔ *t*-C<sub>4</sub>H<sub>9</sub> + *t*-C<sub>4</sub>H<sub>9</sub>, and *t*-C<sub>4</sub>H<sub>9</sub> ↔ *i*-C<sub>4</sub>H<sub>8</sub> + H. Thermochemistry for HME was calculated via group additivity, together with a rate constant of 10<sup>15.4</sup> exp(-31100/T) s<sup>-1</sup> for HME decomposition, as recommended by Manion et al. [5].

For the literature experiments from Awan et al. [6] and Manion et al. [5], 1,3-dimethylbenzene (13DMB) and/or 1,3,5-trimethylbenzene (135TMB) were added to mixtures to act as a radical scavenger, with initial simulations showing that exclusion of these species from the mechanism had a clear influence on the model predictions of species yields, in particular, for CH<sub>4</sub>/C<sub>2</sub>H<sub>6</sub>. We therefore include a skeletal aromatic mechanism which allows for the unimolecular decomposition of these species, including their abstraction reactions involving methyl radicals and hydrogen atoms, and the ipso-substitution reactions of 135TMB + H forming 13DMB + C<sub>2</sub>H<sub>5</sub>, and 13DMB + H forming C<sub>6</sub>H<sub>5</sub>CH<sub>3</sub> + C<sub>2</sub>H<sub>5</sub>. Initial thermochemistry and kinetics for 135TMB and 13DMB were sourced from the recent work of Liu et al. [66]. The kinetics for H-atom abstraction reactions by C<sub>2</sub>H<sub>5</sub> radicals from 135TMB and 13DMB were subsequently updated based on the theoretical results for the

reaction  $\text{C}_6\text{H}_5\text{CH}_3 + \dot{\text{C}}\text{H}_3$  [67], with appropriate corrections to rate constant  $A$ -factors for hydrogen atom degeneracy. Similarly, for the abstraction and addition reactions of  $\dot{\text{H}}$  atom with 135TMB and 13DMB, rate constants for the analogous pathways in  $\text{C}_6\text{H}_5\text{CH}_3$  were adopted based on the rate constants [68] in AramcoMech3.0, considering hydrogen atom degeneracy.

In order to interpret the shock-tube modelling results, rate-of-production and sensitivity analyses have been used to identify important reactions and rate constants. Sensitivity analyses for  $\dot{\text{H}}$  atom concentrations were carried out by individually increasing and decreasing  $A$ -factors for  $\approx 300$  reactions in the kinetic model by factors of two, with the perturbed model then used to simulate the specific experimental measurements of interest. The sensitivity coefficient for a given reaction,  $i$ , at a time,  $t$ , is given by

$$S_i(t) = \log_{10}([\dot{\text{H}}]_{k,2}/[\dot{\text{H}}]_{k/2}) \quad (6),$$

with positive sensitivity coefficients thus indicating reactions which increase  $\dot{\text{H}}$  atom yields, and vice versa for negative coefficients.

A similar series of analyses were carried out for literature experiments, where a broader range of stable alkane, alkene, and diene species were measured. A preliminary brute-force sensitivity analyses for  $\approx 350$  pyrolysis reactions relevant to the primary and secondary chemistry were carried out for various mixtures [5-7]. For each experimentally measured species (e.g.  $\text{CH}_4$ ,  $\text{C}_2\text{H}_6$ ,  $\text{C}_2\text{H}_4$ , etc.), a smaller subset of  $\approx 50$  reaction rate constants whose perturbation by a factor of  $\pm 2$  resulted in a minimum of 5% change in a measured species concentration were identified. For each experimental data point, brute-force sensitivity analyses were carried out for these 50 reactions by varying  $A$ -factors by factors of  $\pm 2$ , and computing the species mole fractions at the experimentally reported conditions of  $T_5$ ,  $p_5$ , residence time ( $\tau$ ), and mixture composition. The sensitivity of a given species concentration,  $\chi_j$ , to a given reaction,  $i$ , was computed *via*  $S_{i,j} = \log_{10}([\chi_j]_{k,2}/[\chi_j]_{k/2})$ . These sensitivity coefficients were also computed in cases where  $\chi_j$  was taken as the ratio of two species mole fractions, e.g. the ratio of ethylene to propene, and so reactions which are important in predicting both the absolute yield of a given species, and the ratio of two species yields, have been identified.

This analysis was repeated for every data point in every literature dataset, and the subsequent sensitivity coefficients for a given species in a given dataset were averaged to arrive at a mean sensitivity coefficient for the mixture. These mean sensitivity coefficients were found to be generally invariant to mixture composition and are reported in Supporting Information.

An important point to note is that the absolute yields of certain species in the literature experiments are rarely sensitive to the primary  $C_5H_{10} + \dot{H}$  or  $\dot{C}_5H_{11}$  chemistry alone. For instance, absolute  $CH_4$  and  $C_2H_6$  yields from the studies of Awan et al. [6] and Manion et al. [5] are sensitive to reactant decomposition reactions (e.g.  $C_5H_{11}I$ , HME,  $C_5H_{10-2}$ ), the reactions of  $\dot{C}H_3$  with radical scavengers/reactants, and the reactions  $\dot{C}H_3 + \dot{C}H_3 (+M) \leftrightarrow C_2H_6 (+M)$  and  $\dot{C}H_3 + \dot{H} (+M) \leftrightarrow CH_4 (+M)$ , which are not the direct focus of the present work.

Unlike Awan et al. and Manion et al. [5, 6], the Comandini et al. [7] experiments were carried out in the absence of radical scavenger, and simulations showed that one cannot predict absolute yields of their reactant, pentyl iodide, or  $CH_4$  and  $C_2H_6$ , without inclusion of some secondary bimolecular reactions to consume the pentyl iodide (e.g.  $C_5H_{11}I + \dot{C}H_3$  abstraction reactions), although the ethylene/propene ratios are insensitive to this chemistry. This caveat in mind, predictions of the current model are generally within a factor of two of all the absolute species concentrations and product ratios reported in the literature. Detailed simulations and sensitivity analysis for all literature species measurements are presented in separate SI documents.

All shock tube simulations were performed assuming a zero-dimensional, constrained-UV homogeneous batch reactor in Chemkin-Pro [69]. Initial fuel and bath gas concentrations,  $T_5$  and  $p_5$  and residence time, as provided in the literature supplementary material were used as the initial simulation conditions [5-7]. The model described above will be denoted as “this work” throughout and any alterations are specifically annotated.

### 3. Theoretical Results

#### 3.1. Thermochemistry

Table 2.7 compares the enthalpies of formation of  $C_5$  species computed in this work with literature data, with the 298 K values in generally good agreement [6, 70]. The Awan et al. [6] unadjusted values (model A) are within  $2.6 \pm 2.68 \text{ kJ mol}^{-1}$  of this work; however, these differences decrease to  $1.05 \pm 1.05 \text{ kJ mol}^{-1}$  if one compares with their best-fit model values.

The enthalpies of formation for the Awan et al. [6] unadjusted model are derived from atomisation energies and RRHO zero point energies. For 1-pentene, the best fit  $\Delta_f H_{298}$  value was derived using  $\Delta_f H_{(l)}$  [1-pentene 298 K] =  $-46.94 \pm 0.42 \text{ kJ mol}^{-1}$  from Wilberg et al. [71] and  $\Delta_{\text{vap}} H_{298\text{K}} = 25.47 \pm 0.1 \text{ kJ mol}^{-1}$  from Steel and Chirico. [72] For (*E*)-2-pentene, the best fit  $\Delta_f H_{298}$  value was derived by averaging the values of  $\Delta_f H_{(l)}$  [(*E*)-2-pentene 298 K] of –

$58.24 \pm 0.42 \text{ kJ mol}^{-1}$  and  $-57.98 \pm 0.76 \text{ kJ mol}^{-1}$  from Wilberg et al. [71] and Good and Smith [73], together with  $\Delta_{\text{vap}}H_{298 \text{ K}} 26.86 \pm 0.09 \text{ kJ mol}^{-1}$  from Steel and Chirico [72].

**Table 2.7:** Comparisons of the Formation Enthalpies Computed in This Work with Literature Data<sup>a</sup>.

Name	Formula	$\Delta_f H_{0\text{K}}$ this work Isodesmic	$\Delta_f H_{0\text{K}}$ this work Atomisation	$\Delta_f H_{298 \text{ K}}$ this work	$\Delta_f H_{0\text{K}}$ [1]	$\Delta_f H_{298\text{K}}$ [1]	$\Delta_f H_{298\text{K}}$ [2]	$\Delta_f H_{298\text{K}}$ [3]
1-pentene	C <sub>5</sub> H <sub>10</sub> -1	$5.29 \pm 0.25$	$7.08 \pm 14.01$	-20.57	4.20	-23.29	-21.50	-21.28
2-pentene	C <sub>5</sub> H <sub>10</sub> -2-E	$-5.07 \pm 0.29$	$-3.43 \pm 14.31$	-31.81	-5.10	-32.18	-31.25	-30.33
1-pentyl	$\dot{\text{C}}_5\text{H}_{11}$ -1	$86.45 \pm 0.76$	$86.95 \pm 16.40$	57.85	90.10	60.10	59.10	60.98
2-pentyl	$\dot{\text{C}}_5\text{H}_{11}$ -2	$73.99 \pm 0.77$	$75.86 \pm 16.21$	44.73	78.30	49.20	46.70	49.27
3-pentyl	$\dot{\text{C}}_5\text{H}_{11}$ -3	$75.40 \pm 0.71$	$77.27 \pm 16.04$	46.95	79.40	50.23	46.40	–
1-penten-1-yl	$\dot{\text{C}}_5\text{H}_9$ 1-1	$247.50 \pm 0.76$	$248.19 \pm 13.53$	224.93	–	–	–	–
1-penten-2-yl	$\dot{\text{C}}_5\text{H}_9$ 1-2	$231.91 \pm 0.77$	$233.06 \pm 13.02$	210.19	–	–	–	–
1-penten-3-yl	$\dot{\text{C}}_5\text{H}_9$ 1-3	$137.77 \pm 0.81$	$138.02 \pm 12.77$	114.31	–	–	–	–
1-penten-4-yl	$\dot{\text{C}}_5\text{H}_9$ 1-4	$193.95 \pm 0.59$	$196.13 \pm 14.78$	172.21	–	–	–	–
1-penten-5-yl	$\dot{\text{C}}_5\text{H}_9$ 1-5	$205.46 \pm 0.83$	$207.68 \pm 14.83$	184.58	–	–	–	–
2-penten-2-yl	$\dot{\text{C}}_5\text{H}_9$ 2-2	$224.62 \pm 1.28$	$225.54 \pm 13.24$	202.19	–	–	–	–
2-penten-3-yl	$\dot{\text{C}}_5\text{H}_9$ 2-3	$225.18 \pm 1.33$	$226.39 \pm 13.29$	203.09	–	–	–	–
2-penten-4-yl	$\dot{\text{C}}_5\text{H}_9$ 2-4	$125.86 \pm 0.83$	$126.10 \pm 12.75$	102.83	–	–	–	–
2-penten-5-yl	$\dot{\text{C}}_5\text{H}_9$ 2-5	$194.40 \pm 2.39$	$196.70 \pm 15.69$	172.74	–	–	–	–

<sup>a</sup>Units: Enthalpies of Formation ( $\text{kJ mol}^{-1}$ ); [1] Awan Model A (G3MP2B3) [6], [2] Awan best-fit model [6], [3] Burcat [70].

The enthalpy of formation at 298 K for 1-pentyl radical was derived using  $\Delta_f H_{(\text{g},298)} [n\text{-pentane}] = -146.8 \pm 0.59 \text{ kJ mol}^{-1}$  from Good [74], and a C–H bond dissociation energy (BDE) of  $423.8 \text{ kJ mol}^{-1}$ . For 2-pentyl radical and 3-pentyl radical, enthalpies of formation at 298 K were derived in the same way as 1-pentyl radical, but using C–H BDEs of 411.5 for 2-pentyl and 411.2  $\text{kJ mol}^{-1}$  for 3-pentyl radical. If one employs the enthalpies of formation values for the three pentyl radicals calculated in this work, along with  $\Delta_f H_{(\text{g})} [n\text{-pentane}(\text{g}) 298 \text{ K}] = -146.8 \pm 0.59 \text{ kJ mol}^{-1}$  from Good [74], BDEs of 422.65, 409.53 and 411.75  $\text{kJ mol}^{-1}$  for 1-pentyl, 2-pentyl and 3-pentyl radical result, which are within  $1.22 \pm 1.43 \text{ kJ mol}^{-1}$  of Awan et al. [6] Differences between this work and Burcat [70] enthalpies of formation are within  $2.46 \pm 2.96 \text{ kJ mol}^{-1}$ .

With the exception of 1-pentene, for which the literature entropies and the result from this work are in good agreement, the differences in the entropies calculated in this work and published in the literature [6, 70] appear larger than those for the enthalpies (Table 2.8).

**Table 2.8:** Comparisons of Entropies Computed in This Work with Literature Data<sup>a</sup>.

Name	Formula	$S_{298\text{ K}}$ this work	$S_{298\text{ K}}$ [1]	$S_{298\text{ K}}$ [2]	$S_{298\text{ K}}$ [3]
1-pentene	C <sub>5</sub> H <sub>10</sub> -1	346.25	347.0	347.0	347.11
( <i>E</i> )-2-pentene	C <sub>5</sub> H <sub>10</sub> -2	342.76	343.2	343.2	370.09
1-pentyl	C <sub>5</sub> H <sub>11</sub> -1	373.44	370.8	370.8	367.17
2-pentyl	C <sub>5</sub> H <sub>11</sub> -2	379.52	375.4	375.4	363.67
3-pentyl	C <sub>5</sub> H <sub>11</sub> -3	380.89	372.7	372.7	–
1-penten-1-yl	C <sub>5</sub> H <sub>9</sub> 1-1	354.10	–	–	–
1-penten-2-yl	C <sub>5</sub> H <sub>9</sub> 1-2	357.37	–	–	–
1-penten-3-yl	C <sub>5</sub> H <sub>9</sub> 1-3	341.61	–	–	–
1-penten-4-yl	C <sub>5</sub> H <sub>9</sub> 1-4	367.53	–	–	–
1-penten-5-yl	C <sub>5</sub> H <sub>9</sub> 1-5	365.82	–	–	–
2-penten-2-yl	C <sub>5</sub> H <sub>9</sub> 2-2	350.23	–	–	–
2-penten-3-yl	C <sub>5</sub> H <sub>9</sub> 2-3	350.72	–	–	–
2-penten-4-yl	C <sub>5</sub> H <sub>9</sub> 2-4	337.28	–	–	–
2-penten-5-yl	C <sub>5</sub> H <sub>9</sub> 2-5	363.20	–	–	357.78

<sup>a</sup>Units: Entropies at 298 K (J K<sup>-1</sup> mol<sup>-1</sup>) [1] Awan Model A (G3MP2B3) [6], [2] Awan best-fit model [6], [3] Burcat [70].

Awan et al. [6] used the same entropy values in both model A (unadjusted results) and their best-fit model, indicating that no optimisation of their RRKM/ME input parameters took place with respect to species entropies. Our computed entropies are on average  $2.75 \pm 6.57$  J K<sup>-1</sup> mol<sup>-1</sup> larger than reported by Awan et al. When we compare our results to those recommended by Burcat, and excluding the 2-pentene entropy which appears to have an erroneous polynomial fit, the differences appear larger, and the present results tend to compare more favourably with the results of Awan et al. [6] than with the Burcat data [70].

Awan et al. [6] and Burcat [70] take a similar approach to the computation of their thermochemistry, and one which is not dissimilar to the current work. Geometries, external rotational constants, and vibrational frequencies are determined with the G3MP2B3 and G3B3 composite methods, respectively, and the translational, vibrational and rotational partition functions are computed with the usual statistical thermodynamics formulae with appropriate corrections for molecular symmetry and electronic level degeneracies.

In their work(s), an-harmonicity arising from torsional/internal rotational modes is accounted for using a 1-dimensional Pitzer-Gwinn [75] like treatment, where the potential energy is approximated *via* symmetric *n*-fold potentials of the form

$$V = 0.5V_{max}\{1 - \cos(n\varphi)\} \quad [14] \quad (7)$$

where *V* is the hindrance potential at angle  $\varphi$ ,  $V_{max}$  is the maximum barrier to rotation, and *n* is the number of minima along the potential. Further corrections are subsequently

employed to correct the hindered rotor partition function for symmetry, for example, the threefold symmetry of methyl rotations and two-fold symmetry of methylene radical ( $-\dot{\text{C}}\text{H}_2$ ) rotors.

To compute energy levels, and hence partition functions and thermochemistry, the moment of inertia, or rotational constant, for the internal rotation is also required, along with an appropriate method to solve the 1-D Schrödinger equation. To rationalise the differences shown in Table 2.8, we have carried out test calculations on the individual and combined effects of the rotational constants and potential energies used in the hindered rotor treatments of this work and Awan et al. [6]. These are described in detail in Appendix A, with most of the discrepancies accounted for through cumulative differences from the treatment of torsional modes.

In contrast, Table 2.9 compares heat capacities for the  $\text{C}_5$  species common to this work, the Awan et al. [6] study and the Burcat database [70]. The differences observed are on a par with those observed for the entropy results presented previously. The Awan et al. [6] heat capacities are greater than those of this work, with mean absolute differences of  $2.7 \pm 3.4 \text{ J mol}^{-1} \text{ K}^{-1}$  computed at 300 K, and  $4.3 \pm 1.5 \text{ J mol}^{-1} \text{ K}^{-1}$  at 1500 K. There are no systematic differences when the Burcat data are compared with the present work, but the mean absolute differences for the six common species are  $3.0 \pm 4.3 \text{ J mol}^{-1} \text{ K}^{-1}$  at 300 K and  $1.7 \pm 2.4 \text{ J mol}^{-1} \text{ K}^{-1}$  at 1500 K. A comparison of the Awan et al. [6] heat capacities with those of Burcat [70] for 1-pentene, 1-pentyl, and 2-pentyl shows that the Awan et al. [6] heat capacities are also systematically greater than those of Burcat at 300 K ( $1.8 \pm 1.3 \text{ J mol}^{-1} \text{ K}^{-1}$ ), and that this difference increases at 1500 K ( $4.4 \pm 1.8 \text{ J mol}^{-1} \text{ K}^{-1}$ ). A further comparison of their (*E*)-2-pentene heat capacities, keeping in mind that the Burcat polynomial may be erroneous, shows that Burcat's recommended heat capacities are 10.5 and 6.6  $\text{J mol}^{-1} \text{ K}^{-1}$  lower than the recommendations of Awan et al. at 300 K and 1500 K, respectively.

These differences in heat capacity can again be attributed in some part to different treatments of torsional an-harmonicity, but also, to differences in harmonic frequencies computed by the G3MP2B3 and G3B3 methods employed by Awan et al. and Burcat, both of which rely on a B3LYP optimisation and frequency analysis with the 6-31G(d) basis set. Some test calculations on the pentyl radicals imply that the application of a scale factor of 0.96–0.97 to our  $\omega\text{B97X-D/aug-cc-pvtz}$  results, which is typical of corrections to frequencies for DFT computations, would resolve the differences in vibrational heat capacities, although differences arising from their different approximations of the hindered rotor contributions would remain.

**Table 2.9:** Comparisons of the Heat Capacities Computed in This Work with Literature Data. Units: ( $\text{J K}^{-1} \text{mol}^{-1}$ ) [a] This work, [b] Burcat [70], [c] Awan et al. [6].

		$C_p$ 300	$C_p$ 400	$C_p$ 500	$C_p$ 600	$C_p$ 800	$C_p$ 1000	$C_p$ 1500
$\text{C}_5\text{H}_{10-1}$	[a]	109.55	135.63	160.85	183.31	217.61	244.22	285.39
	[b]	108.72	136.92	163.55	186.79	221.11	246.52	284.57
	[c]	109.75	140.60	167.39	190.22	225.47	251.22	289.93
$\text{C}_5\text{H}_{10-2-E}$	[a]	107.18	132.97	157.84	180.19	215.15	242.04	284.39
	[b]	101.04	125.87	151.59	175.36	212.32	240.45	281.17
	[c]	111.55	139.56	164.56	186.44	221.38	247.63	287.73
$\dot{\text{C}}_5\text{H}_{11-1}$	[a]	115.77	144.08	171.08	194.92	231.10	259.14	302.80
	[b]	115.17	144.01	171.30	195.41	232.29	260.65	303.74
	[c]	116.76	149.62	178.40	202.98	240.62	267.82	308.34
$\dot{\text{C}}_5\text{H}_{11-2}$	[a]	110.93	138.85	166.10	190.52	227.95	256.73	301.73
	[b]	112.37	139.59	166.67	191.26	229.46	258.84	303.05
	[c]	114.99	145.40	173.09	197.44	235.76	263.96	306.22
$\dot{\text{C}}_5\text{H}_{11-3}$	[a]	111.73	139.00	165.83	190.00	227.27	256.01	301.23
	[b]	115.53	145.65	172.74	196.48	234.11	262.21	304.94
$\dot{\text{C}}_5\text{H}_9-21$	[a]	103.20	129.52	154.07	175.45	207.40	231.71	269.62
	[b]	106.80	133.84	157.70	177.89	207.98	230.96	266.17
$\dot{\text{C}}_5\text{H}_9-25$	[a]	106.19	129.54	152.13	172.35	203.61	227.65	265.50
	[b]	111.44	136.11	158.37	177.67	207.52	230.48	265.95

As a final point on thermochemistry, we have compared our Gibbs free energies as a function of temperature to those of the best fit model of Awan et al. [6] to illustrate how the combined thermochemical effects influence chemical equilibria for the pentyl radicals (Figure AS5 of Appendix A). In the temperature range 300 – 2000 K, we find a maximum difference of  $\approx 7 \text{ J mol}^{-1} \text{ K}^{-1}$  in the Gibbs Free Energy for the 1-pentyl radical at 1000 K, and the worst-case changes in the chemical equilibria for an arbitrary chemical reaction involving any of the pentyl radicals amounts to a factor of 4.5 for the 1-pentyl radical at 300 K. In the temperature range 500 – 2000 K, changes in equilibrium constants, and hence, any rate constants involving pentyl radicals reliant on thermodynamic reversibility, would amount to a factor of approximately  $1.6 \pm 1.1$ , where uncertainties are  $2\sigma$ . In the case of the unimolecular reactions of pentyl radicals and reactions of  $\dot{\text{H}}$  atoms with the pentene isomers, we note that



these changes in thermochemistry are unlikely to significantly influence detailed chemical kinetic modelling predictions of the shock tube data we subsequently model.

### 3.2. Reactions of $\dot{\text{H}}$ with 1-pentene and 2-pentene

Both 1- and 2-pentene have seven plausible reactions with  $\dot{\text{H}}$  atoms (two addition reactions and five abstraction reactions), with 0 K barriers, reaction enthalpies and high-pressure limiting rate constants provided in Table 2.10. 1-pentene has both internal addition ( $\text{C}_2$ , R11), and terminal ( $\text{C}_1$ , R12) addition reactions producing 1-pentyl and 2-pentyl radical respectively. A barrier of  $15.2 \text{ kJ mol}^{-1}$  is computed for the former reaction, which is some  $7.4 \text{ kJ mol}^{-1}$  greater than the terminal addition barrier of  $7.8 \text{ kJ mol}^{-1}$ . The two internal  $\dot{\text{H}}$  atom addition reactions to 2-pentene, forming 2-pentyl radical and 3-pentyl radical, have similar barriers of  $10.9 \text{ (C}_3, \text{R13)}$  and  $11.4 \text{ kJ (C}_2, \text{R14) mol}^{-1}$  respectively.

These addition reaction barriers are found to be substantially lower than those for abstraction. In the case of 1-pentene, a barrier of  $21.9 \text{ kJ mol}^{-1}$  is computed for the abstraction of a secondary allylic hydrogen atom forming  $\dot{\text{C}}_5\text{H}_9\text{-13}$  (R3). The reaction of 2-pentene +  $\dot{\text{H}}$  atom can yield two resonantly stabilised allylic radicals upon abstraction from the primary allylic (R6,  $\dot{\text{C}}_5\text{H}_9\text{-13}$ ) and secondary allylic (R9,  $\dot{\text{C}}_5\text{H}_9\text{-24}$ ) sites, with respective barriers of  $28.94 \text{ kJ mol}^{-1}$  and  $20.96 \text{ kJ mol}^{-1}$  computed.

Figure 2.1 compares the computed high-pressure rate constants (Table 2.10) for the reactions of  $\dot{\text{H}}$  atom with 1- and 2-pentene, along with computed temperature- and pressure-dependent branching ratios for abstraction and addition processes. For both isomers, addition reactions dominate the reaction flux over the entirety of the temperature range as a result of their lower barriers. For 1-pentene, terminal addition is kinetically dominant, and for 2-pentene there is close to a 50:50 ratio between the two internal addition pathways. Abstraction reactions from the allylic sites become increasingly competitive as temperature increases, accounting for approximately 10, 20 and 40% of the branching ratio at 700, 1000 and 1500 K. Figure 2.2 show that the branching ratio between abstraction and addition pathways is effectively pressure-independent for both 1- and 2-pentene.

**Table 2.10:** Computed Energy Barriers, Heats of Reaction, and High-Pressure Limiting Rate Constant Fits for the Reactions of  $\dot{\text{H}}$  with 1- and 2-Pentene. Units ( $AT^n = \text{cm}^3 \text{mol}^{-1} \text{s}^{-1}$ , energies = kJ mol<sup>-1</sup>). R1 – R10 fit between 298 – 2000 K, R11 – R14 fit between 500 – 2000 K.

	Reaction	$\Delta^\ddagger H_{0\text{K}}$	$\Delta_r H_{0\text{K}}$	A	n	$E_a$
R1	$1\text{-C}_5\text{H}_{10} + \dot{\text{H}} \leftrightarrow \dot{\text{C}}_5\text{H}_9\text{1-1} + \text{H}_2$	64.50	27.24	$7.29 \times 10^5$	2.47	53.84
R2	$1\text{-C}_5\text{H}_{10} + \dot{\text{H}} \leftrightarrow \dot{\text{C}}_5\text{H}_9\text{1-2} + \text{H}_2$	51.89	12.53	$4.81 \times 10^6$	2.17	40.50
R3	$1\text{-C}_5\text{H}_{10} + \dot{\text{H}} \leftrightarrow \dot{\text{C}}_5\text{H}_9\text{1-3} + \text{H}_2$	21.89	-83.57	$4.53 \times 10^5$	2.49	10.39
R4	$1\text{-C}_5\text{H}_{10} + \dot{\text{H}} \leftrightarrow \dot{\text{C}}_5\text{H}_9\text{1-4} + \text{H}_2$	31.08	-25.88	$6.56 \times 10^5$	2.46	19.57
R5	$1\text{-C}_5\text{H}_{10} + \dot{\text{H}} \leftrightarrow \dot{\text{C}}_5\text{H}_9\text{1-5} + \text{H}_2$	40.86	-15.71	$5.52 \times 10^4$	2.81	28.38
R6	$(E)\text{-2-C}_5\text{H}_{10} + \dot{\text{H}} \leftrightarrow \dot{\text{C}}_5\text{H}_9\text{2-1} + \text{H}_2$	28.94	-73.24	$1.06 \times 10^4$	2.98	14.13
R7	$(E)\text{-2-C}_5\text{H}_{10} + \dot{\text{H}} \leftrightarrow \dot{\text{C}}_5\text{H}_9\text{2-2} + \text{H}_2$	53.73	15.70	$4.81 \times 10^5$	2.44	42.88
R8	$(E)\text{-2-C}_5\text{H}_{10} + \dot{\text{H}} \leftrightarrow \dot{\text{C}}_5\text{H}_9\text{2-3} + \text{H}_2$	53.50	16.52	$7.35 \times 10^5$	2.39	42.56
R9	$(E)\text{-2-C}_5\text{H}_{10} + \dot{\text{H}} \leftrightarrow \dot{\text{C}}_5\text{H}_9\text{2-4} + \text{H}_2$	20.96	-85.34	$5.47 \times 10^5$	2.47	11.47
R10	$(E)\text{-2-C}_5\text{H}_{10} + \dot{\text{H}} \leftrightarrow \dot{\text{C}}_5\text{H}_9\text{2-5} + \text{H}_2$	42.21	-14.89	$2.52 \times 10^5$	2.63	29.33
R11	$1\text{-C}_5\text{H}_{10} + \dot{\text{H}} \leftrightarrow \dot{\text{C}}_5\text{H}_{11}\text{-1}$	15.20	-136.98	$1.97 \times 10^8$	1.63	9.04
R12	$1\text{-C}_5\text{H}_{10} + \dot{\text{H}} \leftrightarrow \dot{\text{C}}_5\text{H}_{11}\text{-2}$	7.80	-148.16	$7.87 \times 10^8$	1.52	4.12
R13	$(E)\text{-2-C}_5\text{H}_{10} + \dot{\text{H}} \leftrightarrow \dot{\text{C}}_5\text{H}_{11}\text{-2}$	10.92	-137.83	$6.86 \times 10^8$	1.50	6.55
R14	$(E)\text{-2-C}_5\text{H}_{10} + \dot{\text{H}} \leftrightarrow \dot{\text{C}}_5\text{H}_{11}\text{-3}$	11.40	-136.73	$6.02 \times 10^8$	1.51	6.66

Figure 2.2 (a), (b) show the temperature- and pressure-dependencies of the product branching ratios for  $\dot{\text{H}}$  atom addition to 1- and 2-pentene in the temperature range 750 – 1500 K, and at pressure of 0.1, 1 and 10 atm, which is indicative of the conditions of the shock tube data simulated in subsequent sections.

For 1-pentene +  $\dot{\text{H}}$  atoms at 0.1 atm and 1 atm, the chemically activated formation of propene and ethyl radical accounts for 80% of the reaction flux across this temperature range, with direct chemically activated formation of ethylene and *n*-propyl radical accounting for 10–20%. At 10 atm, the importance of stabilisation increases, with formation of stabilised 2-pentyl and 1-pentyl radicals accounting for at least 50% of the reaction flux up to 1000 K.

For 2-pentene +  $\dot{\text{H}}$  atoms a similar situation prevails, with direct chemically activated formation of propene and ethyl radical, and 1-butene and methyl radical, being nearly equivalent under all conditions, and dominant at 0.1 and 1 atm. At 10 atm, stabilisation to form 2-pentyl and 3-pentyl radicals is dominant up to 1050 K, with chemically activated reactions governing the reaction flux at higher temperatures.

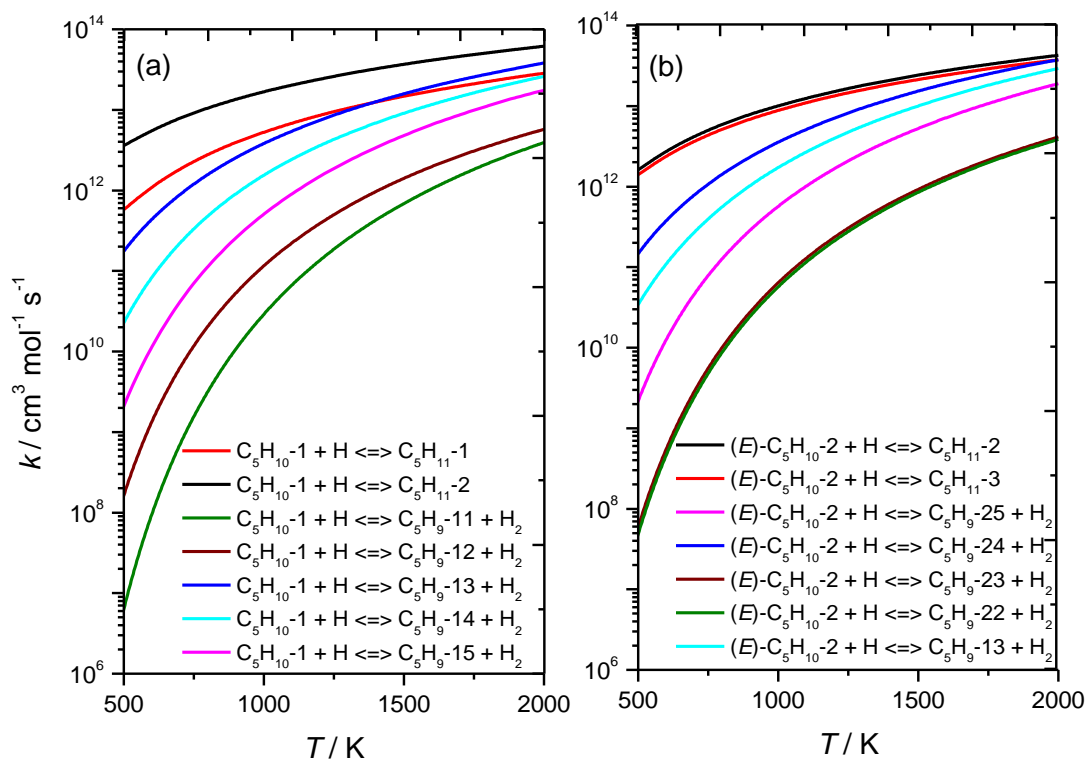


**Figure 2.1.** (Top) high-pressure limit rate constants for the reactions of (a) 1-pentene +  $\dot{\text{H}}$  and (b) 2-pentene +  $\dot{\text{H}}$ .

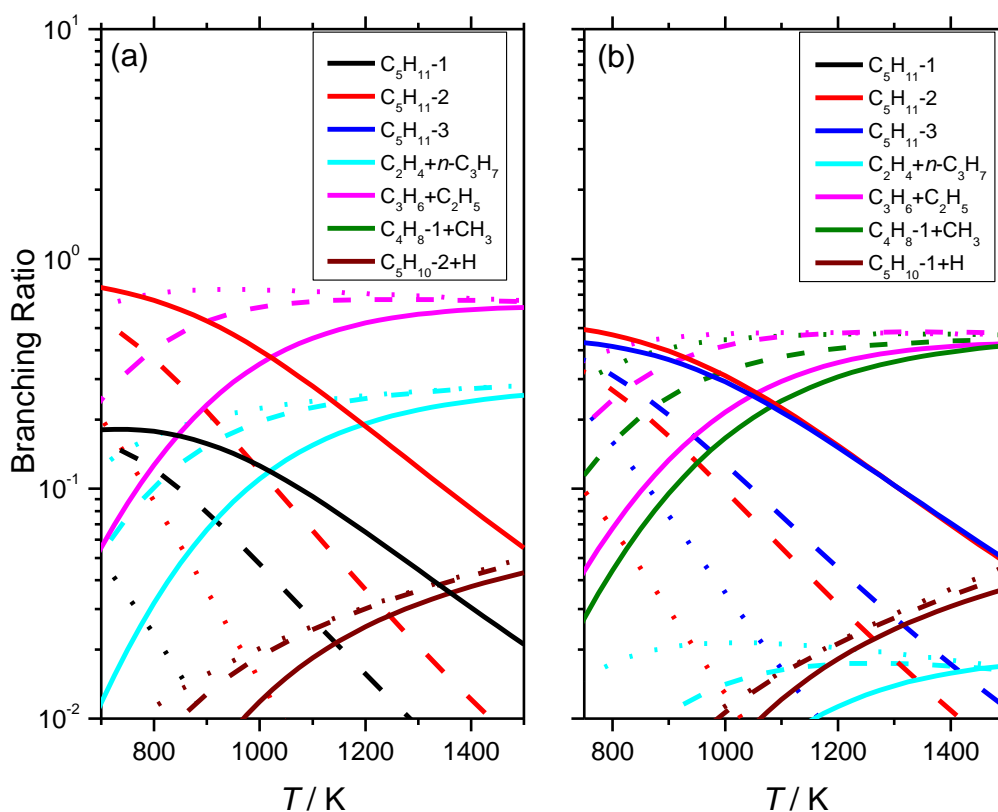


**Figure 2.2.** Temperature and pressure-dependent branching ratios for (a) 1-pentene +  $\dot{H}$  and (b) 2-pentene +  $\dot{H}$  via hydrogen atom addition reactions at 0.1 atm (dotted lines), 1 (dashed lines) and 10 (solid lines) atm.

### 3.3. Reactions of pentyl radicals

The unimolecular reaction mechanism of pentyl radicals is generally well understood [5-14, 28, 29] and only a brief overview of the key features of the potential energy surface from this work is provided here. SI provides a detailed comparison of barriers and rate constants computed in this work with literature data.

The 1-pentyl radical has two decomposition pathways: C–C  $\beta$ -scission (R15) forming ethylene + *n*-propyl radical, and C–H  $\beta$ -scission forming 1-pentene and a  $\dot{H}$  atom, with 0 K barriers of  $123.26 \text{ kJ mol}^{-1}$  and  $153.56 \text{ kJ mol}^{-1}$  computed in this work.

Its isomerisation reactions are slightly more complex, as it can react via 1,2-( $C_1$  to  $C_2$ ) 1,3-( $C_1$  to  $C_3$ ) and 1,4-( $C_1$  to  $C_4$ ) hydrogen atom transfers. For the latter reaction, there exists kinetically distinct equatorial and axial transition states, which cannot be interconverted by internal rotation, Figure 2.3. Barrier heights of  $96.51$  and  $97.36 \text{ kJ mol}^{-1}$  were computed for the two pathways, with the equatorial conformation found to be slightly more stable than its

axial counterpart. Inclusion of the higher energy pathway in our RRKM/ME modelling leads to less than a factor of two increase in the total isomerisation rate constant, although this correction is non-negligible for the modelling of literature experiments [6, 7] on 1-pentyl decomposition.

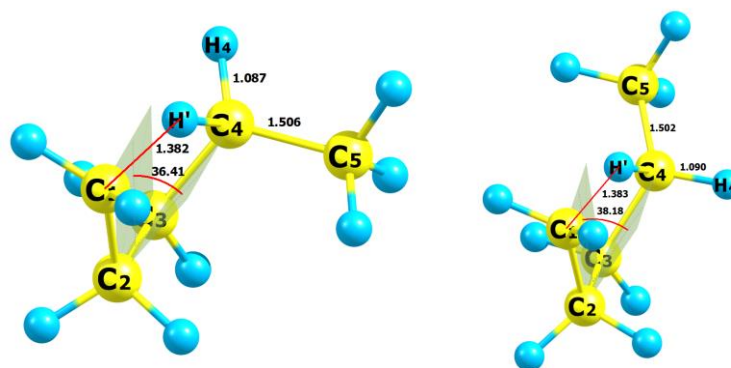


**Figure 2.3.** Axial (left) and equatorial (right) transition states for the 1,4-hydrogen atom transfer reaction of 1-pentyl to 2-pentyl. Figures can be viewed in colour through the online version.

As expected, substantially higher barrier heights of 161.1 and 162.3 kJ mol<sup>-1</sup> were calculated for the 1,2- isomerisation forming 2-pentyl radicals via a 3-membered ring transition state, and the 1,3-isomerisation reactions via a 4-membered ring transition state.

Similarly, 2-pentyl radicals can undergo C–H  $\beta$ -scission to form 2-pentene +  $\dot{\text{H}}$ -atoms (R13) with a barrier height of 148.75 kJ mol<sup>-1</sup>, with C–C  $\beta$ -scission to form propene + ethyl radicals (R16) having a more favourable barrier of 122.9 kJ mol<sup>-1</sup>. Isomerisation of 2-pentyl radicals forming 3-pentyl radicals can also occur via a 3-membered ring transition state (C<sub>2</sub> to C<sub>3</sub>, R20), with a barrier of 166.0 kJ mol<sup>-1</sup> computed for the lowest energy structure, in which the C<sub>2</sub>-bound methyl and C<sub>3</sub>-bound ethyl moieties are in an anti-configuration. The corresponding syn-conformer is energetically disfavoured, with a barrier of 172.4 kJ mol<sup>-1</sup> computed, although both are included in our RRKM/ME analysis. In turn, 3-pentyl radicals can decompose via C–H  $\beta$ -scission to form 1-butene + methyl radicals (R17), with a barrier height of 129.7 kJ mol<sup>-1</sup>, or via C–H  $\beta$ -scission to form 2-pentene +  $\dot{\text{H}}$  atoms (R14) through a barrier of 148.1 kJ mol<sup>-1</sup>.

Whilst these enthalpy effects are dominant at low temperatures, under the experimental conditions of the present work, entropy effects cannot be neglected, and the larger loss of entropy in isomerisation transition states relative to  $\beta$ -scission reactions leads to temperature-dependence in the branching ratios between the two classes of reaction. Figures AS6 and AS7

of Appendix A presents plots of tunnelling-uncorrected pre-exponential factors and entropies of activation for the unimolecular reactions of the pentyl radicals, with the well-known correlation between frequency factors and number of rotors lost in transition state rings observed [23, 76, 77]. Beyond the well-known enthalpy and entropy factors, the energy transfer effects must also be considered and the product branching ratios are also pressure-dependent. Figure 2.4 illustrates the temperature- and pressure-dependent branching ratios for 1-, 2- and 3-pentyl radical unimolecular reactions at 0.1, 1.0 and 10 atm.

Under pyrolysis conditions, the fate of the 2-pentyl and 3-pentyl radicals is clear – the former almost exclusively produces propene and ethyl, with 1-butene and methyl being the solitary decomposition product of 3-pentyl radical. It is interesting to note that significant competition between isomerisation-stabilisation reactions, and reactions forming bimolecular products exists only for the 1-pentyl radical, Figure 2.4 (a). The formation of 2-pentyl radical is dominant up to 825 K, 850 K and 950 K at 0.1 atm, 1.0 atm and 10 atm respectively. At higher temperatures, decomposition to ethylene and propyl radical becomes the dominant pathway, with formation of propene and ethyl through a well-skipping reaction mediated through 2-pentyl also featuring, particularly at low-pressures and high temperatures.

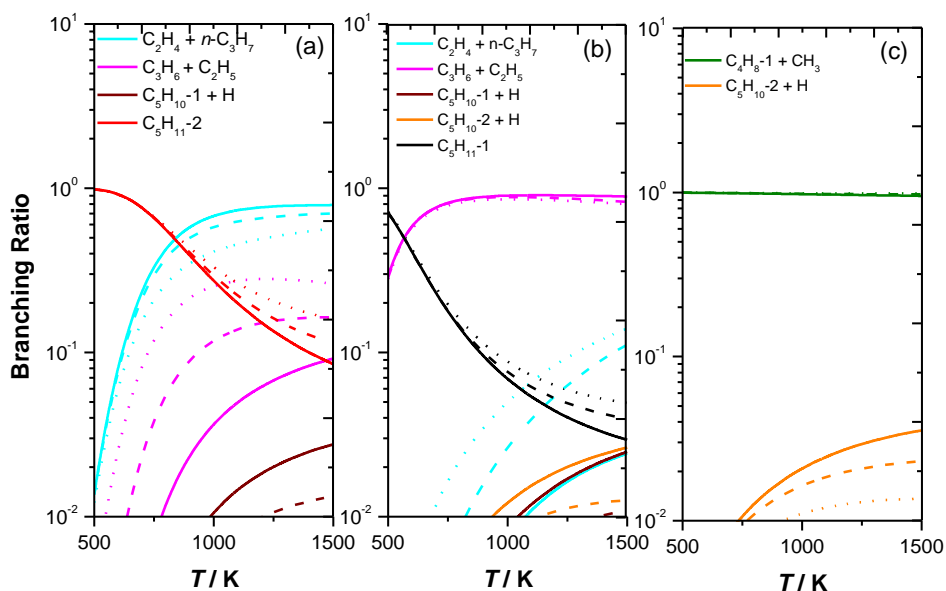


**Figure 2.4.** Branching ratio at 0.1, 1 and 10 atm for (a) 1-pentyl, (b) 2-pentyl and (c) 3-pentyl radicals. Dotted line (0.1 atm), dashed (1 atm) and solid (10 atm).

In terms of the accuracy of our rate constants, high-pressure limiting rate constants for the reactions of 1-pentyl and 2-pentyl are compared with literature studies in detail in SI with varying levels of agreement observed depending on the electronic structure and statistical rate theory approximations employed. Under the high-temperature conditions ( $> 1000$  K) of relevance to this work, most studies agree to within factors of two, although disagreement can be substantially larger at low temperature where differences in barriers, tunnelling corrections, and internal rotor treatments may be enhanced.

The theoretical studies of Yu et al. [10] and combined experimental and theoretical study of Miyoshi et al. [13] provide what are perhaps the best benchmarks results, with both studies in excellent agreement as to the high-pressure limiting rate constant for the reaction  $\dot{C}_5H_{11-1} \rightleftharpoons \dot{C}_5H_{11-2}$ . Yu et al. [10] used this system as a validation of their newly formulated multi-structural variational TST (MS-VTST), which extends the multi-structural (MS) family of methods [78].

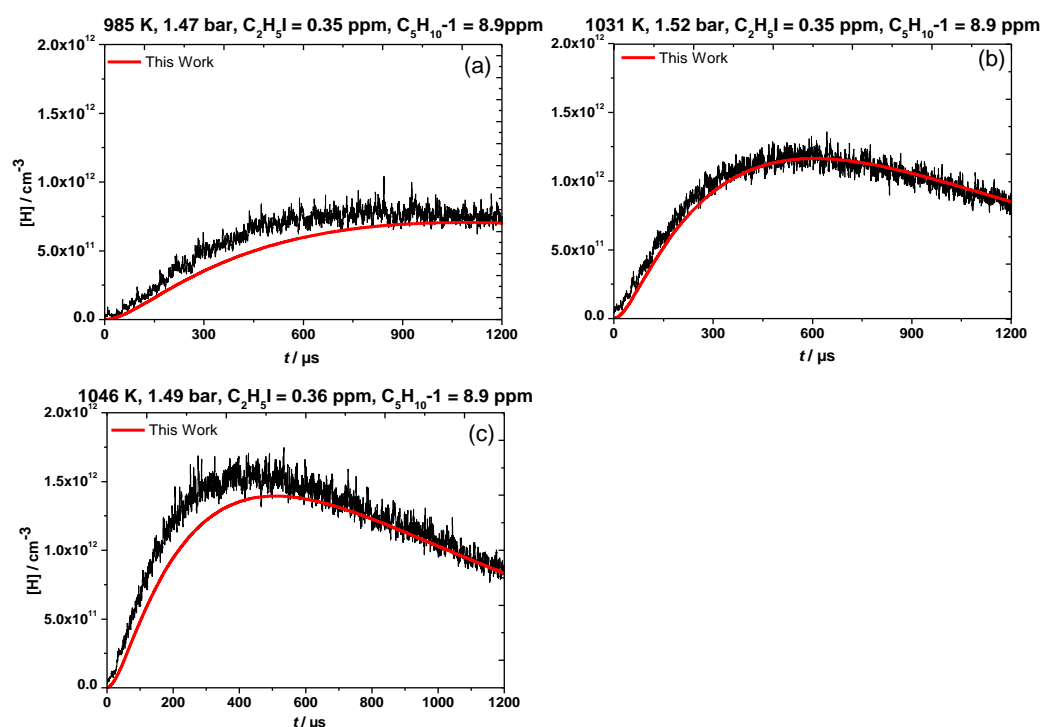
Figure AS4 of Appendix A show that our rate constants for the  $\dot{C}_5H_{11-1} \rightleftharpoons \dot{C}_5H_{11-2}$  reaction are slower than both works, underestimating the Yu et al. [10] result by a factor of  $\approx 7$  at 400 K, with this difference reduced to a factor of approximately two at 1000 K. For the reverse reaction, our rate constant under-predicts that of Yu et al. [10] to a lesser extent, and is within a factor of two from 300–2000 K.

Our computed barriers are in excellent agreement with those of Yu et al., over-predicting their CCSD(T)-F12b/jul-cc-pVTZ//M06-2X/MG3S result by  $\approx 1$  kJ mol<sup>-1</sup>, which accounts for a factor of 1.4 difference at low temperatures where disagreement is largest. Indeed, tunnelling corrections are more important at these temperatures, with our Eckart tunnelling correction factor of 14.1 at 400 K underestimating the small curvature tunnelling correction of Yu et al. [10] by a factor of two. The remaining factor of 3–4 difference can be assigned to their treatment of multi-structural torsional an-harmonicity, variational effects, differences in electronic structure methods, and symmetry corrections, which are somewhat difficult to disentangle.

Despite the apparent importance of multi-structural an-harmonicity, the entropies we compute for 1-pentyl radical with a straight-forward 1-dimensional hindered rotor treatment is in quite good agreement with multi-structural an-harmonic results from Zheng et al. [78], our entropies being 0.95, 2.34, 4.34 J mol<sup>-1</sup> K<sup>-1</sup> less than theirs at 298.15, 400 and 600 K, and one might expect these differences to be diminished for the transition states which are conformationally less complex than the pentyl radicals.

## 4. Detailed Kinetic Modelling

### 4.1. $\dot{\text{H}}$ -ARAS Experiments



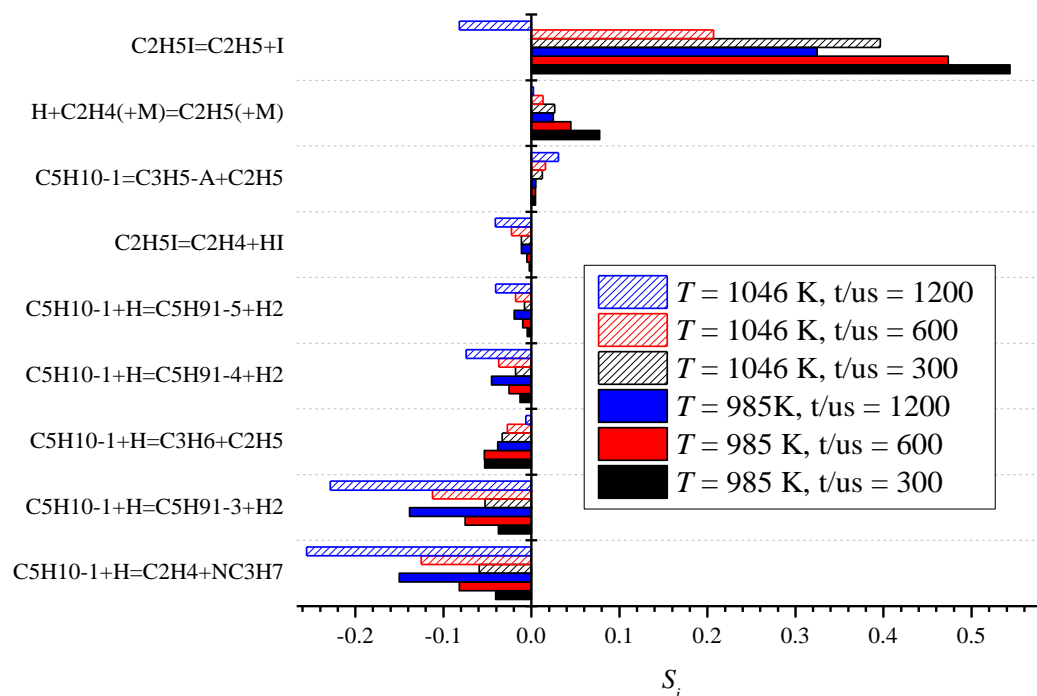
**Figure 2.5.** Experimental (black) and simulated (red)  $\dot{\text{H}}$ -atom profiles for  $\text{C}_2\text{H}_5\text{I}/1\text{-pentene}/\text{Ar}$  mixtures at (a) 985 K, (b) 1031 K and (c) 1046 K.

Figure 2.5 presents experimentally measured and simulated  $\dot{\text{H}}$  atom profiles for  $\text{C}_2\text{H}_5\text{I}/1\text{-pentene}/\text{Ar}$  mixtures with the model capable of predicting the qualitative and quantitative trends observed experimentally. Accompanying sensitivity and rate-of-production analyses are presented in Figure 2.6 and Figure 2.7 respectively. The most important  $\dot{\text{H}}$  atom production pathways are the decomposition of  $\text{C}_2\text{H}_5\text{I}$  to  $\dot{\text{C}}_2\text{H}_5$  and  $\dot{\text{I}}$ , with the subsequent decomposition of  $\dot{\text{C}}_2\text{H}_5$  to ethylene and  $\dot{\text{H}}$  atom being facile, and the rate limiting C-I fission reaction is expectedly more sensitive.

Of the reactions of 1-pentene, the major pathways consuming  $\dot{\text{H}}$  atoms are the chemically activated pathways forming propene and ethyl radicals ( $> 45.6\%$ ), and ethylene and propyl radicals ( $> 14.3\%$ ). Despite the fact that the former pathway consumes three times more  $\dot{\text{H}}$  atoms compared to the latter, it is much less inhibiting, as the ethyl radicals formed can readily decompose to recycle  $\dot{\text{H}}$  atoms, whereas the products of the latter pathway are ethylene and  $\dot{\text{C}}\text{H}_3$  radicals.  $\dot{\text{H}}$  atom addition leading to the formation of stabilised 2-pentyl and 1-pentyl consume 12% and 4% of the 1-pentene at 985 K, with the more important pathway

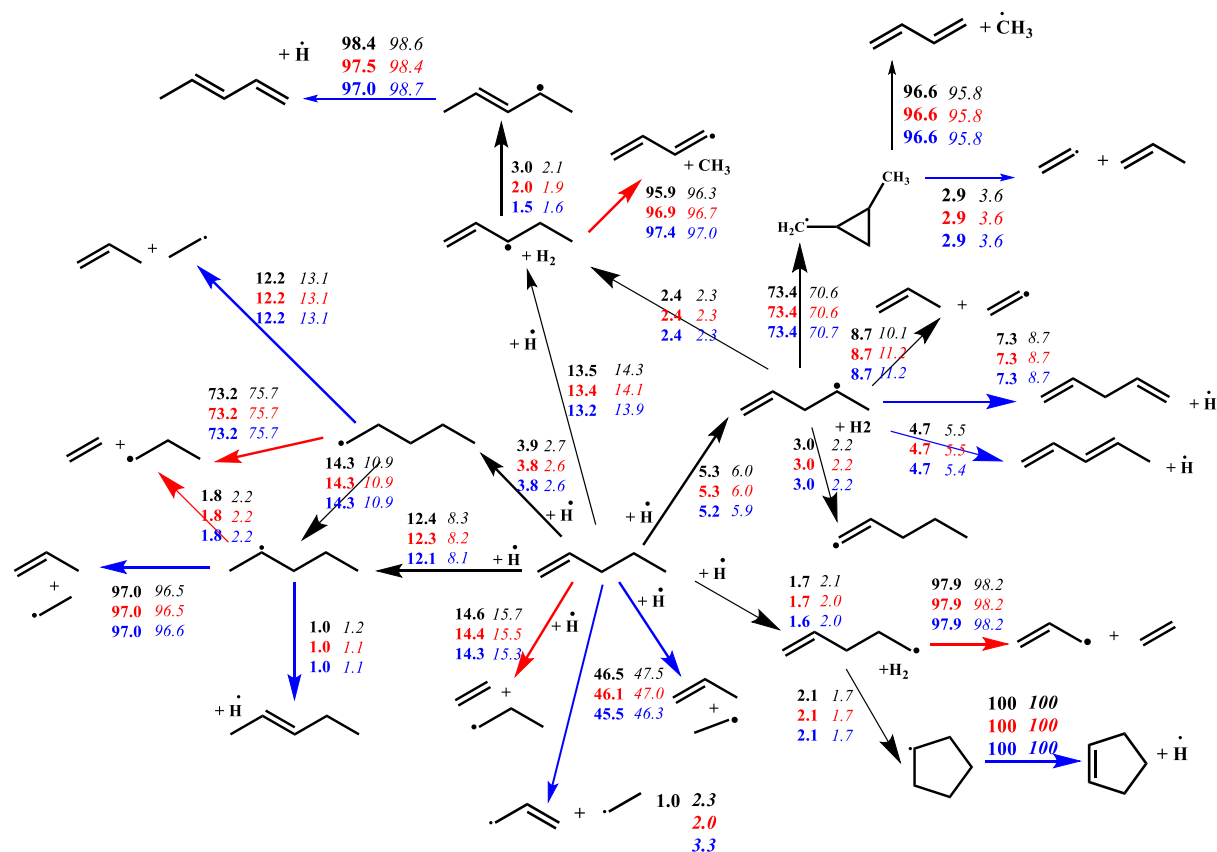


forming 2-pentyl radical only mildly inhibiting as the 2-pentyl radical rapidly decomposes to products which regenerate  $\dot{\text{H}}$  atoms.



**Figure 2.6.** Sensitivity analysis to  $\dot{\text{H}}$  atom concentrations for  $\text{C}_2\text{H}_5\text{I}/1\text{-pentene}/\text{Ar}$  mixtures at 985 K and 1046 K and at times of 300, 600 and 1200  $\mu\text{s}$ .

Abstraction reactions from allylic and alkyl sites account for close to 20% of 1-pentene consumption, with all three pathways found to be inhibiting. The dominant abstraction pathway forming the resonantly stabilised  $\dot{\text{C}}_5\text{H}_9\text{-13}$  radicals consume  $\approx 13\%$  of the 1-pentene, and is the second most inhibiting reaction with respect to  $\dot{\text{H}}$ -atoms yields, as the subsequent decomposition of the pentenyl radicals lead largely to the formation of 1,3-butadiene and methyl radicals. The unimolecular decomposition of 1-pentene consumes less than 1% of the reactant, and is found to be the only 1-pentene-specific reaction which produces  $\dot{\text{H}}$ -atoms, and therefore, it is the only reaction of 1-pentene which has a positive sensitivity coefficient, albeit, a small one.



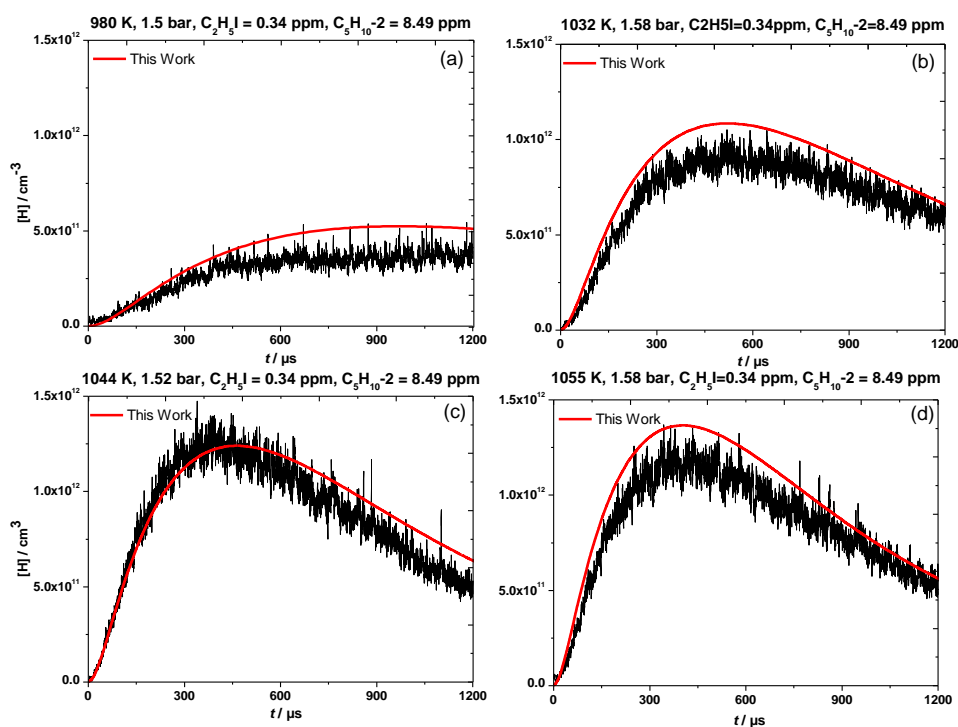
**Figure 2.7.** Rate of production analysis for  $\dot{\text{H}}$  atoms for the  $\text{C}_2\text{H}_5/1\text{-pentene}/\text{Ar}$  experiments at 985 K (bold) and 1046 K (italics). at 300  $\mu\text{s}$  (black), 600  $\mu\text{s}$  (red) and 1200  $\mu\text{s}$  (blue). Solid blue arrows represent  $\dot{\text{H}}$ -atom producing pathways, while red arrows represent  $\dot{\text{H}}$  atom consumption pathways.

Figure 2.8 shows the corresponding experimental and simulation results for  $\text{C}_2\text{H}_5/2\text{-pentene}/\text{Ar}$  mixtures, with the model again found to give good agreement with experiment. The important chemical reactions are delineated in the sensitivity and rate-of-production analyses presented in Figure 2.9 and Figure 2.10. As in the case of 1-pentene, the unimolecular decomposition of 2-pentene, forming  $\dot{\text{C}}\text{H}_3$  and  $\dot{\text{C}}_4\text{H}_7\text{1-3}$ , is the only reaction of the reactant species which is found to promote  $\dot{\text{H}}$ -atom production, as the  $\dot{\text{C}}_4\text{H}_7\text{1-3}$  radical decomposes to form 1,3-butadiene and  $\dot{\text{H}}$  atoms almost exclusively. The importance of this reaction tends to increase with increasing temperature, and at longer reaction times.

The major consumption pathways of  $\dot{\text{H}}$  atoms are the addition reactions, which consume  $\approx 70\%$  of the reactant. The dominant pathways are the chemically activated reactions forming propene and ethyl radicals, and 1-butene and  $\dot{\text{C}}\text{H}_3$ , which both consume 20–30% of the 2-pentene. The latter reaction forming 1-butene and  $\dot{\text{C}}\text{H}_3$  is the most inhibiting reaction with respect to  $\dot{\text{H}}$  atom predictions, as the pathway forming propene and ethyl radicals regenerates

$\dot{\text{H}}$  atoms via ethyl radical decomposition. The stabilisation pathways forming 2-pentyl and 3-pentyl radicals are relatively less important, consuming 15–20% of the reactant. The pathway forming 3-pentyl radical is found to inhibit  $\dot{\text{H}}$ -atom production given that 3-pentyl decomposes to form 1-butene and  $\dot{\text{C}}\text{H}_3$ , and stabilisation forming 2-pentyl does not inhibit  $\dot{\text{H}}$  atom production due to the subsequent formation of propene and ethyl radicals, which ultimately recycle  $\dot{\text{H}}$  atoms.

Abstraction reactions are also found to be important, consuming up to 25% of 2-pentene. The pathways forming the resonantly stabilised  $\dot{\text{C}}_5\text{H}_9$ 1-3 *via* abstraction at the  $\text{C}_1$  position, and  $\dot{\text{C}}_5\text{H}_9$ 2-4 *via* abstraction at the  $\text{C}_4$  site, are dominant. Both reactions inhibit  $\dot{\text{H}}$  atom production as they largely lead to the formation of 1-butene and  $\dot{\text{C}}\text{H}_3$  radicals, with the pathways which recycle  $\dot{\text{H}}$ -atom with  $\text{C}_5\text{H}_8$  dienes of lesser importance.



**Figure 2.8.** Experimental (black) and simulated (red)  $\dot{\text{H}}$  atom concentrations for  $\text{C}_2\text{H}_5\text{I}/2$ -pentene/Ar mixtures at (a) 980 K (b) 1032 K and (c) 1044 K and (d) 1055 K.

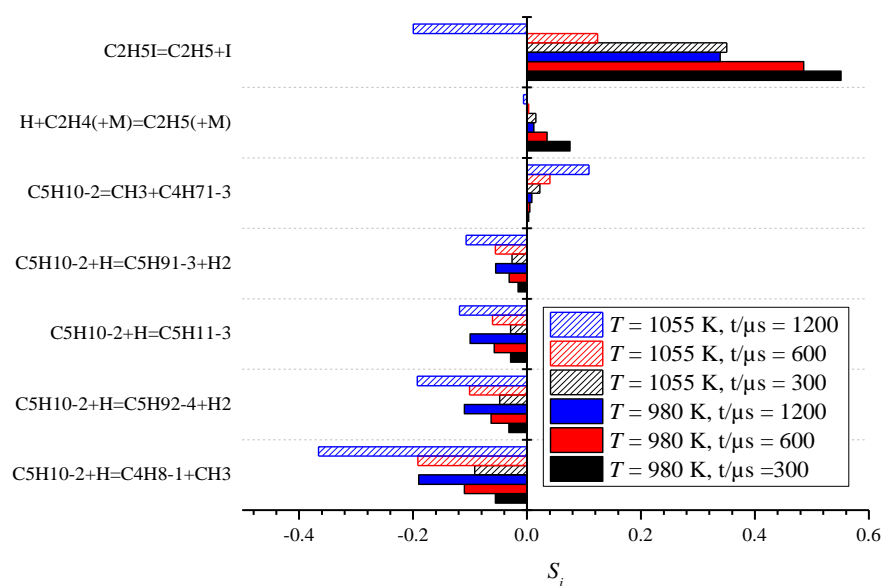


**Figure 2.9.** Sensitivity analysis to  $\dot{H}$  atom concentrations for  $C_2H_5I/1$ -pentene/Ar mixtures at 980 and 1055 K and times of 300, 600 and 1200  $\mu s$ .

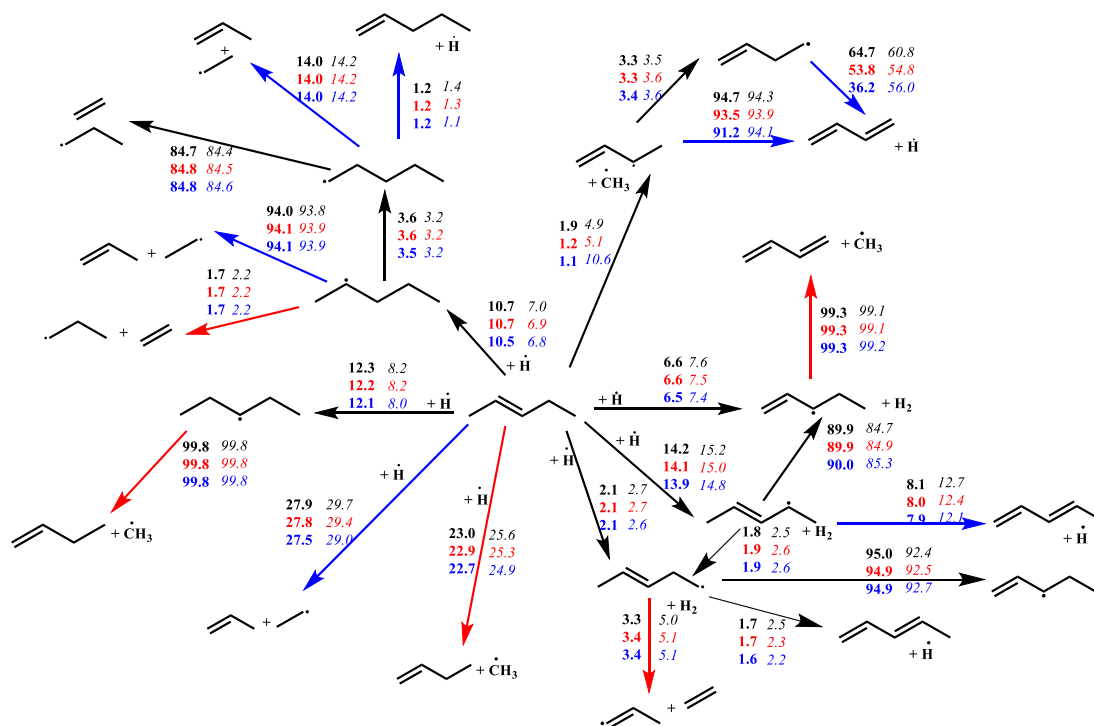


**Figure 2.10.** Rate of production analysis for  $\dot{H}$  atoms for  $C_2H_5I/2$ -pentene/Ar mixtures at 980 K (bold) and 1055 K (italics), at 300  $\mu s$  (black), 600  $\mu s$  (red) and 1200  $\mu s$  (blue). Solid blue arrows represent  $\dot{H}$ -atom producing pathways, while red arrows represent  $\dot{H}$ -atom consumption pathways.

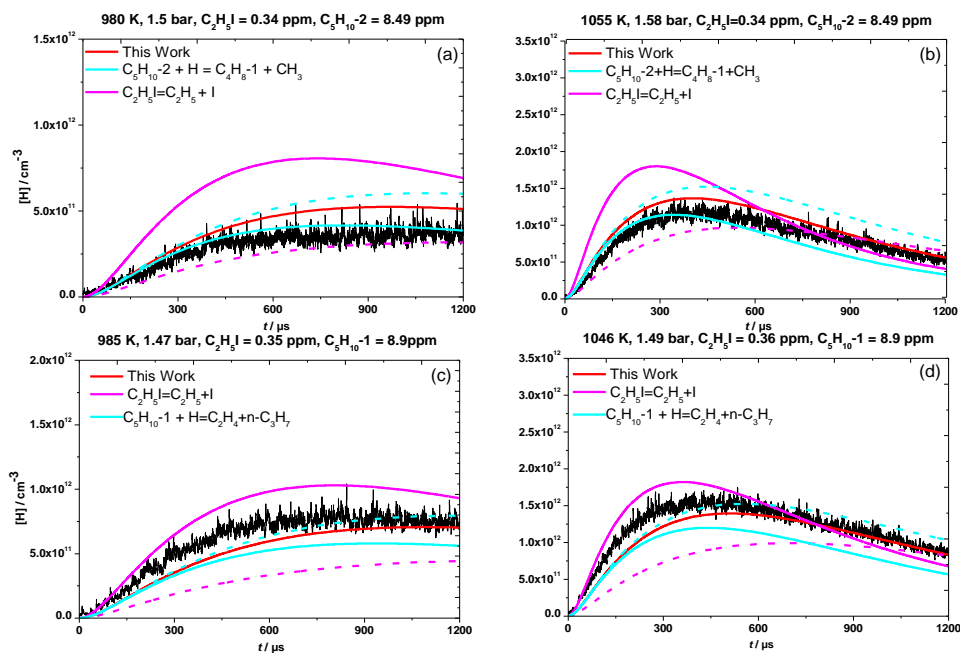


**Figure 2.11.** Model predictions (colour) of measured (black)  $\dot{\text{H}}$  atom profiles upon factor of two perturbations to the most promoting and inhibiting reactions for 2-pentene (top) and 1-pentene (bottom). Solid lines illustrate the result of increasing a rate constant by a factor of two, and vice versa for dashed lines.

Figure 2.11 illustrates the effect of changing the most sensitive promoting and inhibiting reactions within the un-optimized model by factors of  $\pm 2$ . Whilst the uncertainty in the rate constant for unimolecular decomposition of  $\text{C}_2\text{H}_5\text{I}$  is not this large, it illustrates that it largely controls the initial formation of  $\dot{\text{H}}$ -atoms, and a slight increase to this rate constant would improve agreement with experiment on short timescales. For both 1-pentene and 2-pentene, the most inhibiting reactions are those which lead to the production of alkenes and  $\dot{\text{C}}\text{H}_3$  radicals, and these rate constants largely influence the predictions of  $\dot{\text{H}}$ -atom concentrations at later times once  $\dot{\text{H}}$ -atom yields have reached a maximum.

## 4.2. Literature Experiments

The experimental conditions of important literature studies are presented in Table AS2 and Figure AS1 of Appendix A. A comprehensive comparison of the predictions of the unoptimized model from this work against literature data [5-7, 14] and sensitivity analyses for the same are also provided therein.

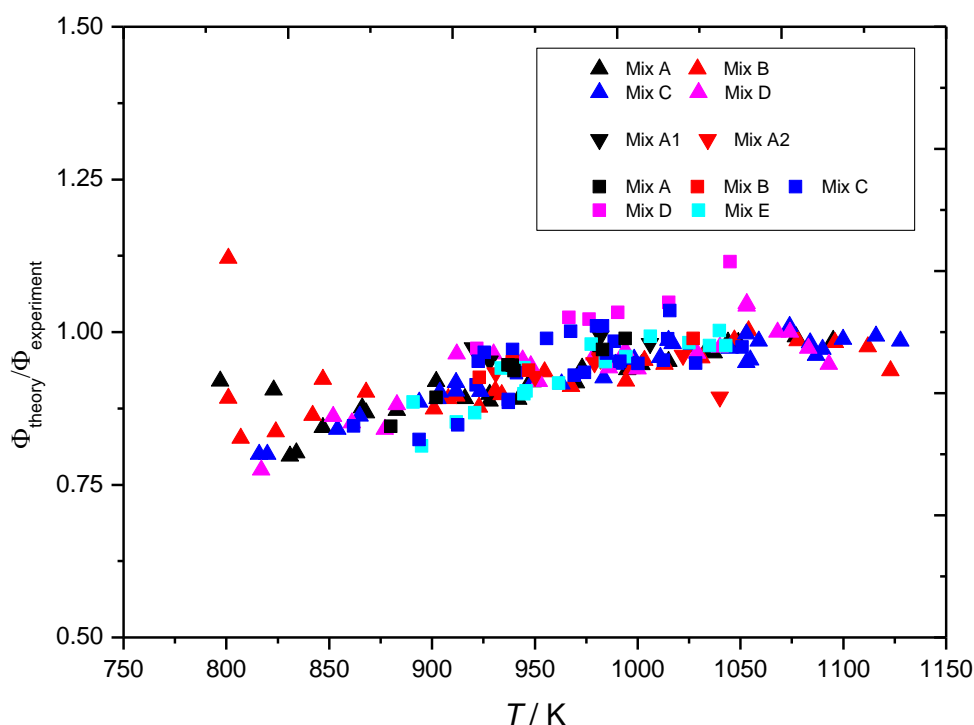


**Figure 2.12.** Comparison of the experimentally measured and theoretically predicted ratios ( $\Phi$ ) of ethylene to propene from the studies of Awan et al.[6] (■) and Comandini et al.[7] (UIC: ▲, NIST: ▼).  $\Phi = X_{\text{ethylene}}/X_{\text{propene}}$ , where X is the mole fraction.

For the experiments of Awan et al. [6] and Comandini et al. [7] the ethylene/propene ratio is the crucial measurement, which is largely determined by the branching ratio between  $1\text{-pentyl} \rightleftharpoons \text{ethylene} + \text{propyl}$  relative to its isomerisation to form 2-pentyl, with the latter decomposing to form propene and ethyl radical. Figure 2.12 presents comparisons of experimental ethylene to propene product ratios with the predictions of the model from this work, with theory and experiment agreeing to within 25% at low temperatures (800 K), and to within 10% at temperature above 1000 K. Sensitivity analyses presented in supplementary material confirm this ratio is most sensitive to the direct decomposition of  $1\text{-pentyl} \leftrightarrow \text{ethylene} + \text{propyl}$ , which increases the predicted ratio due to the effective production of two

ethylene molecules and a methyl radical, and the isomerisation of 1-pentyl  $\rightleftharpoons$  2-pentyl, which ultimately leads to the prediction of propene, ethylene and a  $\dot{\text{H}}$ -atom. Sensitivity analyses also show that the well-skipping reaction 1-pentyl  $\leftrightarrow$  propene + ethyl also reduces this ratio.

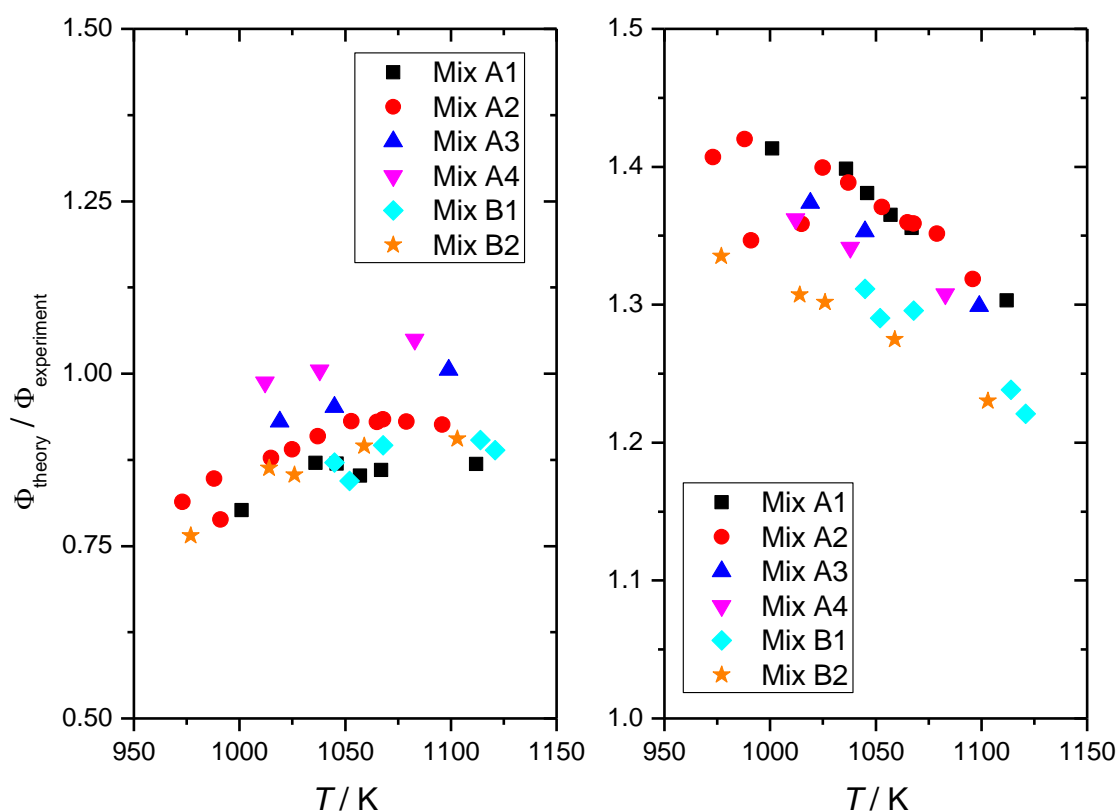


**Figure 2.13.** Comparison of the experimentally measured and theoretically predicted ratios ( $\Phi$ ) of (a) ethylene to butene and (b) propene to butene from the study of Manion et al.[5].  $\Phi = X_{\text{species}}/X_{\text{butene}}$  where  $X$  = mole fraction.

The experiments of Manion et al. [5] differ from those of Awan et al. [6] and Comandini et al. [7] in that they probe the reactions of  $\dot{\text{H}}$  atoms with 2-pentene, and the corresponding reactions of 2-pentyl and 3-pentyl radicals, which lead to the formation of ethylene, propene and butene through addition reactions, and 1,3-butadiene via  $\dot{\text{H}}$  atom abstraction reactions. Figure 2.13 illustrates the performance of the current mechanism in predicting the ratios of ethylene to 1-butene, and propene to 1-butene, with these important ratios predicted to within 25% and 45%, respectively.

Sensitivity analyses show that the ethylene to 1-butene and propene to 1-butene ratios are dominated by the competition between  $\dot{\text{H}}$  atom addition reactions of 2-pentene at the  $\text{C}_2$  and  $\text{C}_3$  positions. Addition at the  $\text{C}_3$  position leads to the formation of propene and ethyl radicals,

and hence ethylene, through chemical activation, hence increasing these ratios. This reaction is in direct competition with addition at the C<sub>2</sub> position, which solely leads to formation of 1-butene and  $\dot{\text{C}}\text{H}_3$  radicals.

Sensitivity analysis also shows that under the experimental conditions of Manion et al. [5] the ratio of ethylene to propene is governed by a more complex spectrum of reactions than the same ratio as measured by Awan et al. [6] and Comandini et al. [7], with the sensitivity of the reactions of radical precursors (HME, *tert*-butyl radical) and scavengers (trimethylbenzene +  $\dot{\text{H}}$ ) on a par with the reactions of 2-pentene +  $\dot{\text{H}}$ . Indeed the reactions of *tert*-butyl radical are amongst the most sensitive in terms of predicted propene yields, and hence ratios of ethylene to propene, as it contributes directly to the formation of propene via isomerisation to *i*- $\dot{\text{C}}_4\text{H}_9$  and the subsequent decomposition of *i*- $\dot{\text{C}}_4\text{H}_9$  to produce C<sub>3</sub>H<sub>6</sub> and  $\dot{\text{C}}\text{H}_3$  radicals.

## 5. Conclusions

Small-molecular-weight alkenes are amongst the most important species in combustion given they are components of virtually all real-world fuels, with pentenes of particular importance as components of gasoline. To contribute to the development of combustion models for these species, we have studied the potential energy surfaces of relevance to the reactions of hydrogen with 1- and 2-pentene in detail.

Thermochemical data for species of relevance to the  $\dot{\text{C}}_5\text{H}_{11}$  PES were calculated as a function of temperature with enthalpies of formation derived from an isodesmic reaction network built upon benchmark literature data and electronic structure calculations. High-pressure limiting and temperature- and pressure-dependent rate constants have been calculated using Rice Ramsperger-Kassel Marcus (RRKM) theory with a 1-dimensional Master Equation (ME) analysis. The theoretical data are implemented in a detailed chemical kinetic model in order to simulate a wide range of literature pyrolysis data, including new hydrogen atomic resonance absorption spectrometry ( $\dot{\text{H}}$ -ARAS) experiments which provide the first measurements of the global rates of reaction of  $\dot{\text{H}}$  atoms with 1- and 2-pentene. The theoretical results predict the  $\dot{\text{H}}$ -ARAS experiment well, and rate-of-production and sensitivity analyses show that there is competition between  $\dot{\text{H}}$  atom addition and abstraction reactions under the conditions of the  $\dot{\text{H}}$ -ARAS experiments. For the addition reactions, there is further competition between chemically activated and collisionally stabilised products.

Furthermore, past experimental and theoretical studies on the title reactions and on corresponding decomposition reactions of 1-, 2- and 3-pentyl radicals have been reviewed



and available data simulated. The rate constants computed in this study tend to agree with literature data to within factors of two under high temperature conditions ( $>1000$  K), with our model capable of reproducing experimentally measured species profiles to within factors of two or better. The current model should provide a useful basis for those who wish to model a variety of practical combustion scenarios (e.g. shock-tubes, rapid-compression machines, flames, jet-stirred reactors).

Despite the good agreement between our un-optimised model predictions and high-temperature shock tube data, there is some disagreement between theoretical studies at lower temperatures (300 – 600 K). Whilst the current theoretical calculations and chemical kinetic model likely super cede many of these works in terms of utility for combustion modelling, there are important factors which this work, and few others [10, 78], have not considered in their thermochemical and kinetics computations, including the influence of vibrational anharmonicity (including umbrella modes), the treatment of multidimensional torsions, and variational effects. Future work should aim to address these topics with the aim of developing a more comprehensive RRKM/ME model to use as a basis for combustion modelling.

### **Supporting Information**

MESS input and output files; tabulated single point energies; tabulated isodesmic reactions; thermochemical values for all  $C_5$  species in NASA polynomial format; Chemkin format/PLOG rate constant fits, mechanism and thermochemistry files used in simulations (ZIP)

### **Acknowledgements**

We would like to acknowledge the support of Science Foundation Ireland in funding this project under project number 15/IA/3177, and also to the Irish Centre for High-End Computing, ICHEC, under project numbers ngchec037c, ngche042c and ngche058c for use of computational resources. Sebastian Peukert also acknowledges funding from the German Research Foundation (DFG) under grant number SCHU 1369/24; RFBR-16-58-12014. The authors would also like to acknowledge Dr. Stephen Klippenstein for his help with the MESS code.

## References

- [1] S. Kikui, H. Nakamura, T. Tezuka, S. Hasegawa, K. Maruta, Study on combustion and ignition characteristics of ethylene, propylene, 1-butene and 1-pentene in a micro flow reactor with a controlled temperature profile, *Combust. Flame* 163 (2016) 209-219.
- [2] S.M. Burke, W. Metcalfe, O. Herbinet, F. Battin-Leclerc, F.M. Haas, J. Santner, F.L. Dryer, H.J. Curran, An experimental and modeling study of propene oxidation. Part 1: speciation measurements in jet-stirred and flow reactors, *Combust. Flame* 161 (2014) 2765-2784.
- [3] Y. Li, C.-W. Zhou, K.P. Somers, K. Zhang, H.J. Curran, The oxidation of 2-butene: a high pressure ignition delay, kinetic modeling study and reactivity comparison with isobutene and 1-butene, *Proc. Combust. Inst.* 36 (2017) 403-411.
- [4] C.-W. Zhou, Y. Li, E. O'Connor, K.P. Somers, S. Thion, C. Keesee, O. Mathieu, E.L. Petersen, T.A. DeVerter, M.A. Oehlschlaeger, et al., A comprehensive experimental and modeling study of isobutene oxidation, *Combust. Flame* 167 (2016) 353-379.
- [5] J.A. Manion, I.A. Awan, The decomposition of 2-pentyl and 3-pentyl radicals, *Proc. Combust. Inst.* 34 (2013) 537-545.
- [6] I.A. Awan, D.R. Burgess, Jr., J.A. Manion, Pressure dependence and branching ratios in the decomposition of 1-pentyl radicals: shock tube experiments and master equation modeling, *J. Phys. Chem. A* 116 (2012) 2895-2910.
- [7] A. Comandini, I.A. Awan, J.A. Manion, Thermal decomposition of 1-pentyl radicals at high pressures and temperatures, *Chem. Phys. Lett.* 552 (2012) 20-26.
- [8] B. Sirjean, E. Dames, H. Wang, W. Tsang, Tunneling in Hydrogen-Transfer Isomerization of n-Alkyl Radicals, *J. Phys. Chem. A* 116 (2012) 319-332.
- [9] A.C. Davis, J.S. Francisco, Ab Initio Study of Hydrogen Migration across n-Alkyl Radicals, *J. Phys. Chem. A* 115 (2011) 2966-2977.
- [10] T. Yu, J. Zheng, D. Truhlar, Multi-structural variational transition state theory. Kinetics of the 1,4-hydrogen shift isomerization of the pentyl radical with torsional anharmonicity, *Chem. Sci.* 2 (2011) 2199-2213.
- [11] J.J. Zheng, D.G. Truhlar, Direct Dynamics Study of Hydrogen-Transfer Isomerization of 1-Pentyl and 1-Hexyl Radicals, *J. Phys. Chem. A* 113 (2009) 11919-11925.
- [12] L.C. Jitariu, L.D. Jones, S.H. Robertson, M.J. Pilling, I.H. Hillier, Thermal rate coefficients via variational transition state theory for the unimolecular decomposition/isomerization of 1-pentyl radical: ab initio and direct dynamics calculations, *J. Phys. Chem. A* 107 (2003) 8607-8617.
- [13] A. Miyoshi, J. Widjaja, N. Yamauchi, M. Koshi, H. Matsui, Direct investigations on the thermal unimolecular isomerization reaction of 1-pentyl radicals, *Proc. Combust. Inst.* 29 (2002) 1285-1293.
- [14] N. Yamauchi, A. Miyoshi, K. Kosaka, M. Koshi, H. Matsui, Thermal Decomposition and Isomerization Processes of Alkyl Radicals, *J. Phys. Chem. A* 103 (1999) 2723-2733.
- [15] K.P. Somers, H.J. Curran, U. Burke, C. Banyon, H.M. Hakka, F. Battin-Leclerc, P.-A. Glaude, S. Wakefield, R.F. Cracknell, The importance of endothermic pyrolysis reactions in the understanding of diesel spray combustion, *Fuel* 224 (2018) 302-310.
- [16] V.B. Mokrushin, V.; Tsang, W.; Zachariah, M.; Knyazev, V.D.; McGivern W.S., ChemRate, National Institute of Standards and Technology, Gaithersburg, Maryland, (1996-2011).
- [17] V.D. Knyazev, I.R. Slagle, Unimolecular Decomposition of n-C<sub>4</sub>H<sub>9</sub> and iso-C<sub>4</sub>H<sub>9</sub> Radicals, *J. Phys. Chem. A* 100 (1996) 5318-5328.
- [18] J.A. Kerr, M.J. Parsonage, Evaluated kinetic data on gas phase addition reactions. Reactions of atoms and radicals with alkenes, alkynes and aromatic compounds, 1972.

- [19] M. Saeys, M.-F. Reyniers, G.B. Marin, V. Van Speybroeck, M. Waroquier, Ab initio group contribution method for activation energies for radical additions, *AIChE Journal* 50 (2004) 426-444.
- [20] V.D. Knyazev, W. Tsang, Chemically and thermally activated decomposition of secondary butyl radical, *J. Phys. Chem. A* 104 (2000) 10747-10765.
- [21] V.D. Knyazev, I.A. Dubinsky, I.R. Slagle, D. Gutman, Unimolecular Decomposition of T-C<sub>4</sub>H<sub>9</sub> Radical, *J. Phys. Chem.* 98 (1994) 5279-5289.
- [22] R.M. Marshall, The rate constant for the intramolecular isomerization of pentyl radicals, *Int. J. Chem. Kinet* 22 (1990) 935 - 950.
- [23] K.W. Watkins, On the rate constant for n-pentyl radical isomerization, *Can. J. Chem.* 50 ( 1972).
- [24] L. Endrenyi, D.J.L. Roy, The Isomerization of n-Pentyl and 4-Oxo-1-pentyl Radicals in the Gas Phase, *J. Phys. Chem.* 70 (1966) 4081-4084.
- [25] A. Ratkiewicz, B. Bankiewicz, T.N. Truong, Kinetics of thermoneutral intermolecular hydrogen migration in alkyl radicals, *Phys. Chem. Chem. Phys* 12 (2010) 10988-10995.
- [26] B. Bankiewicz, L.K. Huynh, A. Ratkiewicz, T.N. Truong, Kinetics of 1,4-Hydrogen Migration in the Alkyl Radical Reaction Class, *J. Phys. Chem. A* 113 (2009) 1564-1573.
- [27] S.H. Robertson, M.J. Pilling, L.C. Jitariu, I.H. Hillier, Master equation methods for multiple well systems: application to the 1-,2-pentyl system, *Phy. Chem. Chem. Phys* 9 (2007) 4085-4097.
- [28] C.J. Hayes, D.R. Burgess, Kinetic Barriers of H-Atom Transfer Reactions in Alkyl, Allylic, and Oxoallylic Radicals as Calculated by Composite Ab Initio Methods, *J. Phys. Chem. A* 113 (2009) 2473-2482.
- [29] D.M. Matheu, W.H. Green, J.M. Grenda, Capturing pressure-dependence in automated mechanism generation: reactions through cycloalkyl intermediates, *Int. J. Chem. Kinet.* 35 (2003) 95-119.
- [30] C.-W. Zhou, Y. Li, U. Burke, C. Banyon, K.P. Somers, S. Ding, S. Khan, J.W. Hargis, T. Sikes, O. Mathieu, e. al, An experimental and chemical kinetic modeling study of 1,3-butadiene combustion: Ignition delay time and laminar flame speed measurements, *Combust. Flame* 197 (2018) 423-438.
- [31] M.J. Frisch, G.W. Trucks, H.B. Schlegel, G.E. Scuseria, M.A. Robb, J.R. Cheeseman, G. Scalmani, V. Barone, G.A. Petersson, H. Nakatsuji, et. al., *Gaussian 09*, 2009.
- [32] M.J. Frisch, G.W. Trucks, H.B. Schlegel, G.E. Scuseria, M.A. Robb, J.R. Cheeseman, G. Scalmani, V. Barone, G.A. Petersson, H. Nakatsuji, et. al., *Gaussian 16 Rev. B.01*, Wallingford, CT, 2016.
- [33] J.-D. Chai, M. Head-Gordon, Long-range corrected hybrid density functionals with damped atom-atom dispersion corrections, *Phys. Chem. Chem. Phys.* 10 (2008) 6615-6620.
- [34] T.H. Dunning, Gaussian-basis sets for use in correlated molecular calculations .1. The atoms boron through neon and hydrogen, *J. Chem. Phys.* 90 (1989) 1007-1023.
- [35] Y. Georgievskii, J.A. Miller, M.P. Burke, S.J. Klippenstein, Reformulation and solution of the master equation for multiple-well chemical reactions, *J. Phys. Chem. A* 117 (2013) 12146-12154.
- [36] C.F. Goldsmith, G.R. Magoon, W.H. Green, Database of small molecule thermochemistry for combustion, *J. Phys. Chem. A* 116 (2012) 9033-9057.
- [37] T.J. Lee, P.R. Taylor, A Diagnostic for Determining the Quality of Single-Reference Electron Correlation Methods, *Int. J. Quantum Chem.*, doi:10.1002/qua.560360824(1989) 199-207.
- [38] B. Ruscic, R.E. Pinzon, M.L. Morton, G. von Laszewski, S.J. Bittner, S.G. Nijsure, K.A. Amin, M. Minkoff, A.F. Wagner, Introduction to active thermochemical tables: several “key” enthalpies of formation revisited, *J. Phys. Chem. A* 108 (2004) 9979-9997.

- [39] B. Ruscic, R.E. Pinzon, G.v. Laszewski, D. Kodeboyina, A. Burcat, D. Leahy, D. Montoy, A.F. Wagner, Active thermochemical tables: thermochemistry for the 21st century, *J. Phys.* 16 (2005) 561-570.
- [40] S.J. Klippenstein, L.B. Harding, B. Ruscic, Ab initio computations and active thermochemical tables hand in hand: heats of formation of core combustion species, *J. Phys. Chem. A* 121 (2017) 6580-6602.
- [41] J.M. Simmie, K.P. Somers, Benchmarking compound methods (CBS-QB3, CBS-APNO, G3, G4, W1BD) against the active thermochemical tables: a litmus test for cost-effective molecular formation enthalpies, *J. Phys. Chem. A* 119 (2015) 7235-7246.
- [42] K.P. Somers, J.M. Simmie, Benchmarking compound methods (CBS-QB3, CBS-APNO, G3, G4, W1BD) against the active thermochemical tables: formation enthalpies of radicals, *J. Phys. Chem. A* 119 (2015) 8922-8933.
- [43] J.M. Simmie, K.P. Somers, W.K. Metcalfe, H.J. Curran, Substituent effects in the thermochemistry of furans: A theoretical (CBS-QB3, CBS-APNO and G3) study, *J. Chem. Thermodyn.* 58 (2013) 117-128.
- [44] J.M. Simmie, G. Black, H.J. Curran, J.P. Hinde, Enthalpies of formation and bond dissociation energies of lower alkyl hydroperoxides and related hydroperoxy and alkoxy radicals, *J. Phys. Chem. A* 112 (2008) 5010-5016.
- [45] B.J. McBride, S. Gordon, Computer program for calculating and fitting thermodynamic functions, (1992).
- [46] H.S. Johnston, J. Heicklen, Tunnelling corrections for unsymmetrical Eckart potential energy barriers, *J. Phys. Chem.* 66 (1962) 532-533.
- [47] A.W. Jasper, J.A. Miller, Lennard-Jones parameters for combustion and chemical kinetics modeling from full-dimensional intermolecular potentials, *Combust. Flame* 161 (2014) 101-110.
- [48] S. Peukert, P. Yatsenko, M. Fikri, C. Schulz, High-Temperature Rate Constants for the Reaction of Hydrogen Atoms with Tetramethoxysilane and Reactivity Analogies between Silanes and Oxygenated Hydrocarbons, *J. Phys. Chem. A* 122 (2018) 5289-5298.
- [49] S. Peukert, P. Sela, D. Nativel, J. Herzler, M. Fikri, C. Schulz, Direct Measurement of High-Temperature Rate Constants of the Thermal Decomposition of Dimethoxymethane, a Shock Tube and Modeling Study, *J. Phys. Chem. A* 122 (2018) 7559-7571.
- [50] T. Bentz, M. Szöri, B. Viskolcz, M. Olzmann, Pyrolysis of Ethyl Iodide as Hydrogen Atom Source: Kinetics and Mechanism in the Temperature Range 950-1200K, 2011.
- [51] A. Matsugi, K. Suma, A. Miyoshi, Kinetics and Mechanisms of the Allyl + Allyl and Allyl + Propargyl Recombination Reactions, *J. Phys. Chem. A* 115 (2011) 7610-7624.
- [52] A.Y. Chang, J.W. Bozzelli, A.M. Dean, Kinetic Analysis of Complex Chemical Activation and Unimolecular Dissociation Reactions using QRRK Theory and the Modified Strong Collision Approximation, *Zeitschrift für Physikalische Chemie*, 2000, pp. 1533.
- [53] A.M. Dean, Predictions of pressure and temperature effects upon radical addition and recombination reactions, *J. Phys. Chem.* 89 (1985) 4600 - 4608.
- [54] J.W. Bozzelli, A.Y. Chang, A.M. Dean, Molecular density of states from estimated vapor phase heat capacities, *Int. J. Chem. Kinet.* 29 (1997) 161-170.
- [55] E.R. Ritter, J.W. Bozzelli, THERM: Thermodynamic property estimation for gas phase radicals and molecules, *Int. J. Chem. Kinet.* 23 (1991) 767-778.
- [56] T.C. Brown, K.D. King, T.T. Nguyen, Kinetics of primary processes in the pyrolysis of cyclopentanes and cyclohexanes, *The Journal of Physical Chemistry* 90 (1986) 419-424.
- [57] W. Tsang, Thermal decomposition of cyclopentane and related compounds, *Int. J. Chem. Kinet.* 10 (1978) 599-617.
- [58] M. Taniewski, Investigations on the thermal decomposition of olefins, *Proc. Royal Soc. Lond. Series A. Mathematical and Physical Sciences* 265 (1962) 519-537.

- [59] R. Kalinenko, E. Buravtseva, N. Nametkin, G. Bach, W. Zychlinskii, G. Zimmermann, Variation of reaction-rate constants with hydrocarbon chain-length in the pyrolysis of paraffins and alpha-olefins in different types of reactors., *Kinetics and Catalysis* 24 (1983) 873-879.
- [60] H.K. Shibatani, H. , Thermal Decomposition of Alkenes. II. Thermal Decomposition of 1-Pentene, *Nippon Kagaku Kaishi*, 2 (1973).
- [61] Y. Li, S.J. Klippenstein, C.-W. Zhou, H.J. Curran, Theoretical Kinetics Analysis for H Atom Addition to 1,3-Butadiene and Related Reactions on the  $\dot{C}_4H_7$  Potential Energy Surface, *J. Phys. Chem. A* 121 (2017) 7433-7445.
- [62] Y. Sun, C.-W. Zhou, K.P. Somers, H.J. Curran, Ab Initio/Transition-State Theory Study of the Reactions of  $\dot{C}_5H_9$  Species of Relevance to 1,3-Pentadiene, Part I: Potential Energy Surfaces, Thermochemistry, and High-Pressure Limiting Rate Constants, *The Journal of Physical Chemistry A* 123 (2019) 9019-9052.
- [63] J.A. Miller, S.J. Klippenstein, The  $H + C_2H_2 (+M) \rightleftharpoons C_2H_3 (+M)$  and  $H + C_2H_2 (+M) \rightleftharpoons C_2H_5 (+M)$  reactions: Electronic structure, variational transition-state theory, and solutions to a two-dimensional master equation, *Phys. Chem. Chem. Phys.* 6 (2004) 1192-1202.
- [64] W. Tsang, Chemical Kinetic Data Base for Combustion Chemistry. Part 3: Propane, *J. Phys. Chem. ref. data.* 17 (1988) 887-951.
- [65] W. Tsang, Chemical Kinetic Data Base for Combustion Chemistry Part V. Propene, *J. Phys. Chem. ref. data.* 20 (1991) 221-273.
- [66] Y.-X. Liu, Z.-Y. Tian, Oxidation chemistry of four C<sub>9</sub>H<sub>12</sub> isomeric transportation fuels: Experimental and modeling studies, *Combustion and Flame* 205 (2019) 165-179.
- [67] S.-H. Li, J.-J. Guo, R. Li, F. Wang, X.-Y. Li, Theoretical Prediction of Rate Constants for Hydrogen Abstraction by OH, H, O, CH<sub>3</sub>, and HO<sub>2</sub> Radicals from Toluene, *J. Phys. Chem. A* 120 (2016) 3424-3432.
- [68] Y. Zhang, K.P. Somers, M. Mehl, W.J. Pitz, R.F. Cracknell, H.J. Curran, Probing the antagonistic effect of toluene as a component in surrogate fuel models at low temperatures and high pressures. A case study of toluene/dimethyl ether mixtures, *Proc. Combust. Inst.* 36 (2017) 413-421.
- [69] A Chemkin-Pro - ANSYS Reaction Design: San Diego.
- [70] A. Burcat, B. Ruscic, Third millenium ideal gas and condensed phase thermochemical database for combustion (with update from active thermochemical tables), Argonne National Lab.(ANL), Argonne, IL (United States), 2005.
- [71] K. Wiberg, D. Wasserman, E. Martin, Enthalpies of hydration of alkenes. II: the n-heptenes and n-pentenes, *J. Phys. Chem.* 88 (1984) 3684-3688.
- [72] W.V. Steele, R.D. Chirico, Thermodynamic Properties of Alkenes (Mono-Olefins Larger than C<sub>4</sub>), *J. Phys. Chem. ref. data.* 22 (1993) 377-430.
- [73] W.D. Good, N.K. Smith, The enthalpies of combustion of the isomeric pentenes in the liquid state. A warning to combustion calorimetrists about sample drying, *J. Chem. Thermodyn.* 11 (1979) 111-118.
- [74] W.D. Good, The enthalpies of combustion and formation of n-octane and 2,2,3,3-tetramethylbutane, *J. Chem. Thermodyn.* 4 (1972) 709-714.
- [75] K.S. Pitzer, W.D. Gwinn, Energy Levels and Thermodynamic Functions for Molecules with Internal Rotation : I. Rigid Frame with Attached Tops, *Molecular Structure and Statistical Thermodynamics*, pp. 33-46.
- [76] H.J. Curran, P. Gaffuri, W.J. Pitz, C.K. Westbrook, A Comprehensive Modeling Study of n-Heptane Oxidation, *Combust. Flame* 114 (1998) 149-177.

[77] K. Wang, S.M. Villano, A.M. Dean, Reactivity–Structure-Based Rate Estimation Rules for Alkyl Radical H Atom Shift and Alkenyl Radical Cycloaddition Reactions, *J. Phys. Chem. A* 119 (2015) 7205-7221.

[78] J. Zheng, T. Yu, E. Papajak, I.M. Alecu, S.L. Mielke, D.G. Truhlar, Practical methods for including torsional anharmonicity in thermochemical calculations on complex molecules: The internal-coordinate multi-structural approximation, *Phys. Chem. Chem. Phys.* 13 (2011) 10885-10907.

# **Chapter 3 : A Theoretical Study of the Reaction of Hydrogen Atoms with Three Pentene Isomers; 2-Methyl-1-Butene, 2-Methyl-2-Butene, and 3-Methyl-1-Butene.**

Published in: *J. Phys. Chem. A*.124(51) (2020) 10649–10666

Publication Date: December 15, 2020

DOI: <https://doi.org/10.1021/acs.jpca.0c06389>

## Author Contributions

- (1) Jennifer Power: Performed electronic structure calculations, modelling work and wrote the manuscript
- (2) Kieran P. Somers: Provided input for theoretical and modelling work. Reviewed the manuscript prior and post review process.
- (3) Shashank Nagaraja: Performed pyrolysis experiments.
- (4) Weronika Wyrebak: Performed electronic structure calculations.
- (5) Henry J. Curran: Managed the project throughout and reviewed the manuscript prior and post review process.





## Abstract

This paper presents a comprehensive potential energy surface (PES) for hydrogen atom addition to and abstraction from 2-methyl-1-butene, 2-methyl-2-butene, and 3-methyl-1-butene and the subsequent  $\beta$ -scission, and H-atom transfer reactions. Thermochemical parameters for species on the  $\dot{C}_5H_{11}$  potential energy surface (PES) were calculated as a function of temperature (298 – 2000 K), using a series of isodesmic reactions to determine the formation enthalpies. High-pressure limiting and pressure-dependent rate constants were calculated using Rice-Ramsperger-Kassel-Marcus theory with a one-dimensional master equation. A number of studies have highlighted the fact that  $C_5$  intermediate species play a role in poly-aromatic hydrocarbon formation and that a fuel's chemical structure can be key in understanding the intermediate species formed during fuel decomposition.

Rate constant recommendations for both  $\dot{H}$  atom addition to, and abstraction from, linear and branched alkenes have subsequently been proposed by incorporating our earlier work on 1- and 2-pentene, and these can be used in mechanisms of larger alkenes for which calculations do not exist. The current set of rate constants for the reactions of  $\dot{H}$  atoms with both linear and branched  $C_5$  alkenes, including their chemically activated pathways, are the first available in the literature of any reasonable fidelity for combustion modelling and are important for gasoline mechanisms. Validation of our theoretical results with pyrolysis experiments of 2-methyl-1-butene, 2-methyl-2-butene, and 3-methyl-1-butene at 2 bar in a single pulse shock tube (SPST) were carried out, with satisfactory agreement observed.

## 1. Introduction

Alkenes are key components of commercial fuels and are formed as intermediates during the pyrolysis and oxidation of alkanes. Despite their importance, alkenes have not been as extensively studied as alkanes, especially pentene, which is a major component of gasoline [1, 2]. Understanding alkene combustion chemistry is therefore important in our understanding of all hydrocarbon fuel combustion and hierarchical mechanism development [3]. Based on previous studies of propene [4] and the butene isomers [5, 6], it was found that  $\dot{H}$  atom addition to the  $C=C$  double bond plays an important role in controlling experimental high-temperature ignition delay times (IDTs), laminar burning velocities (LBVs) and species profiles measured as a function of temperature and/or time in jet-stirred and flow reactors.

Recent studies have shown that reactions of  $C_5$  hydrocarbon intermediate species play a role in aromatic ring formation combustion processes [7], and that PAH formation pathways can depend on the specific chemical structure of the fuel molecule. Therefore, a deeper

understanding of fuel specific decomposition pathways and isomer specific combustion is of great interest, especially for C<sub>5</sub> fuels, for which few studies exist [8-10].

Following our previous work on the reactions of hydrogen atoms with 1- and 2-pentene [2] (C<sub>5</sub>H<sub>10-1</sub> and C<sub>5</sub>H<sub>10-2</sub>), this study will focus on the reactions of hydrogen atoms with three branched pentene isomers; 2-methyl-1-butene (2M1B or aC<sub>5</sub>H<sub>10</sub>), 2-methyl-2-butene (2M2B or bC<sub>5</sub>H<sub>10</sub>) and 3-methyl-1-butene (3M1B or cC<sub>5</sub>H<sub>10</sub>).

**Table 3.1:** List of Experimental and Theoretical Data of Related Studies.

Year	Author	Fuel	Type of study	Measurement	Method
2015	Westbrook et al. [11]	2M2B	Experimental / Modelling	Ignition delay times & species mole fractions	shock-tube and jet-stirred reactor
2017	Cheng et al.[12]	<i>n</i> -C <sub>5</sub> H <sub>12</sub> , C <sub>5</sub> H <sub>10-1</sub> , C <sub>5</sub> H <sub>10-2</sub> , 2M2B	Experimental / Modelling	Laminar flame speeds	Constant volume combustion bomb
2017	Ruwe et al.[9]	2M2B	Experimental	Species mole fractions	Flame sampling molecular beam mass spectrometry / vacuum-ultraviolet single-photon ionisation
2018	Ruwe et al.[10]	<i>n</i> -C <sub>5</sub> H <sub>12</sub> , C <sub>5</sub> H <sub>10-1</sub> , 2M2B	Experimental	Species mole fractions	Flame sampling molecular beam mass spectrometry / vacuum-ultraviolet single-photon ionisation
2018	Zhong et al.[13]	2M2B	Experimental	Laminar flame speeds	Constant volume combustion bomb
2019	Leon et al.[8]	<i>n</i> -C <sub>5</sub> H <sub>12</sub> , 2M2B	Experimental / Modelling	Species mole fractions	Flame sampling molecular beam mass spectrometry / vacuum-ultraviolet single-photon ionisation
2020	Nagaraja et al.[14]	C <sub>5</sub> H <sub>10-1</sub> , C <sub>5</sub> H <sub>10-2</sub> , 2M1B, 2M2B, 3M1B	Experimental / Modelling	Species mole fractions	ωB97XD /aug-cc-pVTZ / Single-pulse shock-tube / gas chromatography/mass spectrometry
2020	Arafin et al.[15]	2M1B, 2M2B, 3M1B	Experimental / Modelling	IDTs & carbon monoxide (CO) time histories	Shock-tube / laser absorption

There have been a number of experimental and mechanistic studies of 2M2B [8-13] but there are few theoretical studies available for all of the branched pentene isomers. 2M2B has a RON of 97.3 and a MON of 84.7, thus showing a high octane sensitivity and anti-knock properties, and is therefore a promising fuel for engine applications [11, 16]. 2M2B can also serve as a model compound for larger hydrocarbons containing linear and branched structures. However, the formation of allylic radicals due to the presence of multiple allylic bonds, influences the fuel specific reaction kinetics which include the formation pathways to PAHs as the resonantly stabilised radicals accumulate in high concentrations and do not undergo scission to smaller radicals [17, 18].

Westbrook et al. [11] carried out experimental studies on the oxidation of 2M2B, measuring IDTs behind reflected shock waves and fuel, intermediate and product species mole fractions in a jet-stirred reactor (JSR). These JSR experiments were the first to report detailed species measurements for an unsaturated, branched hydrocarbon larger than isobutene.

Cheng et al. [12] carried out an experimental and kinetic modelling study of C<sub>5</sub>H<sub>10</sub>-1, C<sub>5</sub>H<sub>10</sub>-2, 2M2B and *n*-C<sub>5</sub>H<sub>12</sub> (*n*-pentane) in laminar flames using a constant volume combustion bomb. They were able to study the roles of differences between alkanes and alkenes and of the branched structures in flame speed measurements. It was found that the laminar flame speeds increased in the order: 2M2B < *n*-C<sub>5</sub>H<sub>12</sub> < C<sub>5</sub>H<sub>10</sub>-2 < C<sub>5</sub>H<sub>10</sub>-1.

Ruwe et al. [9] studied the consumption and hydrocarbon growth processes in a 2M2B flame using flame sampling molecular beam mass spectrometry (MBMS) with vacuum-ultraviolet single-photon ionisation in order to gain new insights into its combustion chemistry, which is expected to be dominated by allylic-type resonantly stabilised radicals. Their experimental data are in the form of isomer-resolved species mole fraction profiles as a function of height above the burner. The results imply that 2M2B consumption proceeds through H-atom abstraction at the allylic carbon sites as well as  $\dot{\text{H}}$  atom addition reactions to the double bond.

To understand the fuel-structure-dependent C<sub>5</sub> chemistry involved in PAH formation Ruwe et al. [10] subsequently studied the high temperature oxidation kinetics of *n*-C<sub>5</sub>H<sub>12</sub>, C<sub>5</sub>H<sub>10</sub>-1 and 2M2B experimentally in laminar non-premixed opposed-flow diffusion flames. Molecular beam mass spectrometry (MBMS) employing electron ionisation (EI) was used for the simultaneous detection of nearly all species involved in the combustion process. Supportive MBMS measurements using single-photon ionisation (PI) by tuneable synchrotron-generated vacuum-ultraviolet (VUV) radiation was used to gain insight into the fuel-specific reaction kinetics of PAH formation tendencies for the C<sub>5</sub>H<sub>10</sub>-1 and 2M2B flames. It was shown that the formation tendency of species, such as PAHs yielded through mass growth reactions increases considerably in the order *n*-C<sub>5</sub>H<sub>12</sub> < C<sub>5</sub>H<sub>10</sub>-1 < 2M2B.

Zhong et al. [13] studied the pressure dependence of laminar flame speed of 2M2B/air flames in the 1.0 – 10 bar range in a spherical constant volume bomb. An empirical correlation describing the dependence of laminar flame speed was proposed and validated by experimental laminar flame speed results.

Leon et al. [8] developed a mechanism based upon previously validated mechanisms [19-23] in order to identify the important carbon growth reactions in a 2M2B flame compared to

an  $n$ -C<sub>5</sub>H<sub>12</sub> flame. To make the mechanism more comprehensive, rate constants and their temperature dependencies were then subsequently added to this mechanism by using existing ones in the literature and analogies where required. Agreement of their mechanism with speciation data for 2M2B and their newly measured mole fraction data for a fuel-rich ( $\phi = 1.8$ )  $n$ -C<sub>5</sub>H<sub>12</sub> flame, in which species profiles up to phenol were quantified using the low-pressure flame apparatus coupled with flame-sampling molecular-beam mass spectrometry (PI-MBMS) were then found to be satisfactory.

Nagaraja et al. [14], performed a single pulse shock-tube study, where five pentene isomers were pyrolyzed in a single pulse shock-tube using gas chromatography–mass spectrometry (GC–MS) analyses to identify product species for C<sub>5</sub>H<sub>10</sub>-1, C<sub>5</sub>H<sub>10</sub>-2, 2M1B, 2M2B and 3M1B which were then quantified using flame ionisation detection (FID) to demonstrate the effect of fuel molecular structure on pyrolysis. The simulations performed were conducted using NUIGMech1.0 [14, 24-27], including preliminary quantum chemical results from the present study which are discussed in detail herein.

To the best of our knowledge, the most recent study of the pentene isomers is by Arafin et al. [15], where a shock-tube and laser absorption study was carried out on 2M1B, 2M2B and 3M1B, measuring IDTs and carbon monoxide (CO) time histories behind reflected shock waves at high temperatures (1350 – 1630 K) and pressures (8.3 – 10.5 atm) for stoichiometric mixtures of 0.075% fuel in O<sub>2</sub>/Ar. It was found that 3M1B is fastest to ignite, while 2M1B dissociates earlier but ignites later than 2M2B. Their measured CO time-histories were compared with mechanisms from Leon/Ruwe [8], AramcoMech3.0 [28] and Westbrook et al. [11]. The Westbrook et al. [11] model performed better than AramcoMech3.0 and that of Leon/Ruwe et al. in predicting the slopes of accelerated CO formation near ignition and the rapid CO depletion for all three isomers. However, it falls short in capturing IDTs and the initial rate of CO formation.

While these studies give an excellent insight into the understanding of C<sub>5</sub> combustion, the mechanisms used rely on rate rules and estimates with analogous reactions for kinetic parameters. As fore-mentioned, limited theoretical studies exist in the literature for all of the pentene isomers. One of the main aims of the current work is to therefore provide accurate kinetics and thermochemistry using the same level of theory for the reactions of  $\dot{H}$  atoms with all of the pentene isomers, which can be used in the development of combustion models. Also, the discrepancies observed between the rate constants calculated in the current work and other literature studies [8, 11, 29] suggests that a refinement of these reaction systems is necessary.

This study is the first to address the reactions of  $\dot{\text{H}}$  atoms with 2-methyl-1-butene, 2-methyl-2-butene and 3-methyl-1-butene, and together with our previous paper on 1- and 2-pentene +  $\dot{\text{H}}$ , including  $\dot{\text{H}}$ -ARAS experiments which are the only experiments to directly measure  $\dot{\text{H}}$  +  $\text{C}_5$  alkene chemistry [2], the results are the most comprehensive investigation of these reaction systems. Figure 3.1 illustrates the naming nomenclature for the  $\text{C}_5$  species considered in this work, with Table 3.2 providing the names and structures of these species. Table 3.3 provides a list of reactions considered in this study, with their corresponding reaction number, which will be used throughout. In the current study, there are six  $\dot{\text{H}}$  atom addition/C–H scission reactions, leading to four  $\dot{\text{C}}_5\text{H}_{11}$  radicals. Each radical can isomerise and  $\beta$ -scission and we account for all of them. The H-atom abstraction reactions have also been considered.

Thermochemical parameters for  $\text{C}_5$  species on the  $\dot{\text{C}}_5\text{H}_{11}$  PES are calculated, with the enthalpies of formation determined using a series of isodesmic reactions. High-pressure limiting and pressure-dependent rate constants are also calculated using RRKM/ME analysis for reactions on the  $\dot{\text{C}}_5\text{H}_{11}$  PES, including their chemically activated pathways. Section 2 describes the methodology for both electronic structure calculations and thermochemistry and Section 3 presents the theoretical results and comparisons of these results with literature, where possible. Section 4 presents the kinetic modelling results of the experiments by Nagaraja et al. [14].

Additionally, rate constant recommendations for both  $\dot{\text{H}}$  atom addition to, and abstraction from, linear and branched alkenes have been proposed and provide a useful tool for the use in mechanisms of larger alkenes for which calculations do not exist.

## 2. Computational Details

### 2.1. Electronic Structure Calculations

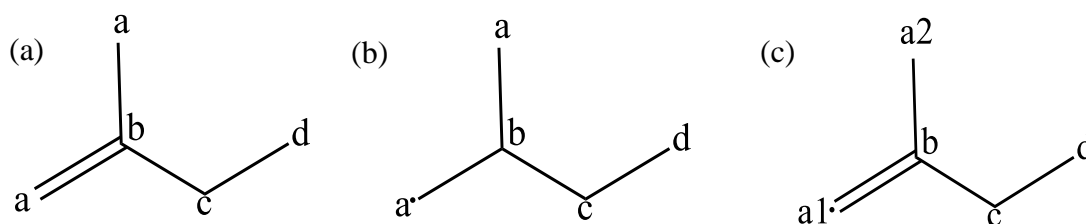
The methods are similar to those in our previous studies and were adopted for all of the electronic structure calculations using Gaussian 09 and 16 [30, 31]. Since many of the species have multiple equilibrium geometries, conformational searches were carried out to obtain the minimum energy structure of all PES minima and saddle points, with details of the conformational sampling described in our earlier study [2]. The resulting lowest-energy-conformer was optimised using the  $\omega\text{B97XD}$  /aug-cc-pVTZ method, with harmonic frequency analysis simultaneously carried out to verify the nature of each stationary point, with a single imaginary frequency indicative of a saddle point structure.

Low frequency torsional modes were treated via relaxed PES scans carried out with a ten degree increment at the  $\omega$ B97XD/6-311++G(d,p) level of theory. The potential energies as a function of dihedral angle were then used as input for a 1-D hindered rotor approximation as implemented in MESS [32]. Single point energies for minima and saddle points were calculated at the CCSD(T)/cc-pVXZ and MP2/cc-pVXZ (where X = D, T and Q) levels of theory. The resulting energies were extrapolated to the complete basis set (CBS) limit using the following formula (1) [33].

$$E_{\text{CCSD(T)/CBS}} = E_{\text{CCSD(T)/cc-pVTZ}} + (E_{\text{CCSD(T)/cc-pVTZ}} - E_{\text{CCSD(T)/cc-pVDZ}}) (3^4 / 4^4 - 3^4) + E_{\text{MP2/cc-pVQZ}} + (E_{\text{MP2/cc-pVQZ}} - E_{\text{MP2/cc-pVTZ}}) (4^4 / 5^4 - 4^4) - E_{\text{MP2/cc-pVTZ}} - (E_{\text{MP2/cc-pVTZ}} - E_{\text{MP2/cc-pVDZ}}) (3^4 / 4^4 - 3^4). \quad (1)$$

The  $T_1$  diagnostic for closed shell species is less than  $\sim 0.02$ , and for radicals less than  $\sim 0.03$ , indicating that single reference methods to describe the wave function are appropriate [33, 34]. A table of  $T_1$  values for the different  $C_5$  species and transition states is available in the Supplementary material.

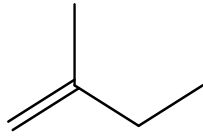
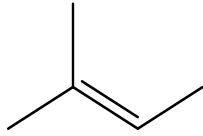
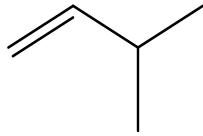
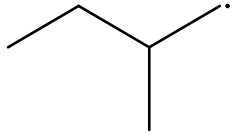
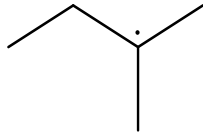
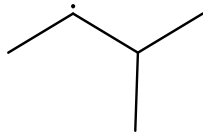
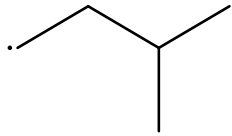
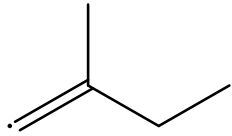
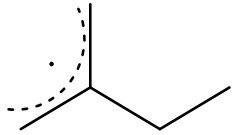
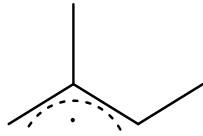
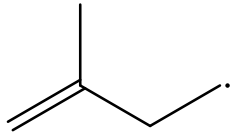
## 2.2. Naming scheme for $C_5$ species on the $\dot{C}_5H_{11}$ PES

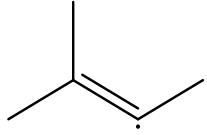
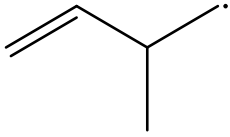
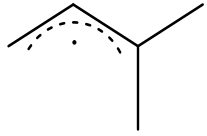
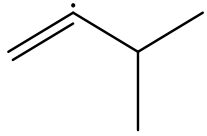
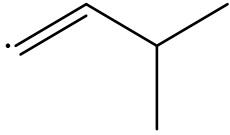


**Figure 3.1.** (a) Schematic of  $aC_5H_{10}$ , (b)  $a\dot{C}_5H_{11}$ , and (c)  $a\dot{C}_5H_9-a1$ .

Figure 3.1(a) presents a schematic of the structures  $aC_5H_{10}$  (2-methyl-1-butene), where the letters a, b, c, and d indicate the positions of the carbon sites. The labelling system is used to assign the position of the double bonds and radical sites. In Figure 3.1(a), 2-methyl-1-butene is written as  $aC_5H_{10}$ , indicating that the C=C double bond is at the “a” position. Thus 2-methyl-2-butene and 3-methyl-1-butene can be written as  $bC_5H_{10}$  and  $cC_5H_{10}$ , respectively. Figure 3.1(b) presents a schematic of the  $a\dot{C}_5H_{11}$  radical, where the radical on the “a” position. Figure 3.1(c) represents the  $a\dot{C}_5H_9-a1$  radical, where the letter following the  $a\dot{C}_5H_9$  name indicates the site of the abstracted hydrogen atom.

**Table 3.2:** C<sub>5</sub> Species Considered in This Work.

Species	Structure
aC <sub>5</sub> H <sub>10</sub>	
bC <sub>5</sub> H <sub>10</sub>	
cC <sub>5</sub> H <sub>10</sub>	
aĊ <sub>5</sub> H <sub>11</sub>	
bĊ <sub>5</sub> H <sub>11</sub>	
cĊ <sub>5</sub> H <sub>11</sub>	
dĊ <sub>5</sub> H <sub>11</sub>	
aĊ <sub>5</sub> H <sub>9</sub> -a1	
aĊ <sub>5</sub> H <sub>9</sub> -a2	
aĊ <sub>5</sub> H <sub>9</sub> -c	
aĊ <sub>5</sub> H <sub>9</sub> -d	

$b\dot{C}_5H_9-c$	
$c\dot{C}_5H_9-a$	
$c\dot{C}_5H_9-b$	
$c\dot{C}_5H_9-c$	
$c\dot{C}_5H_9-d$	

**Table 3.3:** List of Reaction Channels Considered in This Work.

Reaction number	Reaction channel
R1	$aC_5H_{10} + \dot{H} \leftrightarrow a\dot{C}_5H_9-a1 + H_2$
R2	$aC_5H_{10} + \dot{H} \leftrightarrow a\dot{C}_5H_9-a2 + H_2$
R3	$aC_5H_{10} + \dot{H} \leftrightarrow a\dot{C}_5H_9-c + H_2$
R4	$aC_5H_{10} + \dot{H} \leftrightarrow a\dot{C}_5H_9-d + H_2$
R5	$bC_5H_{10} + \dot{H} \leftrightarrow a\dot{C}_5H_9-c + H_2$
R6	$bC_5H_{10} + \dot{H} \leftrightarrow b\dot{C}_5H_9-c + H_2$
R7	$bC_5H_{10} + \dot{H} \leftrightarrow c\dot{C}_5H_9-b + H_2$
R8	$cC_5H_{10} + \dot{H} \leftrightarrow c\dot{C}_5H_9-a + H_2$
R9	$cC_5H_{10} + \dot{H} \leftrightarrow c\dot{C}_5H_9-b + H_2$
R10	$cC_5H_{10} + \dot{H} \leftrightarrow c\dot{C}_5H_9-c + H_2$
R11	$cC_5H_{10} + \dot{H} \leftrightarrow c\dot{C}_5H_9-d + H_2$
R12	$aC_5H_{10} + \dot{H} \leftrightarrow a\dot{C}_5H_{11}$
R13	$aC_5H_{10} + \dot{H} \leftrightarrow b\dot{C}_5H_{11}$
R14	$bC_5H_{10} + \dot{H} \leftrightarrow b\dot{C}_5H_{11}$
R15	$bC_5H_{10} + \dot{H} \leftrightarrow c\dot{C}_5H_{11}$
R16	$cC_5H_{10} + \dot{H} \leftrightarrow c\dot{C}_5H_{11}$
R17	$cC_5H_{10} + \dot{H} \leftrightarrow d\dot{C}_5H_{11}$
R18	$a\dot{C}_5H_{11} \leftrightarrow C_3H_6 + \dot{C}_2H_5$
R19	$a\dot{C}_5H_{11} \leftrightarrow C_4H_8-1 + \dot{C}H_3$



R20	$b\dot{C}_5H_{11} \leftrightarrow iC_4H_8 + \dot{C}H_3$
R21	$c\dot{C}_5H_{11} \leftrightarrow C_4H_8-2 + \dot{C}H_3$
R22	$d\dot{C}_5H_{11} \leftrightarrow C_2H_4 + i\dot{C}_3H_7$
R23	$a\dot{C}_5H_{11} \rightleftharpoons b\dot{C}_5H_{11}$
R24	$a\dot{C}_5H_{11} \rightleftharpoons c\dot{C}_5H_{11}$
R25	$a\dot{C}_5H_{11} \rightleftharpoons d\dot{C}_5H_{11}$
R26	$b\dot{C}_5H_{11} \rightleftharpoons c\dot{C}_5H_{11}$
R27	$b\dot{C}_5H_{11} \rightleftharpoons d\dot{C}_5H_{11}$
R28	$c\dot{C}_5H_{11} \rightleftharpoons d\dot{C}_5H_{11}$

### 2.3. Thermochemistry

**Table 3.4:** Formation Enthalpies and Uncertainties ( $2\sigma$ ) via Isodesmic and Atomisation Methods.

Species	Isodesmic (0 K, kJ mol <sup>-1</sup> )	Isodesmic ( $2\sigma$ )	Atomisation (0 K, kJ mol <sup>-1</sup> )	Atomisation ( $2\sigma$ )	Burcat[35] (0 K, kJ mol <sup>-1</sup> )
aC <sub>5</sub> H <sub>10</sub>	-9.37	0.23	-7.78	14.03	-6.61 ± 8
bC <sub>5</sub> H <sub>10</sub>	-15.50	0.35	-13.95	14.29	-13.21 ± 8
cC <sub>5</sub> H <sub>10</sub>	-1.91	0.29	-0.43	13.81	-1.60 ± 8
a $\dot{C}_5H_{11}$	82.72	0.70	82.49	16.42	
b $\dot{C}_5H_{11}$	61.99	0.66	62.36	16.65	74.74 ± 8
c $\dot{C}_5H_{11}$	70.20	0.85	70.40	16.25	
d $\dot{C}_5H_{11}$	79.34	0.86	79.43	16.43	85.76 ± 8
a $\dot{C}_5H_9$ -a1	235.25	0.66	236.12	13.42	
a $\dot{C}_5H_9$ -a2	138.59	0.78	139.26	12.71	
a $\dot{C}_5H_9$ -c	128.97	0.70	129.28	12.81	
a $\dot{C}_5H_9$ -d	191.53	1.08	193.47	15.19	
b $\dot{C}_5H_9$ -c	213.66	0.73	214.65	13.19	
c $\dot{C}_5H_9$ -a	200.09	0.93	201.96	18.42	204.11 ± 8
c $\dot{C}_5H_9$ -b	122.44	0.68	122.21	12.69	126.52 ± 8
c $\dot{C}_5H_9$ -c	226.89	0.82	227.60	13.02	
c $\dot{C}_5H_9$ -d	240.07	0.94	240.86	13.64	243.19 ± 8

Units: enthalpies of formation (kJ mol<sup>-1</sup>).

Table 3.4 presents formation enthalpies and uncertainties ( $2\sigma$ ) computed *via* the isodesmic and atomisation methods. The same approach as in our previous study [2] was used in the current work to calculate the thermochemical properties of all C<sub>5</sub> species on the PES. Quantum chemical composite methods (CBS–QB3, CBS–APNO, G3 AND G4) [36–38] were used to calculate formation enthalpies at 0 K *via* a network of isodesmic reactions suitable for each species, using the most recent ATcT values [35, 39] for the molecular chaperones. Uncertainties in the enthalpies of formation of each species via the isodesmic approach were calculated using the methods described by Simmie et al. [40], and are described in our earlier work [2].

It is again observed that although the isodesmic and atomisation methods give similar nominal 0 K heats of formation, the uncertainties using the isodesmic approach are lower and are between 0.23 – 1.08 kJ mol<sup>-1</sup>. Tables of the isodesmic reactions used to calculate the 0 K heat of formation are provided as Supplementary material (SM). Temperature-dependent enthalpies, entropies and heat capacities were calculated using traditional statistical thermodynamics methods as implemented in MESSPF [32], with Chemkin format NASA polynomials fitted using PAC99 [41]. The fitted polynomials are provided in the Supplementary Material.

#### **2.4. Transition State Theory (TST), Rice Ramsperger–Kassel Marcus (RRKM) and Master Equation**

High-pressure limiting and pressure-dependent rate constants were calculated using RRKM theory with Master Equation (ME) analysis using the master equation system solver program, MESS [32]. Rate constants for thermally and chemically activated reactions are calculated over the temperature and pressure ranges 298 – 2000 K and 0.01 – 1000 respectively, which are fitted in PLOG format and provided as SM. Quantum mechanical tunnelling was accounted for by the inclusion of 1-D tunnelling through Eckart function [42]. For the collisional model, the average downward energy transfer parameter model was the same as our previous study [2] and was estimated as  $\langle \Delta E_{\text{down}}(T) \rangle = 202.5 \times (T/300)^{1.0} \text{ cm}^{-1}$  based on previously optimized values employed in studies of *sec*-butyl[43] and pentyl radical decompositions [44-46]. Lennard-Jones parameters of  $\sigma = 4.04 \text{ \AA}$  and  $\varepsilon = 235 \text{ cm}^{-1}$  were estimated for the  $\dot{\text{C}}_5\text{H}_{11}$  radicals by analogy to  $\text{C}_5\text{H}_{12}$ , whereas  $\sigma = 3.462 \text{ \AA}$  and  $\varepsilon = 89 \text{ cm}^{-1}$  were used for Ar [47].

### **3. Theoretical Results**

#### **3.1. Thermochemistry**

Table 3.5 presents enthalpy of formation comparisons with available literature data. Our values presented are our values computed via the isodesmic approach. There is reasonable agreement found between enthalpies of formation at 298 K computed in this work and literature. The heat of formation values at 298 K by Leon et al. [8] appear to be outliers when compared to those from this work, NIST, Burcat [48] and AramcoMech3.0 [28], Cheng et al. [12] and Westbrook et al. [11] However, as mentioned earlier, it is duly noted in their study [8] and in other studies that these semi-empirical methods used such as PM7 [49] may not be

the most accurate available for all molecules. Differences expressed as mean absolute error (MAE  $\pm 2\sigma$ ) between Leon [8] and this work were found to be  $44.31 \pm 48.74$  kJ mol<sup>-1</sup>.

**Table 3.5:** Enthalpy of Formation Comparisons of C<sub>5</sub> Species with Literature Data.

Name	$\Delta_f H_{298\text{ K}}$ this work	$\Delta_f H_{298\text{ K}}$ NIST	$\Delta_f H_{298\text{ K}}$ Leon [8]	$\Delta_f H_{298\text{ K}}$ Burcat [48]	$\Delta_f H_{298\text{ K}}$ AramcoMech3.0 [28]	$\Delta_f H_{298\text{ K}}$ Cheng [12]	$\Delta_f H_{298\text{ K}}$ Westbrook [11]
aC <sub>5</sub> H <sub>10</sub>	-36.39	-35.1 $\pm$ 0.84	-41.57	-33.92	-37.87	-37.87	-37.87
bC <sub>5</sub> H <sub>10</sub>	-42.52	-41.5 $\pm$ 0.88	-57.03	-39.79	-49.04	-49.04	-49.04
cC <sub>5</sub> H <sub>10</sub>	-28.84	-25.5	-25.42	-28.14	-33.22	-33.22	-33.22
aC <sub>5</sub> H <sub>11</sub>	53.05		5.93		53.27	52.64	53.27
bC <sub>5</sub> H <sub>11</sub>	33.60	28.0 $\pm$ 3.0	-45.00	43.72	30.55	28.75	30.55
cC <sub>5</sub> H <sub>11</sub>	41.02		-23.03		40.38	39.75	40.38
dC <sub>5</sub> H <sub>11</sub>	50.04		2.19	55.71	53.27	52.64	53.27
aC <sub>5</sub> H <sub>9</sub> -a1	213.19						211.48
aC <sub>5</sub> H <sub>9</sub> -a2	114.60		74.55		111.93	111.93	111.93
aC <sub>5</sub> H <sub>9</sub> -c	104.93		51.05		101.89	101.89	104.36
aC <sub>5</sub> H <sub>9</sub> -d	169.41		102.30		167.38	167.38	168.76
bC <sub>5</sub> H <sub>9</sub> -c	191.48						
cC <sub>5</sub> H <sub>9</sub> -a	178.60		121.85	180.35	172.02	172.02	172.02
cC <sub>5</sub> H <sub>9</sub> -b	98.48		45.06	102.48	104.44	104.44	104.53
cC <sub>5</sub> H <sub>9</sub> -c	204.04						
cC <sub>5</sub> H <sub>9</sub> -d	217.11			219.09			

<sup>a</sup>Units: enthalpies of formation (kJ mol<sup>-1</sup>).

Differences in heats of formation at 298 K between NIST database and this work are in reasonable agreement and are within  $2.81 \pm 4.13$  kJ mol<sup>-1</sup>. Agreement between AramcoMech3.0 [28] and this work are also reasonable and are within  $3.30 \pm 4.45$  kJ mol<sup>-1</sup>, while differences between this work and Burcat [48] database are slightly higher at  $3.92 \pm 6.02$  kJ mol<sup>-1</sup>. The thermochemistry adopted by both Cheng et al. [12] and Westbrook et al. [11] in their mechanisms are almost exactly the same as those in AramcoMech3.0 [28], which were calculated using THERM [50] with the exception of a few species. Heats of formation at 298 K by Cheng et al. [12] are within  $3.46 \pm 4.14$  kJ mol<sup>-1</sup>, while the value used by Westbrook et al. [11] is within  $2.89 \pm 4.70$  kJ mol<sup>-1</sup> of those calculated in the current work.

**Table 3.6:** Entropy Comparisons of C<sub>5</sub> Species with Literature Data (Units: J K<sup>-1</sup> mol<sup>-1</sup>).

Name	S <sub>298 K</sub> this work	S <sub>298 K</sub> Leon [8]	S <sub>298 K</sub> Burcat [48]	S <sub>298 K</sub> AramcoMech3.0 [28]	S <sub>298 K</sub> Cheng [12]	S <sub>298 K</sub> Westbrook [11]
aC <sub>5</sub> H <sub>10</sub>	338.18	346.60	342.01	339.27	339.27	339.27
bC <sub>5</sub> H <sub>10</sub>	336.51	356.28	337.68	328.48	328.48	328.48
cC <sub>5</sub> H <sub>10</sub>	336.73	336.70	349.98	334.50	334.50	334.50
aC <sub>5</sub> H <sub>11</sub>	366.17	358.29		364.80	365.01	364.80
bC <sub>5</sub> H <sub>11</sub>	370.87	375.83	359.01	362.62	361.11	362.62
cC <sub>5</sub> H <sub>11</sub>	365.29	370.67		363.00	363.21	363.00
dC <sub>5</sub> H <sub>11</sub>	358.28	353.74	344.87	359.06	359.27	359.07
aC <sub>5</sub> H <sub>9</sub> -a1	347.08					345.43
aC <sub>5</sub> H <sub>9</sub> -a2	339.71	337.89		335.25	335.25	335.26
aC <sub>5</sub> H <sub>9</sub> -c	335.09	348.30		323.33	323.33	323.67
aC <sub>5</sub> H <sub>9</sub> -d	354.18	352.38				352.75
bC <sub>5</sub> H <sub>9</sub> -c	343.93					
cC <sub>5</sub> H <sub>9</sub> -a	355.97		348.53	348.39	354.13	348.40
cC <sub>5</sub> H <sub>9</sub> -b	335.01	342.90	329.88	313.33	313.33	320.11
cC <sub>5</sub> H <sub>9</sub> -c	343.72					
cC <sub>5</sub> H <sub>9</sub> -d	342.18		335.40			

Table 3.6 presents entropy comparisons with available literature data. With the exception of Leon et al. [8], the differences in the entropies calculated in this work and published in literature are larger than those for the enthalpies. Differences between our computed entropies and those by Leon [8] are approximately  $6.88 \pm 11.32 \text{ J K}^{-1} \text{ mol}^{-1}$ , while differences between this work and Burcat [48] and AramcoMech3.0 are  $7.86 \pm 9.12$  and  $6.32 \pm 12.53 \text{ J K}^{-1} \text{ mol}^{-1}$ , respectively. Similar to the formation enthalpies, the entropies reported by Cheng et al. [12] and Westbrook et al. [11] are almost identical to those in AramcoMech3.0 [28] which were calculated using THERM [50] with the exception of a few species. Entropies at 298 K reported by Cheng et al. [12] are within  $5.92 \pm 12.95 \text{ J K}^{-1} \text{ mol}^{-1}$ , while the value used by Westbrook et al. [11] is within  $5.04 \pm 9.15 \text{ J K}^{-1} \text{ mol}^{-1}$  of those calculated in this work.

Table BS2 of Appendix B compares heat capacities for the common  $C_5$  species of NIST, Leon [8], Burcat [48], AramcoMech3.0 [28], Cheng [12] and Westbrook [11] with this work. For where common species exist, differences between this work and NIST are  $5.42 \pm 4.03 \text{ J K}^{-1} \text{ mol}^{-1}$ , however only heat capacity values at 298 K for three species are available. Differences in heat capacities between Leon et al. [8] are the largest and are  $19.52 \pm 16.76 \text{ J K}^{-1} \text{ mol}^{-1}$ . Reasonable agreement is observed for Burcat [48] and AramcoMech3.0 [28] when compared with this work, with differences being within  $3.52 \pm 4.79$  and  $3.70 \pm 9.92 \text{ J K}^{-1} \text{ mol}^{-1}$  for Burcat and AramcoMech3.0, respectively. Again, values reported by Cheng et al. and Westbrook et al. are similar to those in AramcoMech3.0 which were calculated by THERM, with the exception of a few species. The values used by Cheng et al. are within  $2.53 \pm 3.56 \text{ J K}^{-1} \text{ mol}^{-1}$ , while those used by Westbrook et al. are within  $3.20 \pm 4.21 \text{ J K}^{-1} \text{ mol}^{-1}$  of those calculated herein.

### 3.2. Potential energy surface (PES)

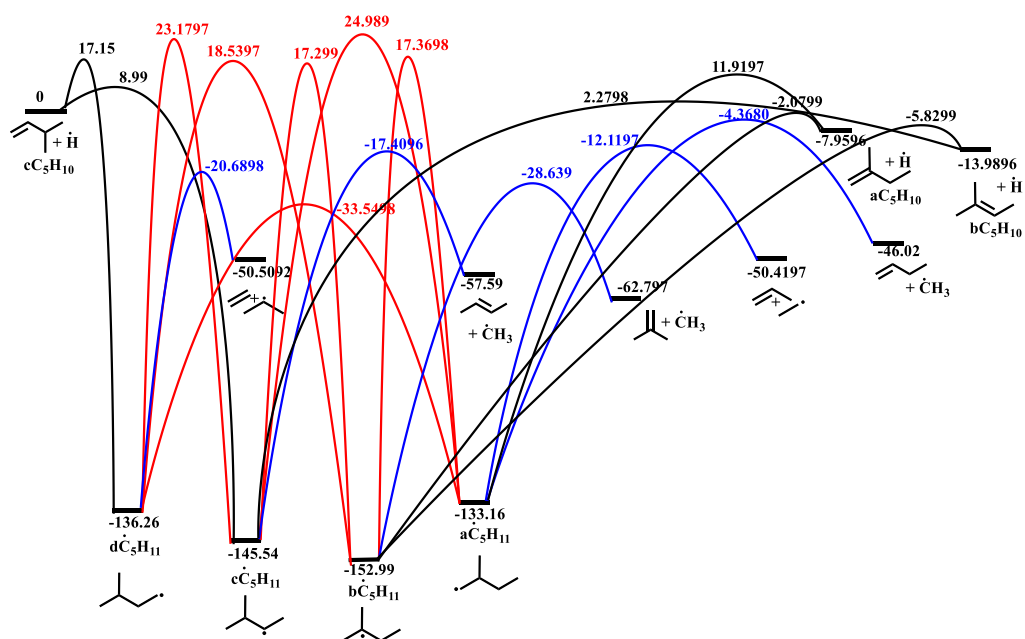


**Figure 3.2.** Potential energy surface for  $\dot{\text{H}}$  atom addition reactions of  $\text{aC}_5\text{H}_{10}$ ,  $\text{bC}_5\text{H}_{10}$  and  $\text{cC}_5\text{H}_{10}$ . Black lines represent  $\dot{\text{H}}$  atom addition reactions. C–C  $\beta$ -scission reactions are presented in blue and  $\dot{\text{H}}$  atom shift isomerisation reactions in red. Energies in  $\text{kJ mol}^{-1}$ .

#### 3.2.1. Reactions of $\dot{\text{H}}$ with the $\text{C}_5\text{H}_{10}$ isomers

Table 3.7 presents 0 K barriers, reaction enthalpies and high-pressure rate constant fits for the reactions of  $\dot{\text{H}}$  with the  $\text{C}_5\text{H}_{10}$  isomers.  $\text{aC}_5\text{H}_{10}$  has both internal addition (R12) and terminal addition (R13) reactions producing  $\text{a}\dot{\text{C}}_5\text{H}_{11}$  and  $\text{b}\dot{\text{C}}_5\text{H}_{11}$  radicals, respectively. An energy barrier of  $19.88 \text{ kJ mol}^{-1}$  is calculated for the internal addition, which is  $14.01 \text{ kJ mol}^{-1}$  greater than the terminal addition barrier of  $5.87 \text{ kJ mol}^{-1}$ . Addition to the terminal carbon is also much more favoured than internal addition as a tertiary radical ( $\text{b}\dot{\text{C}}_5\text{H}_{11}$ ) is formed, which is much more stable than the primary radical formed ( $\text{a}\dot{\text{C}}_5\text{H}_{11}$ ) through internal addition by  $19.83 \text{ kJ mol}^{-1}$ . The site of  $\dot{\text{H}}$  atom addition to the double bond of  $\text{aC}_5\text{H}_{10}$  forming the  $\text{a}\dot{\text{C}}_5\text{H}_{11}$  has a methyl substituent, which sterically hinders its addition, resulting in a higher barrier in comparison to addition to the site forming  $\text{b}\dot{\text{C}}_5\text{H}_{11}$ , which has no methyl substituents (Figure 3.2).

The two internal  $\dot{\text{H}}$  atom addition reactions to  $\text{bC}_5\text{H}_{10}$ , forming  $\text{b}\dot{\text{C}}_5\text{H}_{11}$  (R14) and  $\text{c}\dot{\text{C}}_5\text{H}_{11}$  (R15) radicals, have barriers of  $8.15$  and  $16.26 \text{ kJ mol}^{-1}$ , respectively. Again, it is observed that the addition pathway leading to the formation of a tertiary radical ( $\text{b}\dot{\text{C}}_5\text{H}_{11}$ ) is more favoured, which is to be expected as the stability of radicals increases from primary to tertiary

as there is more potential for hyper-conjugation to take place. Moreover, the site of  $\dot{\text{H}}$  atom addition to the double bond of  $\text{aC}_5\text{H}_{10}$  forming the  $\text{c}\dot{\text{C}}_5\text{H}_{11}$  has two methyl substituents, whereas the site of addition forming the  $\text{b}\dot{\text{C}}_5\text{H}_{11}$  has one. These steric effects again influence the reaction barriers.  $\text{cC}_5\text{H}_{10}$  has both internal (R17) and terminal addition (R16) reactions forming  $\text{c}\dot{\text{C}}_5\text{H}_{11}$  and  $\text{d}\dot{\text{C}}_5\text{H}_{11}$  radicals, with barriers of 17.15 and 8.99  $\text{kJ mol}^{-1}$ , respectively. The barrier to the formation of the secondary radical ( $\text{c}\dot{\text{C}}_5\text{H}_{11}$ ) is 8.16  $\text{kJ mol}^{-1}$  lower in energy than that leading to the formation of the primary radical ( $\text{d}\dot{\text{C}}_5\text{H}_{11}$ ).

**Table 3.7:** Computed Energy Barriers, Heats of Reaction, and High-Pressure Limiting Rate Constant Fits for the Reactions of  $\dot{\text{H}}$  with  $\text{aC}_5\text{H}_{10}$ ,  $\text{bC}_5\text{H}_{10}$  and  $\text{cC}_5\text{H}_{10}$ . Units ( $\text{AT}^n = \text{cm}^3 \text{mol}^{-1} \text{s}^{-1}$ , energies =  $\text{kJ mol}^{-1}$ ). R1 – R17 Fit Between 298 and 2000 K.

	Reaction	$\Delta^\ddagger H_{0\text{K}}$	$\Delta_r H_{0\text{K}}$	$A$	$N$	$E_a$
R1	$\text{aC}_5\text{H}_{10} + \dot{\text{H}} \leftrightarrow \text{a}\dot{\text{C}}_5\text{H}_9\text{-a1} + \text{H}_2$	65.85	30.37	$2.17 \times 10^6$	2.36	56.48
R2	$\text{aC}_5\text{H}_{10} + \dot{\text{H}} \leftrightarrow \text{a}\dot{\text{C}}_5\text{H}_9\text{-a2} + \text{H}_2$	31.45	-64.58	$9.57 \times 10^2$	3.26	15.31
R3	$\text{aC}_5\text{H}_{10} + \dot{\text{H}} \leftrightarrow \text{a}\dot{\text{C}}_5\text{H}_9\text{-c} + \text{H}_2$	21.34	-74.60	$2.79 \times 10^5$	2.62	10.96
R4	$\text{aC}_5\text{H}_{10} + \dot{\text{H}} \leftrightarrow \text{a}\dot{\text{C}}_5\text{H}_9\text{-d} + \text{H}_2$	43.44	-15.44	$3.72 \times 10^5$	2.52	30.17
R5	$\text{bC}_5\text{H}_{10} + \dot{\text{H}} \leftrightarrow \text{a}\dot{\text{C}}_5\text{H}_9\text{-c} + \text{H}_2$	28.12	-68.57	$1.26 \times 10^4$	3.02	13.56
R6	$\text{bC}_5\text{H}_{10} + \dot{\text{H}} \leftrightarrow \text{b}\dot{\text{C}}_5\text{H}_9\text{-c} + \text{H}_2$	52.90	15.77	$4.38 \times 10^5$	2.44	42.26
R7	$\text{bC}_5\text{H}_{10} + \dot{\text{H}} \leftrightarrow \text{c}\dot{\text{C}}_5\text{H}_9\text{-b} + \text{H}_2$	26.89	-74.87	$5.51 \times 10^3$	3.03	13.01
R8	$\text{cC}_5\text{H}_{10} + \dot{\text{H}} \leftrightarrow \text{c}\dot{\text{C}}_5\text{H}_9\text{-a} + \text{H}_2$	42.18	-12.50	$1.49 \times 10^5$	2.72	29.16
R9	$\text{cC}_5\text{H}_{10} + \dot{\text{H}} \leftrightarrow \text{c}\dot{\text{C}}_5\text{H}_9\text{-b} + \text{H}_2$	17.37	-88.86	$1.94 \times 10^6$	2.20	9.67
R10	$\text{cC}_5\text{H}_{10} + \dot{\text{H}} \leftrightarrow \text{c}\dot{\text{C}}_5\text{H}_9\text{-c} + \text{H}_2$	52.35	14.61	$2.63 \times 10^5$	2.48	40.63
R11	$\text{cC}_5\text{H}_{10} + \dot{\text{H}} \leftrightarrow \text{c}\dot{\text{C}}_5\text{H}_9\text{-d} + \text{H}_2$	64.73	27.58	$1.45 \times 10^6$	2.43	54.81
R12	$\text{aC}_5\text{H}_{10} + \dot{\text{H}} \leftrightarrow \text{a}\dot{\text{C}}_5\text{H}_{11}$	19.88	-125.21	$1.33 \times 10^{13}$	0.03	20.91
R13	$\text{aC}_5\text{H}_{10} + \dot{\text{H}} \leftrightarrow \text{b}\dot{\text{C}}_5\text{H}_{11}$	5.87	-145.04	$4.96 \times 10^{15}$	-0.52	11.83
R14	$\text{bC}_5\text{H}_{10} + \dot{\text{H}} \leftrightarrow \text{b}\dot{\text{C}}_5\text{H}_{11}$	8.15	-139.01	$8.98 \times 10^{14}$	-0.38	12.44
R15	$\text{bC}_5\text{H}_{10} + \dot{\text{H}} \leftrightarrow \text{c}\dot{\text{C}}_5\text{H}_{11}$	16.26	-131.56	$9.36 \times 10^{12}$	0.10	16.73
R16	$\text{cC}_5\text{H}_{10} + \dot{\text{H}} \leftrightarrow \text{c}\dot{\text{C}}_5\text{H}_{11}$	8.99	-145.55	$4.07 \times 10^{14}$	-0.24	13.05
R17	$\text{cC}_5\text{H}_{10} + \dot{\text{H}} \leftrightarrow \text{d}\dot{\text{C}}_5\text{H}_{11}$	17.15	-136.27	$5.09 \times 10^{14}$	-0.42	20.07

The  $\dot{\text{H}}$  atom addition reaction barriers are found to be substantially lower than those for abstraction. In the case of  $\text{aC}_5\text{H}_{10}$ , a barrier of 31.45  $\text{kJ mol}^{-1}$  is computed for the abstraction of a primary allylic hydrogen atom forming  $\text{a}\dot{\text{C}}_5\text{H}_9\text{-a2}$  (R2), while a barrier of 21.34  $\text{kJ mol}^{-1}$  is computed for the abstraction of a secondary allylic hydrogen atom (R3). For  $\text{bC}_5\text{H}_{10}$ , two resonantly stabilised allylic radicals can be formed upon abstraction from the primary allylic (R5,  $\text{a}\dot{\text{C}}_5\text{H}_9\text{-c}$ ) and (R7,  $\text{c}\dot{\text{C}}_5\text{H}_9\text{-b}$ ) sites, with respective barriers of 28.12 and 26.89  $\text{kJ mol}^{-1}$  computed. For  $\text{cC}_5\text{H}_{10}$ , abstraction from the tertiary allylic site (R9,  $\text{c}\dot{\text{C}}_5\text{H}_9\text{-b}$ ), has a computed barrier of 17.37  $\text{kJ mol}^{-1}$ .

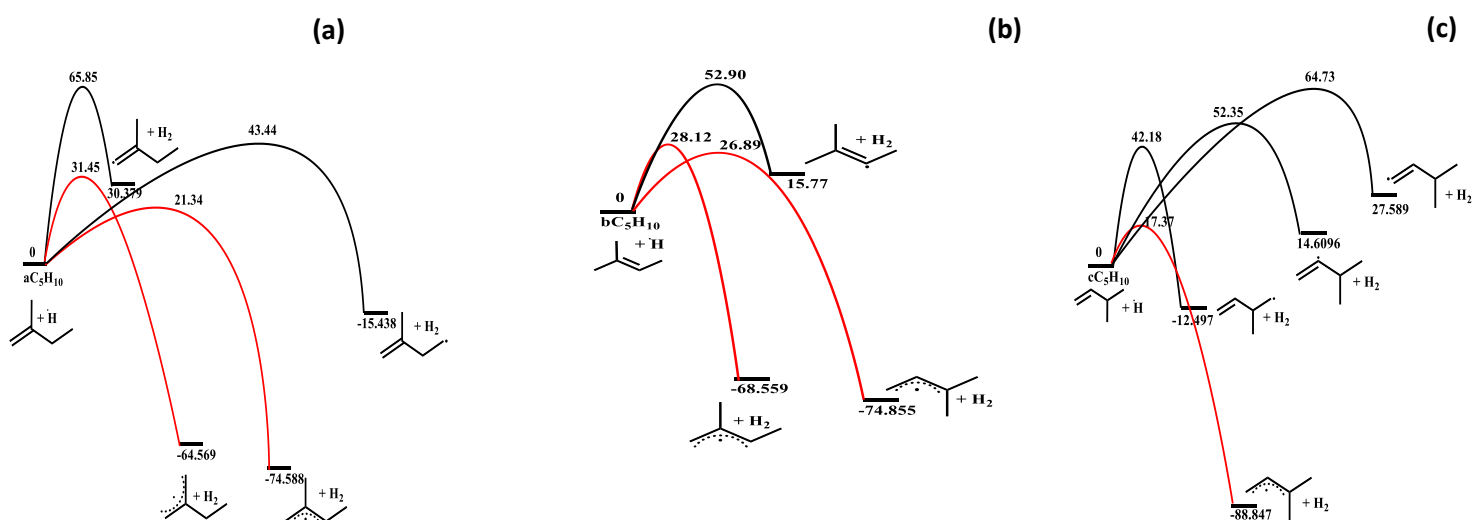


**Figure 3.3.** PES for H-atom abstraction reactions. (a) aC<sub>5</sub>H<sub>10</sub>, (b) bC<sub>5</sub>H<sub>10</sub> and (c) cC<sub>5</sub>H<sub>10</sub>. Red lines represent the reactions which lead to resonantly stabilised radicals. Energies in kJ mol<sup>-1</sup>.

In our previous work on 1- and 2-pentene [2], a barrier of 29.75 kJ mol<sup>-1</sup> was calculated for abstraction of a primary allylic hydrogen atom ( $C_5H_{10-2} + \dot{H} \leftrightarrow \dot{C}_5H_9-13 + H_2$ ). However, as previously described [2], higher-level RO-aug-cc-pVXZ SPEs were carried out for important reaction channels on the  $\dot{C}_5H_{11}$  PES. These calculations showed systematically lower reaction barriers, and a reaction barrier of 28.94 kJ mol<sup>-1</sup> was subsequently computed for abstraction of this primary allylic hydrogen atom [2]. Both values are within ~2.5 kJ mol<sup>-1</sup> of the value computed in this work for (R2,  $aC_5H_{10} + \dot{H} \leftrightarrow a\dot{C}_5H_9-a2 + H_2$ ). For (R5,  $bC_5H_{10} + \dot{H} \leftrightarrow a\dot{C}_5H_9-c + H_2$ ) and (R7,  $bC_5H_{10} + \dot{H} \leftrightarrow c\dot{C}_5H_9-b + H_2$ ), differences in energy barriers for the analogous reaction of ( $C_5H_{10-2} + \dot{H} \leftrightarrow \dot{C}_5H_9-13 + H_2$ ) are within 2.86 kJ mol<sup>-1</sup> for unrestricted (aug-cc-pVXZ) values and 2 kJ mol<sup>-1</sup> for restricted open shell values (RO-aug-cc-pVXZ).

Reaction barriers of 22.31 and 21.41 kJ mol<sup>-1</sup> were calculated for abstraction of secondary allylic hydrogen atoms for  $C_5H_{10-1} + \dot{H} \leftrightarrow \dot{C}_5H_9-13 + H_2$  and  $C_5H_{10-2} + \dot{H} \leftrightarrow \dot{C}_5H_9-24 + H_2$ , respectively [2]. Again barriers for these reaction channels were computed using RO-aug-cc-pVXZ SPEs and were found to be 21.89 and 20.96 kJ mol<sup>-1</sup> for  $C_5H_{10-1} + \dot{H} \leftrightarrow \dot{C}_5H_9-13 + H_2$  and  $C_5H_{10-2} + \dot{H} \leftrightarrow \dot{C}_5H_9-24 + H_2$ , respectively [2]. All values are within 1 kJ mol<sup>-1</sup> of the barrier computed for  $aC_5H_{10} + \dot{H} \leftrightarrow a\dot{C}_5H_9-c + H_2$  calculated in the current work.

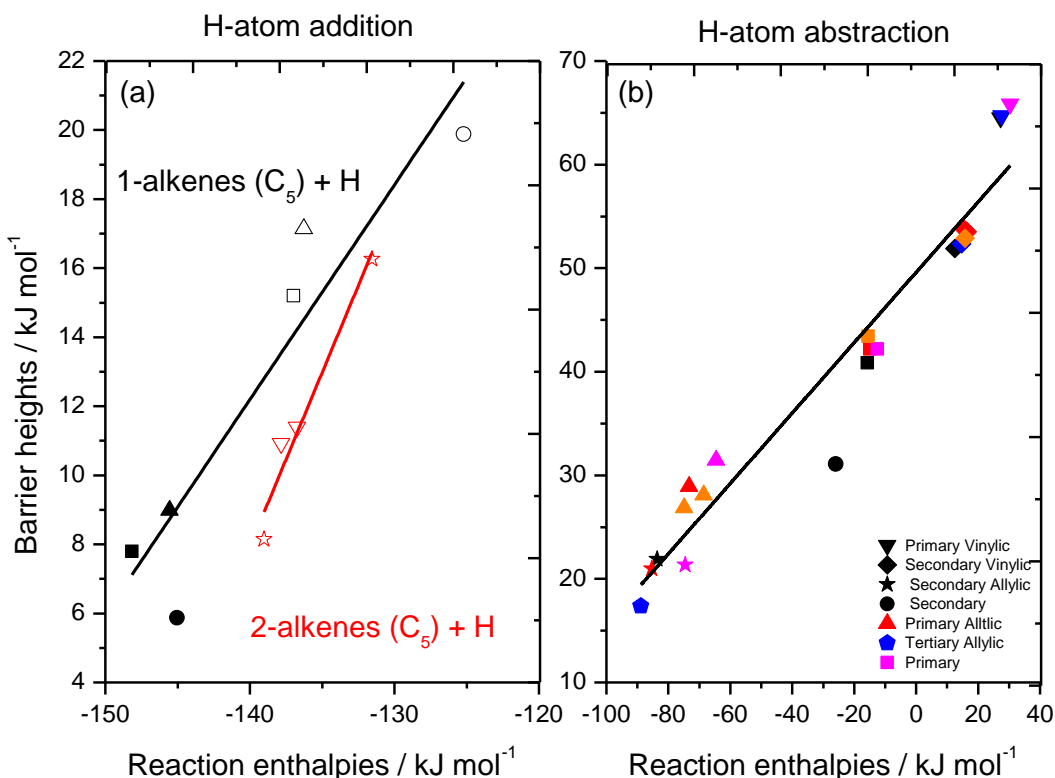


**Figure 3.4.** Evans–Polanyi correlation for (a)  $\dot{\text{H}}$  atom addition to  $\text{C}_5$  alkenes, and (b) H-atom abstraction from  $\text{C}_5$  alkenes. In Fig. 3.4 (a), solid symbols represent external addition reactions of  $\dot{\text{H}}$  atom and open symbols represent internal addition. Different colours correspond to different reactions classes, which are further divided into different symbols to represent different reactants. (1) 1-alkenes, black  $\blacksquare$  1-pentene, black  $\bullet$  2-methyl-1-butene, black  $\blacktriangle$  3-methyl-1-butene. (2) 2-alkenes, red  $\blacktriangledown$  2-pentene, red  $\star$  2-methyl-2-butene. In Fig.3.4 (b), different colours represent different reactants while different symbols correspond to the different abstraction sites. Black (1-pentene), red (2-pentene), magenta (2-methyl-1-butene), orange (2-methyl-2-butene) and blue (3-methyl-1-butene).  $\blacksquare$  (primary),  $\bullet$  (secondary),  $\blacktriangle$  (primary allylic),  $\blacktriangledown$  (primary vinylic),  $\star$  (secondary allylic),  $\blacklozenge$  (secondary vinylic) and  $\blacklozenge$  (tertiary allylic).

Figure 3.4 compares the barrier heights versus reaction enthalpies at 0 K for the reactions of hydrogen atoms with  $\text{C}_5$  alkenes from both our previous work [2] and the current work. The barrier heights and reaction enthalpies for these reactions are listed in Table 3.7. For 1-alkenes, the barrier heights for external addition are consistently lower than internal addition for the same species. In the case of 2-alkenes, both internal  $\dot{\text{H}}$  atom addition reactions for 2-pentene forming the secondary radicals  $\dot{\text{C}}_5\text{H}_{11-2}$  and  $\dot{\text{C}}_5\text{H}_{11-3}$  have similar reaction barriers of



10.92 and 11.4 kJ mol<sup>-1</sup>, respectively. However, for 2-methyl-2-butene, the two internal  $\dot{\text{H}}$  atom addition reactions forming the tertiary ( $\text{b}\dot{\text{C}}_5\text{H}_{11}$ ) and secondary ( $\text{c}\dot{\text{C}}_5\text{H}_{11}$ ) radicals are quite different in barrier heights with barriers of 8.15 and 16.26 kJ mol<sup>-1</sup>, respectively. This is expected as two different radical types are formed. The Evans-Polanyi correlation for  $\dot{\text{H}}$  atom addition to 1-alkenes is fitted to  $\Delta^\ddagger\text{H}_{0\text{K}} = 0.62 (\pm 0.12) \times \Delta_{\text{r}}\text{H}_{0\text{K}} + 99.27 (\pm 16.88)$  kJ mol<sup>-1</sup> with an  $R^2$  of 0.84, while the correlation for  $\dot{\text{H}}$  atom addition to 2-alkenes is fitted to  $\Delta^\ddagger\text{H}_{0\text{K}} = 1.0 (\pm 0.14) \times \Delta_{\text{r}}\text{H}_{0\text{K}} + 148.90 (\pm 19.41)$  kJ mol<sup>-1</sup> with an  $R^2$  of 0.94. For the H-atom abstraction reactions, Fig. 3.4 (b), an Evans-Polanyi correlation was fitted to  $\Delta^\ddagger\text{H}_{0\text{K}} = 0.34 (\pm 0.02) \times \Delta_{\text{r}}\text{H}_{0\text{K}} + 49.54 (\pm 1.0)$  kJ mol<sup>-1</sup>, with an  $R^2$  of 0.94. These Evans-Polanyi correlations may be useful to estimate energy barriers, where literature values are unavailable.

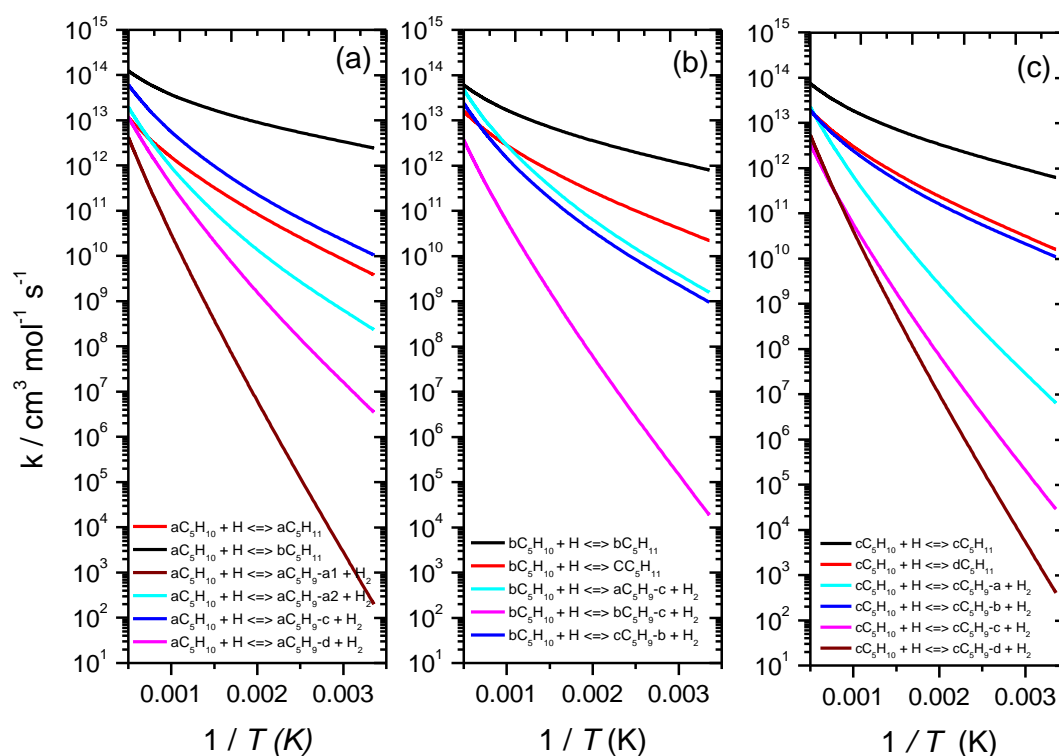


**Figure 3.5.** High-pressure limit rate constants of (a)  $\text{aC}_5\text{H}_{10} + \dot{\text{H}}$ , (b)  $\text{bC}_5\text{H}_{10} + \dot{\text{H}}$  and (c)  $\text{cC}_5\text{H}_{10} + \dot{\text{H}}$ .

Figure 3.5 compares the computed high-pressure limiting rate constants (Table 3.7) for the reactions of a  $\dot{\text{H}}$  atom with  $\text{aC}_5\text{H}_{10}$ ,  $\text{bC}_5\text{H}_{10}$  and  $\text{cC}_5\text{H}_{10}$ . For  $\text{aC}_5\text{H}_{10}$  and  $\text{cC}_5\text{H}_{10}$ , terminal addition is kinetically dominant, and for  $\text{bC}_5\text{H}_{10}$ , internal addition forming the tertiary  $\text{b}\dot{\text{C}}_5\text{H}_{11}$  radical dominates.

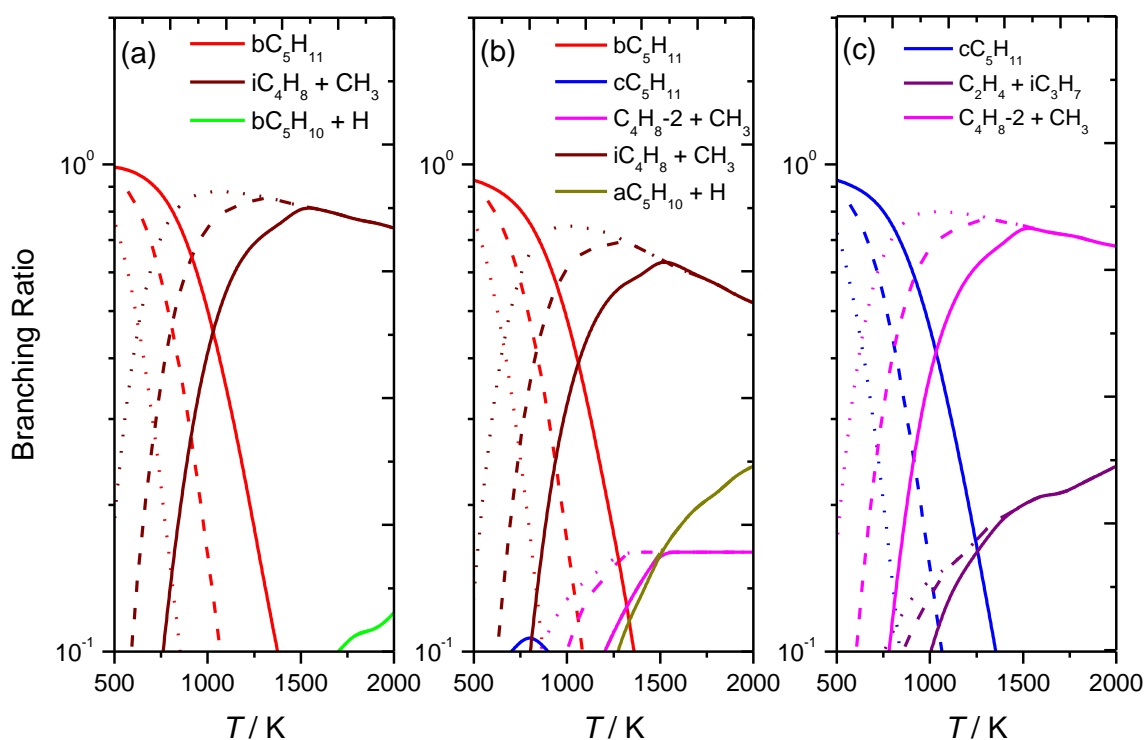


**Figure 3.6.** Temperature- and pressure- dependent branching ratios for (a)  $aC_5H_{10} + \dot{H}$ , (b)  $bC_5H_{10} + \dot{H}$  and (c)  $cC_5H_{10} + \dot{H}$  via hydrogen atom addition reactions at 0.1 atm (dotted lines), 1 atm (dashed lines) and 10 atm (solid lines).

Parts a-c of Figure 3.6 present the temperature- and pressure- dependencies of the product branching ratios for  $\dot{H}$  atom addition to  $aC_5H_{10}$ ,  $bC_5H_{10}$  and  $cC_5H_{10}$  in the temperature range 500–2000 K and at pressures 0.1, 1.0, and 10 atm.

For both  $aC_5H_{10}$  and  $bC_5H_{10}$ , the stabilised formation of the  $b\dot{C}_5H_{11}$  radical through  $\dot{H}$  atom addition is dominant up to 600 K, 800 K and 1000 K at 0.1, 1.0 and 10 atm respectively. The chemically activated formation of isobutene and methyl radical then governs the reaction flux at higher temperatures, which can also be observed in Fig. 3.12 (b). In Fig. 3.6 (a), at higher temperatures and pressures ( $\sim 1700$ – $2000$  K and 10 atm), it is observed (green solid line) that a small percentage ( $\sim 10\%$ ) of the reaction flux goes through a chemically activated pathway to form  $bC_5H_{10} + \dot{H}$  atom.

For  $bC_5H_{10} + \dot{H}$ , Fig. 3.6(b), a small percentage of the reaction flux goes through chemically activated pathways which can form (i)  $aC_5H_{10} + \dot{H}$  (8–24 %) and (ii)  $C_4H_8-2 + \dot{C}H_3$  (10–16 %). In the case of (i)  $aC_5H_{10} + \dot{H}$ , this occurs from 1100 K for 0.1 atm and 1200 K for 1 and 10 atm. For (ii)  $C_4H_8-2 + \dot{C}H_3$ , the flux occurs from 800, 1000 and 1200 K for 0.1, 1.0, and 10 atm, respectively. In the temperature range of  $\sim 700$ – $1000$  K, at 10 atm, it

can be observed that the stabilised formation of  $cC_5H_{11}$  radical formed through  $\dot{H}$  atom addition to  $bC_5H_{10}$  accounts for  $\sim 10\%$  of the reaction flux.

For  $cC_5H_{10}$ , a similar scenario prevails, with the direct  $\dot{H}$  atom addition pathway, forming  $c\dot{C}_5H_{11}$  radical dominating up to 600 K, 800 K and 1000 K at 0.1, 1.0, and 10.0 atm respectively until the chemically activated pathway, forming 2-butene and methyl radical, dominates in the higher temperature range. A small percentage of the flux, through chemical activation forms  $C_2H_4 + iC_3H_7$ . (10 – 24%) from 700, 800 and 1000 K for 0.1, 1.0, at 10 atm, respectively.

### 3.2.1.1. Rate Constant Comparisons

Large differences are observed between the rate constants for  $\dot{H}$  atom addition to  $aC_5H_{10}$ ,  $bC_5H_{10}$  and  $cC_5H_{10}$  calculated in this work and those used in the current models for pentene [8, 11]. In Fig. 3.7 (a), Westbrook et al. [11] used rate constants for external and internal  $\dot{H}$  atom addition to isobutene by analogy based on the recommendation of Curran [29]. At 1000 K, the rate used by Westbrook [11, 29] is a factor of  $\sim 2$  slower than that calculated in this work and the rate constant for internal addition is a factor of  $\sim 3.7$  faster than this work. Those by Leon et al. [8] are a factor of  $\sim 6.8$  and 1.8 slower than the current work at 1000 K for external and internal addition, respectively.

For  $bC_5H_{10} + \dot{H}$  (Fig. 3.7 (b)), Westbrook et al. [11] again used analogies based on Curran [29]. The rates for internal addition to isobutene and internal addition to 1-butene were used, which are a factor of  $\sim 2.82$  and 1.24 slower at 1000 K. Leon et al. [8] are again slower than the current work for the internal addition forming the  $bC_5H_{11}$  and  $cC_5H_{11}$  radical by a factor of  $\sim 3.3$  and 6.4, respectively.

Figure 3.7 (c) presents the rate constants for  $\dot{H}$  atom addition to  $cC_5H_{10}$ . Westbrook et al. [11] used the same analogies as those for  $bC_5H_{10}$ . Their rates [11] are a factor of  $\sim 3$  and  $\sim 1.3$  slower than the ones calculated in this work at 1500 K for external and internal addition, respectively. Leon et al. [8] are a factor of 3.38 and 1.28 times slower at 1000 K than the current work for external and internal addition, respectively. These discrepancies highlight the need for a re-evaluation of these reaction systems, which can also be concluded from the rate constant comparisons for pentyl radical decompositions and alkyl radical additions to olefins in Section 3.2.2.1.

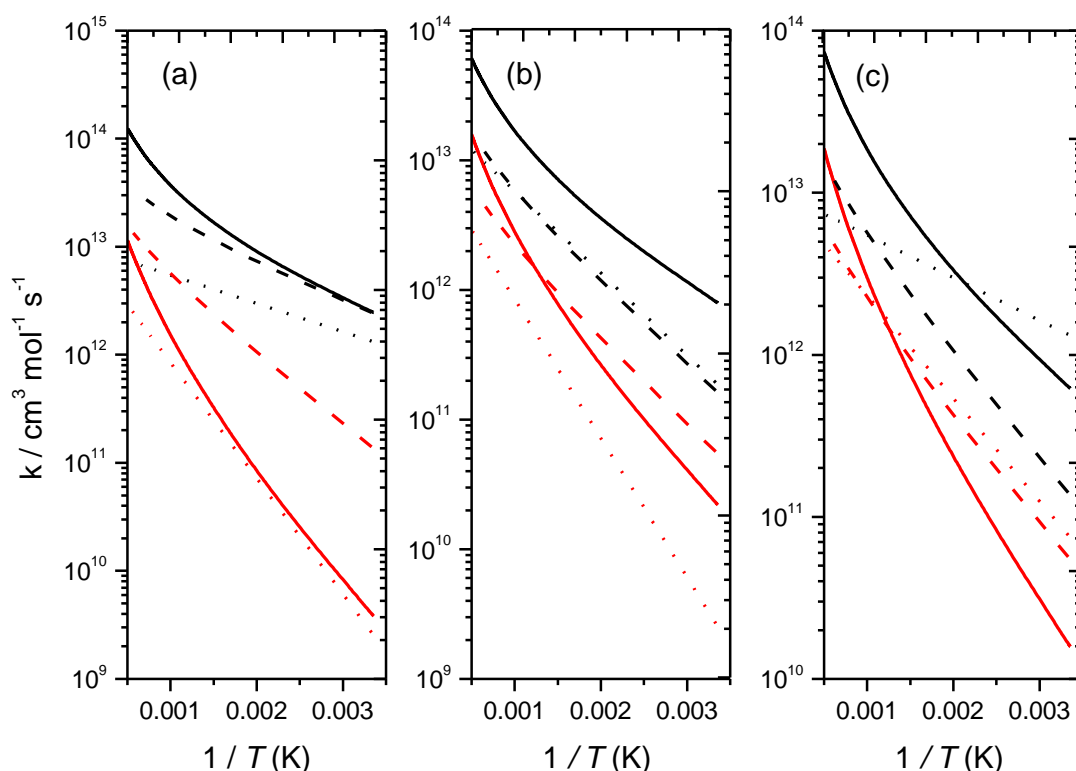


**Figure 3.7.** High-pressure limiting rate constants for  $\dot{\text{H}}$  atom addition to (a)  $\text{aC}_5\text{H}_{10}$ , (b)  $\text{bC}_5\text{H}_{10}$  and (c)  $\text{cC}_5\text{H}_{10}$ . External addition is represented in black, while red represents internal addition. For  $\text{bC}_5\text{H}_{10}$ , black lines represent the formation of the tertiary  $\text{bC}_5\text{H}_{11}$  radical, while red represents the formation of the  $\text{cC}_5\text{H}_{11}$  radical. Solid lines represent the current work and dotted lines represent rate constants by Leon et al. [8] Rate constants used in the models of Westbrook et al. [11] are shown as dashed lines.

Figure 3.8 presents rate constants for both terminal and internal  $\dot{\text{H}}$  atom addition to (a) linear and (b) branched  $\text{C}_5$  alkenes. Preliminary results for the reactions of  $\dot{\text{H}}$  with  $\text{C}_4$  alkenes have been included for comparison. Different trends are observed for addition to linear and branched alkenes.

In the case of linear alkenes, terminal  $\dot{\text{H}}$  atom addition (solid lines) leads to the formation of secondary radicals (red) ( $\text{C}_5\text{H}_{10-1} + \dot{\text{H}} \leftrightarrow \dot{\text{C}}_5\text{H}_{11-2}$  and  $\text{C}_4\text{H}_8-1 + \dot{\text{H}} \leftrightarrow \dot{\text{C}}_4\text{H}_9-2$ ), with the rate constants being very similar. Internal addition (dashed lines) can lead to primary ( $1^\circ$ ) ( $\text{C}_5\text{H}_{10-1} + \dot{\text{H}} \leftrightarrow \dot{\text{C}}_5\text{H}_{11-1}$ ,  $\text{C}_4\text{H}_8-1 + \dot{\text{H}} \leftrightarrow \dot{\text{C}}_4\text{H}_9-1$ ) or secondary ( $2^\circ$ ) radicals (red) ( $\text{C}_5\text{H}_{10-2} + \dot{\text{H}} \leftrightarrow \dot{\text{C}}_5\text{H}_{11-2}$ ,  $\text{C}_5\text{H}_{10-2} + \dot{\text{H}} \leftrightarrow \dot{\text{C}}_5\text{H}_{11-3}$  and  $\text{C}_4\text{H}_8-2 + \dot{\text{H}} \leftrightarrow \dot{\text{C}}_4\text{H}_9-2$ ). The rate constants within each class, i.e. (i) formation of primary radicals through internal addition and (ii) formation of secondary radicals through internal addition are very similar. Also, it can be observed that the

rates for the formation of these primary radicals are slower than formation of the secondary radicals, which can be correlated with radical stability.

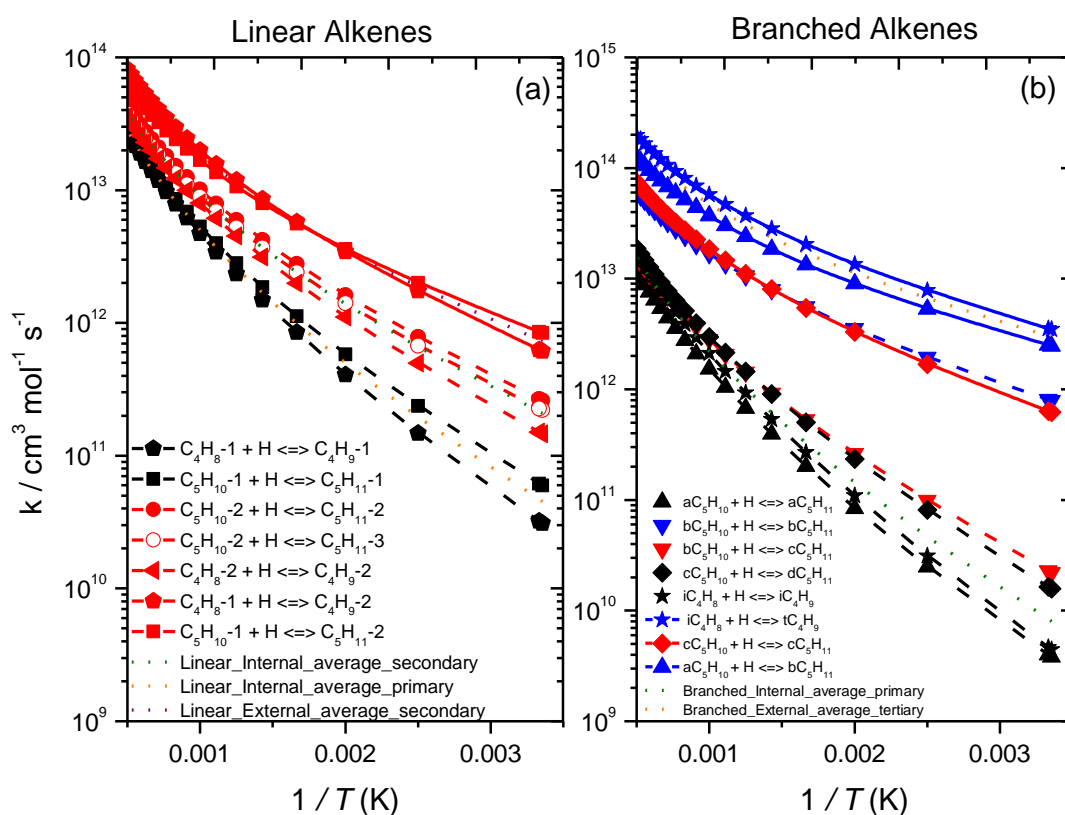


**Figure 3.8.** Rate constants for terminal and internal  $\dot{\text{H}}$  atom addition to (a) linear and (b) branched  $\text{C}_5$  alkenes from previous[2] and current work. Solid and dashed lines represent terminal and internal addition, respectively. Different colours represent different radical types formed. Black (primary), red (secondary) and blue (tertiary). Different symbols correspond to the different reactants.  $\blacksquare$  (1-pentene),  $\bullet$  (2-pentene),  $\blacktriangle$  (2-methyl-1-butene),  $\blacktriangledown$  (2-methyl-2-butene),  $\blacklozenge$  (3-methyl-1-butene),  $\blacklozenge$  (1-butene),  $\blacktriangleleft$  (2-butene) and  $\star$  (iso-butene).

For branched alkenes, terminal  $\dot{\text{H}}$  atom addition can lead to either the formation of tertiary ( $3^\circ$ ) (blue) ( $\text{aC}_5\text{H}_{10} + \dot{\text{H}} \leftrightarrow \text{b}\dot{\text{C}}_5\text{H}_{11}$  and  $\text{iC}_4\text{H}_8 + \dot{\text{H}} \leftrightarrow \text{t}\dot{\text{C}}_4\text{H}_9$ ) or secondary radicals ( $\text{cC}_5\text{H}_{10} + \dot{\text{H}} \leftrightarrow \text{c}\dot{\text{C}}_5\text{H}_{11}$ ) (red). Rate constants for  $\text{aC}_5\text{H}_{10} + \dot{\text{H}} \leftrightarrow \text{b}\dot{\text{C}}_5\text{H}_{11}$  and  $\text{iC}_4\text{H}_8 + \dot{\text{H}} \leftrightarrow \text{t}\dot{\text{C}}_4\text{H}_9$  are in good agreement, with the rate constant forming the secondary radical  $\text{cC}_5\text{H}_{10} + \dot{\text{H}} \leftrightarrow \text{c}\dot{\text{C}}_5\text{H}_{11}$  being slower, which is to be expected. Internal addition (dashed lines) for the branched alkenes can form primary ( $\text{aC}_5\text{H}_{10} + \dot{\text{H}} \leftrightarrow \text{a}\dot{\text{C}}_5\text{H}_{11}$ ,  $\text{cC}_5\text{H}_{10} + \dot{\text{H}} \leftrightarrow \text{d}\dot{\text{C}}_5\text{H}_{11}$  and  $\text{iC}_4\text{H}_8 + \dot{\text{H}} \leftrightarrow \text{i}\dot{\text{C}}_4\text{H}_9$ ), secondary ( $\text{bC}_5\text{H}_{10} + \dot{\text{H}} \leftrightarrow \text{c}\dot{\text{C}}_5\text{H}_{11}$ ) and tertiary radicals ( $\text{bC}_5\text{H}_{10} + \dot{\text{H}} \leftrightarrow \text{b}\dot{\text{C}}_5\text{H}_{11}$ ). Again, a trend is observed such that the rate constants for formation of tertiary radicals are the fastest, followed by secondary and primary radicals, respectively.

Recommended rate constants have been suggested based on (i) whether its addition to a linear or branched alkene (ii) terminal or internal addition and (iii) the type of radical formed. An average of the rate constants within each sub-class was taken as the recommended rate constant and these values are shown as dotted lines in Fig.3.8. If only one rate constant was available, for example in the case of internal addition to a branched alkene forming a secondary radical ( $\text{bC}_5\text{H}_{10} + \dot{\text{H}} \leftrightarrow \text{c}\dot{\text{C}}_5\text{H}_{11}$ ), the rate constant for the reaction is taken as the recommended rate constant. For the rate constant recommendations (Tables 3.8 and 3.9), activation energies are expressed in  $\text{cal mol}^{-1}$  units for ease when implementing into kinetic mechanisms.

**Table 3.8:** Recommended Rate Constants for  $\dot{\text{H}}$  atom Addition to Linear and Branched Alkenes (units:  $\text{cm}^3/\text{mol}/\text{s}/\text{cal}$ ).

Structure	Site	Radical Formed	<i>A</i>	<i>n</i>	<i>E<sub>a</sub></i>	Uncertainty Bounds (Upper, Lower)
Linear	External	2°	7.36E+08	1.55	1144.7	1.15, 1.18
	Internal	1°	1.33E+08	1.69	2248.5	1.32, 1.46
	Internal	2°	5.25E+08	1.53	1612.3	1.24, 1.43
Branched	External	2°	4.07E+14	-0.24	3119.0	-
	External	3°	2.79E+09	1.47	830.9	1.23, 1.29
	Internal	1°	3.42E+07	1.81	2891.9	1.97, 2.1
	Internal	2°	9.36E+12	0.10	3999.0	-
	Internal	3°	8.98E+14	-0.38	2973.0	-

In relation to the uncertainty bounds presented in Tables 8 and 9, upper and lower bounds are given, which are defined as:

$$\text{Upper} = k_{\text{max}} / k_{\text{recommendation}}$$

$$\text{Lower} = k_{\text{recommendation}} / k_{\text{min}}$$

where  $k_{\text{recommendation}}$  refers to the recommended rate coefficient, while  $k_{\text{min}}$  and  $k_{\text{max}}$  refer to the minimum and maximum rate coefficients used in the rate coefficient estimations, respectively.

Figure 3.9 presents high-pressure limiting rate constants for H-atom abstraction from (a) primary, (b) primary allylic, and (c) primary vinylic carbon sites on a per H-atom basis. For each sub-class, a factor of  $\pm 2$  of the recommended rate constant for that class are shown as dotted lines.

Work-in-progress results for C<sub>2</sub> – C<sub>4</sub> alkenes +  $\dot{\text{H}}$  have been included as comparisons. By comparing our rate constants for the same reaction classes; i.e. primary, primary allylic, etc., we have shown that our computed rate constants for the pentene systems are consistent and allow for the definition of rate rules for higher order alkenes. By having a consistent set of rate constants for C<sub>2</sub> – C<sub>4</sub> alkenes +  $\dot{\text{H}}$  using the same level of theory, our results help constrain available models and the development of recommended rate constants which provide a tool for the use in mechanisms of larger alkenes for which calculations do not exist in the literature.

Excellent agreement is observed for H-atom abstraction from the primary carbon sites. Good agreement is also observed for the rates calculated for abstraction from the primary allylic sites, Fig 3.9(b). If the rate constant for  $\text{aC}_5\text{H}_{10} + \dot{\text{H}} \leftrightarrow \text{a}\dot{\text{C}}_5\text{H}_9\text{-a2} + \text{H}_2$  (black line) is taken as the recommended rate constant for abstraction from primary allylic carbon sites, all the other calculated rate constants fall within a factor of ~two of this rate constant (dotted black line), including the rate calculated by Miller and Klippenstein [51] for H-atom abstraction from propene. It can be observed that the rate constants for the reactions  $\text{bC}_5\text{H}_{10} + \dot{\text{H}} \leftrightarrow \text{a}\dot{\text{C}}_5\text{H}_9\text{-c} + \text{H}_2$ ,  $\text{bC}_5\text{H}_{10} + \dot{\text{H}} \leftrightarrow \text{c}\dot{\text{C}}_5\text{H}_9\text{-b} + \text{H}_2$  and  $\text{C}_5\text{H}_{10}\text{-2} + \dot{\text{H}} \leftrightarrow \dot{\text{C}}_5\text{H}_9\text{-13} + \text{H}_2$  are slightly faster at lower temperatures than their analogous comparisons, but this can be attributed to the differences in reaction barriers.

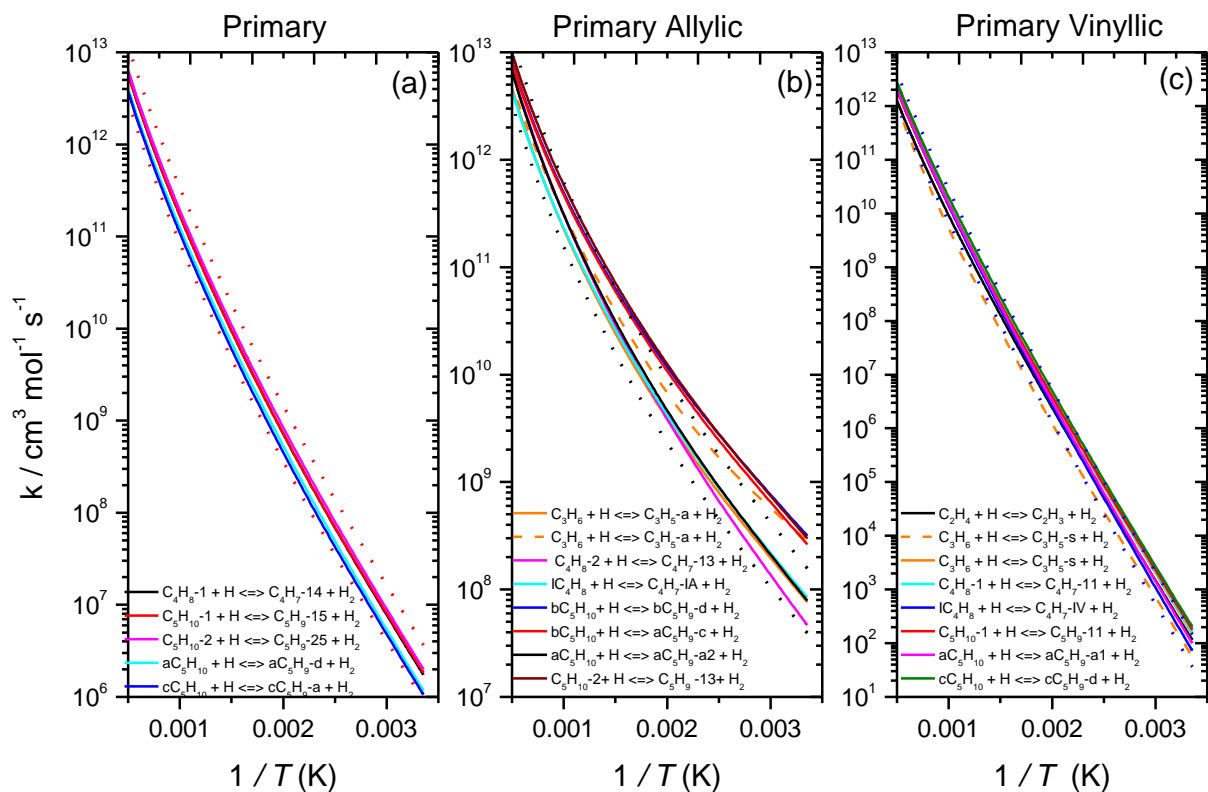


**Figure 3.9.** High-pressure limiting rate constants for H-atom abstraction from (a) primary, (b) primary allylic, and (c) primary vinylic carbon sites. (on a per H-atom basis)

Again, good agreement is found for abstraction rates from primary vinylic sites. If the rate constant for  $iC_4H_8 + \dot{H} \leftrightarrow \dot{C}_4H_{7-iv} + H_2$  (blue) calculated in this work is taken as our recommended value, our rate constants for the other analogous reactions fall within a factor of two of this (dotted blue), including the rate constant calculated by Miller and Klippenstein [51] for the reaction  $C_3H_6 + \dot{H} \leftrightarrow C_3H_{5-s} + H_2$ .



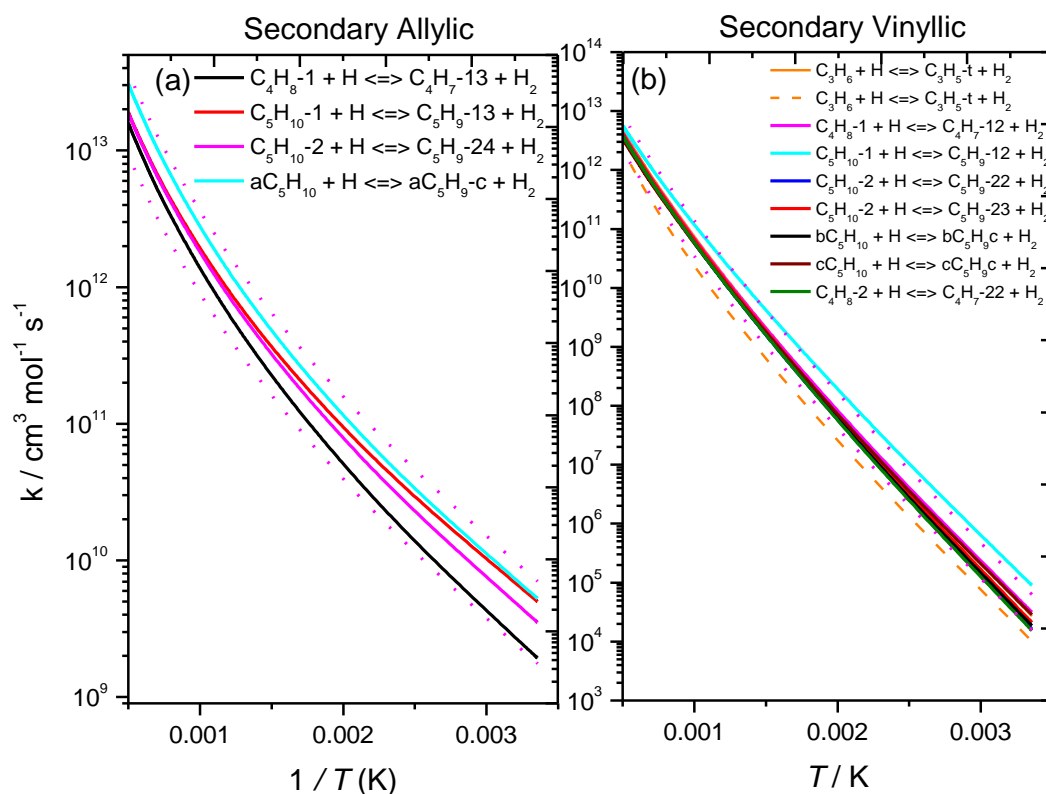


**Figure 3.10.** High-pressure limiting rate constants (on a per H-atom basis) for H-atom abstraction from (a) secondary allylic and (b) secondary vinylic carbon sites.

Figure 3.10 presents high-pressure-limiting H-atom abstraction rate constants on a per H-atom basis for (a) secondary allylic and (b) secondary vinylic carbon sites, with good agreement among our calculated results being observed. For secondary allylic H-atom abstraction, the rate constant for  $\text{C}_5\text{H}_{10-2} + \dot{\text{H}} \leftrightarrow \dot{\text{C}}_5\text{H}_9-24 + \text{H}_2$  is recommended (magenta). The rate constants for the analogous reactions fall within a factor of  $\pm 2$  (dotted magenta) of this recommendation. For secondary vinylic H-atom abstraction, Fig 3.10 (b), the rate constant for  $\text{C}_4\text{H}_8-1 + \dot{\text{H}} \leftrightarrow \dot{\text{C}}_4\text{H}_7-12 + \text{H}_2$  is recommended (magenta). The rate constant from Klippenstein [51] is slightly slower than those calculated in this work by a factor of  $\sim 3$  at 1000 K (dashed orange).

**Table 3.9:** Recommended Rate Constants for H-atom Abstraction From Alkenes<sup>a</sup>

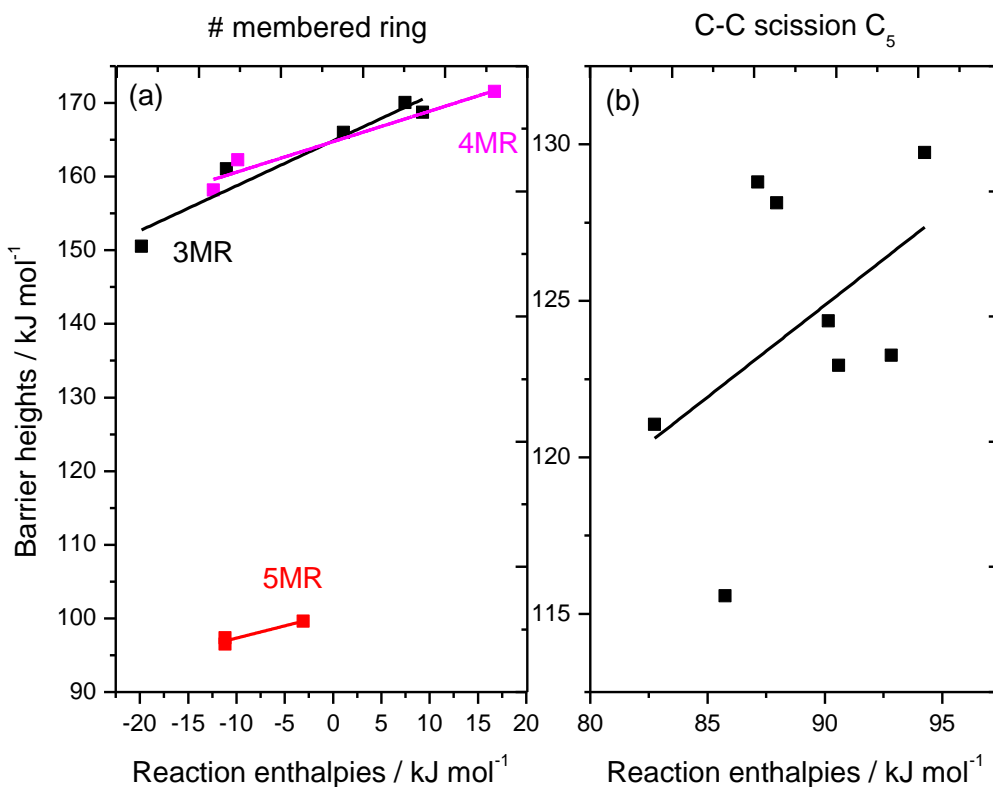
Class	Recommended rate constants			Uncertainty Bounds (Upper, Lower)
	<i>A</i>	<i>n</i>	<i>E<sub>a</sub></i>	
Primary	$1.84 \times 10^{04}$	2.81	6782.	1.17, 1.73
Primary Allylic	$3.37 \times 10^{02}$	3.25	3673.	3.70, 1.53
Primary Vinyllic	$1.36 \times 10^{06}$	2.33	13711.	2.80, 1.68
Secondary Allylic	$2.73 \times 10^{05}$	2.47	2744.	1.63, 1.83
Secondary Vinyllic	$2.11 \times 10^{05}$	2.54	9720.	2.84, 2.05

<sup>a</sup>On a per H-atom basis ( $AT^n = \text{cm}^3 \text{mol}^{-1} \text{s}^{-1}$ , energies =  $\text{cal mol}^{-1}$ ). Fit between 298 and 2000 K.

### 3.2.2. Reactions of Pentyl Radicals

**Table 3.10:** Computed Energy Barriers, Heats of Reaction, and High-Pressure Limiting Rate Constant Fits for the Reactions of Pentyl Radicals. Units ( $AT^n = \text{s}^{-1}$ , Energies =  $\text{kJ mol}^{-1}$ ). R18–R28 Fit between 298 and 2000 K.

	reaction	$\Delta^\ddagger H_{0\text{K}}$	$\Delta_r H_{0\text{K}}$	<i>A</i>	<i>n</i>	<i>E<sub>a</sub></i>
R18	$\text{a}\dot{\text{C}}_5\text{H}_{11} \rightleftharpoons \text{C}_3\text{H}_6 + \dot{\text{C}}_2\text{H}_5$	121.05	82.75	$1.33 \times 10^{16}$	-0.77	128.28
R19	$\text{a}\dot{\text{C}}_5\text{H}_{11} \rightleftharpoons \text{C}_4\text{H}_8\text{-1} + \dot{\text{C}}\text{H}_3$	128.79	87.15	$3.61 \times 10^{15}$	-0.57	136.40
R20	$\text{b}\dot{\text{C}}_5\text{H}_{11} \rightleftharpoons \text{iC}_4\text{H}_8 + \dot{\text{C}}\text{H}_3$	124.36	90.16	$2.90 \times 10^{13}$	0.03	129.83
R21	$\text{c}\dot{\text{C}}_5\text{H}_{11} \rightleftharpoons \text{C}_4\text{H}_8\text{-2} + \dot{\text{C}}\text{H}_3$	128.13	87.96	$5.59 \times 10^{14}$	-0.33	134.31
R22	$\text{d}\dot{\text{C}}_5\text{H}_{11} \rightleftharpoons \text{C}_2\text{H}_4 + \text{i}\dot{\text{C}}_3\text{H}_7$	115.58	85.76	$6.03 \times 10^{16}$	-0.93	123.26
R23	$\text{a}\dot{\text{C}}_5\text{H}_{11} \rightleftharpoons \text{b}\dot{\text{C}}_5\text{H}_{11}$	150.54	-19.83	$3.26 \times 10^{-02}$	3.95	107.61
R24	$\text{a}\dot{\text{C}}_5\text{H}_{11} \rightleftharpoons \text{c}\dot{\text{C}}_5\text{H}_{11}$	158.15	-12.38	$4.45 \times 10^{-15}$	7.52	83.89
R25	$\text{a}\dot{\text{C}}_5\text{H}_{11} \rightleftharpoons \text{d}\dot{\text{C}}_5\text{H}_{11}$	99.62	-3.10	$4.37 \times 10^{-02}$	3.54	61.71
R26	$\text{b}\dot{\text{C}}_5\text{H}_{11} \rightleftharpoons \text{c}\dot{\text{C}}_5\text{H}_{11}$	170.03	7.45	$1.87 \times 10^{-05}$	4.87	120.50
R27	$\text{b}\dot{\text{C}}_5\text{H}_{11} \rightleftharpoons \text{d}\dot{\text{C}}_5\text{H}_{11}$	171.54	16.73	$8.42 \times 10^{-17}$	7.98	97.24
R28	$\text{c}\dot{\text{C}}_5\text{H}_{11} \rightleftharpoons \text{d}\dot{\text{C}}_5\text{H}_{11}$	168.72	9.28	$2.71 \times 10^{-05}$	4.94	121.42



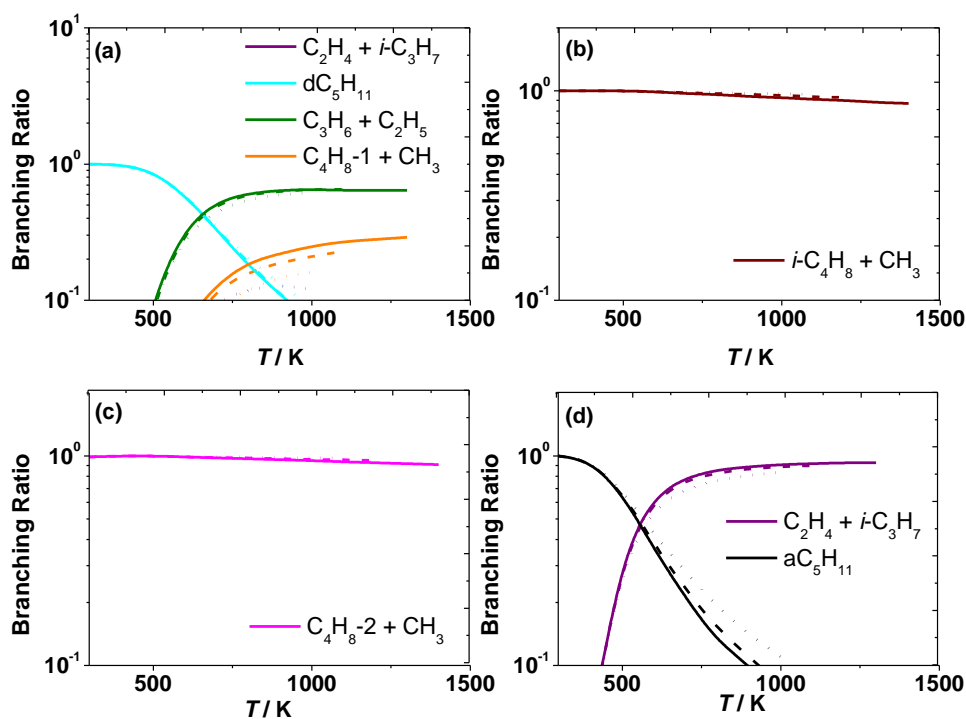
**Figure 3.11.** Evans–Polanyi correlation for (a) H-atom isomerisation, and (b) C–C scission of pentyl radicals.

Figure 3.11 compares the barrier heights versus reaction enthalpies at 0 K for (a) H-atom isomerisation and (b) C–C scission reactions of pentyl radicals from both our previous work [2] and those calculated here. The barrier heights and reaction enthalpies for these reactions are listed in Table 3.10. The Evans-Polanyi correlation for H-atom isomerisation reactions forming 3-membered ring transition states is fitted to  $\Delta^\ddagger H_{0K} = 0.61 (\pm 0.1) \times \Delta_r H_{0K} + 164.86 (\pm 1.1) \text{ kJ mol}^{-1}$  with an  $R^2$  of 0.91, while the correlation for H-atom isomerisation forming a 4-membered ring transition state is fitted to  $\Delta^\ddagger H_{0K} = 0.41 (\pm 0.1) \times \Delta_r H_{0K} + 164.74 (\pm 1.27) \text{ kJ mol}^{-1}$  with an  $R^2$  of 0.90. For H-atom isomerisation reactions forming a 5-membered transition state, the Evans-Polanyi correlation is fitted to  $\Delta^\ddagger H_{0K} = 0.33 (\pm 0.1) \times \Delta_r H_{0K} + 100.65 (\pm 0.85) \text{ kJ mol}^{-1}$  with an  $R^2$  of 0.86. There is a very weak correlation for C–C scission reactions, and no obvious trend was observed.

There are five unimolecular decomposition reactions for the pentyl radicals ( $a\dot{C}_5H_{11}$ ,  $b\dot{C}_5H_{11}$ ,  $c\dot{C}_5H_{11}$  and  $d\dot{C}_5H_{11}$ ). The  $a\dot{C}_5H_{11}$  radical has two decomposition pathways: C–C  $\beta$ -scission (R18) forming propene and ethyl radical and a second (R19) forming 1-butene and methyl radical, with 0 K barriers of 121.05 and 128.79  $\text{kJ mol}^{-1}$ , respectively. Its isomerisation reactions can yield  $b\dot{C}_5H_{11}$  (R23),  $c\dot{C}_5H_{11}$  (R24) and  $d\dot{C}_5H_{11}$  (R25) radicals with

barrier heights of 150.54, 158.15 and 99.62 kJ mol<sup>-1</sup> respectively. The reaction R25 involves a five membered ring transition state and thus has a substantially lower barrier height than R23 and R24, which are three and four membered ring transition states.

For  $b\dot{C}_5H_{11}$ , C–C  $\beta$ -scission occurs (R20), leading to the formation of isobutene and methyl radicals with a barrier height of 124.36 kJ mol<sup>-1</sup>.  $c\dot{C}_5H_{11}$  radicals can form 2-butene and methyl radicals (R21) through C–C  $\beta$ -scission, with a barrier height of 128.13 kJ mol<sup>-1</sup>, while C–C  $\beta$ -scission of  $d\dot{C}_5H_{11}$  radicals (R22) has the lowest reaction barrier of the unimolecular decomposition pathways. Its decomposition leads to the formation of ethylene and *iso*-propyl radicals, with a barrier height of 115.58 kJ mol<sup>-1</sup>. Isomerisation of  $b\dot{C}_5H_{11}$  to  $c\dot{C}_5H_{11}$  (R26), can occur with a barrier height of 170.03 kJ mol<sup>-1</sup>, while isomerisation of  $b\dot{C}_5H_{11}$  to  $d\dot{C}_5H_{11}$  (R27) radicals has a computed barrier of 171.54 kJ mol<sup>-1</sup>. The  $c\dot{C}_5H_{11}$  radical can isomerise to  $d\dot{C}_5H_{11}$ , with a barrier height of 168.72 kJ mol<sup>-1</sup>.



**Figure 3.12.** Branching ratio at 0.1, 1, and 10 atm for (a)  $a\dot{C}_5H_{11}$ , (b)  $b\dot{C}_5H_{11}$ , (c)  $c\dot{C}_5H_{11}$  and (d)  $d\dot{C}_5H_{11}$ . 0.1 atm (dotted lines), 1 atm (dashed lines) and 10 atm (solid lines).

Figure 3.12 illustrates the temperature- and pressure-dependent branching ratios for  $a\dot{C}_5H_{11}$ ,  $b\dot{C}_5H_{11}$ ,  $c\dot{C}_5H_{11}$  and  $d\dot{C}_5H_{11}$  radical unimolecular reactions at 0.1, 1.0, and 10 atm. The isomerisation of  $\dot{C}_5H_{11}$  to  $d\dot{C}_5H_{11}$  is favoured at temperatures up to 600 K for all pressures. At higher temperatures, the formation of propene and ethyl radicals dominates the reaction flux. The fates of the  $b\dot{C}_5H_{11}$  and  $c\dot{C}_5H_{11}$  radicals are clear: the former almost exclusively produces

isobutene and methyl radicals, while  $c\dot{C}_5H_{11}$  radicals primarily produce 2-butene and methyl radicals. For  $d\dot{C}_5H_{11}$  radicals, isomerisation to  $a\dot{C}_5H_{11}$  radicals is favoured at temperatures up to 500 K, while the formation of ethylene and iso-propyl radicals dominates at higher temperatures.

### 3.2.2.1. Rate Constant Comparisons

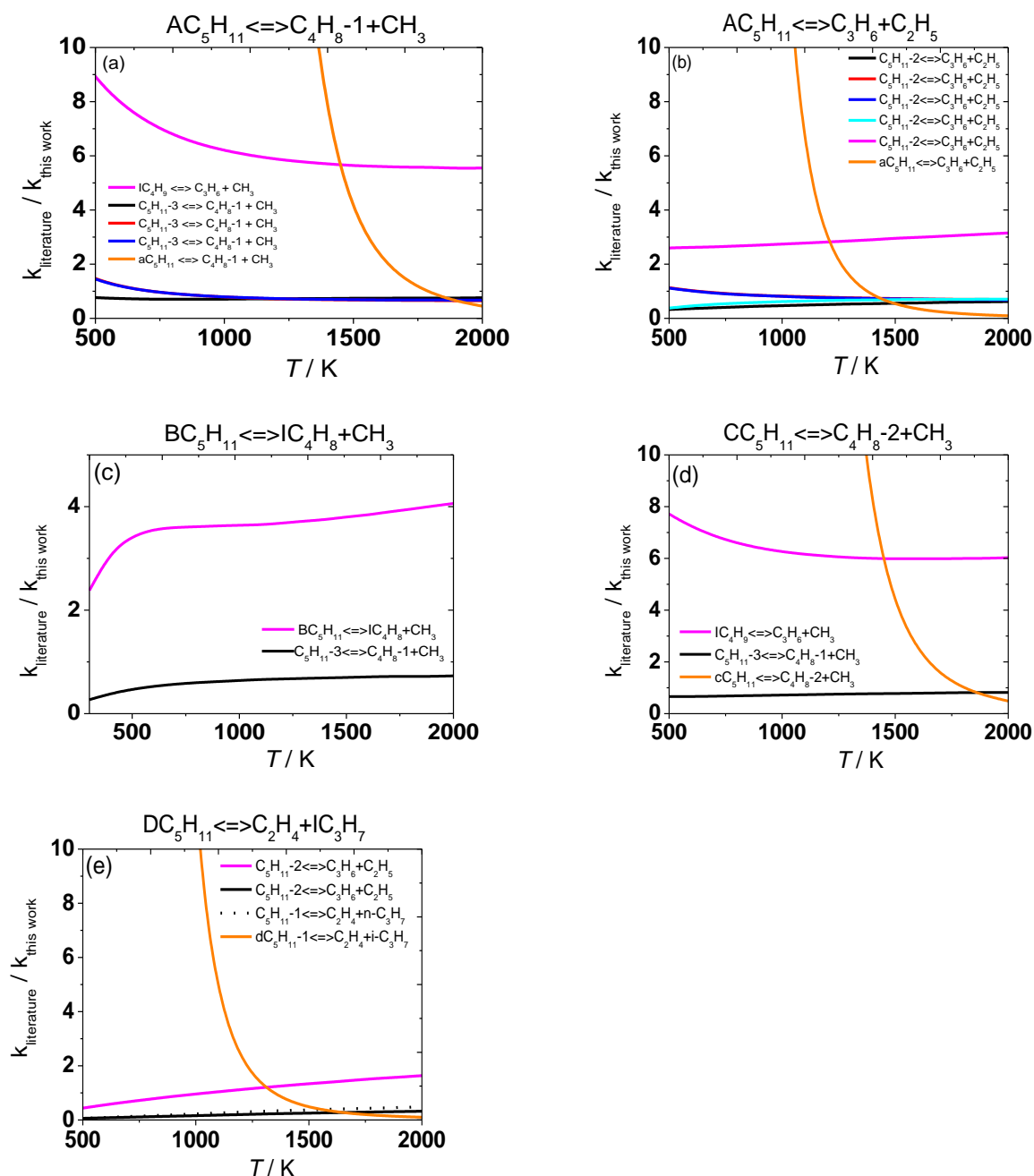


**Figure 3.13.** High-pressure limit rate constant comparisons for pentyl radical decomposition reactions. Rate constants are expressed as a ratio of  $k_{\text{literature}} / k_{\text{this work}}$ . Different literature studies are represented as follows; Power [2] (black), Awan [44] (red), Comandini [45] (blue), Jitariu [52] (cyan), Curran [29] (magenta), and Leon [8] (orange).

There are limited data available for the decomposition of branched pentyl radicals. However we have compared our theoretical results with those used in the current pentene models [11] and analogous reactions from the literature and from our previous study on  $\dot{\text{H}}$  + 1- and 2-pentene [2]. The rate constants by Leon et al. [8] have been plotted but appear to be outliers, except for the reaction  $\text{b}\dot{\text{C}}_5\text{H}_{11} \leftrightarrow \text{iC}_4\text{H}_8 + \dot{\text{C}}\text{H}_3$ , which was taken from the recommendations by Curran [29]. Good agreement is observed between the current work and other literature studies by Awan, Comandini and Jitariu [44, 45, 52]. Our results are within a factor of two of these literature studies for the analogous reactions in the temperature range 500–2000 K and are also consistent with our earlier pentene results. However as noted, large deviations from earlier work are observed. Curran [29] estimated rate constants for  $\text{C}_1$  to  $\text{C}_4$  alkyl and alkoxy radical decomposition. Rate constants for the addition of a radical species to the olefin were studied, with the forward rate expression then being determined through microscopic reversibility. Although these provide very useful tools for the combustion community, the calculated rate constants employed in the current work using ab-initio methods, are more reliable.

Figure 3.13 (a) presents rate constant comparisons for  $\text{a}\dot{\text{C}}_5\text{H}_{11} \leftrightarrow \text{C}_4\text{H}_8\text{-1} + \dot{\text{C}}\text{H}_3$ . Rate constants for the reaction  $\dot{\text{C}}_5\text{H}_{11}\text{-3} \leftrightarrow \text{C}_4\text{H}_8\text{-1} + \dot{\text{C}}\text{H}_3$  from our previous work [2], Awan [44] and Comandini et al. [45] will be used as a comparison for the reaction  $\text{a}\dot{\text{C}}_5\text{H}_{11} \leftrightarrow \text{C}_4\text{H}_8\text{-1} + \dot{\text{C}}\text{H}_3$  calculated here. Additionally, the rate constant recommended by Curran [29] for  $\text{i}\dot{\text{C}}_4\text{H}_9 \leftrightarrow \text{C}_3\text{H}_6 + \dot{\text{C}}\text{H}_3$  will be used as an analogous comparison. The rate constant from our previous work [2] is in excellent agreement, with the rate constants being almost identical. Awan and Comandini et al. [44, 45] are within a factor of  $\sim 1.5$  of this work from 500–2000 K. This difference can be attributed to the difference of  $4.59 \text{ kJ mol}^{-1}$  in reaction barrier, using their [44] “best fit model” energy barrier values. The rate constant from Curran [29] is within a factor of  $\sim 6-7$  from 800 K.

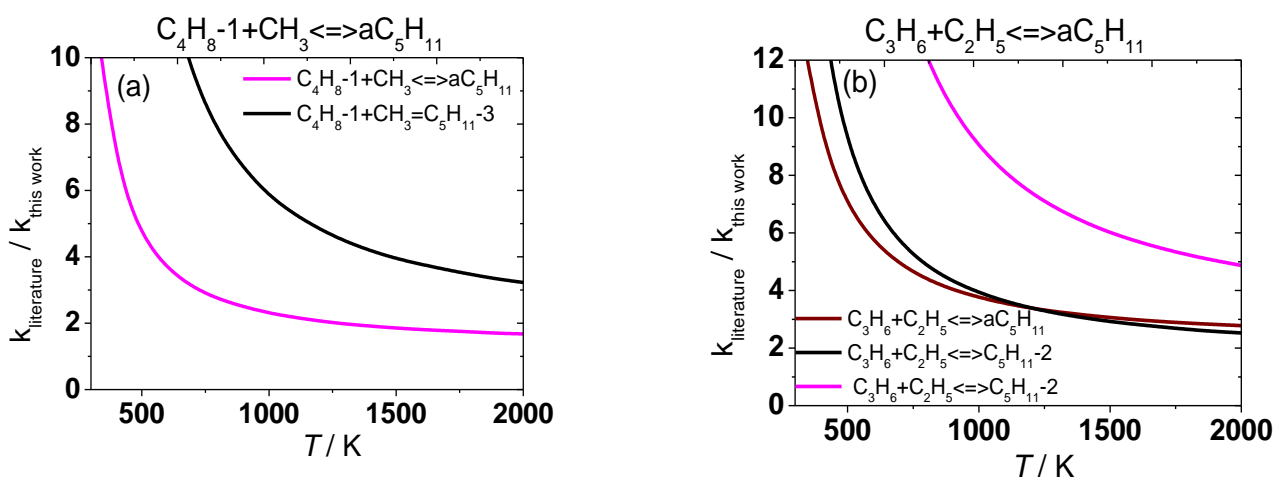
Rate constants for  $\dot{\text{C}}_5\text{H}_{11}\text{-2}$  decomposition to  $\text{C}_3\text{H}_6 + \dot{\text{C}}_2\text{H}_5$  from our previous work [2], Curran [29], Awan [44], Comandini [45] and Jitariu et al. [52] have been used as comparisons for the reaction  $\text{a}\dot{\text{C}}_5\text{H}_{11} \leftrightarrow \text{C}_3\text{H}_6 + \dot{\text{C}}_2\text{H}_5$ , Fig. 3.13(b). Our previous work [2] is a factor of  $\sim 2$  slower than that of the current work at 1000 K, and reduces to a factor of  $\sim 1.6$  at 2000 K. The difference of  $1.89 \text{ kJ mol}^{-1}$  in energy barrier accounts for a factor of 1.3 of this difference at 1000 K. Awan and Comandini et al. [44, 45] are in excellent agreement with this work, with rate constants being within a factor of  $\sim 1.5$  over the temperature range 300–2000 K. Jitariu et al. [52] are a factor of  $\sim 2$  slower than the current work at 600 K, reducing to a factor of  $\sim 1.5$  at  $T > 1200 \text{ K}$ . Again, the difference of 3.35 and  $6.14 \text{ kJ mol}^{-1}$  in energy

barriers between this work and Awan/Comandini and this work and Jitariu, respectively would account for the differences observed. The rate constant recommended by Curran [29] for  $\dot{C}_5H_{11-2} \leftrightarrow C_3H_6 + \dot{C}_2H_5$  is within a factor of 2 – 3 of this work across the temperature range 300 – 2000 K.

Good agreement is observed for the reaction  $b\dot{C}_5H_{11} \leftrightarrow iC_4H_8 + \dot{C}H_3$  between Curran [29] and this work, and is within a factor of 3 – 4. The reaction of  $\dot{C}_5H_{11-3} \leftrightarrow C_4H_8-1 + \dot{C}H_3$  computed in our previous work is a factor of  $\sim 1.4 - 3.6$  slower than that of the current work, with the difference attributed to the difference in reaction barrier of  $3.95 \text{ kJ mol}^{-1}$ .

Figure 3.13(d) presents comparisons for the reaction  $c\dot{C}_5H_{11} \leftrightarrow C_4H_8-2 + \dot{C}H_3$ . Comparisons of our previous work for  $\dot{C}_5H_{11-3} \leftrightarrow C_4H_8-1 + \dot{C}H_3$  is in excellent agreement with the current work and is a factor of  $\sim 1.5$  slower across the entire temperature range. Rate constants by Curran [29] for the decomposition of  $i\dot{C}_4H_9$  radical to  $C_3H_6 + \dot{C}H_3$  is a factor of  $\sim 6 - 7$  times faster than the rate for  $c\dot{C}_5H_{11} \leftrightarrow C_4H_8-2 + \dot{C}H_3$  calculated in this work over the temperature range 600 – 2000 K.

Finally, Fig. 3.13(e) presents rates for the reaction  $d\dot{C}_5H_{11} \rightleftharpoons C_2H_4 + i\dot{C}_3H_7$ . Rate constants by Curran [29] for  $\dot{C}_5H_{11-2} \leftrightarrow C_3H_6 + \dot{C}_2H_5$  is in excellent agreement and is within a factor of  $\sim 1.6$  of the rate  $d\dot{C}_5H_{11} \leftrightarrow C_2H_4 + i\dot{C}_3H_7$  calculated here. Rate constants from our previous work [2] for  $\dot{C}_5H_{11-1} \leftrightarrow C_2H_4 + n\dot{C}_3H_7$  is a factor of  $\sim 4$  slower at 1000 K, reducing to a factor of  $\sim 2$  at 2000 K, which can be attributed to the difference in barrier height of  $7.68 \text{ kJ mol}^{-1}$ . The rate constant for  $\dot{C}_5H_{11-2} \leftrightarrow C_3H_6 + \dot{C}_2H_5$  in our previous work is a factor of  $\sim 6$  times slower at 1000 K, reducing to a factor of  $\sim 3$  at 2000 K. However, our calculated rate constant for  $\dot{C}_5H_{11-2} \leftrightarrow C_3H_6 + \dot{C}_2H_5$  [2] is in excellent agreement with Awan, Comandini and Jitariu et al. for the same reaction [44, 45, 52].



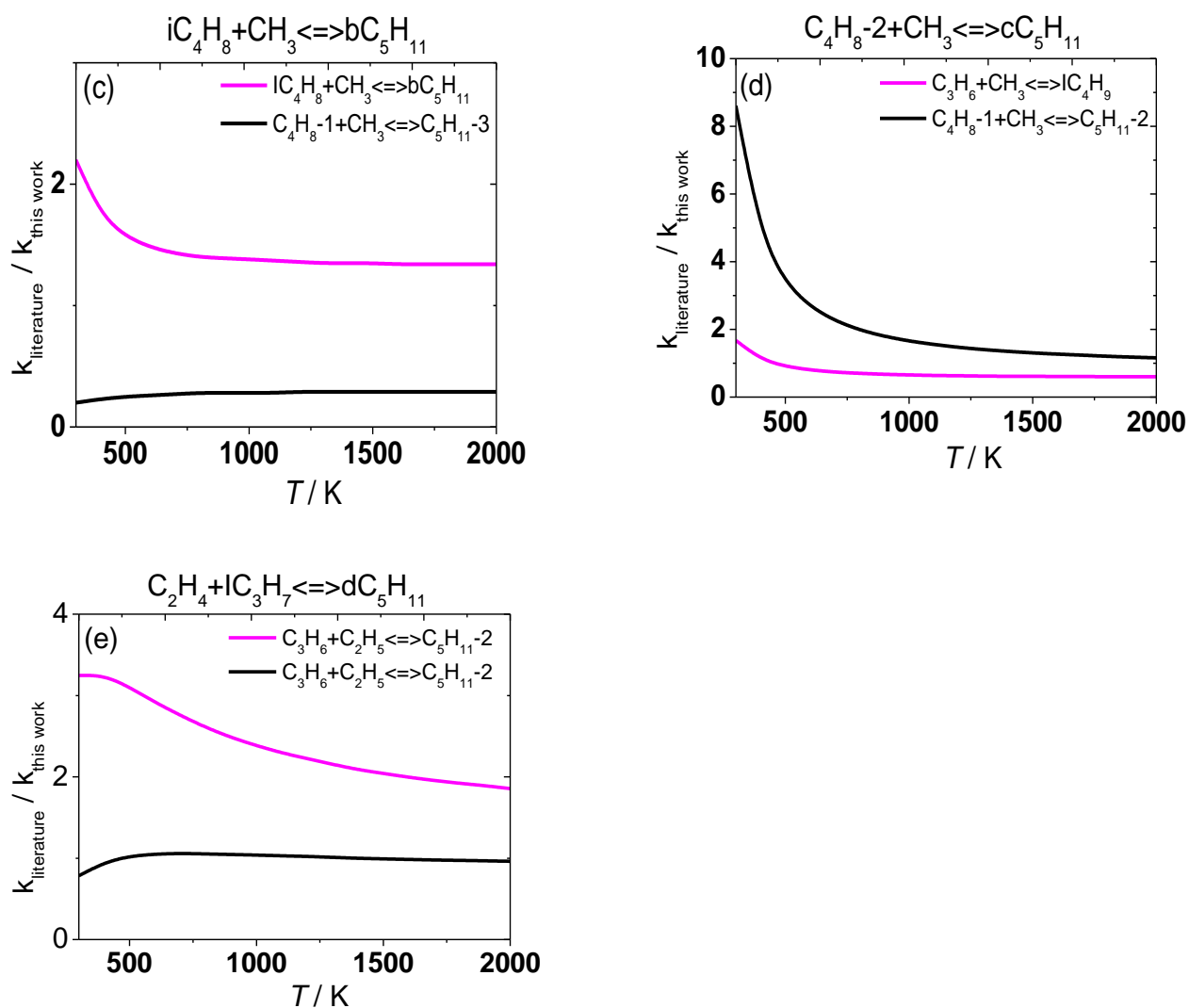


**Figure 3.14.** High-pressure limit rate constant comparisons for alkyl radical additions to olefins. Rate constants are expressed as a ratio of  $k_{\text{literature}} / k_{\text{this work}}$ . Different literature studies are represented as follows; Power [2] (black), Curran [29] (magenta) and Westbrook [11] (wine).

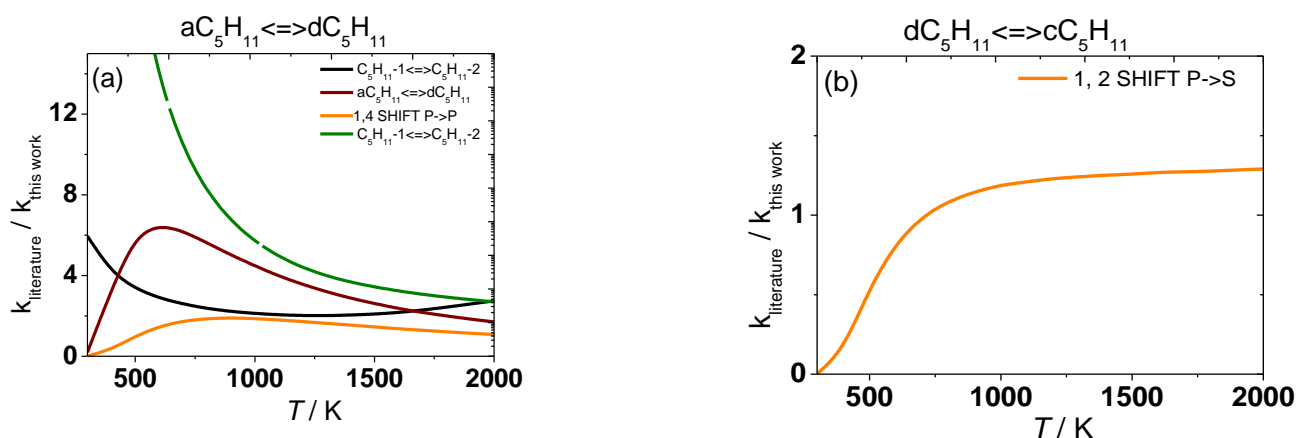
Figure 3.14 presents high-pressure limiting rate constant comparisons for alkyl radical additions to olefins. For the reaction  $\text{C}_4\text{H}_8\text{-1} + \dot{\text{C}}\text{H}_3 \leftrightarrow \text{a}\dot{\text{C}}_5\text{H}_{11}$ , Westbrook et al. [11] adopt a rate constant based on recommendations by Curran [29] for the reaction  $\text{C}_3\text{H}_6 + \dot{\text{C}}\text{H}_3 \leftrightarrow \text{i}\dot{\text{C}}_4\text{H}_9$  and is within a factor of  $\sim 2$  with this work in the temperature range 1000 – 2000 K. The rate for  $\text{C}_4\text{H}_8\text{-1} + \dot{\text{C}}\text{H}_3 \leftrightarrow \dot{\text{C}}_5\text{H}_{11}\text{-3}$  calculated previously [2] is a factor of  $\sim 5$  faster at 1000 K than our rate for  $\text{C}_4\text{H}_8\text{-1} + \dot{\text{C}}\text{H}_3 \leftrightarrow \text{a}\dot{\text{C}}_5\text{H}_{11}$ , reducing to a factor of  $\sim 3$  at 2000 K but is within a factor of  $\sim 2.5$  at 1000 K with the rate adopted by Westbrook et al.



The rate constants used by Westbrook et al. [11] in their model were taken from rate constant recommendations by Curran [29], except for the reaction  $C_3H_6 + \dot{C}_2H_5 \leftrightarrow a\dot{C}_5H_{11}$ . From 800 – 2000 K, the rate adopted by Westbrook [11] is within a factor of  $\sim 4.4$  of the rate computed here and is almost identical to the rate calculated in our previous work for  $C_3H_6 + \dot{C}_2H_5 \leftrightarrow \dot{C}_5H_{11-2}$ . The rate recommended by Curran [29] for  $C_3H_6 + \dot{C}_2H_5 \leftrightarrow \dot{C}_5H_{11-2}$  is a factor of  $\sim 9$  faster at 1000 K and  $\sim 5$  at 2000 K than the rate for  $C_3H_6 + \dot{C}_2H_5 \leftrightarrow a\dot{C}_5H_{11}$  calculated here. However, the value recommended by Curran [29] is within a factor of  $\sim 2.5$  with our computed rate for  $C_3H_6 + \dot{C}_2H_5 \leftrightarrow \dot{C}_5H_{11-2}$  from our previous work over the temperature range 800 – 2000 K [2].

Westbrook adopt the rate constant by Curran [29] for  $iC_4H_8 + \dot{C}H_3 \leftrightarrow b\dot{C}_5H_{11}$ , which is in excellent agreement with the current work. The rate constant for  $C_4H_8-2 + \dot{C}H_3 \leftrightarrow c\dot{C}_5H_{11}$  adopted by Westbrook is taken from Curran [29], using  $C_3H_6 + \dot{C}H_3 \leftrightarrow i\dot{C}_4H_9$  as an analogy, and again excellent agreement is observed, with rate constants being within  $\sim 1.6$  across the entire temperature range. Additionally, rate constants from our previous work for  $C_4H_8-1 + \dot{C}H_3 \leftrightarrow \dot{C}_5H_{11-3}$  are a factor of  $\sim 3$  slower across the entire temperature range. The difference of  $6.24 \text{ kJ mol}^{-1}$  in energy barrier accounts for this difference.

For  $C_2H_4 + i\dot{C}_3H_7 \leftrightarrow d\dot{C}_5H_{11}$ , good agreement is observed. Westbrook [11] adopt the rate recommended by Curran [29] for  $C_3H_6 + \dot{C}_2H_5 \leftrightarrow \dot{C}_5H_{11-2}$  and is within a factor of two across the temperature range 800 – 2000 K. The rate constant for  $C_3H_6 + \dot{C}_2H_5 \leftrightarrow \dot{C}_5H_{11-2}$  from our previous work is also in excellent agreement with the rate  $C_2H_4 + i\dot{C}_3H_7 \leftrightarrow d\dot{C}_5H_{11}$  calculated here, with the discrepancy explained by the difference in energy barrier of  $2.53 \text{ kJ mol}^{-1}$ .



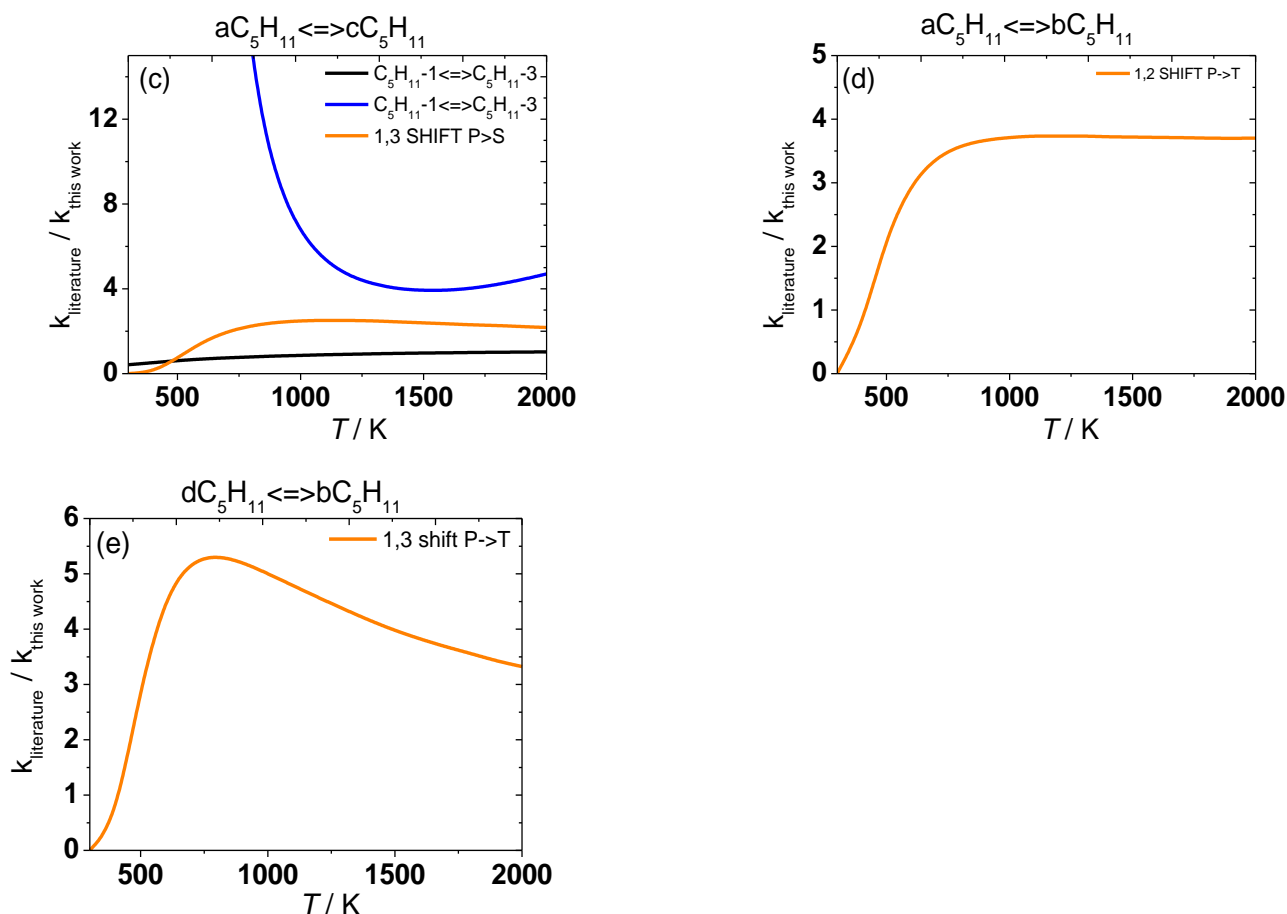


**Figure 3.15.** High-pressure limit rate constant comparisons for H-atom shift isomerisation reactions. Rate constants are expressed as a ratio of  $k_{\text{literature}} / k_{\text{this work}}$ . Different literature studies are represented as follows; Power [2] (black), Comandini [45] (blue), Matheu [53] (orange), Yu [54] (green), and Westbrook [11] (wine). P→P, P→S, and P→T represent hydrogen atom shift from primary carbon to primary, secondary and tertiary carbons, respectively.

Similarly, limited results for the isomerisation reactions for branched pentyl radicals exist, therefore comparisons with what is in the current models [8, 11], analogous reactions from literature and our previous work [2] will be made. Figure 3.15 (a) presents the rate computed for  $a\dot{C}_5H_{11} \rightleftharpoons d\dot{C}_5H_{11}$  with some literature studies of 1,2 H-atom shift through a five-membered ring transition state. At 1000 K, the rate adopted by Westbrook [11] for this reaction is a factor of  $\sim 4.5$  faster than this work, reducing to a factor of  $\sim 2$  at higher temperatures. The rate constant published by Matheu et al. [53] (1,4 isomerisation of a primary to primary) is within a factor of  $\sim 2$  of the rate calculated in this work. The rate constant from our previous work for  $\dot{C}_5H_{11-1} \rightleftharpoons \dot{C}_5H_{11-2}$  is within a factor of 2–3 of our rate constant for  $a\dot{C}_5H_{11} \rightleftharpoons d\dot{C}_5H_{11}$  from 500 K. The difference of  $3.11 \text{ kJ mol}^{-1}$  in energy barrier

would account for a factor of 2.11 at 500 K. Also plotted is the rate constant from Yu et al. [54], who are a factor of  $\sim 5$  faster at 1000 K, reducing to a factor of  $\sim 2$  at higher temperatures, which was also found in our previous work for the reaction  $\dot{C}_5H_{11-1} \rightleftharpoons \dot{C}_5H_{11-2}$ . A further description for comparisons with this rate constant can be found in the supplementary material of our previous work [2]. The main finding was that these multi-structural variational effects seem to influence rate constants at lower temperatures more so than higher temperatures. At higher temperatures, the rate constants calculated in the current and past works are within a factor of two, and our validation against the  $\dot{H}$ -ARAS shock tube experiments show that our rate constants are accurate to within this factor.

For  $d\dot{C}_5H_{11} \rightleftharpoons c\dot{C}_5H_{11}$ , comparison with the rate by Matheu et al. [53] for a 1,2 H-atom isomerisation from primary to secondary is in excellent agreement with the current work. Figure 3.15 (c) presents rate constants for the reaction  $a\dot{C}_5H_{11} \rightleftharpoons c\dot{C}_5H_{11}$ . Matheu et al. [53] rate for (1,3 isomerisation from primary to secondary) are within a factor of  $\sim 2$ – $2.5$  over the entire temperature range with the current work. The rate by Comandini et al. [45] for  $\dot{C}_5H_{11-1} \rightleftharpoons \dot{C}_5H_{11-3}$  is approximately seven times faster at 1000 K, reducing to a factor of five at 2000 K. As discussed in the Supplementary material of our previous work [2], their [44] energy barrier for the reaction  $\dot{C}_5H_{11-1} \rightleftharpoons \dot{C}_5H_{11-3}$  was corrected to  $144.5 \text{ kJ mol}^{-1}$ , which is  $14.95 \text{ kJ mol}^{-1}$  lower than our computed barrier for  $a\dot{C}_5H_{11} \rightleftharpoons c\dot{C}_5H_{11}$ , which would account for the difference. Excellent agreement with our previous work on  $\dot{C}_5H_{11-1} \rightleftharpoons \dot{C}_5H_{11-3}$  is observed.

At temperatures in the range 500 – 2000 K, the rate constant for 1,2 H-atom isomerisation from primary  $\rightleftharpoons$  tertiary by Matheu [53] is within a factor  $\sim 2$  –  $3.7$  of our rate for  $a\dot{C}_5H_{11} \rightleftharpoons b\dot{C}_5H_{11}$ .

Finally, comparison of our rate for  $d\dot{C}_5H_{11} \rightleftharpoons b\dot{C}_5H_{11}$  is presented in Fig.3.15 (e) Matheu et al. [53] are a factor of  $\sim 5$  faster than the rate in the current work at 1000 K, reducing to a factor of  $\sim 3$  at 2000 K.

#### 4. Detailed Kinetic Modelling

All simulations were performed using Chemkin-Pro [55] assuming a constant volume homogeneous batch reactor. The model was developed by implementing our computed thermochemistry and rate constants into NUIGMech1.0 [14, 24-27] which contains our quantum chemical calculations based on this work. This model was then used to simulate recent results from a pyrolysis study of the pentene isomers using the NUIG single pulse shock-tube (dotted lines).

The reaction flux analyses for 2M1B, 2M2B and 3M1B pyrolysis are described in detail by Nagaraja et al. so we shall not reproduce that here. To summarise, propene and isobutene are formed through the chemically activated pathways of  $\dot{H}$  atom addition to 2M1B. The current model over-predicts the mole fraction of isobutene, but propene is sufficiently captured, (Fig. 3.16). Upon H-atom abstraction from the primary and secondary allylic sites of 2M1B, the  $a\dot{C}_5H_9-a2$  and  $a\dot{C}_5H_9-c$  radicals are formed, respectively. The  $a\dot{C}_5H_9-a2$  radical forms allene, while  $a\dot{C}_5H_9-c$  produces isoprene, both of which are captured well by the current model.

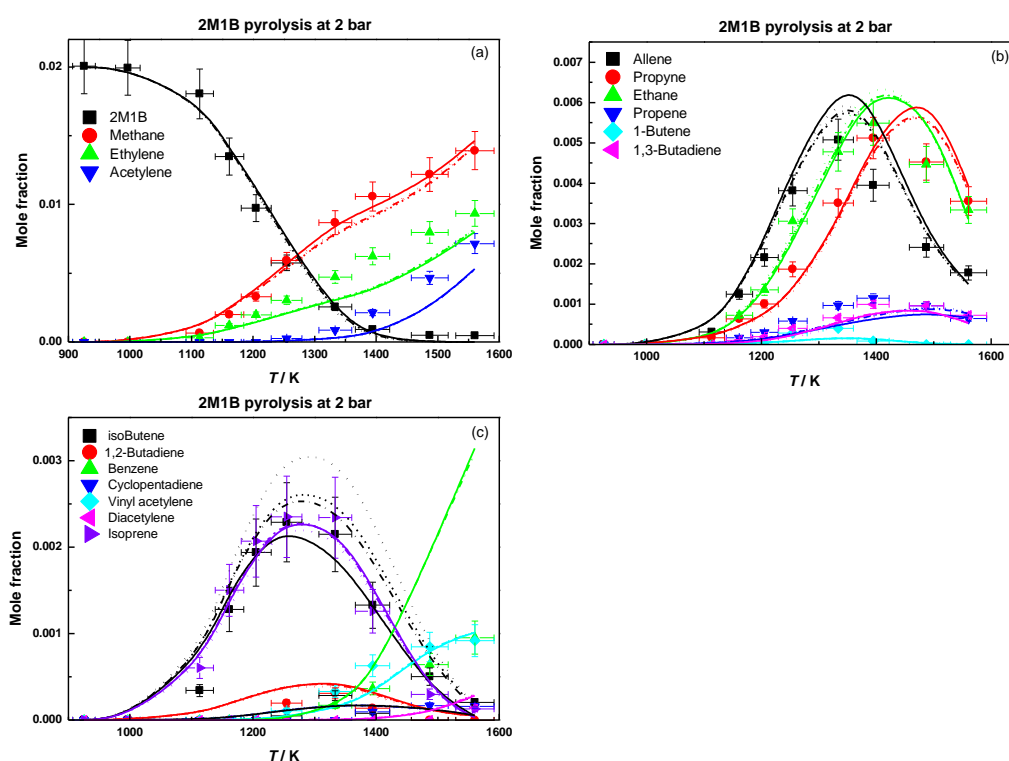


**Figure 3.16.** Species profiles for 2M1B pyrolysis. Dotted lines are model simulations with the current model, dashed lines represent approximate variational effects predictions, dashed-dot lines represent these approximate variational effects along with changes to  $\dot{C}H_3$  abstraction reactions in the current model and solid lines represent all these changes in addition to altering  $\dot{C}H_3$  abstraction from isobutene by a factor of two.

Isobutene and 2-butene are formed through the chemical activated pathways of  $\dot{H}$  atom addition to 2M2B. Similar to 2M1B, the  $a\dot{C}_5H_9-c$  radical is formed via H-atom abstraction, and dissociates to form isoprene +  $\dot{H}$ . All species are captured well by the current model, (Fig. 3.17).

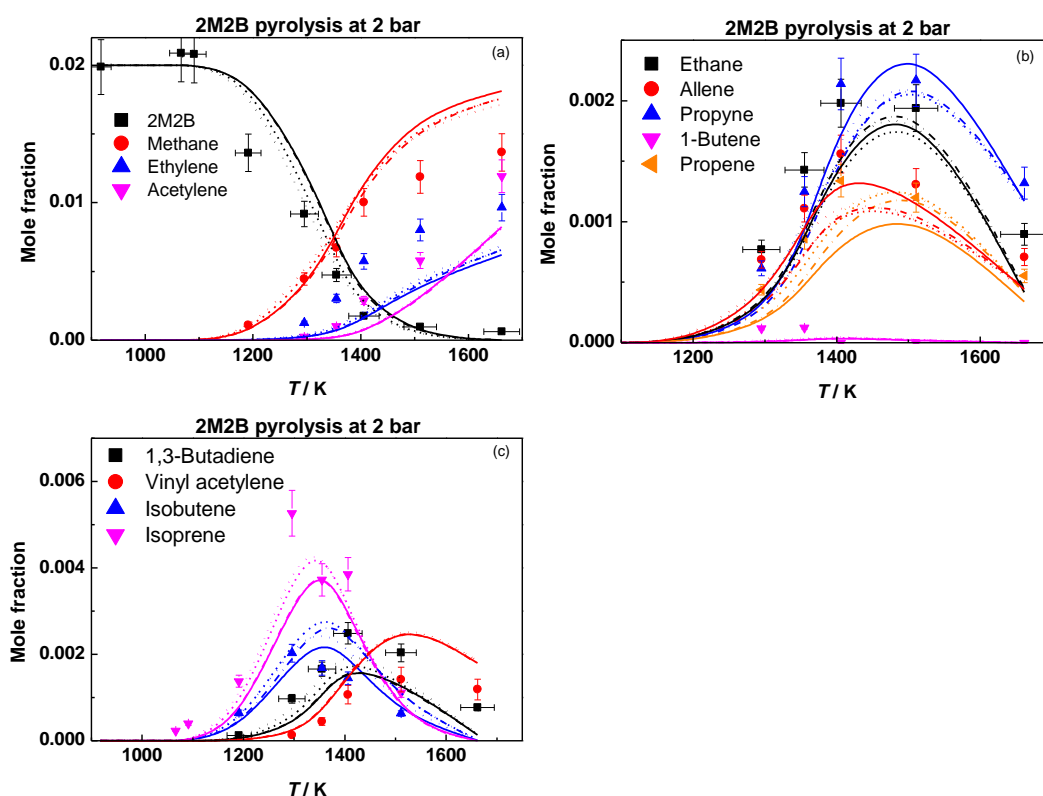


**Figure 3.17.** Species profiles for 2M2B pyrolysis. Dotted lines are model simulations with the current model, dashed lines represent approximate variational effects predictions, dashed-dot lines represent these approximate variational effects along with changes to  $\dot{\text{C}}\text{H}_3$  abstraction reactions in the current model and solid lines represent all these changes in addition to altering  $\dot{\text{C}}\text{H}_3$  abstraction from isobutene by a factor of two.

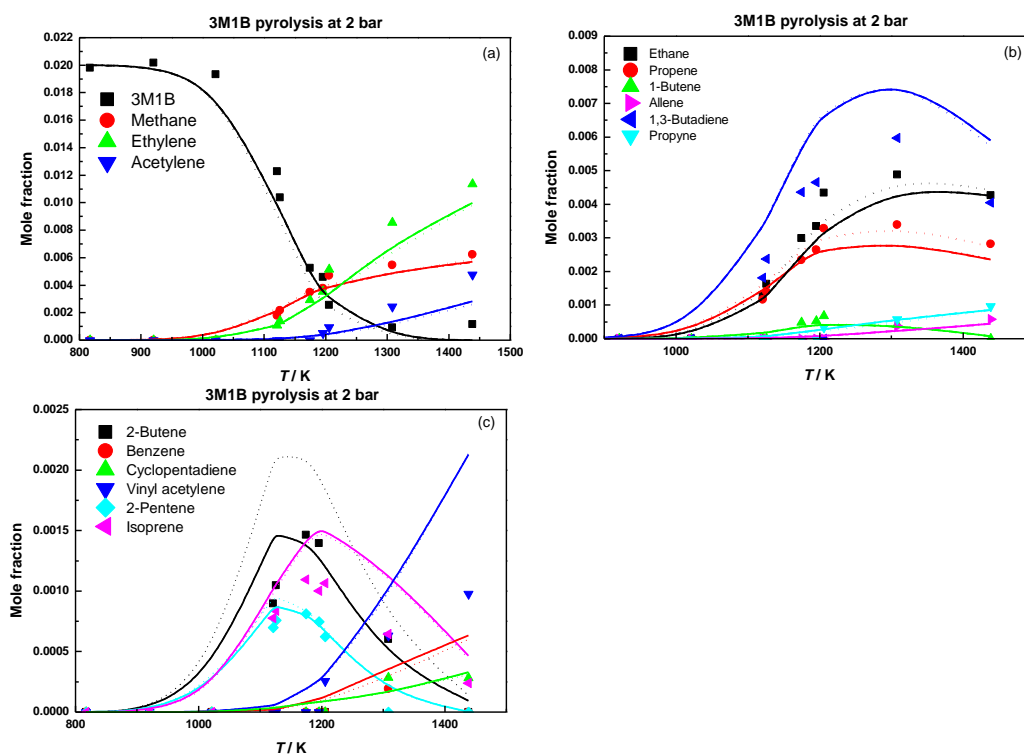


**Figure 3.18.** Species profiles for 3M1B pyrolysis. Dotted lines are model simulations with the current model, dashed lines represent approximate variational effects predictions, dashed-dot lines represent these approximate variational effects along with changes to  $\dot{\text{C}}\text{H}_3$  abstraction reactions in the current model and solid lines represent all these changes in addition to altering  $\dot{\text{C}}\text{H}_3$  abstraction from isobutene by a factor of two.

In the case of 3M1B, ethylene and 2-butene are the products formed via the chemically activated pathways of  $\dot{\text{H}}$  atom addition. It can be observed in Fig.3.18 that ethylene is sufficiently captured, while 2-butene is slightly over-predicted. Upon H-atom abstraction from the tertiary allylic site of 3M1B, the  $\text{c}\dot{\text{C}}_5\text{H}_9\text{-b}$  radical is formed which again dissociates to isoprene, which is captured well by the current model.

Whilst the current model shows a good performance against the ST data, it is worth commenting on the influence of factors which have not been explicitly treated in our RRKM/ME model. Test calculations showed that the inclusion of vibrational anharmonicities has a modest effect, accounting for ~2–5% variations in the calculated high-pressure limiting rate constants (Section 2.0 of Supplementary\_Material\_2. of ESI). Variational effects were found to be completely negligible for isomerisation reactions [52, 56–58] and abstraction reactions, amounting to 15% in the latter case. However, for hydrogen atom addition

reactions, variational effects may be considerable, with test computations implying that the high-pressure limiting rate constant for external  $\dot{\text{H}}$  atom addition to 2M1B is over-estimated by a factor of 2–3. This is in line with the variational effect observed by others for  $\dot{\text{H}}$  atom addition reactions to large molecular weight species [59]. To assess the influence of variational effects on predictions of experimental data, indicative simulations have been carried out and presented in Section 1.0 of Supplementary\_Material\_2 included as ESI, by systematically reducing the rate constants for  $\dot{\text{H}}$  atom addition by a factor of two in the RRKM/ME model and re-computing  $k(T,p)$ . Reductions in the rate constants for the  $\dot{\text{H}}$  atom addition pathways (dashed lines) do not lead to significant changes in the predictions of major species mole fractions for 2M1B and 2M2B. For 2M2B, iso-butene yields were found to increase by up to ~20%, Figure 3.17 (c). For 2M1B isobutene yields decreased by up to 20%, while 2-butene yields decreased by up to 66 % for 3M1B.

For 2M2B, preliminary simulations showed that  $\dot{\text{C}}\text{H}_3$  abstraction from isobutene is a major consumption pathway for isobutene. The rate constant that is currently in the mechanism is twice the rate constant of  $\dot{\text{C}}\text{H}_3$  abstraction from propene [60]. This was changed to the recommended rate constant for  $\dot{\text{C}}\text{H}_3$  from isobutene, with the largest difference being a factor of 1.44 at 298 K [60]. Additionally, the rate constant for  $\dot{\text{C}}\text{H}_3$  abstraction from 2M2B is twice the rate constant for  $\dot{\text{C}}\text{H}_3$  abstraction for primary allylic sites. This was reduced by a factor of two. The combined effect of variational effects and alterations to both these abstraction rate constants is represented by dashed-dotted lines. This results in a slight decrease of isobutene yields for both 2M2B and 2M1B.

Wang et al. [60] quotes an uncertainty of a factor of two in the rate rules. Therefore, the rate constant for  $\dot{\text{C}}\text{H}_3$  abstraction from isobutene was increased by a factor of two. The combined variational effects and abstraction reactions, with the rate constant for  $\dot{\text{C}}\text{H}_3$  abstraction from isobutene increased by a factor of two is represented by solid lines. Increasing this rate constant leads to better agreement in the predicted formation of isobutene from 2M1B and 2M2B. Additionally, for 2M1B and 2M2B, allene and propyne yields also increase since there is an increase in  $i\dot{\text{C}}_4\text{H}_7$  radicals formed. The propene yields decrease due to the increased importance of  $\dot{\text{C}}\text{H}_3$  abstraction from isobutene which competes with  $i\text{C}_4\text{H}_8 + \dot{\text{H}} \leftrightarrow \text{C}_3\text{H}_6 + \dot{\text{C}}\text{H}_3$ .

Since the inclusion of variational effects worsens the agreement with the experiments of Nagaraja et al. [14] in one instance (isobutene mole fractions for 2M2B), the agreement of our non-variational model with experiment is potentially fortuitous as it is dependent on the cancellation of multiple errors, albeit ones which are typical of those found in chemical

kinetic models for species of this size. The uncertainty in these secondary reactions which are based on estimated rate constants [60] is on a par with or greater than the systems studied herein, and test simulations show that modifications of a factor of two in  $\dot{\text{C}}\text{H}_3$  abstraction rate constants coupled with an estimate of variational effects (solid lines) leads to predictions of iso-butene to within a within  $\sim 40\%$  at temperatures greater than  $\sim 1100\text{ K}$  for 2M1B and  $\sim 40\%$  for 2M2B. Theoretical studies of  $\dot{\text{C}}\text{H}_3$  abstraction reactions from alkenes for which theoretical data and direct experimental measurement is currently sparse, especially for larger alkenes [60] would therefore be of use in reducing uncertainty in available kinetic models. Direct measurements of the reactions of  $\dot{\text{H}}$  atoms with branched alkenes would also provide a more direct means to validate the theory presented in this work.

## 5. Conclusions

Alkenes are key components of real-world fuels, with pentenes of particular importance as components of gasoline. This study extends our earlier study on the reactions of hydrogen atoms with 1- and 2-pentene [2] to those with the branched pentene isomers; 2-methyl-1-butene, 2-methyl-2-butene and 3-methyl-1-butene. Together, these results are the most comprehensive investigation of these reaction systems and contribute to the development of combustion models. Thermochemical data for species on the  $\dot{\text{C}}_5\text{H}_{11}$  PES were calculated as a function of temperature with formation enthalpies derived using a network of isodesmic reactions based upon benchmark literature data and electronic structure calculations. Rice-Ramsperger-Kassel-Marcus (RRKM) theory with a one-dimensional master equation (ME) analysis was used to calculate high-pressure-limiting and temperature- and pressure-dependent rate constants. The theoretical results are implemented into a detailed chemical model and simulated against species mole fractions from the pyrolysis study of the pentene isomers using the NUIG single pulse shock-tube. The chemically activated pathways of  $\dot{\text{H}}$  atom addition to each of the pentene isomers, as well as their abstraction reactions were found to be important in capturing the species profiles of the products from pyrolysis, with satisfactory agreement being observed. Although good agreement is observed between our model predictions and experiment, future works should consider addressing VTST, treatment of multi-dimensional torsions, and anharmonic effects in the aim of developing a more comprehensive RRKM/ME model for combustion modelling. Additionally, rate constant recommendations for  $\dot{\text{H}}$  atom addition to and abstraction from linear and branched alkenes have been proposed and serve as a tool for the use in mechanisms of larger alkenes for which calculations do not exist in the literature.



## **Associated Content**

The supplementary material (SM) contains MESS input and output files, tabulated isodesmic reactions, thermochemical values for all C<sub>5</sub> species in NASA polynomial format, Chemkin format PLOG rate constant fits and mechanism/thermochemistry files used in simulations (ZIP).

## **Acknowledgements**

The authors would like to acknowledge the support of Science Foundation Ireland in funding this project under 15/IA/3177 and also to the Irish Centre for High-End Computing, ICHEC, under project numbers ngche058c and ngche080c.

## References

- [1] S. Kikui, H. Nakamura, T. Tezuka, S. Hasegawa, K. Maruta, Study on combustion and ignition characteristics of ethylene, propylene, 1-butene and 1-pentene in a micro flow reactor with a controlled temperature profile, *Combust. Flame* 163 (2016) 209-219.
- [2] J. Power, K.P. Somers, C.-W. Zhou, S. Peukert, H.J. Curran, Theoretical, experimental, and modeling study of the reaction of hydrogen atoms with 1- and 2-pentene, *J. Phys. Chem. A* 123 (2019) 8506-8526.
- [3] M. Mehl, T. Faravelli, F. Giavazzi, E. Ranzi, P. Scorletti, A. Tardani, D. Terna, Detailed chemistry promotes understanding of octane numbers and gasoline sensitivity, *Energy Fuels* 20 (2006) 2391-2398.
- [4] S.M. Burke, W. Metcalfe, O. Herbinet, F. Battin-Leclerc, F.M. Haas, J. Santner, F.L. Dryer, H.J. Curran, An experimental and modeling study of propene oxidation. Part 1: speciation measurements in jet-stirred and flow reactors, *Combust. Flame* 161 (2014) 2765-2784.
- [5] Y. Li, C.-W. Zhou, K.P. Somers, K. Zhang, H.J. Curran, The oxidation of 2-butene: a high pressure ignition delay, kinetic modeling study and reactivity comparison with isobutene and 1-butene, *Proc. Combust. Inst.* 36 (2017) 403-411.
- [6] C.-W. Zhou, Y. Li, E. O'Connor, K.P. Somers, S. Thion, C. Keesee, O. Mathieu, E.L. Petersen, T.A. DeVerter, M.A. Oehlschlaeger, et al., A comprehensive experimental and modeling study of isobutene oxidation, *Combust. Flame* 167 (2016) 353-379.
- [7] M.R. Djokic, K.M. Van Geem, C. Cavallotti, A. Frassoldati, E. Ranzi, G.B. Marin, An experimental and kinetic modeling study of cyclopentadiene pyrolysis: first growth of polycyclic aromatic hydrocarbons, *Combust. Flame* 161 (2014) 2739-2751.
- [8] L. León, L. Ruwe, K. Moshhammer, L. Seidel, K.P. Shrestha, X. Wang, F. Mauss, K. Kohse-Höinghaus, N. Hansen, Chemical insights into the larger sooting tendency of 2-methyl-2-butene compared to n-pentane, *Combust. Flame* 208 (2019) 182-197.
- [9] L. Ruwe, K. Moshhammer, N. Hansen, K. Kohse-Höinghaus, Consumption and hydrocarbon growth processes in a 2-methyl-2-butene flame, *Combust. Flame* 175 (2017) 34-46.
- [10] L. Ruwe, K. Moshhammer, N. Hansen, K. Kohse-Höinghaus, Influences of the molecular fuel structure on combustion reactions towards soot precursors in selected alkane and alkene flames, *Phys. Chem. Chem. Phys.* 20 (2018) 10780-10795.
- [11] C.K. Westbrook, W.J. Pitz, M. Mehl, P.-A. Glaude, O. Herbinet, S. Bax, F. Battin-Leclerc, O. Mathieu, E.L. Petersen, J. Bugler, H.J. Curran, Experimental and kinetic modeling study of 2-methyl-2-butene: allylic hydrocarbon kinetics, *J. Phys. Chem. A* 119 (2015) 7462-7480.
- [12] Y. Cheng, E. Hu, X. Lu, X. Li, J. Gong, Q. Li, Z. Huang, Experimental and kinetic study of pentene isomers and n-pentane in laminar flames, *Proc. Combust. Inst.* 36 (2017) 1279-1286.
- [13] B. Zhong, Z. Zeng, H. Peng, The pressure dependence of laminar flame speed of 2-methyl-2-butene/air flames in the 0.1-1.0 MPa range, *Combust. Sci. Technol.* 190 (2018) 1886-1899.
- [14] S.S. Nagaraja, J. Power, G. Kukkadapu, S. Dong, S.W. Wangon, W.J. Pitz, H.J. Curran, A single pulse shock tube study of pentene isomer pyrolysis, *Proc. Combust. Inst.* 38 (2021).
- [15] L.A. Arafin F, Ninnemann E, Greene R, Rahman RK, Vasu SS, Influence of the double bond position in combustion chemistry of methyl butene isomers: a shock tube and laser absorption study, *Int. J. Chem. Kinet.*, doi:[https://onlinelibrary.wiley.com/doi/abs/10.1002/kin.21396\(2020\)](https://onlinelibrary.wiley.com/doi/abs/10.1002/kin.21396(2020)).

- [16] W.G. Lovell, Knocking characteristics of hydrocarbons, *Ind. Eng. Chem* 40 (1948) 2388-2438.
- [17] H. Wang, Formation of nascent soot and other condensed-phase materials in flames, *Proc. Combust Inst.* 33 (2011) 41-67.
- [18] K. Johansson, M. Head-Gordon, P. Schrader, K. Wilson, H. Michelsen, Resonance-stabilized hydrocarbon-radical chain reactions may explain soot inception and growth, *Science* 361 (2018) 997-1000.
- [19] K. Hoyeremann, F. Mauß, T. Zeuch, A detailed chemical reaction mechanism for the oxidation of hydrocarbons and its application to the analysis of benzene formation in fuel-rich premixed laminar acetylene and propene flames, *Phys. Chem. Chem. Phys* 6 (2004) 3824-3835.
- [20] P. Oßwald, K. Kohse-Höinghaus, U. Struckmeier, T. Zeuch, L. Seidel, L. Leon, F. Mauss, Combustion chemistry of the butane isomers in premixed low-pressure flames, *Z. Phys. Chem* 225 (2011) 1029.
- [21] M. Schenk, L. Leon, K. Moshhammer, P. Oßwald, T. Zeuch, L. Seidel, F. Mauss, K. Kohse-Höinghaus, Detailed mass spectrometric and modeling study of isomeric butene flames, *Combust. Flame* 160 (2013) 487-503.
- [22] A. Nawdiyal, N. Hansen, T. Zeuch, L. Seidel, F. Mauß, Experimental and modelling study of speciation and benzene formation pathways in premixed 1-hexene flames, *Proc. Combust Inst.* 35 (2015) 325-332.
- [23] L. Seidel, K. Moshhammer, X. Wang, T. Zeuch, K. Kohse-Höinghaus, F. Mauss, Comprehensive kinetic modeling and experimental study of a fuel-rich, premixed n-heptane flame, *Combust. Flame* 162 (2015) 2045-2058.
- [24] S.S. Nagaraja, J. Liang, S. Dong, S. Panigrahy, A. Sahu, G. Kukkadapu, S.W. Wagnon, W.J. Pitz, H.J. Curran, A hierarchical single-pulse shock tube pyrolysis study of C<sub>2</sub>–C<sub>6</sub> 1-alkenes, *Combust. Flame* 219 (2020) 456-466.
- [25] M. Baigmohammadi, V. Patel, S. Nagaraja, A.K. Ramalingam, S. Martinez, S. Panigrahy, A.A.E. Mohamed, K.P. Somers, U. Burke, K.A. Heufer, A. Pekalski, H.J. Curran, Comprehensive experimental and simulation study of the ignition delay time characteristics of binary blended methane, ethane, and ethylene over a wide range of temperature, pressure, equivalence ratio, and dilution., *Energy Fuels* 34 (2020) 8808-8823.
- [26] M. Baigmohammadi, V. Patel, S. Martinez, S. Panigrahy, A. Ramalingam, U. Burke, K.P. Somers, K.A. Heufer, A. Pekalski, H.J. Curran, A comprehensive experimental and simulation study of ignition delay time characteristics of single fuel C<sub>1</sub>–C<sub>2</sub> hydrocarbons over a wide range of temperatures, pressures, equivalence ratios, and dilutions, *Energy Fuels* 34 (2020) 3755-3771.
- [27] A.A.E.-S. Mohamed, S. Panigrahy, A.B. Sahu, G. Bourque, H.J. Curran, An experimental and modeling study of the auto-ignition of natural gas blends containing C<sub>1</sub>–C<sub>7</sub> n-alkanes, *Proc. Combust. Inst.* 38 (2021).
- [28] C.-W. Zhou, Y. Li, U. Burke, C. Banyon, K.P. Somers, S. Ding, S. Khan, J.W. Hargis, T. Sikes, O. Mathieu, e. al, An experimental and chemical kinetic modeling study of 1,3-butadiene combustion: Ignition delay time and laminar flame speed measurements, *Combust. Flame* 197 (2018) 423-438.
- [29] H.J. Curran, Rate constant estimation for C<sub>1</sub> to C<sub>4</sub> alkyl and alkoxy radical decomposition, *Int. J. Chem. Kinet.* 38 (2006) 250-275.
- [30] M.J. Frisch, G.W. Trucks, H.B. Schlegel, G.E. Scuseria, M.A. Robb, J.R. Cheeseman, G. Scalmani, V. Barone, G.A. Petersson, H. Nakatsuji, e. al., *Gaussian 09*, 2009.
- [31] M.J. Frisch, G.W. Trucks, H.B. Schlegel, G.E. Scuseria, M.A. Robb, J.R. Cheeseman, G. Scalmani, V. Barone, G.A. Petersson, H. Nakatsuji, e. al., *Gaussian 16 Rev. B.01*, Wallingford, CT, 2016.

- [32] Y. Georgievskii, J.A. Miller, M.P. Burke, S.J. Klippenstein, Reformulation and solution of the master equation for multiple-well chemical reactions, *J. Phys. Chem. A* 117 (2013) 12146-12154.
- [33] C.F. Goldsmith, G.R. Magoon, W.H. Green, Database of small molecule thermochemistry for combustion, *J. Phys. Chem. A* 116 (2012) 9033-9057.
- [34] S.J. Klippenstein, L.B. Harding, Kinetics of the H+NCO reaction, *Proc. Combust. Inst.* 32 (2009) 149-155.
- [35] B. Ruscic, R.E. Pinzon, G.v. Laszewski, D. Kodeboyina, A. Burcat, D. Leahy, D. Montoy, A.F. Wagner, Active thermochemical tables: thermochemistry for the 21st century, *J. Phys.* 16 (2005) 561-570.
- [36] J.M. Simmie, K.P. Somers, Benchmarking compound methods (CBS-QB3, CBS-APNO, G3, G4, W1BD) against the active thermochemical tables: a litmus test for cost-effective molecular formation enthalpies, *J. Phys. Chem. A* 119 (2015) 7235-7246.
- [37] K.P. Somers, J.M. Simmie, Benchmarking compound methods (CBS-QB3, CBS-APNO, G3, G4, W1BD) against the active thermochemical tables: formation enthalpies of radicals, *J. Phys. Chem. A* 119 (2015) 8922-8933.
- [38] J.M. Simmie, K.P. Somers, W.K. Metcalfe, H.J. Curran, Substituent effects in the thermochemistry of furans: A theoretical (CBS-QB3, CBS-APNO and G3) study, *J. Chem. Thermodyn.* 58 (2013) 117-128.
- [39] B. Ruscic, R.E. Pinzon, M.L. Morton, G. von Laszewski, S.J. Bittner, S.G. Nijsure, K.A. Amin, M. Minkoff, A.F. Wagner, Introduction to active thermochemical tables: several “key” enthalpies of formation revisited, *J. Phys. Chem. A* 108 (2004) 9979-9997.
- [40] J.M. Simmie, G. Black, H.J. Curran, J.P. Hinde, Enthalpies of formation and bond dissociation energies of lower alkyl hydroperoxides and related hydroperoxy and alkoxy radicals, *J. Phys. Chem. A* 112 (2008) 5010-5016.
- [41] B.J. McBride, S. Gordon, Computer program for calculating and fitting thermodynamic functions, (1992).
- [42] H.S. Johnston, J. Heicklen, Tunnelling corrections for unsymmetrical Eckart potential energy barriers, *J. Phys. Chem.* 66 (1962) 532-533.
- [43] V.D. Knyazev, W. Tsang, Chemically and thermally activated decomposition of secondary butyl radical, *J. Phys. Chem. A* 104 (2000) 10747-10765.
- [44] I.A. Awan, D.R. Burgess, Jr., J.A. Manion, Pressure dependence and branching ratios in the decomposition of 1-pentyl radicals: shock tube experiments and master equation modeling, *J. Phys. Chem. A* 116 (2012) 2895-2910.
- [45] A. Comandini, I.A. Awan, J.A. Manion, Thermal decomposition of 1-pentyl radicals at high pressures and temperatures, *Chem. Phys. Lett.* 552 (2012) 20-26.
- [46] J.A. Manion, I.A. Awan, The decomposition of 2-pentyl and 3-pentyl radicals, *Proc. Combust. Inst.* 34 (2013) 537-545.
- [47] A.W. Jasper, J.A. Miller, Lennard-Jones parameters for combustion and chemical kinetics modeling from full-dimensional intermolecular potentials, *Combust. Flame* 161 (2014) 101-110.
- [48] A. Burcat, B. Ruscic, Third millennium ideal gas and condensed phase thermochemical database for combustion (with update from active thermochemical tables), Argonne National Lab.(ANL), Argonne, IL (United States), 2005.
- [49] J.J.P. Stewart, Optimization of parameters for semiempirical methods VI: more modifications to the NDDO approximations and re-optimization of parameters, *J. Mol. Model.* 19 (2013) 1-32.
- [50] E.R. Ritter, J.W. Bozzelli, THERM: Thermodynamic property estimation for gas phase radicals and molecules, *Int. J. Chem. Kinet.* 23 (1991) 767-778.

- [51] J.A. Miller, S.J. Klippenstein, Dissociation of propyl radicals and other reactions on a C<sub>3</sub>H<sub>7</sub> potential, *J. Phys. Chem. A* 117 (2013) 2718-2727.
- [52] L.C. Jitariu, L.D. Jones, S.H. Robertson, M.J. Pilling, I.H. Hillier, Thermal rate coefficients via variational transition state theory for the unimolecular decomposition/isomerization of 1-pentyl radical: ab initio and direct dynamics calculations, *J. Phys. Chem. A* 107 (2003) 8607-8617.
- [53] D.M. Matheu, W.H. Green, J.M. Grenda, Capturing pressure-dependence in automated mechanism generation: reactions through cycloalkyl intermediates, *Int. J. Chem. Kinet.* 35 (2003) 95-119.
- [54] T. Yu, J. Zheng, D. Truhlar, Multi-structural variational transition state theory. Kinetics of the 1,4-hydrogen shift isomerization of the pentyl radical with torsional anharmonicity, *Chem. Sci.* 2 (2011) 2199-2213.
- [55] A Chemkin-Pro - ANSYS Reaction Design: San Diego.
- [56] J.J. Zheng, D.G. Truhlar, Direct Dynamics Study of Hydrogen-Transfer Isomerization of 1-Pentyl and 1-Hexyl Radicals, *J. Phys. Chem. A* 113 (2009) 11919-11925.
- [57] A. Ratkiewicz, B. Bankiewicz, Kinetics of 1,5-Hydrogen Migration in Alkyl Radical Reaction Class, *J. Phys. Chem. A* 116 (2012) 242-254.
- [58] B. Bankiewicz, L.K. Huynh, A. Ratkiewicz, T.N. Truong, Kinetics of 1,4-Hydrogen Migration in the Alkyl Radical Reaction Class, *J. Phys. Chem. A* 113 (2009) 1564-1573.
- [59] A.W. Jasper, N. Hansen, Hydrogen-assisted isomerizations of fulvene to benzene and of larger cyclic aromatic hydrocarbons, *Proc. Combust Inst.* 34 (2013) 279-287.
- [60] K. Wang, S.M. Villano, A.M. Dean, Reactions of allylic radicals that impact molecular weight growth kinetics, *Phys. Chem. Chem. Phys.* 17 (2015) 6255-6273.

# **Chapter 4 : A hierarchical study of the reactions of hydrogen atoms with alkenes: A theoretical study of the reactions of hydrogen atoms with C<sub>2</sub> – C<sub>4</sub> alkenes**

Published in: *J. Phys. Chem. A*.125(23) (2021) 5124–5145

Publication Date: June 8, 2021

DOI: <https://doi.org/10.1021/acs.jpca.1c03168>

## Author Contributions

- (1) Jennifer Power: Performed electronic structure calculations, modelling work and wrote the manuscript
- (2) Kieran P. Somers: Performed electronic structure calculations and provided input for theoretical and modelling work. Reviewed the manuscript prior and post review process.
- (3) Shashank S. Nagaraja: Performed pyrolysis experiments.
- (4) Henry J. Curran: Managed the project throughout and reviewed the manuscript prior and post review process.



## Abstract

The present study complements our previous studies on the reactions of hydrogen atoms with  $C_5$  alkene species including 1- and 2-pentene and the branched isomers (2-methyl-1-butene, 2-methyl-2-butene, and 3-methyl-1-butene), by studying the reactions of hydrogen atoms with  $C_2 - C_4$  alkenes (ethylene, propene, 1- and 2-butene, and isobutene). The aim of the current work is to develop a hierarchical set of rate constants for  $\dot{H}$  atom addition reactions to  $C_2 - C_5$  alkenes, both linear and branched, which can be used in the development of chemical kinetic models. High-pressure limiting and pressure-dependent rate constants are calculated using Rice-Ramsperger-Kassel-Marcus (RRKM) theory and a one-dimensional master equation (ME). Rate constant recommendations for  $\dot{H}$  atom addition and abstraction reactions in addition to alkyl radical decomposition reactions are also proposed and provide a useful tool for use in mechanisms of larger alkenes for which calculations do not exist. Additionally, validation of our theoretical results with single-pulse shock-tube pyrolysis experiments is carried out. An improvement in species mole fractions predictions for alkene pyrolysis is observed, showing the relevance of the present study.

## 1. Introduction

Alkenes are important intermediates formed during the oxidation and pyrolysis of larger alkanes and are key components of hydrocarbon fuels. An understanding of their combustion chemistry is therefore important in our understanding of hydrocarbon fuel combustion. The reactions of  $\dot{H}$  atom across the  $C=C$  double bond plays an important role in controlling experimental high-temperature ignition delay times (IDTs), flame speeds and species profiles measured as a function of temperature and/or time in jet-stirred and flow reactors [1-3].

In the current work, the reactions of  $\dot{H}$  atoms with  $C_2 - C_4$  alkenes are studied, while the reactions of  $\dot{H}$  atom addition to  $C_5$  alkenes were studied previously [4, 5]. There have been a number of theoretical and experimental studies of  $\dot{H}$  atoms with  $C_2 - C_4$  alkenes [6-19]. This study aims to complement these by providing a comprehensive hierarchical set of rate constants for  $\dot{H}$  atom addition and abstraction potential energy surfaces (PES's), including their chemically activated pathways for  $C_2 - C_5$  alkenes, determined at the same levels of theory. By having a consistent set of rate constants for  $C_2 - C_5$  alkenes +  $\dot{H}$  atoms calculated at the same level of theory, our results help constrain available models and the development



of recommended rate constants which provide a tool for use in mechanisms of larger alkenes for which calculations do not exist in the literature.

Ethylene is the smallest alkene in our series and has been extensively studied [6, 10-19]. Miller and Klippenstein [17] studied the kinetics of  $\dot{\text{H}} + \text{C}_2\text{H}_2$  and  $\dot{\text{H}} + \text{C}_2\text{H}_4$ , including their reverse dissociation reactions using variational transition state theory (VTST) and a 2-D master equation. Matsugi [16] performed direct trajectory calculations on  $\dot{\text{C}}_2\text{H}_5$  radical dissociation and discovered a reaction pathway that directly eliminates  $\text{H}_2$  from  $\dot{\text{C}}_2\text{H}_5$ , leading to the formation of vinyl ( $\dot{\text{C}}_2\text{H}_3$ ) radicals. The resulting  $\dot{\text{C}}_2\text{H}_3$  radicals can dissociate to  $\text{C}_2\text{H}_2 + \dot{\text{H}}$ . They suggest that this may be an explanation for the unexpectedly slow  $\dot{\text{H}}$  atom formation previously observed in photo-dissociation experiments of  $\dot{\text{C}}_2\text{H}_5$  radicals [21, 22]. Barker et al. [6] studied the reaction of  $\dot{\text{H}} + \text{C}_2\text{H}_4$  as a function of He pressure at room temperature with three experimental techniques; (i) a discharge flow system with Lyman- $\alpha$  photometry, (ii) a time resolved Lyman- $\alpha$  photometric system and (iii) a discharge flow system with time-of-flight mass spectrometry. Rate constants were obtained in both excess ethylene and hydrogen environments and an experimental value for the third body recombination coefficient for  $\dot{\text{H}} + \dot{\text{C}}\text{H}_3 (+\text{M})$  was obtained.

Michael et al. [12] used Lyman- $\alpha$  photometry to obtain the pressure dependence of the  $\dot{\text{H}} + \text{C}_2\text{H}_4$  reaction at room temperature. Through computer simulation analysis, the rate constants were adjusted for  $\dot{\text{H}}$  atom depletion in reactions subsequent to the initial reaction. Experiments at high pressures of He permitted extrapolation to the high-pressure limit of the rate constant. Lee et al. [9] experimentally measured the rate constant for the  $\dot{\text{H}} + \text{C}_2\text{H}_4$  reaction as a function of temperature (198 – 320 K) at high pressures of Ar bath gas using the flash photolysis-resonance fluorescence technique. Sugawara et al. [14] measured the high-pressure limiting rate constants of  $\dot{\text{H}}$  and  $\dot{\text{D}}$  atom addition to  $\text{C}_2\text{H}_4$ ,  $\text{C}_2\text{H}_3\text{D}$ ,  $\text{C}_2\text{D}_4$ ,  $\text{C}_2\text{H}_2$  and  $\text{C}_2\text{D}_2$  in the temperature range 206 – 461 K using pulse radiolysis-resonance absorption.

Pacey et al. [13] performed pyrolysis experiments on ethane at 902 K and concentrations of  $1.8 \times 10^{-4} - 4.5 \times 10^{-3} \text{ mol L}^{-1}$  in a flow system. Rate constants for the reactions  $\dot{\text{C}}_2\text{H}_5 + \dot{\text{C}}_2\text{H}_5 \leftrightarrow \text{C}_4\text{H}_{10}$  and  $\dot{\text{C}}_2\text{H}_5 + \dot{\text{C}}_2\text{H}_5 \leftrightarrow \text{C}_2\text{H}_6 + \text{C}_2\text{H}_4$  were determined. Moreover, pressure-dependent rate constants for  $\text{C}_2\text{H}_6 \leftrightarrow \dot{\text{C}}\text{H}_3 + \dot{\text{C}}\text{H}_3$  and  $\dot{\text{C}}_2\text{H}_5 \leftrightarrow \text{C}_2\text{H}_4 + \dot{\text{H}}$  were determined using unimolecular reaction rate theory. Lightfoot et al. [10] measured the rate constant of the reaction  $\dot{\text{H}} + \text{C}_2\text{H}_4 \leftrightarrow \dot{\text{C}}_2\text{H}_5$  as a function of temperature and pressure, over the temperature and pressure ranges 285 – 604 K and 50 – 600 Torr respectively, using laser flash photolysis/resonance fluorescence, with helium diluent.

Feng et al. [7] investigated the unimolecular decomposition of  $\dot{C}_2H_5$  radicals in helium over the temperature and pressure ranges 876 – 1094 K and 0.8 – 14.3 Torr, respectively in time-resolved experiments. The reaction was isolated for quantitative study in a heated tubular reactor coupled to a photoionisation mass spectrometer. Hanning et al. [8] studied the reaction  $\dot{H} + C_2H_4 \leftrightarrow \dot{C}_2H_5$  at 800 K in He. Exciplex laser flash photolysis at 193.3 nm of ethene-helium mixtures was used to generate  $\dot{H}$  atoms, which were detected using time-resolved resonance fluorescence. Rate coefficients for the forward and reverse reactions were deduced from measurements of the equilibrium constant and relaxation rate coefficient at nine pressures in the range 97 – 600 Torr. More recently, Yang et al. [15] investigated the decomposition of ethyl iodide and subsequent dissociation of ethyl radicals behind incident shock waves in a diaphragm-less shock tube using laser schlieren (LS) densitometry ( $1150 \leq T \leq 1870$  K, and  $55 \leq p \leq 123 \pm 3$  Torr).

Fewer studies exist for the reactions of  $\dot{H}$  atoms with propene and the butene isomers. Experimental studies of  $\dot{H}$  atoms with propene include [20, 23-32], with the most recent one by Chen et al. [20] studying the temperature and pressure dependence of the product branching ratio of the  $\dot{H} +$  propene reaction. This was done behind reflected shock waves in a diaphragm-less shock-tube using the  $\dot{H}$ -ARAS technique in the temperature range 1065 – 1306 K at 1 and 2 bar. Quantum chemistry calculations were also performed at the CCSD(T)/CBS//CCSD/6-311++G(3df,2p) level of theory. The predicted high-pressure limit rate constant ratio for terminal versus non-terminal addition agrees well with that reported by Manion et al. [19] for the analogous reaction of  $\dot{H}$  atoms with butene. Both Chen et al. [20] and Manion et al. [19] state that their predicted branching ratio for terminal versus non-terminal addition differ to that calculated by Miller and Klippenstein who studied the dissociation of propyl radicals and other reactions on the  $\dot{C}_3H_7$  PES [18]. With minor adjustments to several of the barrier heights, Miller and Klippenstein showed excellent agreement between their theoretical values and experimental results available in the literature over a wide range of conditions.

Manion and Awan [19] investigated the kinetics of terminal and internal  $\dot{H}$  atom addition to 1-alkenes. Single-pulse shock tube methods were employed to thermally generate  $\dot{H}$  atoms and their reactions with 1-butene were investigated over the temperature and pressure ranges of 880 – 1120 K and 145 – 245 kPa, respectively. Relative and absolute rate constants for the displacement of methyl and ethyl radicals by  $\dot{H}$  atoms were determined and related to the high-pressure limit rate constant for  $\dot{H}$  atom addition to the terminal and internal sites of 1-butene. It was found that addition to the terminal site is favoured by a factor of  $2.6 \pm 0.4$  at

1000 K. These results were combined with data from lower temperatures and used by Manion and Awan to derive rate constants in the temperature range 220 – 2000 K. They state that these branching ratio expressions should approximate the behaviour of other un-branched 1-olefins and can thus be used as estimates for unstudied 1-olefins in detailed kinetic models describing pyrolysis and combustion conditions. A factor of three discrepancy was noted in the branching ratio for terminal to internal  $\dot{\text{H}}$  atom addition by comparing their current experimental results with the theoretical study [18], and they suggest that the difference observed is well outside the experimental errors of their study and any expected differences for 1-butene.

Wang et al. [33] studied the reaction kinetics of H-atom abstraction from  $\text{C}_4 - \text{C}_6$  alkenes by  $\dot{\text{H}}$  atoms and  $\dot{\text{C}}\text{H}_3$  radicals using the G4 composite method with CTST and Eckart tunneling corrections. The study provides the first systematic study on the key initiation abstraction reaction classes for alkenes with  $\dot{\text{H}}$  atoms and  $\dot{\text{C}}\text{H}_3$  radicals. However, large discrepancies are observed between the Wang et al. [33] calculations and those already present in the literature and calculated in this work.

Nagaraja et al. [32] performed a single-pulse shock-tube study on the pyrolysis of 2%  $\text{C}_2 - \text{C}_6$  1-alkenes at 2 bar in the temperature range 900 – 1800 K, with reactant intermediate and product species obtained and quantified using gas chromatography-mass spectrometry analysis.

One of the aims of the present study is to investigate the ratio of terminal to internal  $\dot{\text{H}}$  atom addition to  $\text{C}_2 - \text{C}_5$  alkenes taking into account our past studies [4, 5] of the  $\text{C}_5$  alkenes since discrepancies remain in the literature. Rate constant recommendations for  $\dot{\text{H}}$  atom addition, abstraction and alkyl radical decomposition reactions will also be made and should serve as a useful tool for their use in mechanisms for larger alkenes where calculations do not exist.

Section 2 describes the computational methods employed in the current work and Section 3 presents the theoretical results including comparisons with literature studies, where available. Section 4 presents our simulation results compared to the shock tube pyrolysis experiments of Nagaraja et al. [32].

**Table 4.1:** Summary of Experimental and Theoretical Studies Relevant to  $C_2 - C_4$  alkenes +  $\dot{H}$ .

Year	Author	Reaction(s)	$T$ (K)	$p$ (kPa)	Method
2020	Nagaraja et al. [32]	pyrolysis of $C_2 - C_6$ 1-alkenes	900 – 1800	200	Experiment single pulse shock tube (SPST)
2020	Chen et al. [20]	$\dot{H} + C_3H_6$	1065 – 1306	100 – 200	Theory/Experiment $\dot{H}$ -ARAS / shock-tube CCSD(T)/CBS//CCSD/6-311++G(3df,2p)
2018	Wang et al. [33]	$C_4 - C_6$ alkenes + $\dot{H}$ and $\dot{C}H_3$			Theory G4 composite method
2015	Manion et al. [19]	$\dot{H} + C_4H_8-1$	880 – 1120	145 – 245	Experiment single pulse shock tube (SPST)
2013	Matsugi et al. [16]	photodissociation of $\dot{C}_2H_5$	–	–	Theory direct trajectory calculations $\omega$ B97X-D / 6-31 + G(d,p)
2013	Miller et al. [18]	dissociation of propyl radicals & other reactions on $\dot{C}_3H_7$ potential	–	0 – HPL	Theory CCSD(T)/cc-pVTZ MP2/6-311++G(d,p)
2012	Yang et al. [15]	decomposition of ethyl iodide / dissociation of $\dot{C}_2H_5$ radicals	1150 – 1870	7.3 – 16.4	Experiment diaphragmless shock tube / laser schlieren (LS) densitometry
2011	Rosado-Reyes et al. [28]	$\dot{H} + C_3H_6$	922 – 1200	150 – 340	Experiment single pulse shock tube (SPST)
2004	Miller et al. [17]	$\dot{H} + C_2H_2$ and $C_2H_4$	300 – 2000	>0.13 / HPL	Theory variational transition state theory (VTST), 2D master equation
1993	Hanning et al. [8]	$\dot{H} + C_2H_4$	800	12.9 – 80.0	Experiment exciplex laser flash photolysis / time-resolved resonance fluorescence

1993	Feng et al. [7]	Unimolecular decomposition of $\dot{\text{C}}_2\text{H}_5$	876 – 1094	0.1 – 1.9	Experiment heated tubular reactor / to a photoionisation mass spectrometer
1993	Seakins et al. [23]	$i\dot{\text{C}}_3\text{H}_7$ decomposition	720 – 910	–	Experiment Laser flash photolysis / photoionisation mass spectrometry
1992	Tsang [35]	Database for hydrocarbon pyrolysis		–	Theory Estimate
1992	Hidaka et al. [29]	Thermal decomposition of $\text{C}_3\text{H}_6$	1200 – 1800	–	Experiment Laser kinetic absorption spectroscopy / GC
1991	Tsang [36]	Database for hydrocarbon pyrolysis	–	–	Theory Estimate
1989	Loser et al. [30]	$\dot{\text{H}}$ atom abstraction by allyl radicals from fuels	–	–	Theory BSBL
1987	Lightfoot et al. [10]	$\dot{\text{H}} + \text{C}_2\text{H}_4$	285 – 604	6.7 – 80.0	Experiment laser flash photolysis / resonance fluorescence
1986	Munk et al. [25]	$i\dot{\text{C}}_3\text{H}_7$ and $i\dot{\text{C}}_3\text{H}_7\text{O}_2$	298	101	Experiment UV absorption / pulse photolysis
1984	Pacey et al. [13]	Pyrolysis of $\text{C}_2\text{H}_6$	902	HPL	Experiment flow system
1982	Watanabe et al. [27]	$\dot{\text{H}} + \text{C}_3\text{H}_6$	200 – 500	–	Experiment Pulse radiolysis resonance absorption
1982	Harris et al. [31]	$\dot{\text{H}} + \text{C}_3\text{H}_6 / \text{C}_4\text{H}_8$	298 – 455	–	Experiment Flash photolysis resonance fluorescence
1981	Sugawara et al. [14]	$\dot{\text{H}}$ and D-atom addition to $\text{C}_2\text{H}_4$ , $\text{C}_2\text{H}_3\text{D}$ , $\text{C}_2\text{D}_4$ ,	206 – 461	–	Experiment

		$C_2H_2$ and $C_2D_2$			Pulse radiolysis-resonance absorption.
1978	Lee et al. [9]	$\dot{H} + C_2H_4$	198 – 320	0.13	Experiment flash photolysis-resonance fluorescence (FP-RF) technique
1973	Michael et al. [12]	$\dot{H} + C_2H_4$	–	–	Experiment Lyman $\alpha$ photometry
1972	Kerr et al. [24]	Evaluated kinetic data on gas phase addition reactions	–	–	
1971	Kurylo et al. [26]	$\dot{H} + C_3H_6$	298	–	Experiment Resonance fluorescence of Lyman $\alpha$ radiation
1970	Barker et al. [6]	$\dot{H} + C_2H_4$	–	–	Experiment Discharge Flow System with Lyman- $\alpha$ Photometry, Time resolved Lyman- $\alpha$ Photometric System and Discharge Flow System with Time-of-Flight Mass Spectrometry

## 2. Computational Details

### 2.1. Electronic structure calculations

As mentioned earlier, we have employed the same methods here as those used in our previous studies [4, 5] to carry out all electronic structure calculations, thus the description here is brief. All calculations were carried out using Gaussian 09 [37] and Gaussian 16 [38]. Conformational searches were performed, with the resulting lowest energy conformer optimised at the  $\omega$ B97XD [39] / aug-cc-pVTZ [40] level of theory. An harmonic frequency analysis was simultaneously performed at the same level of theory to verify the nature of each stationary point.

Low-frequency torsional modes were treated via relaxed PES scans in 10-degree increments with the  $\omega$ B97XD/6-311++G(d,p) [39] method, with the potential energies as a function of dihedral angle used as input for a one-dimensional (1-D) hindered rotor approximation as implemented in the Master Equation System Solver (MESS) [41].

To compute reaction barrier heights, single point energies for minima and transition states were calculated at the CCSD(T)/cc-pVXZ and MP2/cc-pVXZ (where X = D, T and Q) levels of theory. The resulting energies were extrapolated to the complete basis set (CBS) limit using the following formula (1) [42, 43]:

$$E_{\text{CCSD(T)/CBS}} = E_{\text{CCSD(T)/cc-pVTZ}} + (E_{\text{CCSD(T)/cc-pVTZ}} - E_{\text{CCSD(T)/cc-pVDZ}}) (3^4 / 4^4 - 3^4) + E_{\text{MP2/cc-pVQZ}} + (E_{\text{MP2/cc-pVQZ}} - E_{\text{MP2/cc-pVTZ}}) (4^4 / 5^4 - 4^4) - E_{\text{MP2/cc-pVTZ}} - (E_{\text{MP2/cc-pVTZ}} - E_{\text{MP2/cc-pVDZ}}) (3^4 / 4^4 - 3^4). \quad (1)$$

The  $T_1$  diagnostic for minima and transition state species is  $\leq \sim 0.03$ , indicating that single reference methods to describe the wave function are appropriate [42]. However, for the  $\dot{\text{C}}_2\text{H}_3$  radical well and the transition states of  $\dot{\text{H}}$  atom addition to and abstraction from  $\text{C}_2\text{H}_4$ , the  $T_1$  diagnostics are 0.04, 0.038 and 0.352, respectively. As a result, for the  $\text{C}_2$  and  $\text{C}_3$  reaction systems, ROCCSD(T)/aug-cc-pVXZ, (where X = T and Q) single point energies were also calculated since they were computationally achievable. The energies were extrapolated to the CBS limit using the formula (2):

$$E_{\text{ROCCSD(T)/CBS}} = E_{\text{ROCCSD(T)/aug-cc-pVQZ}} + (E_{\text{ROCCSD(T)/aug-cc-pVQZ}} - E_{\text{ROCCSD(T)/aug-cc-pVTZ}}) * 4^4 / (5^4 - 4^4) \quad (2)$$

with the resulting  $T_1$  diagnostics falling below 0.03. The largest difference in energy barriers as a result of using the two formulas was for H-atom abstraction from the primary vinylic sites of  $\text{C}_2\text{H}_4$  and  $\text{C}_3\text{H}_6$ , where differences of 1.57 and 1.39  $\text{kJ mol}^{-1}$  respectively, were observed. These differences in energy barriers increased the rate constants for these reactions by a factor of 1.87 and 1.71 at 298 K.

## 2.2. Thermochemistry

The methods employed to calculate the thermochemical parameters of species are identical to those used in our previous studies [4, 5], with 0 K formation enthalpies determined via the isodesmic approach using the most recent ATcT values for the molecular and radical chaperones, and uncertainties computed using methods described by Simmie et al. [44]. Temperature-dependent enthalpies, entropies, and heat capacities were calculated using traditional statistical thermodynamic methods as implemented in MESSPF [41], with Chemkin format polynomials fitted using PAC99 [45], and are provided as Supplementary material (SM).

## 2.3. Transition-State Theory (TST), Rice-Ramsperger-Kassel-Marcus (RRKM), and Master Equation (ME) Calculations

High-pressure limiting and pressure-dependent rate constants were calculated for the C<sub>2</sub> – C<sub>4</sub> PESs using RRKM/ME as implemented in MESS [41], in which tunnelling is accounted for via an asymmetric Eckart model [46]. To model collisional energy transfer, a single exponential down model was used and is estimated to be  $\langle \Delta E_{\text{down}}(T) \rangle = 75 \times (T/300)^{1.05} \text{ cm}^{-1}$  for the  $\dot{\text{C}}_2\text{H}_5$  PES [17] and  $\langle \Delta E_{\text{down}}(T) \rangle = 200 \times (T/300)^{0.75} \text{ cm}^{-1}$  for the  $\dot{\text{C}}_3\text{H}_7$  and  $\dot{\text{C}}_4\text{H}_9$  PESs [47-50].

## 3. Theoretical Results

### 3.1. Thermochemistry

Table 4.2 presents formation enthalpies, along with their  $2\sigma$  uncertainties computed via isodesmic and atomisation methods. Also presented are ATcT [51, 52], ANL0 [53], and ANL1 [53] formation enthalpies with  $2\sigma$  uncertainties. The current study uses the most recent ATcT values for the molecular and radical chaperones [51, 52]. Similar to previous work [4, 5], ATcT, ANL0 and ANL1 formation enthalpies do not exist for the species  $\dot{\text{C}}_4\text{H}_7\text{-11}$ ,  $\dot{\text{C}}_4\text{H}_7\text{-12}$ ,  $\dot{\text{C}}_4\text{H}_7\text{-13}$ ,  $\dot{\text{C}}_4\text{H}_7\text{-14}$ ,  $\dot{\text{C}}_4\text{H}_7\text{-22}$ ,  $i\dot{\text{C}}_4\text{H}_7$ , and  $i\dot{\text{C}}_4\text{H}_7\text{-i1}$ . Quantum chemical composite methods (CBS–QB3, CBS–APNO, G3, and G4) [55-57] were therefore used to calculate their formation enthalpies at 0 K via isodesmic reactions suitable for each species, using ATcT values as chaperones.



**Table 4.2:** Formation Enthalpies and Uncertainties ( $2\sigma$ ) Computed via Isodesmic and Atomisation Methods, Together with ATcT, ANL0, and ANL1 Formation Enthalpies and Uncertainties.

Species	isodesmic (0 K, kJ mol <sup>-1</sup> )	isodesmic ( $2\sigma$ )	atomisation (0 K, kJ mol <sup>-1</sup> )	atomisation ( $2\sigma$ )	ATcT [51, 52] (0 K, kJ mol <sup>-1</sup> )	ANL0 [53]	ANL1 [53]	Burcat [54] (0 K, kJ mol <sup>-1</sup> )
C <sub>2</sub> H <sub>4</sub>	60.60	0.45	61.36	3.85	60.88	60.20	60.20	61.03
$\dot{C}_2$ H <sub>5</sub>	131.65	0.74	131.06	6.65	131.06	131.30	131.00	130.77
$\dot{C}_2$ H <sub>3</sub>	301.49	0.96	301.26	5.41	301.13	300.90	300.50	300.87
C <sub>3</sub> H <sub>6</sub>	35.03	0.36	35.85	7.33	34.93	34.50	–	35.01
n $\dot{C}_3$ H <sub>7</sub>	117.78	0.66	118.15	9.75	118.34	118.20	–	119.15
i $\dot{C}_3$ H <sub>7</sub>	105.33	0.92	105.71	9.63	105.32	105.10	–	108.24
$\dot{C}_3$ H <sub>5</sub> -s	277.86	0.87	278.38	7.53	278.22	278.40	–	276.29
$\dot{C}_3$ H <sub>5</sub> -t	262.28	0.95	262.80	6.86	262.98	263.00	–	–
$\dot{C}_3$ H <sub>5</sub> -a	177.44	2.00	179.03	6.69	180.03	179.60	–	180.40
C <sub>4</sub> H <sub>8</sub> -1	21.15	0.20	22.40	10.66	21.00	21.30	–	20.82
C <sub>4</sub> H <sub>8</sub> -2	9.40	0.25	10.63	10.86	9.38	9.60	–	9.39
$\dot{C}_4$ H <sub>9</sub> -1	102.20	0.77	102.52	13.08	102.74	103.20	–	105.91
$\dot{C}_4$ H <sub>9</sub> -2	90.76	0.74	91.55	12.82	90.84	90.90	–	94.95
$\dot{C}_4$ H <sub>7</sub> -11	263.61	0.79	263.97	10.27	–	–	–	262.76
$\dot{C}_4$ H <sub>7</sub> -12	248.88	0.81	249.16	9.84	–	–	–	248.45
$\dot{C}_4$ H <sub>7</sub> -13	152.70	0.81	152.04	9.48	–	–	–	153.55
$\dot{C}_4$ H <sub>7</sub> -14	222.83	0.77	224.34	12.26	–	–	–	220.92
$\dot{C}_4$ H <sub>7</sub> -22	239.46	1.24	240.21	9.97	–	–	–	239.74
iC <sub>4</sub> H <sub>8</sub>	3.61	0.31	5.19	10.72	4.01	4.20	–	3.46
i $\dot{C}_4$ H <sub>9</sub>	96.14	0.73	96.38	12.91	97.17	–	–	97.92
t $\dot{C}_4$ H <sub>9</sub>	73.86	0.73	75.31	13.23	75.60	–	–	79.72
i $\dot{C}_4$ H <sub>7</sub>	153.25	0.81	153.73	9.49	–	–	–	155.27
i $\dot{C}_4$ H <sub>7</sub> -i1	250.60	0.70	251.18	10.45	–	–	–	–

Excellent agreement is observed between this work and the ATcT [51, 52] values, with differences, expressed as mean absolute error ( $\text{MAE} \pm 2\sigma$ ), being on average  $0.59 \pm 1.38 \text{ kJ mol}^{-1}$ . Differences between this work and ANL0 [53] and ANL1 [53] computations are on average  $0.57 \pm 1.03$  and  $0.68 \pm 0.60 \text{ kJ mol}^{-1}$ , respectively. Differences between this work and Burcat [54] are slightly higher at  $1.58 \pm 3.2 \text{ kJ mol}^{-1}$ . Comparisons between isodesmic and atomisation values calculated in the current work are in excellent agreement, with a MAE of  $0.76 \pm 0.93 \text{ kJ mol}^{-1}$ . As discussed in our previous work [4, 5], although the isodesmic and atomisation methods give similar nominal 0 K heats of formation, the isodesmic method is often used to achieve “chemical accuracy”. Our computed final heat of formation uncertainties for the isodesmic reactions are between  $0.36$  and  $2.00 \text{ kJ mol}^{-1}$ .

**Table 4.3:** Comparisons of the Formation Enthalpies Computed in This Work with Literature Data.

Species	$\Delta_f H_{298\text{K}}$ (this work)	$\Delta_f H_{298\text{K}}$ (Goldsmith) [42]	$\Delta_f H_{298\text{K}}$ (ATcT) [51, 52]	$\Delta_f H_{298\text{K}}$ (Burcat) [54]
C <sub>2</sub> H <sub>4</sub>	51.99	52.30	52.36	52.50
C <sub>2</sub> H <sub>5</sub>	120.61	120.92	119.99	119.70
C <sub>2</sub> H <sub>3</sub>	297.29	297.90	296.93	296.58
C <sub>3</sub> H <sub>6</sub>	19.88	19.25	19.93	20.00
nC <sub>3</sub> H <sub>7</sub>	100.23	101.67	100.94	101.32
iC <sub>3</sub> H <sub>7</sub>	87.92	88.70	88.45	90.19
C <sub>3</sub> H <sub>5</sub> -s	267.07	268.19	267.38	265.53
C <sub>3</sub> H <sub>5</sub> -t	251.79	253.13	252.58	237.65
C <sub>3</sub> H <sub>5</sub> -a	165.55	169.87	168.31	168.60
C <sub>4</sub> H <sub>8</sub> -1	-0.21	-0.00	0.05	-0.03
C <sub>4</sub> H <sub>8</sub> -2	-11.30	-11.30	-11.18	-11.19
C <sub>4</sub> H <sub>9</sub> -1	78.86	80.75	80.23	81.80
C <sub>4</sub> H <sub>9</sub> -2	68.02	69.45	66.07	70.22
C <sub>4</sub> H <sub>7</sub> -11	246.82	248.11	–	245.87
C <sub>4</sub> H <sub>7</sub> -12	232.66	–	–	231.16
C <sub>4</sub> H <sub>7</sub> -13	135.21	137.65	–	136.11
C <sub>4</sub> H <sub>7</sub> -14	206.50	208.36	–	204.60
C <sub>4</sub> H <sub>7</sub> -22	223.32	225.10	–	223.85
iC <sub>4</sub> H <sub>8</sub>	-17.60	-17.15	-17.05	-17.57
iC <sub>4</sub> H <sub>9</sub>	72.29	74.48	73.18	73.79
tC <sub>4</sub> H <sub>9</sub>	50.77	54.39	50.30	55.04
iC <sub>4</sub> H <sub>7</sub>	134.68	139.32	–	137.60
iC <sub>4</sub> H <sub>7</sub> -i1	233.84	–	–	–

Table 4.3 presents 298 K formation enthalpies between this work and literature data, with the results generally in good agreement. Differences between this work and Goldsmith [42] are on average  $1.56 \pm 2.61$  kJ mol<sup>-1</sup>. Excellent agreement is observed between this work and ATcT, with a MAE of  $0.76 \pm 1.43$  kJ mol<sup>-1</sup>. The values reported by Burcat [54] are within  $2.01 \pm 5.90$  kJ mol<sup>-1</sup> of this work.

**Table 4.4:** Comparisons of Entropies Computed in This Work with Literature Data.

Species	$S_{298\text{ K}}$ (this work)	$S_{298\text{ K}}$ (Goldsmith) [42]	$S_{298\text{ K}}$ (Burcat) [54]
C <sub>2</sub> H <sub>4</sub>	218.66	218.82	219.32
$\dot{\text{C}}_2\text{H}_5$	247.38	247.27	242.98
$\dot{\text{C}}_2\text{H}_3$	233.38	233.47	233.66
C <sub>3</sub> H <sub>6</sub>	266.10	266.10	266.66
n $\dot{\text{C}}_3\text{H}_7$	289.91	289.95	290.46
i $\dot{\text{C}}_3\text{H}_7$	295.05	288.28	290.11
$\dot{\text{C}}_3\text{H}_5\text{-s}$	271.27	271.54	271.31
$\dot{\text{C}}_3\text{H}_5\text{-t}$	273.48	273.63	266.06
$\dot{\text{C}}_3\text{H}_5\text{-a}$	257.07	257.32	257.88
C <sub>4</sub> H <sub>8</sub> -1	307.77	306.27	305.37
C <sub>4</sub> H <sub>8</sub> -2	295.67	295.81	296.33
$\dot{\text{C}}_4\text{H}_9\text{-1}$	331.26	328.44	307.63
$\dot{\text{C}}_4\text{H}_9\text{-2}$	331.85	330.54	327.42
$\dot{\text{C}}_4\text{H}_7\text{-11}$	312.91	311.71	311.28
$\dot{\text{C}}_4\text{H}_7\text{-12}$	315.08	—	300.37
$\dot{\text{C}}_4\text{H}_7\text{-13}$	300.56	301.25	306.09
$\dot{\text{C}}_4\text{H}_7\text{-14}$	321.80	315.89	317.35
$\dot{\text{C}}_4\text{H}_7\text{-22}$	310.77	311.28	313.26
iC <sub>4</sub> H <sub>8</sub>	293.21	293.72	287.45
i $\dot{\text{C}}_4\text{H}_9$	319.07	319.66	304.66
t $\dot{\text{C}}_4\text{H}_9$	318.97	318.82	323.39
i $\dot{\text{C}}_4\text{H}_7$	293.08	293.72	300.80
i $\dot{\text{C}}_4\text{H}_7\text{-i1}$	305.54	—	—

Table 4.4 presents comparisons of entropies calculated in this work and the literature, with differences being larger than those observed for the enthalpies. Differences between Goldsmith [42] and this work are on average  $1.13 \pm 3.72$  J K<sup>-1</sup> mol<sup>-1</sup>, while differences between those recommended by Burcat [54] and calculated here are on average  $5.09 \pm 11.64$  J K<sup>-1</sup> mol<sup>-1</sup>. In the case of i $\dot{\text{C}}_3\text{H}_7$ , the lowest energy conformer has Cs symmetry, with an assigned symmetry factor of one. If it is assumed that the symmetry factor of i $\dot{\text{C}}_3\text{H}_7$  is two, the entropy value drops from 295.05 to 289.29 J K<sup>-1</sup> mol<sup>-1</sup>, which is now only 1.01 J K<sup>-1</sup> mol<sup>-1</sup> larger than the value computed by Goldsmith and 0.82 J K<sup>-1</sup> mol<sup>-1</sup> lower than that by

Burcat [54]. For the  $\dot{C}_4H_7-14$  radical, our computed entropy is 5.91 and 4.45 J K<sup>-1</sup> mol<sup>-1</sup> larger than Goldsmith [42] and Burcat [54], respectively. However, Goldsmith [42] reports an uncertainty of 5.86 J K<sup>-1</sup> mol<sup>-1</sup> for their reported entropy for  $\dot{C}_4H_7-14$ , and our value falls within this range.

**Table 4.5:** Comparisons of Heat Capacities Computed Here with Literature Data.

Species	Study	$C_p$						
		300	400	500	600	800	1000	1500
$C_2H_4$	This Work	42.04	51.22	60.64	69.19	82.07	92.25	108.54
	Goldsmith	42.68	52.30	61.50	69.87	82.84	92.88	109.20
	Burcat	43.05	52.64	62.27	70.93	83.89	94.09	109.58
$\dot{C}_2H_5$	This Work	50.83	60.85	70.92	80.13	94.66	106.31	125.31
	Goldsmith	51.46	61.92	71.96	80.75	95.40	107.11	125.94
	Burcat	50.86	61.26	71.64	81.13	96.05	107.91	126.21
$\dot{C}_2H_3$	This Work	43.02	50.42	57.32	63.28	72.12	79.19	90.65
	Goldsmith	43.51	51.46	58.16	63.60	72.80	79.50	91.21
	Burcat	42.20	49.42	56.30	62.33	71.37	78.58	89.98
$C_3H_6$	This Work	62.80	77.74	92.34	105.50	125.94	141.81	166.99
	Goldsmith	64.43	79.91	94.56	107.11	127.61	143.09	168.20
	Burcat	64.71	80.19	95.03	108.28	128.79	144.61	168.44
$n\dot{C}_3H_7$	This Work	71.53	88.04	103.86	117.96	139.72	156.80	184.17
	Goldsmith	72.38	89.96	105.86	119.24	141.42	158.16	185.35
	Burcat	71.61	88.44	104.39	118.52	140.27	157.27	183.71
$i\dot{C}_3H_7$	This Work	67.68	83.16	99.11	113.83	136.88	154.91	183.44
	Goldsmith	68.62	84.94	100.83	115.06	138.49	156.06	184.51
	Burcat	65.81	81.67	97.76	112.60	136.04	154.33	182.33
$\dot{C}_3H_5-s$	This Work	62.51	75.45	87.65	98.44	115.11	128.06	148.67
	Goldsmith	64.02	77.40	89.54	99.58	116.32	129.29	149.37
	Burcat	63.63	76.53	88.46	98.97	115.47	128.30	148.22
$\dot{C}_3H_5-t$	This Work	61.98	74.30	86.40	97.33	114.35	127.61	148.57
	Goldsmith	63.18	76.15	87.86	98.74	115.90	128.87	149.37
	Burcat	61.94	76.98	90.79	102.80	121.04	134.95	155.57
$\dot{C}_3H_5-a$	This Work	61.33	76.91	90.74	102.38	119.28	132.16	152.54
	Goldsmith	62.34	78.24	92.05	102.93	120.08	133.05	153.13
	Burcat	62.12	77.74	91.51	103.04	119.77	132.52	152.17
$C_4H_8-1$	This Work	84.31	105.66	125.90	143.81	171.31	192.50	225.95
	Goldsmith	87.03	109.20	129.29	146.44	173.64	194.56	227.61
	Burcat	85.96	106.28	126.08	144.16	173.16	195.04	227.47
$C_4H_8-2$	This Work	85.63	105.06	124.29	141.89	169.82	191.32	225.43
	Goldsmith	88.28	108.78	127.61	144.77	172.38	193.30	226.77
	Burcat	88.03	108.22	127.84	145.62	173.80	195.38	227.77
$\dot{C}_4H_9-1$	This Work	93.56	116.39	137.92	156.88	185.81	208.19	243.65
	Goldsmith	96.23	119.24	140.58	158.57	187.86	210.04	245.18

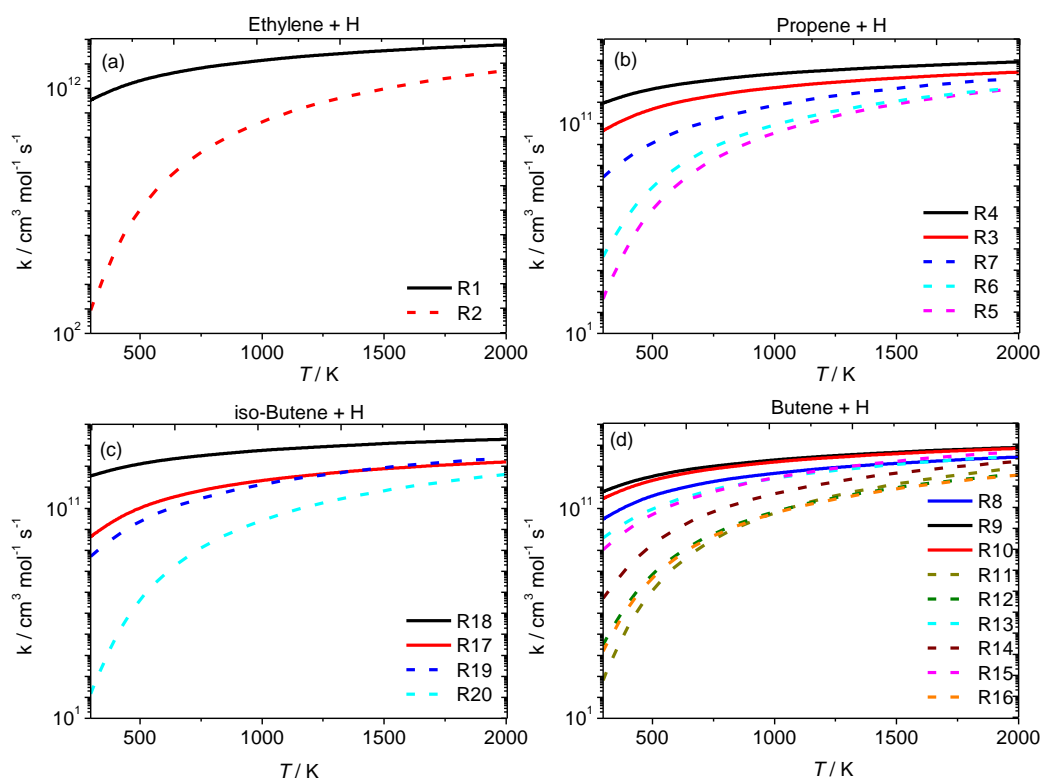
	Burcat	94.98	118.67	140.97	160.63	190.76	213.94	249.44
$\dot{C}_4H_9-2$	This Work	90.04	111.14	132.42	151.82	181.88	205.36	242.30
	Goldsmith	91.63	113.80	135.14	153.97	184.10	207.53	243.93
	Burcat	86.79	109.43	131.47	151.27	181.88	205.47	241.32
$\dot{C}_4H_7-11$	This Work	84.17	103.50	121.34	136.89	160.62	178.88	207.72
	Goldsmith	86.19	106.27	123.85	138.91	162.34	180.33	208.78
	Burcat	84.05	103.05	120.71	136.20	160.05	178.45	206.63
$\dot{C}_4H_7-12$	This Work	83.70	102.27	120.04	135.77	159.75	178.27	207.41
	Goldsmith							
	Burcat	84.33	103.88	121.97	137.87	162.53	181.46	210.28
$\dot{C}_4H_7-13$	This Work	81.56	101.65	120.62	137.24	162.13	181.10	210.74
	Goldsmith	83.26	103.76	122.59	138.49	163.59	182.42	211.71
	Burcat	81.15	101.15	120.07	136.69	161.70	180.78	209.69
$\dot{C}_4H_7-14$	This Work	83.27	102.21	120.16	135.94	159.76	178.10	207.05
	Goldsmith	86.61	105.86	123.43	138.49	161.92	179.91	208.36
	Burcat	85.14	104.57	122.89	138.96	163.17	181.76	210.14
$\dot{C}_4H_7-22$	This Work	83.12	99.93	116.93	132.58	157.36	176.52	206.64
	Goldsmith	84.94	102.81	119.24	134.31	158.41	178.24	207.94
	Burcat	83.51	99.85	116.58	132.13	157.01	176.30	205.65
$iC_4H_8$	This Work	86.01	106.46	125.84	143.20	170.72	191.87	225.62
	Goldsmith	88.28	109.20	128.87	145.60	172.80	193.72	227.19
	Burcat	86.44	109.53	130.81	149.22	176.71	197.59	228.66
$i\dot{C}_4H_9$	This Work	95.21	118.37	139.73	158.34	186.70	208.68	243.73
	Goldsmith	96.65	120.92	142.26	160.25	188.70	210.46	245.18
	Burcat	98.56	122.36	143.90	162.52	191.01	212.96	246.99
$t\dot{C}_4H_9$	This Work	88.45	108.45	129.49	149.13	180.04	204.10	241.76
	Goldsmith	90.79	111.29	132.21	151.04	182.00	205.85	243.09
	Burcat	82.78	104.42	126.31	146.47	178.31	202.90	240.05
$i\dot{C}_4H_7$	This Work	80.50	102.35	121.72	138.17	162.72	181.35	210.69
	Goldsmith	82.01	104.18	123.43	139.33	164.01	182.42	211.71
	Burcat	82.59	103.51	122.32	138.44	162.74	181.30	209.76
$i\dot{C}_4H_7-i1$	This Work	85.77	103.91	120.75	135.71	159.46	177.78	207.03
	Goldsmith	–	–	–	–	–	–	–
	Burcat	–	–	–	–	–	–	–

Table 4.5 presents heat capacities for the  $C_2 - C_4$  species calculated in this work, by Goldsmith [42] and present in the Burcat database [54]. Good agreement is observed, with a MAE of  $1.69 \pm 1.5 \text{ J mol}^{-1} \text{ K}^{-1}$  observed between this work and Goldsmith [42]. Differences between this work and the Burcat database [54] are slightly higher, with a MAE of  $1.87 \pm 3.36 \text{ J K}^{-1} \text{ mol}^{-1}$ .

### 3.2. Reactions of $\dot{\text{H}}$ atoms with $\text{C}_2\text{H}_4$ , $\text{C}_3\text{H}_6$ , $\text{C}_4\text{H}_8$ -1, $\text{C}_4\text{H}_8$ -2, and $\text{iC}_4\text{H}_8$

**Table 4.6:** Computed Energy Barriers, Heats of Reaction, and High-Pressure Limiting Rate Constant (298 – 2000 K) for the Reactions of  $\dot{\text{H}}$  Atoms with  $\text{C}_2 - \text{C}_4$  Alkenes. Units ( $AT^n = \text{cm}^3 \text{mol}^{-1} \text{s}^{-1}$ , Energies  $\text{kJ mol}^{-1}$ ).

		Reaction	$\Delta^\ddagger H_{0\text{K}}$	$\Delta_r H_{0\text{K}}$	$A$	$n$	$E_a$
C <sub>2</sub>	R1	$\text{C}_2\text{H}_4 + \dot{\text{H}} \leftrightarrow \dot{\text{C}}_2\text{H}_5$	11.18	-146.48	$1.15 \times 10^{15}$	-0.41	14.73
	R2	$\text{C}_2\text{H}_4 + \dot{\text{H}} \leftrightarrow \dot{\text{C}}_2\text{H}_3 + \text{H}_2$	63.12	24.09	$4.79 \times 10^{05}$	2.55	51.77
C <sub>3</sub>	R3	$\text{C}_3\text{H}_6 + \dot{\text{H}} \leftrightarrow \text{n}\dot{\text{C}}_3\text{H}_7$	15.61	-132.97	$6.25 \times 10^{15}$	-0.73	19.34
	R4	$\text{C}_3\text{H}_6 + \dot{\text{H}} \leftrightarrow \text{i}\dot{\text{C}}_3\text{H}_7$	8.39	-146.83	$1.02 \times 10^{14}$	-0.03	11.43
	R5	$\text{C}_3\text{H}_6 + \dot{\text{H}} \leftrightarrow \dot{\text{C}}_3\text{H}_5\text{-s} + \text{H}_2$	63.97	27.14	$1.21 \times 10^{06}$	2.43	53.96
	R6	$\text{C}_3\text{H}_6 + \dot{\text{H}} \leftrightarrow \dot{\text{C}}_3\text{H}_5\text{-t} + \text{H}_2$	51.95	12.04	$3.11 \times 10^{05}$	2.51	40.36
	R7	$\text{C}_3\text{H}_6 + \dot{\text{H}} \leftrightarrow \dot{\text{C}}_3\text{H}_5\text{-a} + \text{H}_2$	31.09	-71.88	$6.97 \times 10^{02}$	3.24	13.93
C <sub>4</sub>	R8	$\text{C}_4\text{H}_8\text{-1} + \dot{\text{H}} \leftrightarrow \dot{\text{C}}_4\text{H}_9\text{-1}$	16.04	-136.49	$2.23 \times 10^{14}$	-0.27	18.47
	R9	$\text{C}_4\text{H}_8\text{-1} + \dot{\text{H}} \leftrightarrow \dot{\text{C}}_4\text{H}_9\text{-2}$	9.32	-147.65	$6.06 \times 10^{15}$	-0.60	14.59
	R10	$\text{C}_4\text{H}_8\text{-2} + \dot{\text{H}} \leftrightarrow \dot{\text{C}}_4\text{H}_9\text{-2}$	12.52	-136.08	$1.56 \times 10^{15}$	-0.42	15.68
	R11	$\text{C}_4\text{H}_8\text{-1} + \dot{\text{H}} \leftrightarrow \dot{\text{C}}_4\text{H}_7\text{-11} + \text{H}_2$	64.81	27.38	$2.01 \times 10^{06}$	2.44	54.53
	R12	$\text{C}_4\text{H}_8\text{-1} + \dot{\text{H}} \leftrightarrow \dot{\text{C}}_4\text{H}_7\text{-12} + \text{H}_2$	52.29	13.06	$2.11 \times 10^{05}$	2.54	40.67
	R13	$\text{C}_4\text{H}_8\text{-1} + \dot{\text{H}} \leftrightarrow \dot{\text{C}}_4\text{H}_7\text{-13} + \text{H}_2$	22.85	-82.85	$2.37 \times 10^{05}$	2.56	12.24
	R14	$\text{C}_4\text{H}_8\text{-1} + \dot{\text{H}} \leftrightarrow \dot{\text{C}}_4\text{H}_7\text{-14} + \text{H}_2$	42.70	-14.76	$1.23 \times 10^{05}$	2.71	29.03
	R15	$\text{C}_4\text{H}_8\text{-2} + \dot{\text{H}} \leftrightarrow \dot{\text{C}}_4\text{H}_7\text{-13} + \text{H}_2$	33.51	-69.77	$2.60 \times 10^{04}$	2.95	15.36
	R16	$\text{C}_4\text{H}_8\text{-2} + \dot{\text{H}} \leftrightarrow \dot{\text{C}}_4\text{H}_7\text{-22} + \text{H}_2$	54.25	15.91	$1.21 \times 10^{04}$	2.41	43.19
	R17	$\text{iC}_4\text{H}_8 + \dot{\text{H}} \leftrightarrow \text{i}\dot{\text{C}}_4\text{H}_9$	21.15	-124.43	$9.67 \times 10^{13}$	-0.21	22.08
	R18	$\text{iC}_4\text{H}_8 + \dot{\text{H}} \leftrightarrow \text{t}\dot{\text{C}}_4\text{H}_9$	6.13	-145.60	$7.89 \times 10^{15}$	-0.53	11.98
	R19	$\text{iC}_4\text{H}_8 + \dot{\text{H}} \leftrightarrow \text{i}\dot{\text{C}}_4\text{H}_7 + \text{H}_2$	30.50	-63.73	$4.45 \times 10^{03}$	3.08	14.81
	R20	$\text{iC}_4\text{H}_8 + \dot{\text{H}} \leftrightarrow \text{i}\dot{\text{C}}_4\text{H}_7\text{-i1} + \text{H}_2$	66.75	32.19	$2.60 \times 10^{06}$	2.34	57.34



**Figure 4.1.** High pressure limit rate constants for the reactions of (a) ethylene +  $\dot{\text{H}}$ , (b) propene +  $\dot{\text{H}}$ , (c) isobutene +  $\dot{\text{H}}$ , and (d) 1- and 2-butene +  $\dot{\text{H}}$ .

Figure 4.1 compares the high-pressure limiting rate constants (Table 4.6), for (a) ethylene +  $\dot{\text{H}}$ , (b) propene +  $\dot{\text{H}}$ , (c) isobutene +  $\dot{\text{H}}$ , and (d) 1- and 2-butene +  $\dot{\text{H}}$ . Hydrogen atom addition to, and abstraction from, ethylene have computed energy barriers of 11.2 and 63.1  $\text{kJ mol}^{-1}$ , respectively. Terminal  $\dot{\text{H}}$  atom addition to propene has a computed energy barrier of 8.4  $\text{kJ mol}^{-1}$ , which is 7.2  $\text{kJ mol}^{-1}$  lower than that for internal addition. As expected,  $\dot{\text{H}}$  atom abstraction from the primary allylic site of propene is favored, with an energy barrier of 31.1  $\text{kJ mol}^{-1}$ . Abstraction of the two  $\dot{\text{H}}$  atoms on the primary vinylic site have similar barriers of 63.7 and 64.6  $\text{kJ mol}^{-1}$ , leading to *cis*- and *trans*- configurations of  $\dot{\text{C}}_3\text{H}_5$ -s, respectively. Terminal  $\dot{\text{H}}$  atom addition to isobutene forming the tertiary  $\text{t}\dot{\text{C}}_4\text{H}_9$  radical has a computed barrier of 6.1  $\text{kJ mol}^{-1}$ , which is 15.0  $\text{kJ mol}^{-1}$  lower than internal addition forming the primary  $\text{i}\dot{\text{C}}_4\text{H}_9$  radical. Abstraction from the primary allylic site has a computed barrier of 30.5  $\text{kJ mol}^{-1}$ . Terminal and internal  $\dot{\text{H}}$  atom addition can exist for 1-butene, with respective barriers of 9.3 and 16.0  $\text{kJ mol}^{-1}$ , while abstraction from the primary allylic site has a barrier of 22.85  $\text{kJ mol}^{-1}$ . Internal addition to 2-butene and abstraction from the primary allylic site have respective barriers of 12.5 and 33.5  $\text{kJ mol}^{-1}$ .

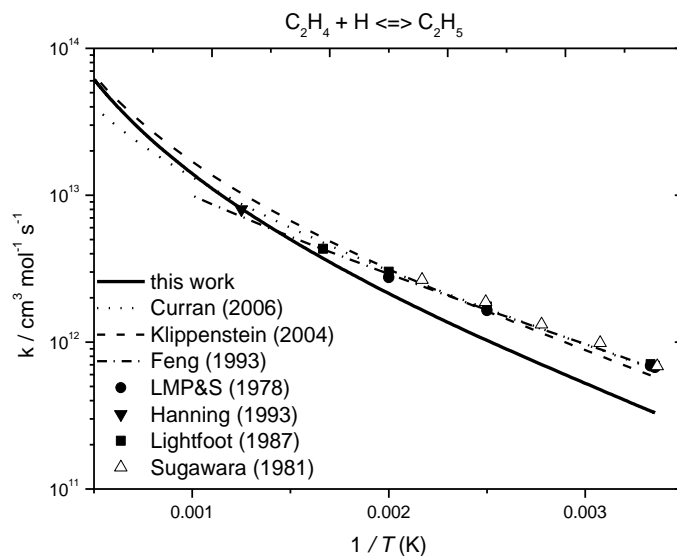


**Figure 4.2.** High-pressure limiting rate constant comparisons for the reactions of  $\dot{\text{H}}$  atom addition with ethylene. Solid lines represent the current work (ROCCSD(T)/aug-cc-pVXZ), dotted (Curran [58]), dashed (Miller and Klippenstein [17]), dashed-dotted (Feng et al. [7]), ● (Lee et al. [9]), ▲ (Hanning et al. [8]), ■ (Lightfoot et al. [10]), and △ (Sugawara et al. [14]).

Figure 4.2. compares theoretical and experimental data [8-10, 14] for the reaction  $\text{C}_2\text{H}_4 + \dot{\text{H}} \leftrightarrow \dot{\text{C}}_2\text{H}_5$ . Also plotted is the rate constant recommendation from Curran et al. [58] and the transition state theory fit to the experiments by Feng et al. [7], with good agreement being observed. The largest difference observed between the current work and Miller and Klippenstein [17] is a factor of 1.75 at 300 K. The difference in energy barrier of  $0.54 \text{ kJ mol}^{-1}$  and the quoted uncertainty of their fits to replicate the master equation results of  $\pm 20\%$ , which would account for an accumulative difference of  $\sim 1.5$ .



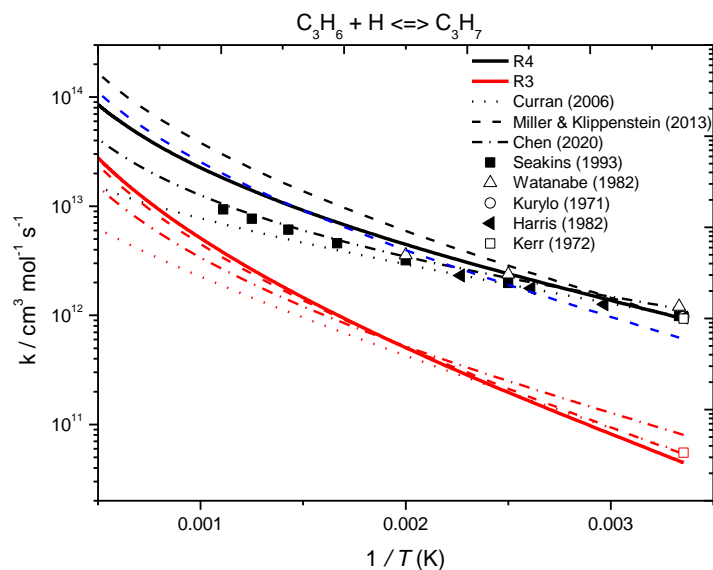


**Figure 4.3.** High-pressure limiting rate constant comparisons for the reactions of  $\dot{\text{H}}$  atom addition to propene. Solid lines represent the current work (ROCCSD(T)/aug-cc-pVXZ), dotted (Curran [58]), dashed (Miller and Klippenstein [18]), dashed-dotted (Chen [20]), ■ (Seakins et al. [23]),  $\triangle$  (Watanabe et al.[27]),  $\circ$  (Kurylo et al. [26]),  $\blacktriangleleft$  (Harris et al. [31]), and  $\square$  (Kerr et al. [24]).

Figure 4.3 presents high-pressure limiting rate constant comparisons for the  $\dot{\text{H}}$  atom addition reactions to propene. Relatively good agreement is observed between the current work and theory and experiments from the literature. In order to improve agreement with experiment, Miller and Klippenstein [18] altered some reaction barriers, including those for terminal and internal H-atom addition and H-atom abstraction from the primary allylic site of propene. The adjusted rate constant for internal addition to propene (red) is in excellent agreement with the one calculated in the current work and the adjusted energy barrier of  $15.5 \text{ kJ mol}^{-1}$  is almost identical to  $15.6 \text{ kJ mol}^{-1}$  calculated in the current work, as shown in Table 4.6. The rate constant for terminal addition (black) is approximately a factor of two faster than that calculated here. However, as mentioned by Chen et al. [20], the higher values reported by Miller and Klippenstein may be attributed to input data errors. An error in symmetry number affects the energy barriers and pressure dependent rate constant expressions. If the effect of symmetry reduced the rate constant by a factor of  $\sim 1.5$  (dashed blue line, Fig 4.3), it would be in good agreement with that calculated here.

The rate constants reported by Chen et al. [20] are within a factor of two of the current work over the temperature range 298 – 2000 K. Differences in energy barriers computed in

this work and that by Chen are 3.01 and 2.49 kJ mol<sup>-1</sup> for non-terminal addition and terminal addition, respectively. The recommendations by Curran et al. [58] are in good agreement at T < 800 K, but differences become larger at higher temperatures, with a factor of ~5 discrepancy observed at 2000 K.

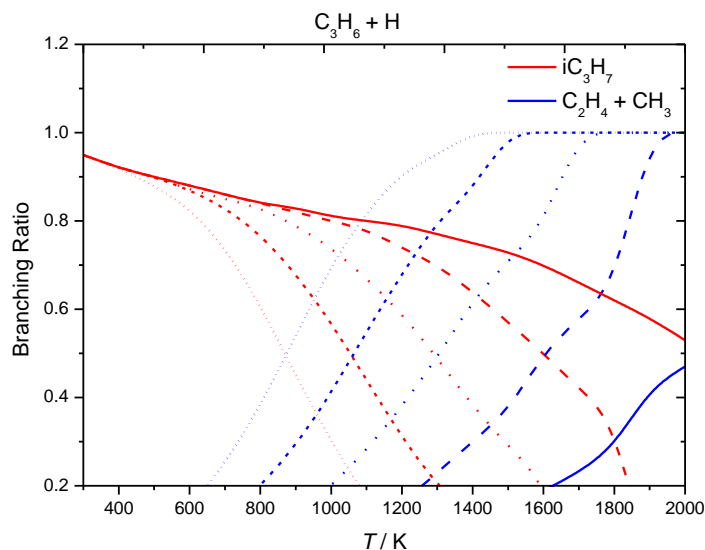


**Figure 4.4.** Temperature- and pressure-dependent branching ratios for propene +  $\dot{\text{H}}$  via hydrogen atom addition reactions at 0.1 (short-dotted lines), 1 (short-dashed lines), 10 (dotted lines), 100 (dashed lines), and 1000 (solid lines) atm.

Figure 4.4 presents the temperature- and pressure-dependencies of the product branching ratios for  $\dot{\text{H}}$  atom addition to propene in the temperature range 298 – 2000 K and at pressures of 0.1, 1.0, 10, and 100 atm. At 0.1 atm  $\dot{\text{H}}$  atom addition to propene forming  $\dot{\text{iC}}_3\text{H}_7$  radicals is favoured at temperatures up to 800 K, until the formation of  $\text{C}_2\text{H}_4$  and  $\dot{\text{C}}\text{H}_3$  dominates. For pressures of 1.0, 10, 100 atm, the formation of  $\dot{\text{iC}}_3\text{H}_7$  is favoured at temperatures up to ~1000 K, 1200 K, and 1500 K, respectively.

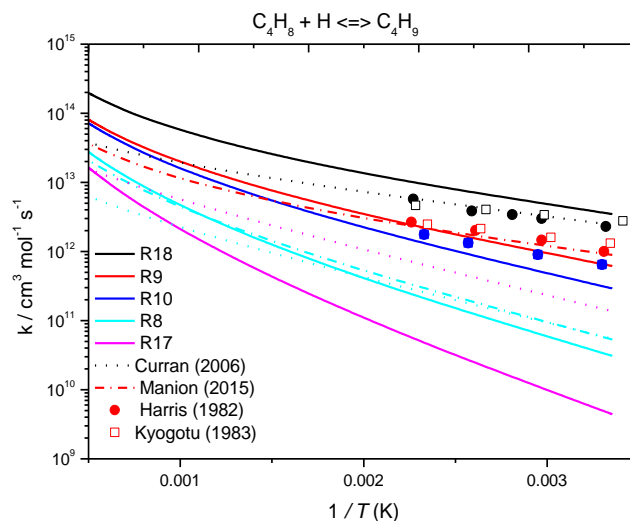


**Figure 4.5.** High-pressure limiting rate constant comparisons for the reactions of  $\dot{\text{H}}$  atom addition to the butene isomers. Solid lines represent the current work (ROCCSD(T)/aug-cc-pVXZ) dotted (Curran [58]), dash-dotted (Manion et al.[19]),  $\bullet$  (Harris et al. [31]), and  $\square$  (Kyogotu et al. [59]).

Figure 4.5 presents high-pressure limiting rate constant comparisons for the reactions of  $\dot{\text{H}}$  atom addition to the butene isomers. Larger differences are observed for the reactions of  $\dot{\text{H}}$  atoms with  $\text{C}_4$  alkenes calculated here and in the literature. For terminal addition to 1-butene, the rate constants determined by Manion et al. [19] and in this work are within a factor of  $\sim 2.22$  over the temperature range 298 – 2000 K. The rate constants for internal addition to 1-butene are in excellent agreement and are within a factor of  $\sim 1.3$ . Additionally, the current calculations are in relatively good agreement with the experimental data by Kyogotu et al. [59] and Harris et al. [31]. For terminal addition to isobutene, the recommendations by Curran et al. [58] are again in good agreement at lower temperatures but there is a larger deviation of a factor of five observed at 2000 K. The largest difference is observed for internal addition to isobutene. However, the difference in rate constants calculated in the current work for internal addition to 1-butene and isobutene is consistent with the difference in the computed barrier heights of  $5.1 \text{ kJ mol}^{-1}$ , accounting for the factor of seven discrepancy at low temperatures. Curran’s recommendation is a factor of  $\sim 30$  times faster at 298 K. The rate constant recommendation used is 2.5 times the recommendation used for internal addition to propene. However, it was found that our calculations for internal addition to propene is  $\sim 10$  times faster than that to isobutene at 298 K, which can be attributed to the

energy barrier for internal addition to propene being  $\sim 5.54 \text{ kJ mol}^{-1}$  lower than that for isobutene.

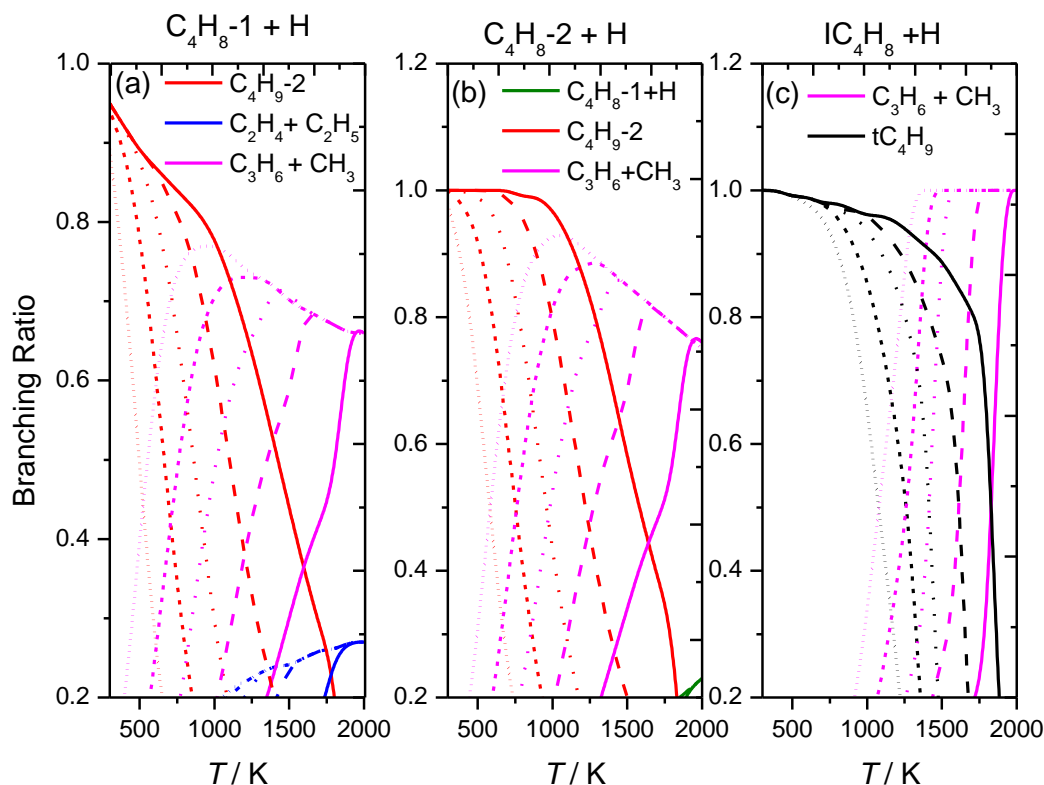


**Figure 4.6.** Temperature- and pressure-dependent branching ratios for (a) 1-butene, (b) 2-butene and (c) isobutene via hydrogen atom addition reactions at 0.1 (short-dotted lines), 1 (short-dashed lines), 10 (dotted lines), 100 (dashed lines), and 1000 (solid lines) atm.

Figure 4.6 shows the temperature- and pressure-dependencies of the product branching ratios for  $\dot{\text{H}}$  atom addition to (a) 1- and (b) 2-butene and (c) isobutene in the temperature range 298 – 2000 K and at pressures of 0.1, 1.0, 10, and 100 atm. For both 1- and 2-butene, at 0.1 atm,  $\dot{\text{H}}$  atom addition forming the  $\dot{\text{C}}_4\text{H}_9\text{-2}$  radical is favoured at temperatures up to 500 K. The formation of  $\text{C}_3\text{H}_6$  and  $\dot{\text{C}}\text{H}_3$  then dominates the reaction flux at higher temperatures. Similar trends are observed in both Figs. 4. 6(a) and (b) at 1.0, 10, and 100 atm. However the formation of  $\dot{\text{C}}_4\text{H}_9\text{-2}$  is favoured at temperatures up to  $\sim 700$ , 900, and 1200K, respectively. In the case of isobutene,  $\dot{\text{H}}$  atom addition forming  $t\dot{\text{C}}_4\text{H}_9$  radicals is favoured at temperatures up to 1000 K at 0.1 atm, whereas at higher temperatures the formation of  $\text{C}_3\text{H}_6$  and  $\dot{\text{C}}\text{H}_3$  dominates. The same trends are observed at 1.0, 10, and 100 atm. However the formation of  $t\dot{\text{C}}_4\text{H}_9$  radicals is favoured at temperatures up to 1200, 1400, and 1600 K, respectively.

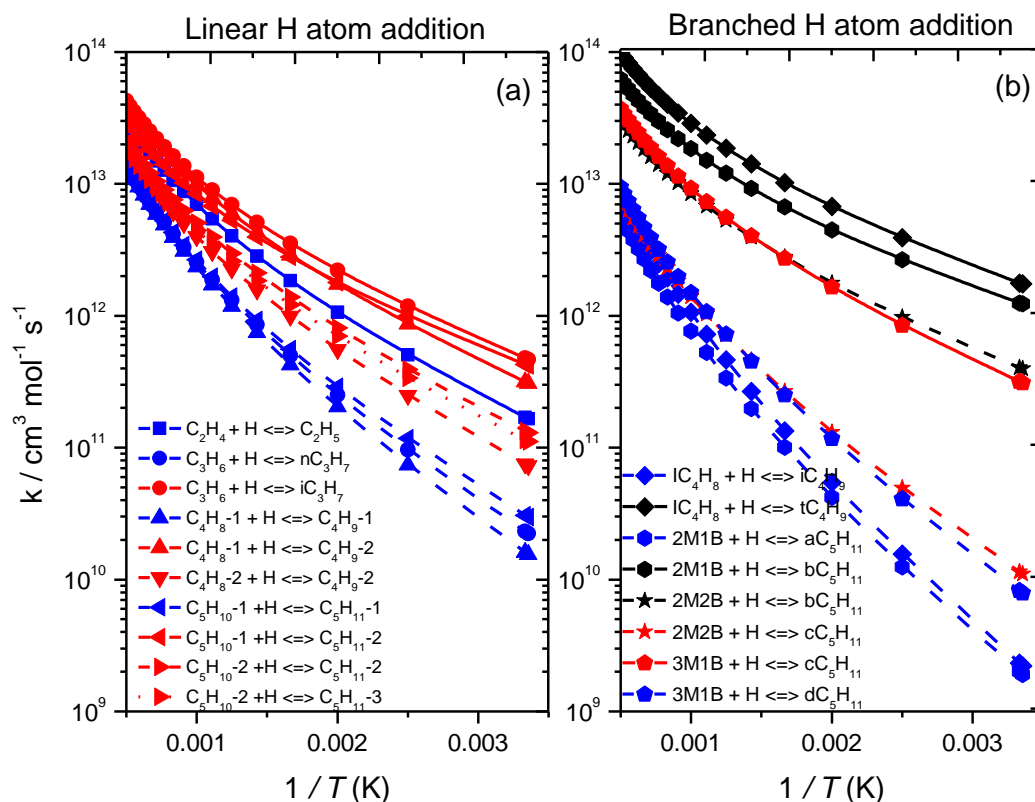


**Figure 4.7.** Rate constants (symmetry uncorrected) for terminal and internal  $\dot{\text{H}}$  atom addition to (a) linear and (b) branched  $\text{C}_2 - \text{C}_5$  alkenes from previous [4, 5] and current work. Solid and dashed lines represent terminal and internal addition, respectively. Different colours represent different radical types formed. Black (tertiary), red (secondary) and blue (primary). Different symbols correspond to the different reactants.  $\blacksquare$  (ethylene),  $\bullet$  (propene),  $\blacktriangle$  (1-butene),  $\blacktriangledown$  (2-butene),  $\blacklozenge$  (isobutene),  $\blacktriangleleft$  (1-pentene),  $\blacktriangleright$  (2-pentene),  $\blacklozenge$  (2-methyl-1-butene),  $\star$  (2-methyl-2-butene), and  $\blacklozenge$  (3-methyl-1-butene).

Figure 4.7 presents rate constants for  $\dot{\text{H}}$  atom addition reactions, which are reported with no symmetry or optical isomer corrections between the transition state and reactants – i.e. the reaction path degeneracy is set to one. Table S1 of SM presents the symmetry factors for the reactants and transition states prior to this change. As expected, external  $\dot{\text{H}}$  atom addition to each of the alkenes (solid lines) dominates over internal addition (dashed lines). For the linear alkenes, both external and internal  $\dot{\text{H}}$  atom addition can lead to the formation of primary (blue) or secondary radicals (red). The rate constants for external addition to propene, 1-butene and 1-pentene are similar with respective barrier heights of 8.4, 9.3 and 7.8  $\text{kJ mol}^{-1}$ . However, the rate constant for external addition to ethylene is approximately a factor of two slower than external addition to propene and 1-butene at 500 K, reducing to a factor of  $\sim 1.4$

at 2000 K. This difference can be attributed to the difference in energy barrier of  $\sim 2.8$  kJ mol<sup>-1</sup>. This can also be correlated with radical stability as a primary radical is formed in the case of ethylene, while secondary radicals are formed for propene, 1-butene and 1-pentene.

Internal  $\dot{H}$  atom addition to linear alkenes form either primary ( $C_3H_6 + \dot{H} \leftrightarrow n\dot{C}_3H_7$ ,  $C_4H_8-1 + \dot{H} \leftrightarrow \dot{C}_4H_9-1$ , and  $C_5H_{10}-1 + \dot{H} \leftrightarrow \dot{C}_5H_{11}-1$ ) or secondary radicals ( $C_4H_8-2 + \dot{H} \leftrightarrow \dot{C}_4H_9-2$ ,  $C_5H_{10}-2 + \dot{H} \leftrightarrow \dot{C}_5H_{11}-2$ , and  $C_5H_{10}-2 + \dot{H} \leftrightarrow \dot{C}_5H_{11}-3$ ). Rate constants for internal addition to propene, 1-butene and 1-pentene are similar. Rate constants for internal addition to 2-pentene are almost identical, with internal addition to 2-butene being slightly slower. However, this can be attributed to an energy barrier difference of  $\sim 1.6$  kJ mol<sup>-1</sup>. The branched alkenes have been described previously [5], so we shall not re-iterate here. A trend was observed in that the rate constants for formation of tertiary radicals are the fastest, followed by secondary and primary radicals, respectively [5]. In the rate rule determinations, two rules were proposed for internal  $\dot{H}$  atom addition to branched alkenes (one for addition to a branched alkene where the branching occurs at the double bond and a second for where the branching does not occur at the double bond. For the cases where branching occurs at the double bond ( $iC_4H_8 + \dot{H} \leftrightarrow i\dot{C}_4H_9$  and  $2M1B + \dot{H} \leftrightarrow a\dot{C}_5H_{11}$ ), the energy barriers are similar, being 21.15 and 19.9 kJ mol<sup>-1</sup>, and are higher than that for  $3M1B + \dot{H} \leftrightarrow d\dot{C}_5H_{11}$  (17.15 kJ mol<sup>-1</sup>), where the branching does not occur at the double bond.

Recommended rate constants were suggested based on (i) whether addition is to a linear or branched alkene (ii) whether it is terminal or internal addition and (iii) the type of radical formed. An average of the rate constants within each sub-class was taken as the recommended rate constant. If only one rate constant was available, for example in the case of internal addition to a branched alkene forming a secondary radical ( $bC_5H_{10} + \dot{H} \leftrightarrow c\dot{C}_5H_{11}$ ), the rate constant for the reaction is taken as the recommended rate constant. For the rate constant recommendations presented in Tables 4.7, 4.9 and 4.11, the activation energies are expressed in cal mol<sup>-1</sup> units for ease in implementing into kinetic mechanisms.

In relation to the uncertainty bounds presented in, upper and lower bounds are given, which are defined as:

$$\text{Upper} = k_{\text{max}} / k_{\text{recommendation}}$$

$$\text{Lower} = k_{\text{recommendation}} / k_{\text{min}}$$

where  $k_{\text{recommendation}}$  refers to the recommended rate coefficient and  $k_{\text{min}}$  and  $k_{\text{max}}$  refer to the minimum and maximum rate coefficients used in the determinations of the recommended rate coefficients, respectively. Appropriate symmetry corrections must be applied to these recommendations for use in rate rule determinations.

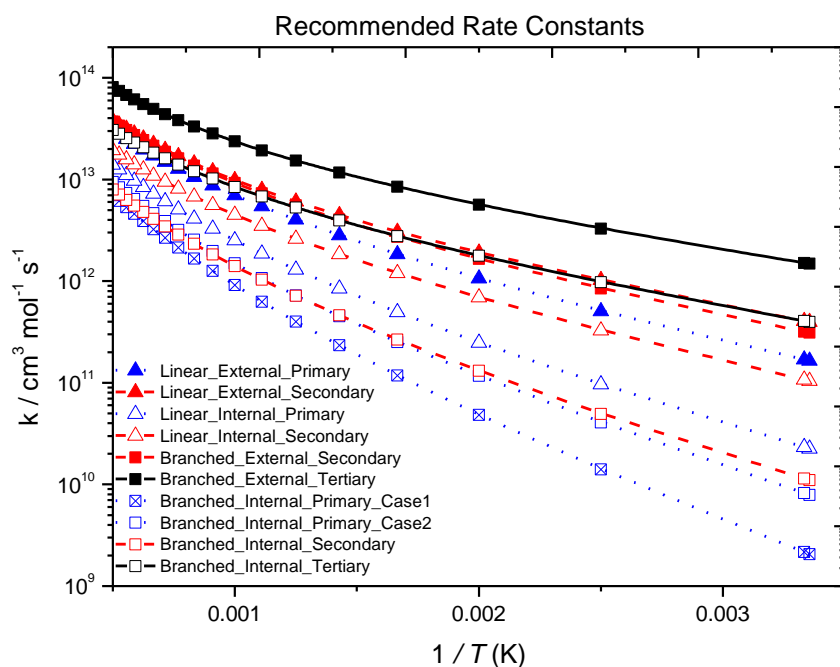


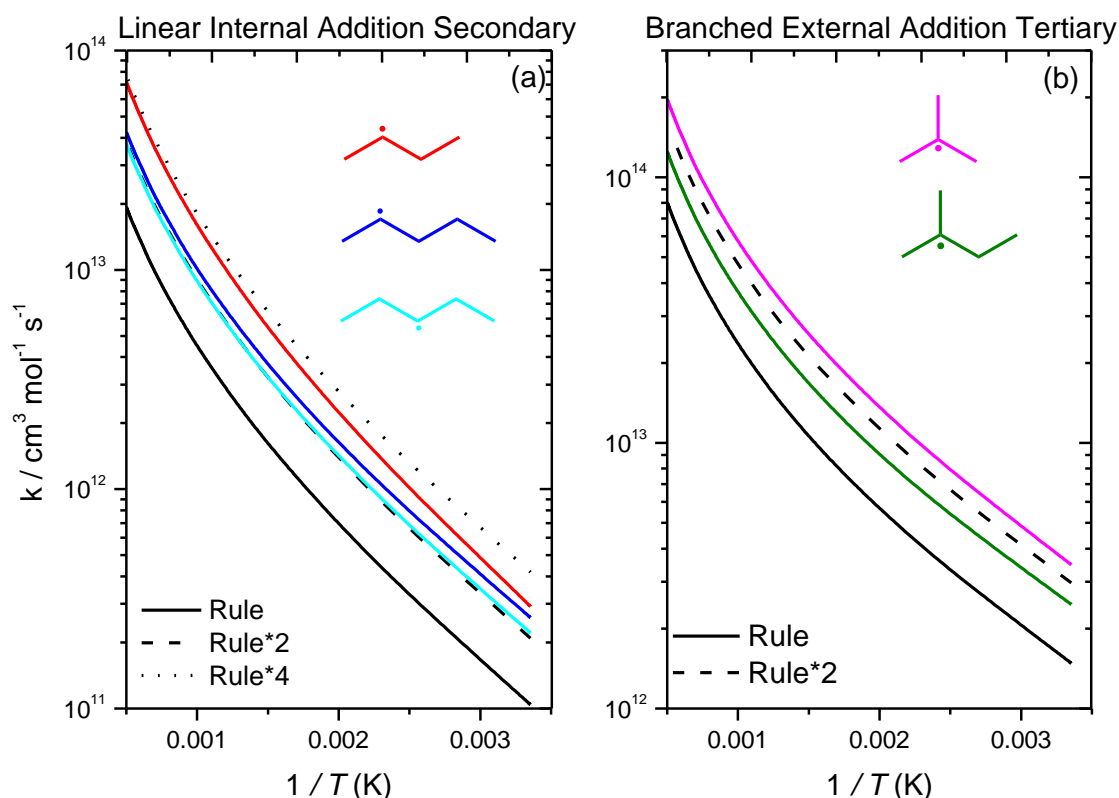
**Figure 4.8.** Rate constant recommendations (symmetry uncorrected) for  $\dot{\text{H}}$  atom addition to linear ( $\blacktriangle$ ) and branched ( $\blacksquare$ )  $\text{C}_2 - \text{C}_5$  alkenes. Solid, dashed and dotted lines represent the formation of tertiary, secondary and primary radicals, respectively. Open symbols are internal C-atom additions, solid symbols are external C-atom additions.

**Table 4.7:** Rate Constant Recommendations (Symmetry Uncorrected) for  $\dot{\text{H}}$  atom Addition to Linear and Branched Alkenes ( $\text{C}_2 - \text{C}_5$ ).

Structure	Site	Radical Formed	$A$	$n$	$E_a$	Uncertainty Bounds (Upper, Lower)
Linear	External	$1^\circ$	$2.40 \times 10^{08}$	1.60	1526.	—
	External	$2^\circ$	$4.35 \times 10^{08}$	1.54	1144.	1.17, 1.23
	Internal	$1^\circ$	$7.79 \times 10^{07}$	1.67	2276.	1.32, 1.45
	Internal	$2^\circ$	$2.74 \times 10^{08}$	1.52	1621.	1.24, 1.43
Branched	External	$2^\circ$	$4.21 \times 10^{08}$	1.54	1292.	—
	External	$3^\circ$	$1.42 \times 10^{09}$	1.47	836.	1.22, 1.29
	Internal_Case1	$1^\circ$	$2.27 \times 10^{07}$	1.78	3326.	1.18, 1.21
	Internal_Case2	$1^\circ$	$4.29 \times 10^{07}$	1.71	2677.	—
	Internal	$2^\circ$	$5.09 \times 10^{07}$	1.65	2401.	—
	Internal	$3^\circ$	$5.45 \times 10^{08}$	1.47	1070.	—

**Table 4.8:** Symmetry Corrections to be Applied to Rate Constant Recommendations for  $\dot{\text{H}}$  Atom Addition to Alkenes.

$\sigma$ Reactant	$\sigma$ Transition State	Symmetry Corrected / Symmetry Uncorrected
1	0.5	2
2	0.5	4
2	1.0	2
4	2.0	2



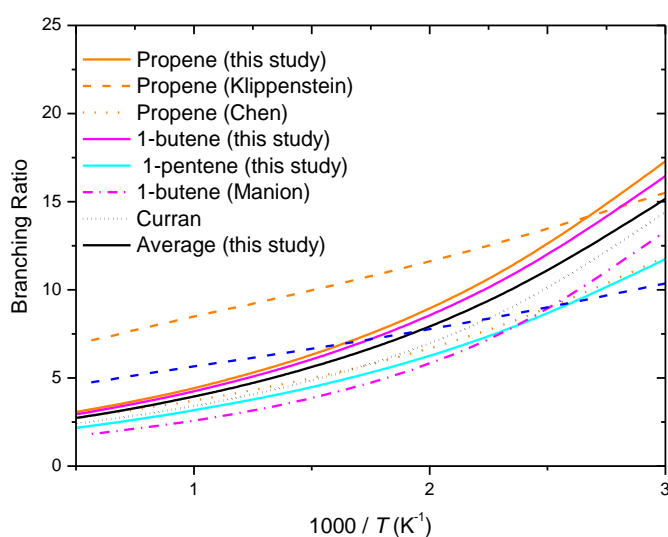
**Figure 4.9.** Examples of the application of the proposed rules for  $\dot{\text{H}}$  atom addition to alkenes.

Figure 4.9 illustrates an example of the rules proposed for (a) internal  $\dot{\text{H}}$  addition to a linear alkene forming a secondary radical and (b) external addition to a branched alkene forming a tertiary radical. The rule is represented by a black solid line. Factors of two and four variations in the rule are represented by dashed and dotted lines, respectively. The coloured lines represent the symmetry corrected rate constants for each respective reaction, with the uncertainty bounds presented in Table 7. Presented in Fig. 4.9(a) are the recommended rate constants (symmetry uncorrected) which is multiplied by four for  $\text{C}_4\text{H}_8\text{-2} + \dot{\text{H}} \leftrightarrow \dot{\text{C}}_4\text{H}_9\text{-2}$  since the reactant has a symmetry factor of two and the transition state has a symmetry factor of 0.5. For  $\text{C}_5\text{H}_{10}\text{-2} + \dot{\text{H}} \leftrightarrow \dot{\text{C}}_5\text{H}_{11}\text{-2}$  and  $\text{C}_5\text{H}_{10}\text{-2} + \dot{\text{H}} \leftrightarrow \dot{\text{C}}_5\text{H}_{11}\text{-3}$ , the rule is



multiplied by two, since the reactant has a symmetry factor of one, and both TSs have a symmetry factor of 0.5. As mentioned earlier, Table S1 of SM presents the symmetry factors for reactants and transition states prior to changing them to one. It was found that this change decreased each  $\dot{H}$  atom addition rate constant for both linear and branched alkenes by a factor of two, with the exception of  $C_4H_8-2 + \dot{H} \leftrightarrow \dot{C}_4H_9-2$ , which is explained above.

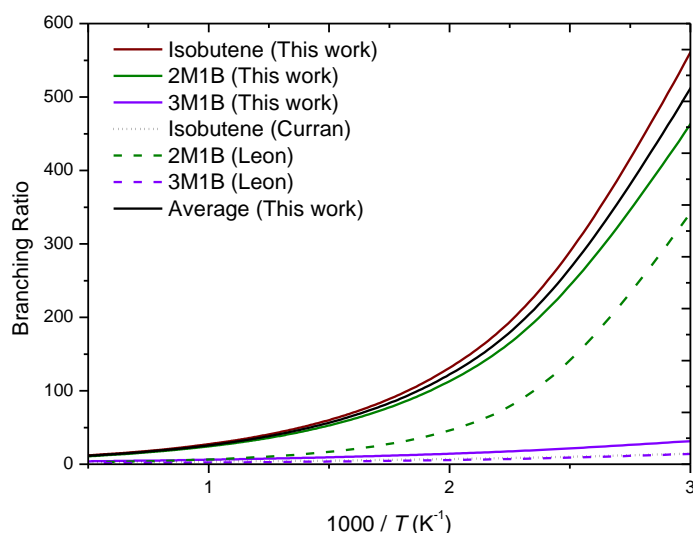
### 3.2.1. Branching ratios of terminal/internal $\dot{H}$ atom addition to linear and branched alkenes



**Figure 4.10.** Branching ratio for terminal to internal  $\dot{H}$  atom addition to (a) linear and (b) branched 1-alkenes.

As discussed earlier, Manion et al. [19] carried out a shock-tube study to investigate the kinetics of terminal and internal  $\dot{H}$  atom addition to 1-butene. They observed a factor of three discrepancy in the branching ratio for terminal/internal  $\dot{H}$  atom addition compared to that calculated by Miller and Klippenstein [18] for the  $\dot{H} +$  propene reactions. Manion et al. [19] state that the difference is well outside the experimental error of their experiments or the expected differences for 1-butene. One of the aims of the current work is thus to investigate the branching ratio of terminal to internal  $\dot{H}$  atom addition in 1-alkenes. Branching ratios for  $\dot{H}$  atom addition to linear 1-alkenes for  $C_2$ – $C_5$  alkenes are plotted in Fig. 4.10. The branching ratios for propene and 1-butene calculated in the current work are within 5% of each other while our calculated branching ratio for 1-pentene is approximately 40–48% lower than that for propene. Non-terminal addition to pentene is  $\sim 1.33$  –  $1.92$  times faster than that for propene and 1-butene at  $T < 300$  K. However, terminal addition to propene and 1-butene is

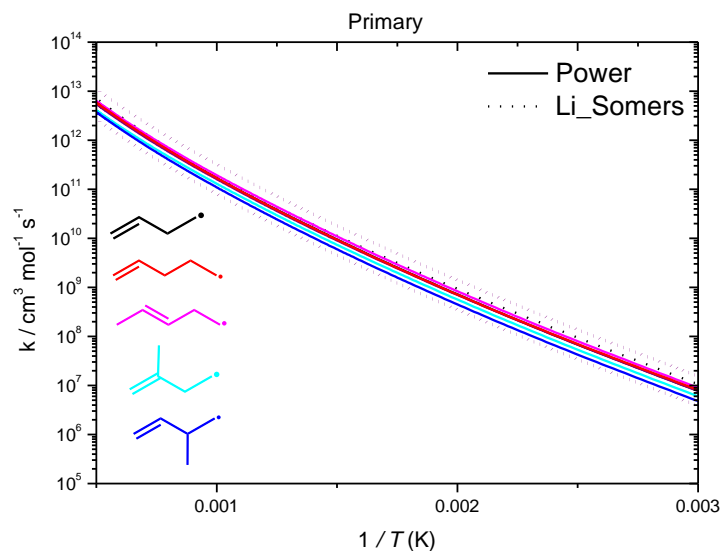
1.2 – 1.38 times faster than for 1-pentene at  $T > 1000$  K. The solid black line represents an average of the calculated rate constants for external addition to a linear 1-alkene forming a secondary radical to internal addition to a linear alkene forming a primary radical and is in excellent agreement with Curran’s recommendation [58], with the branching ratios being within 10% of each other. This average branching ratio is also in good agreement with Manion’s branching ratio for 1-butene and is within a factor of 1.57 at 2000 K. The dashed blue line is the branching ratio for terminal/non-terminal addition if the rate constant for terminal addition by Miller and Klippenstein [18] was reduced by a factor of 1.5. This adjusted branching ratio still differs with that of Manion’s by a factor of  $\sim 2.6$  and a factor of 1.5 – 2.0 of the branching ratios calculated in the current work at 2000 K.



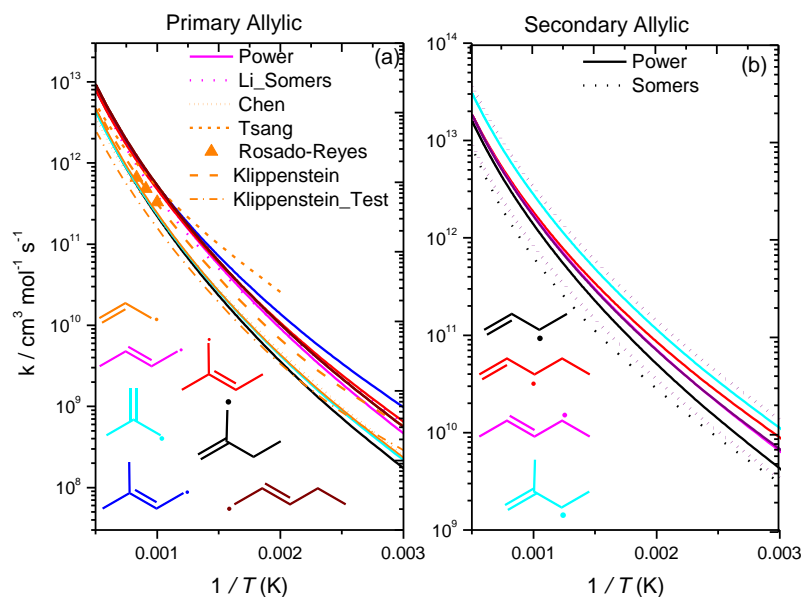
**Figure 4.11.** Branching ratio for terminal to internal  $\dot{\text{H}}$  atom addition to branched 1-alkenes.

Figure 4.11 presents branching ratios for terminal to internal  $\dot{\text{H}}$  atom addition to branched 1-alkenes. 2-methyl-1-butene (2M1B) and isobutene have a branching ratio of 24.2 and 27.2, respectively at 1000 K. These branching ratios are significantly higher than 3-methyl-1-butene, where the branching ratio of terminal to internal  $\dot{\text{H}}$  atom addition is 6.21 at 1000 K. This is due to branching at the position of the double bond. This results in terminal addition to 2M1B and isobutene forming a tertiary radical, which is more stable than a secondary radical formed through terminal addition to 3M1B, resulting in faster rate constants for terminal addition. Again, the solid black line represents the branching ratio of our recommended rate constants of external addition to branched 1-alkene forming a tertiary radical to internal addition to a branched alkene forming a primary radical. As mentioned earlier, large deviations in rate constants for isobutene are observed between this work and

the recommendations by Curran [58], particularly for internal  $\dot{H}$  atom addition. However, Curran does state that no experimental studies for internal  $\dot{H}$  atom addition existed, so the rate constant recommendation was taken as 2.5 times the rate constant of internal  $\dot{H}$  atom addition to propene. Manion [19] states in his study that their [19] rates should not be applied to 1-olefins that have branching at the double bond position. We also observe that branching at the double bond significantly influences the branching ratio of 1-olefins and explains the difference as why the branching ratio from Curran is lower than that of the current work. Additionally, Manion [19] states that direct information is lacking on the impact of branching removed from the double bond, but they believe it would have a minimal effect, which is also supported by our calculations here, where our calculated branching ratio for 3M1B is 6.21 at 1000 K. Our calculated branching ratios for propene, 1-butene and 1-pentene are 4.42, 4.24 and 3.17, respectively at 1000 K.



**Figure 4.12.** High-pressure limiting rate constants for H-atom abstraction from alkylic (primary) carbon sites on a per H-atom basis.



**Figure 4.13.** High-pressure limiting rate constants for H-atom abstraction from allylic carbon sites on a per H-atom basis.

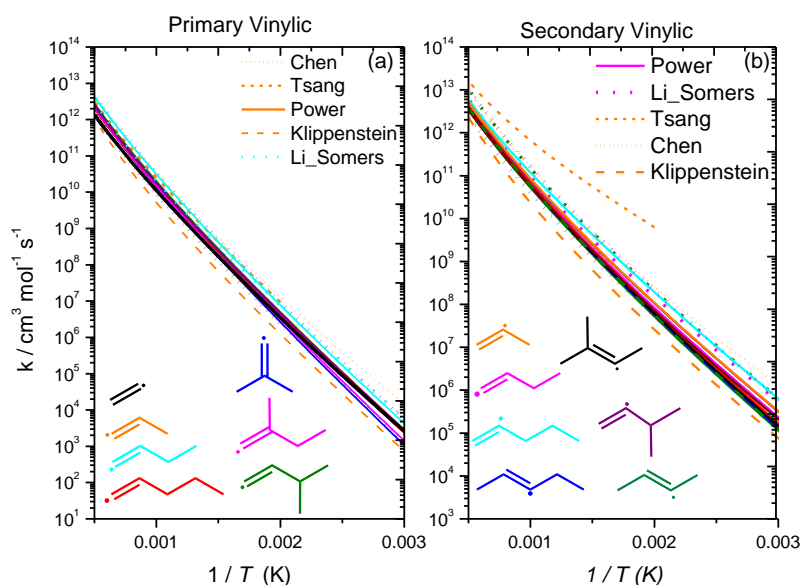


**Figure 4.14.** High-pressure limiting rate constants for H-atom abstraction from vinylic carbon sites on a per H-atom basis.

Rate constant comparisons for the H-atom abstraction reactions from  $C_2 - C_4$  alkenes were discussed in our previous studies [4, 5] on the reactions of  $\dot{H}$  atoms with the pentene isomers, so we shall be brief here. As mentioned earlier, excellent agreement is observed for H-atom abstraction from the primary carbon sites, Fig. 4.12. An average of our computed rate constants for abstraction from the primary carbon site as well as the rate calculated by Li and

Somers [2] is taken as the recommended rate constant. Good agreement is also observed for the abstraction reactions from the primary allylic and vinylic carbon sites.

For H-atom abstraction from the primary allylic carbon sites, a trend was observed in which abstraction from 2-alkenes is faster than that from 1-alkenes, Fig. 4.13(a). As a result, two rate constant recommendations were proposed. The average energy barriers for abstraction from the primary allylic site of 1-alkenes and 2-alkenes computed in this work are 31.0 and 28.6 kJ mol<sup>-1</sup>, respectively which accounts for most of the difference observed. The difference observed at higher temperatures can be attributed to the difference in entropy of activation. For the rate constant recommendation for 1-alkenes, an average of the rates calculated in this work and previous studies as well as that by Chen is taken.

For 2-alkenes, an average of our computed rate constants and the rate constant by Li and Somers is taken as the recommended value. For comparison purposes, the rate constant calculated by Miller and Klippenstein was decreased by a factor of two since this was another reaction for which they altered the energy barrier. The altered rate constant agrees well with the rate constant calculated in the current work and with that from Chen. Moreover, for abstraction from the secondary allylic and primary vinylic carbon site, an average of our calculated rates and that by Li and Somers is taken as the recommended rate constant. For abstraction from the secondary vinylic site, an average of our computed rate constants, Li and Somers, Chen and Miller and Klippenstein is taken. A factor of two uncertainty is applied to these recommendations and are represented by dotted purple lines in Figs. 4.12 – 4.14. For clarity reasons, the factor of two uncertainty is not shown for Fig.4.13 (a) since there are two recommended rate constants.

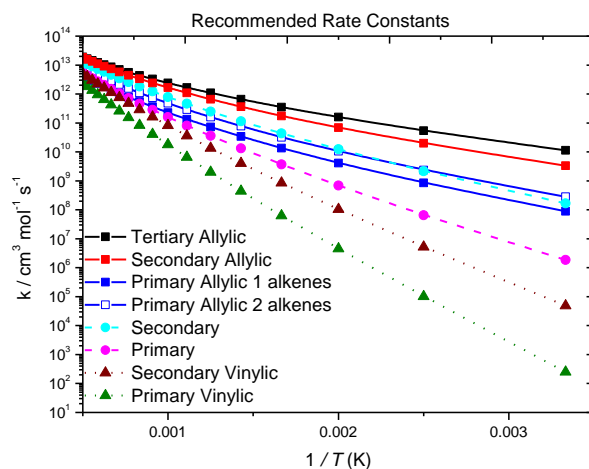


**Figure 4.15.** Rate constant recommendations for H-atom abstraction from C<sub>2</sub> – C<sub>5</sub> alkenes. Solid (allylic), dashed (alkyl) and dotted (vinylic).

**Table 4.9:** Recommended Rate Constants for H-atom Abstraction from Alkenes on a per H-atom basis. ( $A.T^n = \text{cm}^3 \text{mol}^{-1} \text{s}^{-1}$ , Energies =  $\text{cal mol}^{-1}$ ). Fit between 300 and 2000 K.

Class	$A$	$n$	$E_a$	Uncertainty Bounds (Upper, Lower)
Primary	$4.69 \times 10^{04}$	2.68	6959.	1.42, 1.35
Primary Allylic: 1 alkenes	$9.14 \times 10^{02}$	3.06	3582.	1.10, 1.28
Primary Allylic: 2 alkenes	$1.32 \times 10^{03}$	3.08	3203.	1.19, 1.50
Primary Vinylic	$2.72 \times 10^{05}$	2.54	12819.	2.39, 2.95
Secondary	$4.08 \times 10^{05}$	2.44	4734.	–
Secondary Allylic	$1.06 \times 10^{05}$	2.59	2654.	1.67, 2.67
Secondary Vinylic	$2.41 \times 10^{05}$	2.55	9611.	2.09, 2.02
Tertiary Allylic	$2.10 \times 10^{06}$	2.19	2329.	–

$\text{cm}^3 / \text{mol/s/cal units}$ .

### 3.3. Reactions of alkyl radicals

#### 3.3.1. Ethyl ( $\dot{\text{C}}_2\text{H}_5$ ) radical

Ethyl radicals are formed via  $\dot{\text{H}}$  atom addition to ethylene ( $11.2 \text{ kJ mol}^{-1}$ ). C–H  $\beta$ -scission of ethyl radicals can also occur with a barrier height of  $157.7 \text{ kJ mol}^{-1}$ .

**Table 4.10:** Computed Energy Barriers, Heats of Reaction, and High-Pressure Limiting Rate Constant Fits for the Reactions of  $\text{C}_3$ – $\text{C}_4$  alkyl radicals. Units ( $AT^n = \text{s}^{-1}$ , Energies =  $\text{kJ mol}^{-1}$ ). Fit Between 298 and 2000 K.

Reaction	$\Delta^\ddagger H_{0\text{K}}$	$\Delta_f H_{0\text{K}}$	$A$	$n$	$E_a$
$n\dot{\text{C}}_3\text{H}_7 \rightleftharpoons i\dot{\text{C}}_3\text{H}_7$	158.09	–13.86	$2.22 \times 10^{05}$	2.05	129.83
$n\dot{\text{C}}_3\text{H}_7 \leftrightarrow \text{C}_2\text{H}_4 + \dot{\text{C}}\text{H}_3$	127.91	91.40	$1.10 \times 10^{16}$	–0.72	135.31
$\dot{\text{C}}_4\text{H}_9-1 \rightleftharpoons \dot{\text{C}}_4\text{H}_9-2$	162.78	–11.15	$8.80 \times 10^{-05}$	4.82	111.84
$\dot{\text{C}}_4\text{H}_9-1 \leftrightarrow \text{C}_2\text{H}_4 + \dot{\text{C}}_2\text{H}_5$	124.29	89.93	$3.64 \times 10^{15}$	–0.58	130.33
$\dot{\text{C}}_4\text{H}_9-2 \leftrightarrow \text{C}_3\text{H}_6 + \dot{\text{C}}\text{H}_3$	129.45	93.21	$1.87 \times 10^{14}$	–0.20	134.93
$i\dot{\text{C}}_4\text{H}_9 \rightleftharpoons \dot{\text{C}}_4\text{H}_9-t$	150.21	–21.17	$8.08 \times 10^{01}$	3.03	116.48
$i\dot{\text{C}}_4\text{H}_9 \leftrightarrow \text{C}_3\text{H}_6 + \dot{\text{C}}\text{H}_3$	129.86	86.81	$1.46 \times 10^{17}$	–0.91	137.99

#### 3.3.2. Propyl ( $n\dot{\text{C}}_3\text{H}_7$ and $i\dot{\text{C}}_3\text{H}_7$ ) radicals

Once  $n\dot{\text{C}}_3\text{H}_7$  radicals are formed via internal  $\dot{\text{H}}$  atom addition to propene, they can undergo C–C  $\beta$ -scission to form ethylene and  $\dot{\text{C}}\text{H}_3$  radicals with an energy barrier of  $127.9 \text{ kJ mol}^{-1}$ , which is more favourable (by  $30.2 \text{ kJ mol}^{-1}$ ) than isomerisation to  $i\dot{\text{C}}_3\text{H}_7$  radicals. They can also undergo C–H  $\beta$ -scission, with an energy barrier of  $148.6 \text{ kJ mol}^{-1}$ . The  $i\dot{\text{C}}_3\text{H}_7$  radicals formed can undergo a  $\dot{\text{H}}$  atom elimination reaction, with an energy barrier of  $155.2 \text{ kJ mol}^{-1}$ .

### 3.3.3. Butyl ( $\dot{\text{C}}_4\text{H}_9\text{-1}$ and $\dot{\text{C}}_4\text{H}_9\text{-2}$ ) radicals

$\dot{\text{C}}_4\text{H}_9\text{-1}$  radicals are formed via internal  $\dot{\text{H}}$  atom addition to 1-butene, while terminal addition leads to the formation of  $\dot{\text{C}}_4\text{H}_9\text{-2}$  radicals.  $\dot{\text{C}}_4\text{H}_9\text{-2}$  radicals are also formed through internal  $\dot{\text{H}}$  atom addition to 2-butene. C–C  $\beta$ -scission of  $\dot{\text{C}}_4\text{H}_9\text{-1}$  radicals can occur forming ethylene and  $\dot{\text{C}}_2\text{H}_5$  radicals, with a barrier height of 124.3 kJ mol<sup>-1</sup>, which is more favourable (by 33.5 kJ mol<sup>-1</sup>) than isomerisation to  $\dot{\text{C}}_4\text{H}_9\text{-2}$  radicals. Additionally, C–H  $\beta$ -scission of  $\dot{\text{C}}_4\text{H}_9\text{-1}$  radicals can occur with a barrier height of 152.5 kJ mol<sup>-1</sup>. Two transition states are available for the reaction  $\dot{\text{C}}_4\text{H}_9\text{-1} \rightleftharpoons \dot{\text{C}}_4\text{H}_9\text{-2}$ , one occurring through a 3-membered ring and the second one occurring through a 4-membered ring, with barrier heights of 160.6 and 162.8 kJ mol<sup>-1</sup>, respectively. C–C  $\beta$ -scission of  $\dot{\text{C}}_4\text{H}_9\text{-2}$  can also occur, forming propene and a  $\dot{\text{C}}\text{H}_3$  radical, with an energy barrier of 129.45 kJ mol<sup>-1</sup>, while C–H  $\beta$ -scission of  $\dot{\text{C}}_4\text{H}_9\text{-2}$  has a barrier height of 148.6 kJ mol<sup>-1</sup>.

### 3.3.4. Branched butyl ( $i\dot{\text{C}}_4\text{H}_9$ and $t\dot{\text{C}}_4\text{H}_9$ ) radicals

Internal  $\dot{\text{H}}$  atom addition to isobutene forms  $i\dot{\text{C}}_4\text{H}_9$  radicals, while terminal addition forms  $t\dot{\text{C}}_4\text{H}_9$  radicals. C–H  $\beta$ -scission of  $i\dot{\text{C}}_4\text{H}_9$  radicals can occur, with a barrier height of 145.6 kJ mol<sup>-1</sup>. However, C–C  $\beta$ -scission of  $i\dot{\text{C}}_4\text{H}_9$  radicals, forming propene and  $\dot{\text{C}}\text{H}_3$  radicals is more favoured, with a reaction barrier of 129.9 kJ mol<sup>-1</sup>. Isomerisation of  $i\dot{\text{C}}_4\text{H}_9$  to  $t\dot{\text{C}}_4\text{H}_9$  occurs with a higher energy barrier of 150.2 kJ mol<sup>-1</sup>. C–H  $\beta$ -scission of  $t\dot{\text{C}}_4\text{H}_9$  can occur, with a barrier height of 151.7 kJ mol<sup>-1</sup>.

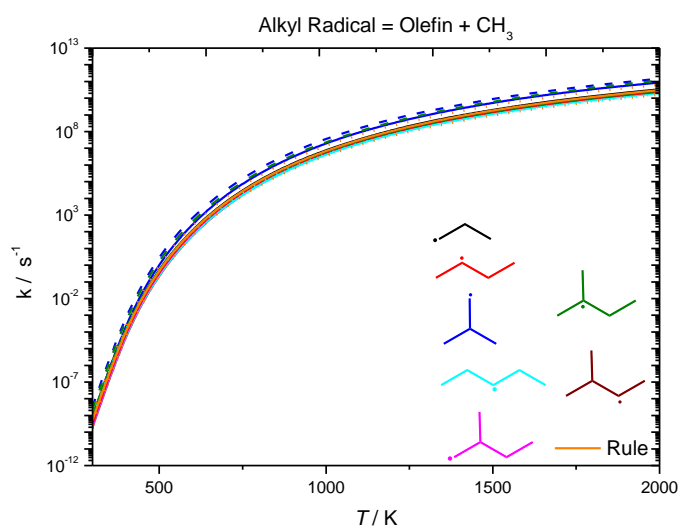


**Figure 4.16.** High-pressure limiting rate constants for alkyl radical decomposition, forming (a) olefin +  $\dot{\text{C}}\text{H}_3$ . Solid (current work), dashed (Curran), dotted (Awan) and short-dotted (Comandini).

Figure 4.16 presents high-pressure limiting rate constants for alkyl radical decomposition reactions forming an olefin +  $\dot{\text{C}}\text{H}_3$ . For comparison, rate constants for alkyl radical decomposition from our previous work on  $\text{C}_5$  alkenes in addition to other literature sources [4, 58, 60-62] are plotted. The rate constant for the reaction  $i\dot{\text{C}}_4\text{H}_9 \leftrightarrow \text{C}_3\text{H}_6 + \dot{\text{C}}\text{H}_3$  recommended by Curran [58] is a factor of 2.74 – 1.67 times faster than that calculated in this work in the temperature range 500 – 2000 K. With the exception of this reaction, all other rate constants calculated in this work for alkyl radicals leading to the formation of an olefin and a  $\dot{\text{C}}\text{H}_3$  radical are within a factor of 1.55 of our computed rate constant for  $n\dot{\text{C}}_3\text{H}_7 \leftrightarrow \text{C}_2\text{H}_4 + \dot{\text{C}}\text{H}_3$  over the temperature range 298 – 2000 K. The rate constant calculated in this work for  $i\dot{\text{C}}_4\text{H}_9 \leftrightarrow \text{C}_3\text{H}_6 + \dot{\text{C}}\text{H}_3$  is a factor of 2.54 – 3.08 times faster than  $n\dot{\text{C}}_3\text{H}_7 \leftrightarrow \text{C}_2\text{H}_4 + \dot{\text{C}}\text{H}_3$ . This may be due to the fact that  $i\dot{\text{C}}_4\text{H}_9$  radicals have three degenerate sites for C–C  $\beta$ -scission to take place.

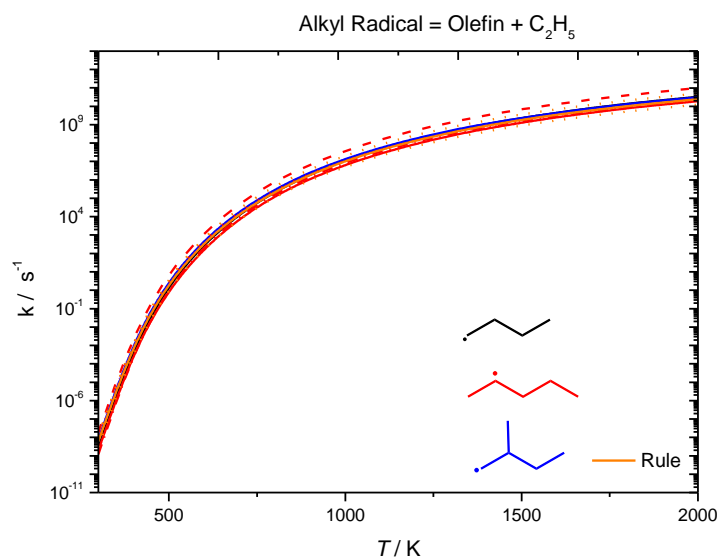


**Figure 4.17.** High-pressure limiting rate constants for alkyl radical decomposition, forming an olefin +  $\dot{\text{C}}_2\text{H}_5$ . Solid (current work), dashed (Curran), dotted (Awan), short-dotted (Comandini), and dashed-dotted (Jitariu).

Reasonable agreement is observed for the reactions of alkyl radicals forming an olefin and  $\dot{\text{C}}_2\text{H}_5$  radicals calculated previously and in this work. In Fig.4.17, the rate constant recommendation by Curran [58] for the reaction  $\dot{\text{C}}_5\text{H}_{11-2} \leftrightarrow \text{C}_3\text{H}_6 + \dot{\text{C}}_2\text{H}_5$  is the fastest in comparison to the other analogous reactions. The Curran recommendation [58] is a factor of ~9.5 – 5.0 times faster than our calculated rate constant for  $\dot{\text{C}}_5\text{H}_{11-2} \leftrightarrow \text{C}_3\text{H}_6 + \dot{\text{C}}_2\text{H}_5$  calculated previously over the temperature range 300 – 2000 K [4]. The value from Awan and



Comandini [60, 61] is a factor of  $\sim 3.4$  times faster than our previous work [4] for the same reaction at 500 K, with the rate constants converging at higher temperatures. Jitariu et al. [62] are in excellent agreement with our previous work for the reaction  $\dot{C}_5H_{11-2} \leftrightarrow C_3H_6 + \dot{C}_2H_5$  [4], with the rate constants being within a factor of  $\sim 1.3$ . The rate constant for the reaction  $a\dot{C}_5H_{11} \leftrightarrow C_3H_6 + \dot{C}_2H_5$  calculated in our most recent study [5] is a factor of  $\sim 3$  times faster at 500 K than our calculated rate constant for  $\dot{C}_5H_{11-2} \leftrightarrow C_3H_6 + \dot{C}_2H_5$  [4]. An energy barrier difference of  $1.9 \text{ kJ mol}^{-1}$  accounts for a factor of 1.6 of this difference. For the decomposition of an alkyl radical forming an olefin and an ethyl radical, an average of the rate constants calculated in our current and previous studies [4, 5] as well as those by Awan, Comandini and Jitariu [4, 58, 60-62] is taken, with a factor of two of the recommended represented as orange dotted lines.

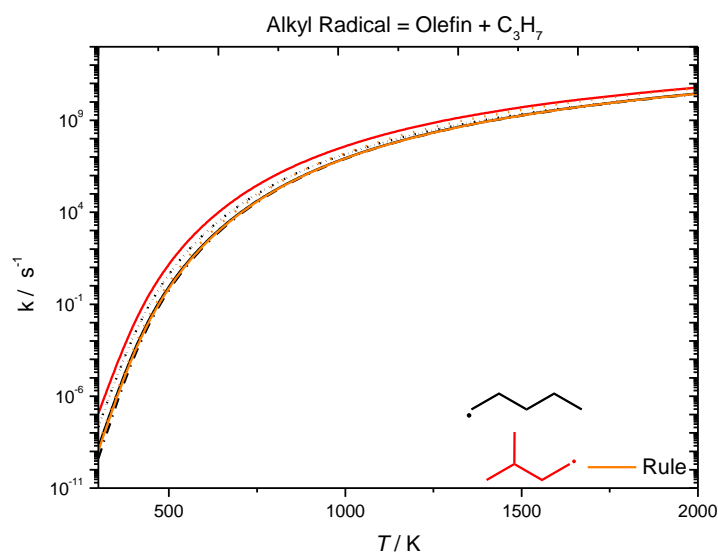


**Figure 4.18.** High-pressure limiting rate constants for alkyl radical decomposition, forming an olefin +  $\dot{C}_3H_7$ . Solid (current work), dotted (Awan), short-dotted (Comandini), and dashed-dotted (Jitariu).

Figure 4.18 presents rate constant comparisons for alkyl radical decomposition forming an olefin and propyl radicals. The reactions  $\dot{C}_5H_{11-1} \leftrightarrow C_2H_4 + n\dot{C}_3H_7$  and  $d\dot{C}_5H_{11} \leftrightarrow C_2H_4 + i\dot{C}_3H_7$  are plotted for comparison. The rate constants for the reaction  $\dot{C}_5H_{11-1} \leftrightarrow C_2H_4 + n\dot{C}_3H_7$  by Awan [60], Comandini [61] and Jitariu et al. [62] are in good agreement with our previously calculated rate constant [4]. At 500 K, the values from Awan [60] and Comandini [61] are a factor of  $\sim 4.5$  times faster than our calculated rate constant for this reaction at 500 K, with the rate constants converging at high temperatures. The difference of  $7.76 \text{ kJ mol}^{-1}$  in

the energy barrier accounts for the observed difference. Larger differences are observed between the values calculated in this work and by Awan and Comandini at temperatures below 500 K, therefore the recommended rate constant for  $\dot{C}_5H_{11-1} \leftrightarrow C_2H_4 + n\dot{C}_3H_7$  is taken as an average of the rate calculated in the current work and by Jitariu et al. [62]. The rate constant by Jitariu et al. is in excellent agreement with our calculated rate constant for the same reaction [4]. Our calculated rate constant for  $d\dot{C}_5H_{11} \leftrightarrow C_2H_4 + i\dot{C}_3H_7$  is also plotted in this graph, which is taken as the recommended rate constant for alkyl radical decomposition forming an olefin and an  $i\dot{C}_3H_7$  radical.

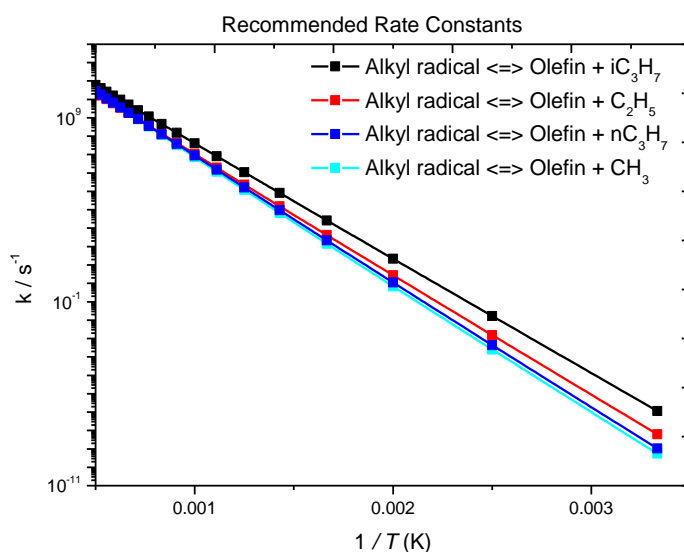


**Figure 4.19.** Rate constant recommendations for alkyl radical decomposition to olefin + radical.

**Table 4.11:** Recommended Rate Constants for Alkyl Radical Decomposition Forming an Olefin + Radical. ( $AT^n = s^{-1}$ , Energies =  $cal\ mol^{-1}$ ). Fit between 300 K and 2000 K.

Class	$A$	$n$	$E_a$	Uncertainty Bounds (Upper, Lower)
alkyl radical $\leftrightarrow$ olefin + $\dot{C}H_3$	$2.54 \times 10^{10}$	1.04	30573.	2.86, 3.71
alkyl radical $\leftrightarrow$ olefin + $\dot{C}_2H_5$	$5.20 \times 10^{11}$	0.57	29308.	1.34, 3.11
alkyl radical $\leftrightarrow$ olefin + $n\dot{C}_3H_7$	$9.62 \times 10^{11}$	0.55	30678.	1.61, 2.60
alkyl radical $\leftrightarrow$ olefin + $i\dot{C}_3H_7$	$6.87 \times 10^{12}$	0.31	28225.	—

#### 4. Detailed kinetic modelling

All simulations were performed using Chemkin-Pro assuming a constant volume homogeneous batch reactor. As described in our previous study of the pentene isomers [5], test computations implied that the high-pressure limiting rate constant for external H atom

addition to 2M1B was over-estimated by a factor of 2 – 3, which is also in line with the variational effect observed by Jasper and Hansen [63] for  $\dot{\text{H}}$  atom addition to large molecular weight species. To assess the influence of variational effects on predictions of experimental data, indicative simulations are carried out by systematically reducing the rate constants for  $\dot{\text{H}}$  atom addition by a factor of two in the RRKM/ME model and re-computing  $k(T,p)$ . The NUIGMech1.2 model includes our computed rate constants and thermochemistry from our previous studies on the pentene isomers [4, 5] and the approximate variational effect results of the current work. This model was then used to simulate the recent results from a pyrolysis study of 1-alkenes using the NUIG single pulse shock-tube [32] and is represented by solid lines. Dashed lines represent model predictions of NUIGMech1.1. Improvements in species mole fractions are observed, particularly for 2-butene and isobutene pyrolysis. The supporting information contains PLOG fits for both the approximate variational results and the original unadjusted results.

#### 4.1. Ethylene pyrolysis

Figure 4.20 presents species profiles for ethylene pyrolysis at 2 bar [32]. The reaction path analysis was already described by Nagaraja et al. [32] so we shall be brief here. H-atom abstraction by  $\dot{\text{H}}$  atoms from ethylene leads to the production of vinyl radicals, with vinyl radicals decomposing to acetylene +  $\dot{\text{H}}$ . Through the incorporation of the rate constants calculated in this work (NUIGMech1.2), there is a slight improvement in the species profiles for both ethylene and acetylene. The rate constant for H-atom abstraction from ethylene is approximately a factor of two slower, which reduces the amount of vinyl radical produced, which in turn decreases the production of acetylene and  $\dot{\text{H}}$  atoms.

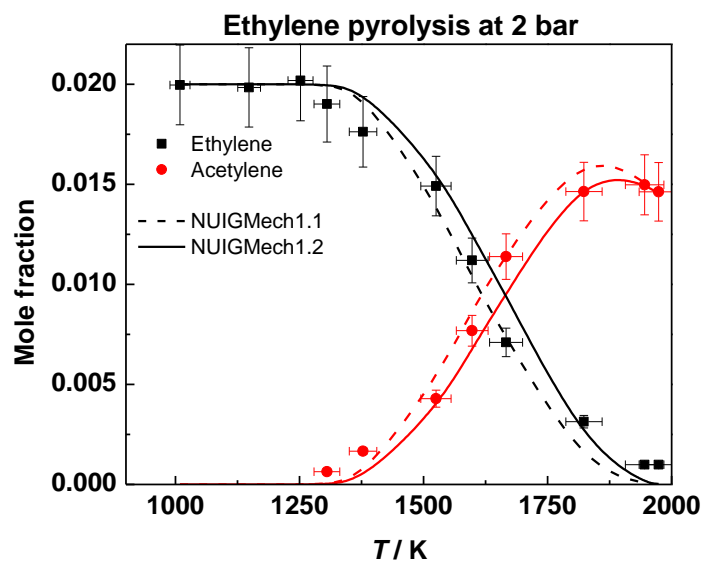


**Figure 4.20.** Species profiles for ethylene pyrolysis at 2 bar. Dashed lines represent NUIGMech1.1 and solid lines represent NUIGMech1.2.

#### 4.2. Propene pyrolysis

Figure 4.21 presents species profiles for propene pyrolysis at 2 bar [32]. Both  $\dot{H}$  atom addition and abstraction reactions are the main consumption pathways for propene.  $\dot{H}$  atom addition to propene and the subsequent decomposition of propyl radical, leads to the formation of ethylene and a methyl radical. Abstraction of an allylic H-atom by  $\dot{H}$  atoms or  $\dot{C}H_3$  radicals leads to the formation of allyl and  $H_2$  and  $CH_4$ . Allyl radicals are converted to allene, which subsequently isomerises to propyne or undergoes H-atom abstraction to form propargyl radicals, which in turn produces benzene. Acetylene is formed by the decomposition of vinyl radicals, the reaction of  $\dot{H}$  atoms with allene and propyne, and the  $\beta$ -scission of propen-1-yl radical.

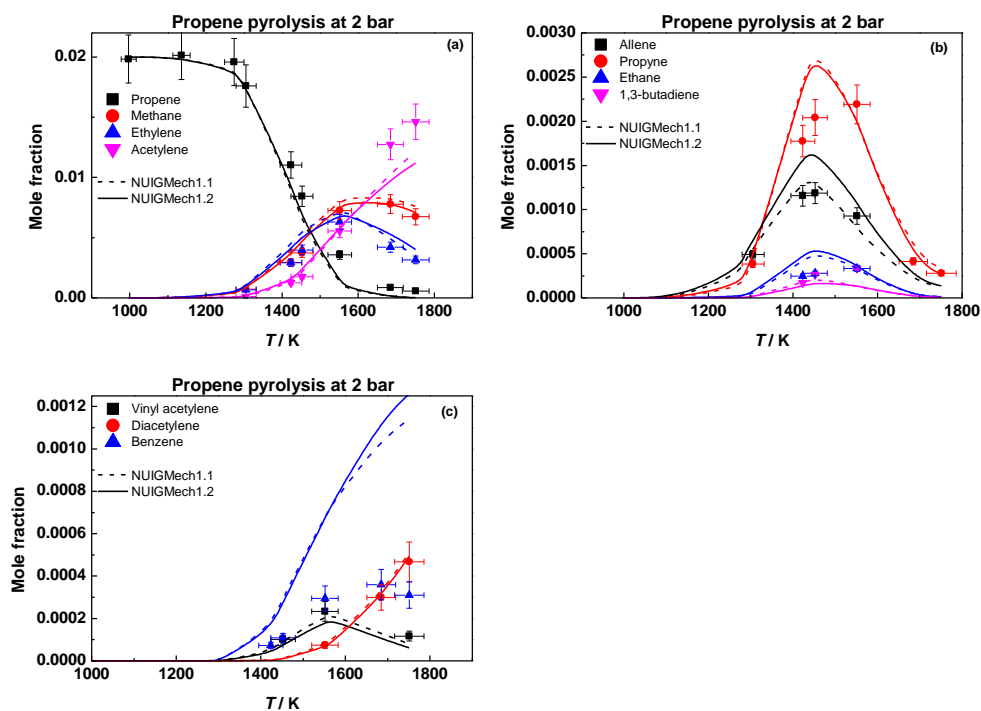


**Figure 4.21.** Species profiles for propene pyrolysis at 2 bar. Dashed lines represent NUIGMech1.1 and solid lines represent NUIGMech1.2.

### 4.3. 1-Butene pyrolysis

Figure 4.22 presents species profiles for 1-butene pyrolysis at 2 bar [32]. The pyrolysis chemistry is quite similar to that of propene, with both  $\dot{H}$  atom addition and abstraction reactions being important pathways.  $\dot{H}$  atom addition to 1-butene produces propene and a  $\dot{C}H_3$  radical and ethylene and a  $\dot{C}_2H_5$  radical via two chemically activated pathways. Ethyl radicals decompose to ethylene +  $\dot{H}$ . Hydrogen atom abstraction by  $\dot{H}$  or  $\dot{C}H_3$  leads to the formation of  $\dot{C}_4H_7$ 1-3, which in turn forms 1,3-butadiene. Methane is formed primarily by H-atom abstraction by  $\dot{C}H_3$  radicals from the fuel and other stable species. Acetylene is mainly produced by the decomposition of vinyl radicals and the reactions of  $\dot{H}$  atoms with allene and propyne.

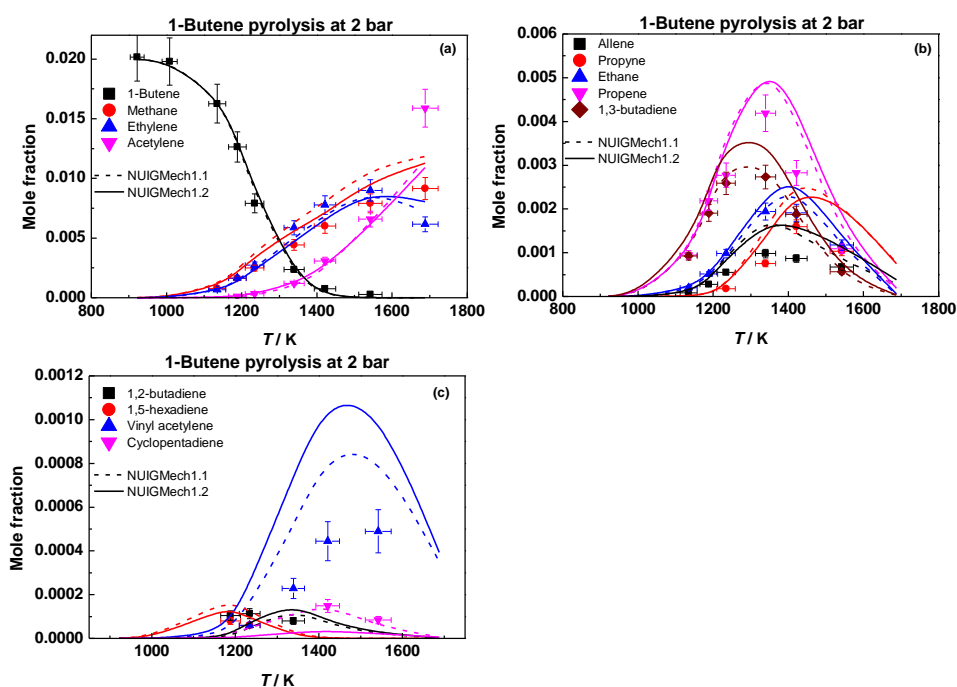


**Figure 4.22.** Species profiles for 1-butene pyrolysis at 2 bar. Dashed lines represent NUIGMech1.1 and solid lines represent NUIGMech1.2

#### 4.4. Trans 2-butene pyrolysis

Figure 4.23 presents species profiles for 2-butene pyrolysis at 2 bar [32]. Again, the pyrolysis chemistry is quite similar to that of propene and 1-butene.  $\dot{H}$  atom addition to 2-butene forms propene and  $\dot{C}H_3$  radicals through a chemically activated pathway. H-atom abstraction by  $\dot{H}$  or  $\dot{C}H_3$  leads to the formation of  $\dot{C}_4H_7$ 1-3, which in turn forms 1,3-butadiene. The rate constant for H-atom abstraction from 2-butene forming  $\dot{C}_4H_7$ 1-3 calculated in this work is a factor of 2.5 times slower than that used in NUIGMech1.1, which in turn reduces the species mole fraction of 1,3-butadiene. For the propene species profiles, there is an improvement in the predictions through the incorporation of the calculations computed in the current work. The production of propene, as previously stated comes from the chemically activated pathway of  $\dot{H}$  atom addition to 2-butene. The rate constants in NUIGMech1.1 are based on QRRK/MSM estimates and are approximately a factor of ~seven times faster than those in NUIGMech1.2 at 1400 K. Again, methane is mainly produced by H-atom abstraction by  $\dot{C}H_3$  from the fuel and other stable species. Acetylene is mainly produced by the decomposition of vinyl radicals and the reactions of  $\dot{H}$  atoms with allene and propyne.

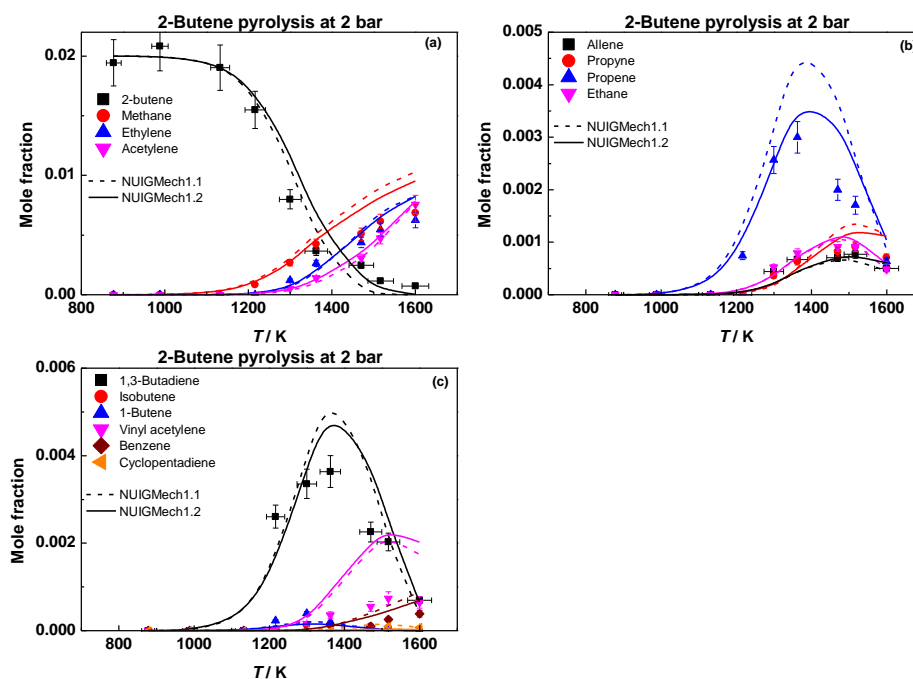


**Figure 4.23.** Species profiles for 2-butene pyrolysis at 2 bar. Dashed lines represent NUIGMech1.1 and solid lines represent NUIGMech1.2.

#### 4.5. Isobutene pyrolysis

Figure 4.24 presents species profiles for isobutene pyrolysis at 2 bar [32]. H-atom abstraction from isobutene leads to the formation of  $i\dot{C}_4H_7$  radicals, which decompose to produce allene and  $\dot{C}H_3$  radicals. The resulting allene then isomerises to propyne. Propene is primarily formed through the chemically activated pathway of  $\dot{H}$  atom reaction to isobutene. There is an improvement in the propene predictions with the current model, due to the rate constant for the chemically activated pathway of  $\dot{H}$  atom addition to isobutene being approximately a factor of seven times slower at 1400 K.

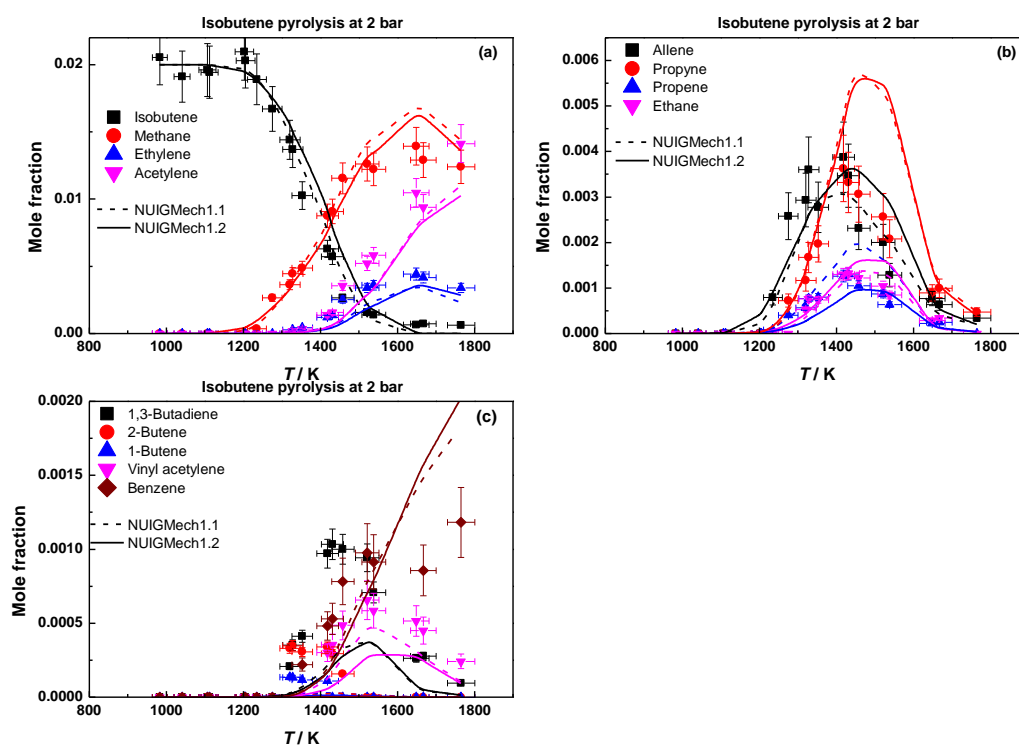


**Figure 4.24.** Species profiles for isobutene pyrolysis at 2 bar. Dashed lines represent NUIGMech1.1 and solid lines represent NUIGMech1.2.

## 5. Chemically activated pathways

### 5.1. Effect of pressure

From the simulations, it is observed that the chemically activated pathways for the reaction of  $\dot{\text{H}}$  atoms with alkenes are important in capturing the species profiles of the products during pyrolysis and oxidation. Taking propene as an example, which is described in Figure 4.4 above, the formation of stabilised  $i\dot{\text{C}}_3\text{H}_7$  radicals through the reaction of  $\dot{\text{H}}$  atoms with propene dominates at temperatures up to 800, 1000, 1200, and 1500 at pressures of 0.1, 1, 10, and 100 atm respectively. The chemically activated pathway  $\text{C}_3\text{H}_6 + \dot{\text{H}} \leftrightarrow [n\dot{\text{C}}_3\text{H}_7]^* \leftrightarrow \text{C}_2\text{H}_4 + \dot{\text{C}}\text{H}_3$  then dominates the reaction flux at higher temperatures. At 1000 atm, the formation of stabilised  $i\dot{\text{C}}_3\text{H}_7$  radicals dominates over the entire temperature range.

At 1000 K and 0.1 atm, 70% of the reaction flux goes through this chemically activated pathway for  $\text{C}_3\text{H}_6 + \dot{\text{H}}$ . However, as the pressure increases, this percentage reduces, and the stabilisation reaction channel becomes more favourable. The percentage reaction flux going through this chemically activated pathway is 41%, 20%, 7% and 2% for pressures of 1, 10, 100, and 1000 atm respectively. It is therefore important to have accurate rate constants for



the chemically activated pathways on these potential energy surfaces in order to predict the species mole fractions across a wide range of temperatures and pressures.

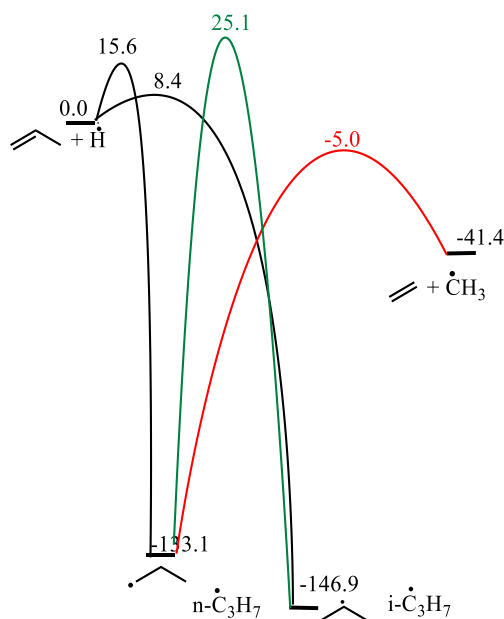


**Figure 4.25.** Potential energy surface for  $\dot{\text{H}}$  atom addition reactions of propene. Energies in  $\text{kJ mol}^{-1}$ .

Below is a list of some of the chemically activated pathways forming some of the major products of pyrolysis calculated in the current study and in previous ones [4,5].

- $\text{C}_3\text{H}_6 + \dot{\text{H}} \leftrightarrow [\text{n}\dot{\text{C}}_3\text{H}_7]^* \leftrightarrow \text{C}_2\text{H}_4 + \dot{\text{C}}\text{H}_3$
- $\text{C}_4\text{H}_8\text{-1} + \dot{\text{H}} \leftrightarrow [\dot{\text{C}}_4\text{H}_9\text{-1}]^* \leftrightarrow \text{C}_2\text{H}_4 + \dot{\text{C}}_2\text{H}_5$
- $\text{C}_4\text{H}_8\text{-1} + \dot{\text{H}} \leftrightarrow [\dot{\text{C}}_4\text{H}_9\text{-2}]^* \leftrightarrow \text{C}_3\text{H}_6 + \dot{\text{C}}\text{H}_3$
- $\text{C}_4\text{H}_8\text{-2} + \dot{\text{H}} \leftrightarrow [\dot{\text{C}}_4\text{H}_9\text{-2}]^* \leftrightarrow \text{C}_3\text{H}_6 + \dot{\text{C}}\text{H}_3$
- $\text{iC}_4\text{H}_8 + \dot{\text{H}} \leftrightarrow [\text{i}\dot{\text{C}}_4\text{H}_9]^* \leftrightarrow \text{C}_3\text{H}_6 + \dot{\text{C}}\text{H}_3$

Moreover, chemically activated pathways were also found to be important for the reactions of  $\dot{\text{H}}$  with the pentene isomers in our previous studies [4,5].

- $\text{C}_5\text{H}_{10}\text{-1} + \dot{\text{H}} \leftrightarrow [\dot{\text{C}}_5\text{H}_{11}\text{-1}]^* \leftrightarrow \text{C}_2\text{H}_4 + \text{n-}\dot{\text{C}}_3\text{H}_7$
- $\text{C}_5\text{H}_{10}\text{-1} + \dot{\text{H}} \leftrightarrow [\dot{\text{C}}_5\text{H}_{11}\text{-2}]^* \leftrightarrow \text{C}_3\text{H}_6 + \dot{\text{C}}_2\text{H}_5$
- $\text{C}_5\text{H}_{10}\text{-2} + \dot{\text{H}} \leftrightarrow [\dot{\text{C}}_5\text{H}_{11}\text{-2}]^* \leftrightarrow \text{C}_3\text{H}_6 + \dot{\text{C}}_2\text{H}_5$
- $\text{C}_5\text{H}_{10}\text{-2} + \dot{\text{H}} \leftrightarrow [\dot{\text{C}}_5\text{H}_{11}\text{-3}]^* \leftrightarrow \text{C}_4\text{H}_8\text{-1} + \dot{\text{C}}\text{H}_3$
- $\text{aC}_5\text{H}_{10} + \dot{\text{H}} \leftrightarrow [\text{a}\dot{\text{C}}_5\text{H}_{11}]^* \leftrightarrow \text{C}_3\text{H}_6 + \dot{\text{C}}_2\text{H}_5$
- $\text{aC}_5\text{H}_{10} + \dot{\text{H}} \leftrightarrow [\text{a}\dot{\text{C}}_5\text{H}_{11}]^* \leftrightarrow \text{C}_4\text{H}_8\text{-1} + \dot{\text{C}}\text{H}_3$
- $\text{aC}_5\text{H}_{10} + \dot{\text{H}} \leftrightarrow [\text{b}\dot{\text{C}}_5\text{H}_{11}]^* \leftrightarrow \text{iC}_4\text{H}_8 + \dot{\text{C}}\text{H}_3$
- $\text{bC}_5\text{H}_{10} + \dot{\text{H}} \leftrightarrow [\text{b}\dot{\text{C}}_5\text{H}_{11}]^* \leftrightarrow \text{iC}_4\text{H}_8 + \dot{\text{C}}\text{H}_3$
- $\text{bC}_5\text{H}_{10} + \dot{\text{H}} \leftrightarrow [\text{c}\dot{\text{C}}_5\text{H}_{11}]^* \leftrightarrow \text{C}_4\text{H}_8\text{-2} + \dot{\text{C}}\text{H}_3$
- $\text{cC}_5\text{H}_{10} + \dot{\text{H}} \leftrightarrow [\text{c}\dot{\text{C}}_5\text{H}_{11}]^* \leftrightarrow \text{C}_4\text{H}_8\text{-2} + \dot{\text{C}}\text{H}_3$



## 5.2. Effect of molecular size

As the size of the molecule increases from propene to 1-butene, the effect of chemical activation becomes greater, especially at lower pressures. At 1000 K and 0.1 atm, for 1-butene 99% of the reaction flux proceeds through the chemically activated pathways compared to 70% for propene.

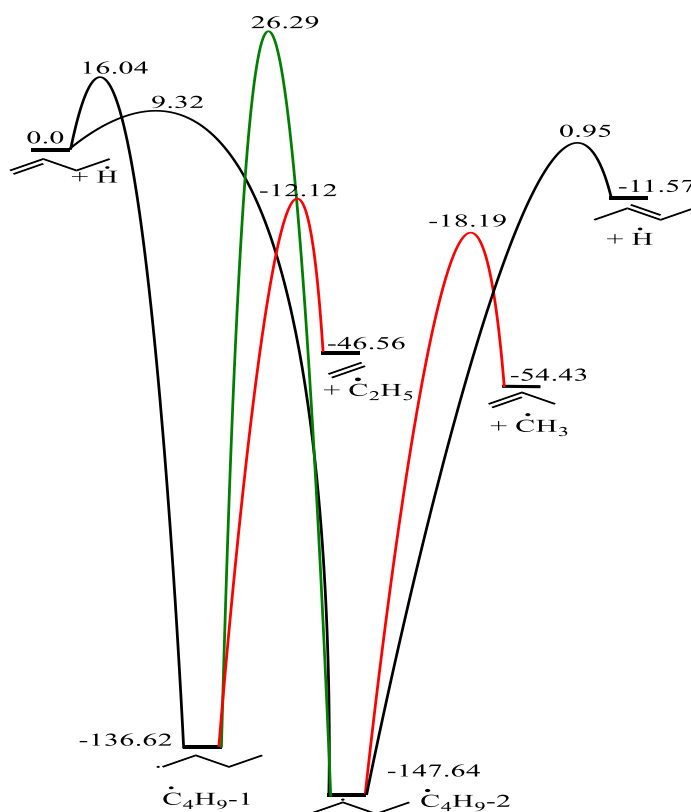


**Figure 4.26.** Potential energy surface for  $\dot{\text{H}}$ -atom addition reactions of 1- and 2-butene. Energies in  $\text{kJ mol}^{-1}$ .

For the pentene isomers, it was shown that  $> 95\%$  of the reaction flux proceeds through the chemically activated pathways at 1000 K and 0.1 atm [4,5], which is similar to butene. As the pressure increases, this percentage reduces to 93%, 65%, 25% and 4% at pressures of 1, 10, 100, and 1000 atm, respectively for 1-butene, compared to 41%, 20%, 7% and 2% for propene. The formation of stabilised  $\dot{\text{C}}_4\text{H}_9-2$  radicals through the reaction of  $\dot{\text{H}}$  atoms with 1-butene then dominates, which can be seen in Figure 4.6(a). A similar situation prevails for 2-butene, Figure 4.6(b) where 98%, 87%, 57%, 20% and 3% proceeds through chemical activation at 0.1, 1, 10, 100 and 1000 atm. In the case of isobutene, 33% of the reaction flux goes through the chemically activated pathways at 1000 K and 0.1 atm, with the formation of

stabilised  $t\dot{C}_4H_9$  radicals then dominating the reaction flux. It is not until a temperature of 1200 K is reached that chemical activation is considerable, accounting for 74% at 0.1 atm, Figure 4.6(c). It is observed that the effect of chemical activation becomes greater as the molecular size increases from propene to butene. However, as the molecular size increases from butene to pentene the effect of chemical activation is similar.

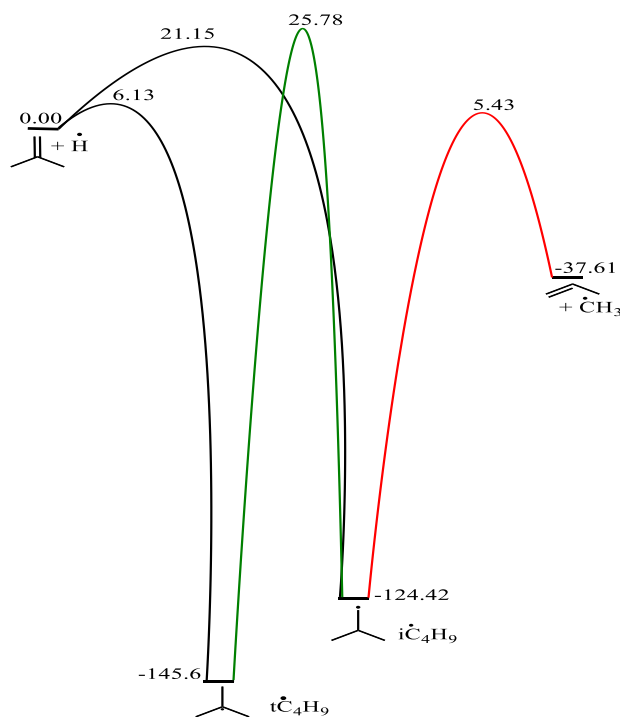


**Figure 4.27.** Potential energy surface for  $\dot{H}$ -atom addition reactions of isobutene. Energies in  $\text{kJ mol}^{-1}$ .

## 6. Conclusions

To contribute to the development of combustion models, a hierarchical set of rate constants for the reactions of  $\dot{H}$  atom with  $C_2 - C_5$  alkenes, and the subsequent C–C and C–H  $\beta$ -scission and  $\dot{H}$  atom transfer reactions using the same level of theory now exist. The reactions for the linear and branched  $C_5$  alkenes were performed in our previous studies, while calculations for  $C_2 - C_4$  species are performed in the current work. Thermochemical data are calculated as a function of temperature, with enthalpies of formation determined from an isodesmic network, which is built upon benchmark literature data and electronic structure calculations. High-pressure limiting and temperature- and pressure-dependent rate constants are calculated using RRKM theory with a 1-D master equation (ME) analysis. Rate constant recommendations for  $\dot{H}$  atom addition/abstraction and alkyl radical decomposition

are proposed and serve as a useful tool in mechanisms for larger alkenes for which calculations do not exist.

As mentioned in our earlier work [5], test computations implied that the high-pressure limiting rate constant for  $\dot{H}$  atom addition were over-estimated by a factor of 2 – 3, which is also in line with the variational effect observed by others for  $\dot{H}$  atom addition reactions to large molecular weight species [63]. To determine the influence of variational effects on model predictions, indicative simulations are carried out by systematically reducing the rate constants for  $\dot{H}$  atom addition by a factor of two in the RRKM/ME model and re-computing  $k(T,p)$ . Similarly to our earlier work [5], it is found that the chemically activated pathways for  $\dot{H}$  atom addition to alkenes, as well as their abstraction reactions, are found to be important in capturing the species profiles of the products from pyrolysis. Although good agreement is observed between our model predictions and experiment, future work should consider to address VTST, the treatment of multi-dimensional torsions, and an-harmonic effects with the aim of developing a more comprehensive RRKM/ME model for combustion modelling.

### **Supporting Information**

MESS input and output files, thermochemical values in NASA polynomial format and Chemkin format PLOG rate constant fits are provided in the supporting information.

### **Acknowledgements**

The authors acknowledge the support of Science Foundation Ireland in funding this project under Grant 15/IA/3177 and also to the Irish Centre for High-End Computing, ICHEC, under project numbers ngche058c and ngche080c.

## References

- [1] S.M. Burke, W. Metcalfe, O. Herbinet, F. Battin-Leclerc, F.M. Haas, J. Santner, F.L. Dryer, H.J. Curran, An experimental and modeling study of propene oxidation. Part 1: speciation measurements in jet-stirred and flow reactors, *Combust. Flame* 161 (2014) 2765-2784.
- [2] Y. Li, C.-W. Zhou, K.P. Somers, K. Zhang, H.J. Curran, The oxidation of 2-butene: a high pressure ignition delay, kinetic modeling study and reactivity comparison with isobutene and 1-butene, *Proc. Combust. Inst.* 36 (2017) 403-411.
- [3] C.-W. Zhou, Y. Li, E. O'Connor, K.P. Somers, S. Thion, C. Keesee, O. Mathieu, E.L. Petersen, T.A. DeVerter, M.A. Oehlschlaeger, et al, A comprehensive experimental and modeling study of isobutene oxidation, *Combust. Flame* 167 (2016) 353-379.
- [4] J. Power, K.P. Somers, C.-W. Zhou, S. Peukert, H.J. Curran, Theoretical, experimental, and modeling study of the reaction of hydrogen atoms with 1- and 2-pentene, *J. Phys. Chem. A* 123 (2019) 8506-8526.
- [5] J. Power, K.P. Somers, S.S. Nagaraja, W. Wyrebak, H.J. Curran, Theoretical study of the reaction of hydrogen atoms with three pentene isomers: 2-methyl-1-butene, 2-methyl-2-butene, and 3-methyl-1-butene, *J. Phys. Chem. A* 124 (2020) 10649-10666.
- [6] J.R. Barker, D.G. Keil, J. Michael, D.T. Osborne, Reaction  $H + C_2H_4$ : Comparison of three experimental techniques, *J. Chem. Phys.* 52 (1970) 2079-2088.
- [7] Y. Feng, J. Niiranen, A. Bencsura, V. Knyazev, D. Gutman, W. Tsang, Weak collision effects in the reaction  $C_2H_5 \rightleftharpoons C_2H_4 + H$ , *J. Phys. Chem. A* 97 (1993) 871-880.
- [8] M. Hanning-Lee, N.B. Green, M. Pilling, S. Robertson, Direct observation of equilibration in the system  $H + C_2H_4 \rightleftharpoons C_2H_5$ : standard enthalpy of formation of the ethyl radical, *J. Phys. Chem.* 97 (1993) 860-870.
- [9] J. Lee, J. Michael, W. Payne, L. Stief, Absolute rate of the reaction of atomic hydrogen with ethylene from 198 to 320 K at high pressure, *J. Chem. Phys.* 68 (1978) 1817-1820.
- [10] P.D. Lightfoot, M.J. Pilling, Temperature and pressure dependence of the rate constant for the addition of hydrogen atoms to ethylene, *J. Phys. Chem.* 91 (1987) 3373-3379.
- [11] L.A. Mertens, I.A. Awan, D.A. Sheen, J.A. Manion, Evaluated site-specific rate constants for reaction of isobutane with H and  $CH_3$ : shock tube experiments combined with bayesian model optimization, *J. Phys. Chem. A* 122 (2018) 9518-9541.
- [12] J. Michael, D. Osborne, G. Suess, Reaction  $H + C_2H_4$ : Investigation into the effects of pressure, stoichiometry, and the nature of the third body species, *J. Chem. Phys.* 58 (1973) 2800-2806.
- [13] P.D. Pacey, J.H. Wimalasena, Kinetics and thermochemistry of the ethyl radical. The induction period in the pyrolysis of ethane, *J. Phys. Chem.* 88 (1984) 5657-5660.
- [14] K.-I. Sugawara, K. Okazaki, S. Sato, Temperature dependence of the rate constants of H and D-atom additions to  $C_2H_4$ ,  $C_2H_3D$ ,  $C_2D_4$ ,  $C_2H_2$ , and  $C_2D_2$ , *Bulletin of the Chemical Society of Japan* 54 (1981) 2872-2877.
- [15] X. Yang, R.S. Tranter, High-temperature dissociation of ethyl radicals and ethyl iodide, *Int. J. Chem. Kinet.* 44 (2012) 433-443.
- [16] A. Matsugi, Roaming Dissociation of Ethyl Radicals, *J. Phys. Chem. Lett.* 4 (2013) 4237-4240.
- [17] J.A. Miller, S.J. Klippenstein, The  $H + C_2H_2 (+M) \rightleftharpoons C_2H_3 (+M)$  and  $H + C_2H_4 (+M) \rightleftharpoons C_2H_5 (+M)$  reactions: Electronic structure, variational transition-state theory, and solutions to a two-dimensional master equation, *Phys. Chem. Chem. Phys.* 6 (2004) 1192-1202.
- [18] J.A. Miller, S.J. Klippenstein, Dissociation of propyl radicals and other reactions on a  $C_3H_7$  potential, *J. Phys. Chem. A* 117 (2013) 2718-2727.

- [19] J.A. Manion, I.A. Awan, Evaluated kinetics of terminal and non-terminal addition of hydrogen atoms to 1-alkenes: a shock tube study of H+ 1-butene, *J.Phys.Chem.A* 119 (2015) 429-441.
- [20] W.Y. Chen, T.N. Nguyen, M.C. Lin, N.S. Wang, H. Matsui, Experimental and theoretical studies on the reaction of H atom with C<sub>3</sub>H<sub>6</sub>, *Int. J. Chem. Kinet.*, (2020).
- [21] T. Gilbert, T.L. Grebner, I. Fischer, P. Chen, Microcanonical rates for the unimolecular dissociation of the ethyl radical, *J.Chem.Phys* 110 (1999) 5485-5488.
- [22] M. Steinbauer, J. Giegerich, K.H. Fischer, I. Fischer, The photodissociation dynamics of the ethyl radical, C<sub>2</sub>H<sub>5</sub>, investigated by velocity map imaging, *J.Chem.Phys* 137 (2012) 014303.
- [23] P. Seakins, S. Robertson, M. Pilling, I. Slagle, G. Gmurczyk, A. Bencsura, D. Gutman, W. Tsang, Kinetics of the unimolecular decomposition of isopropyl: weak collision effects in helium, argon, and nitrogen, *J.Phys.Chem* 97 (1993) 4450-4458.
- [24] J.A. Kerr, M.J. Parsonage, Evaluated kinetic data on gas phase addition reactions. Reactions of atoms and radicals with alkenes, alkynes and aromatic compounds, 1972.
- [25] J. Munk, P. Pagsberg, E. Ratajczak, A. Sillesen, Spectrokinetic studies of i-C<sub>3</sub>H<sub>7</sub> and i-C<sub>3</sub>H<sub>7</sub>O<sub>2</sub> radicals, *Chem. Phys. Lett* 132 (1986) 417-421.
- [26] M.J. Kurylo, N.C. Peterson, W. Braun, Temperature and pressure effects in the addition of H atoms to propylene, *J.Chem.Phys* 54 (1971) 4662-4666.
- [27] T. Watanabe, T. Kyogoku, S. Tsunashima, S. Sato, S. Nagase, Kinetic isotope effects in the H+ C<sub>3</sub>H<sub>6</sub>→ C<sub>3</sub>H<sub>7</sub> reaction, *Bulletin of the Chemical Society of Japan* 55 (1982) 3720-3723.
- [28] C.M. Rosado-Reyes, J.A. Manion, W. Tsang, H atom attack on propene, *J.Phys.Chem.A* 115 (2011) 2727-2734.
- [29] Y. Hidaka, T. Nakamura, H. Tanaka, A. Jinno, H. Kawano, T. Higashihara, Shock tube and modeling study of propene pyrolysis, *Int. J. Chem. Kinet.* 24 (1992) 761-780.
- [30] U. Löser, K. Scherzer, K. Weber, Abschätzung kinetischer Daten für H-Transferreaktionen mit Hilfe der Bond Strength-Bond Length (BSBL)-Methode, *Zeitschrift für Physikalische Chemie* 270 (1989) 237-245.
- [31] G. Harris, J. Pitts Jr, Absolute rate constants and temperature dependencies for the gas phase reactions of H atoms with propene and the butenes in the temperature range 298 to 445 K, *J.Chem.Phys* 77 (1982) 3994-3997.
- [32] S.S. Nagaraja, J. Liang, S. Dong, S. Panigrahy, A. Sahu, G. Kukkadapu, S.W. Wagnon, W.J. Pitz, H.J. Curran, A hierarchical single-pulse shock tube pyrolysis study of C<sub>2</sub>–C<sub>6</sub> 1-alkenes, *Combust. Flame* 219 (2020) 456-466.
- [33] Q.-D. Wang, Z.-W. Liu, Reaction Kinetics of Hydrogen Atom Abstraction from C<sub>4</sub>–C<sub>6</sub> Alkenes by the Hydrogen Atom and Methyl Radical, *J.Phys.Chem.A* 122 (2018) 5202-5210.
- [34] H. Wang, E. Dames, B. Sirjean, D. Sheen, R. Tangko, A. Violi, J. Lai, F. Egolfopoulos, D. Davidson, R. Hanson, A high-temperature chemical kinetic model of n-alkane (up to n-dodecane), cyclohexane, and methyl-, ethyl-, n-propyl and n-butyl-cyclohexane oxidation at high temperatures, *JetSurF version 2* (2010) 19.
- [35] W. Tsang, Chemical kinetic data base for hydrocarbon pyrolysis, *Industrial & engineering chemistry research* 31 (1992) 3-8.
- [36] W. Tsang, Chemical kinetic data base for combustion chemistry part V. Propene, *J.Phys.Chem.Ref.Data* 20 (1991) 221-273.
- [37] M.J. Frisch, G.W. Trucks, H.B. Schlegel, G.E. Scuseria, M.A. Robb, J.R. Cheeseman, G. Scalmani, V. Barone, G.A. Petersson, H. Nakatsuji, et. al., *Gaussian 09*, 2009.
- [38] M.J. Frisch, G.W. Trucks, H.B. Schlegel, G.E. Scuseria, M.A. Robb, J.R. Cheeseman, G. Scalmani, V. Barone, G.A. Petersson, H. Nakatsuji, et. al., *Gaussian 16 Rev. B.01*, Wallingford, CT, 2016.

- [39] J.-D. Chai, M. Head-Gordon, Long-range corrected hybrid density functionals with damped atom-atom dispersion corrections, *Phys. Chem. Chem. Phys.* 10 (2008) 6615-6620.
- [40] T.H. Dunning, Gaussian-basis sets for use in correlated molecular calculations .1. The atoms boron through neon and hydrogen, *J. Chem. Phys.* 90 (1989) 1007-1023.
- [41] Y. Georgievskii, J.A. Miller, M.P. Burke, S.J. Klippenstein, Reformulation and solution of the master equation for multiple-well chemical reactions, *J. Phys. Chem. A* 117 (2013) 12146-12154.
- [42] C.F. Goldsmith, G.R. Magoon, W.H. Green, Database of small molecule thermochemistry for combustion, *J. Phys. Chem. A* 116 (2012) 9033-9057.
- [43] J.A. Miller, S.J. Klippenstein, The recombination of propargyl radicals and other reactions on a C<sub>6</sub>H<sub>6</sub> potential, *J. Phys. Chem. A* 107 (2003) 7783-7799.
- [44] J.M. Simmie, G. Black, H.J. Curran, J.P. Hinde, Enthalpies of formation and bond dissociation energies of lower alkyl hydroperoxides and related hydroperoxy and alkoxy radicals, *J. Phys. Chem. A* 112 (2008) 5010-5016.
- [45] B.J. McBride, S. Gordon, Computer program for calculating and fitting thermodynamic functions, 1992.
- [46] H.S. Johnston, J. Heicklen, Tunnelling corrections for unsymmetrical Eckart potential energy barriers, *J. Phys. Chem.* 66 (1962) 532-533.
- [47] Y. Li, S.J. Klippenstein, C.-W. Zhou, H.J. Curran, Theoretical kinetics analysis for H atom addition to 1,3-butadiene and related reactions on the C<sub>4</sub>H<sub>7</sub> potential energy surface, *J. Phys. Chem. A* 121 (2017) 7433-7445.
- [48] A. Miyoshi, Computational studies on the reactions of 3-butenyl and 3-butenylperoxy radicals, *Int. J. Chem. Kinet.* 42 (2010) 273-288.
- [49] S.J. Klippenstein, J.A. Miller, The addition of hydrogen atoms to diacetylene and the heats of formation of i-C<sub>4</sub>H<sub>3</sub> and n-C<sub>4</sub>H<sub>3</sub>, *J. Phys. Chem. A* 109 (2005) 4285-4295.
- [50] S.J. Klippenstein, J.A. Miller, A.W. Jasper, Kinetics of propargyl radical dissociation, *J. Phys. Chem. A* 119 (2015) 7780-7791.
- [51] B. Ruscic, R.E. Pinzon, G.v. Laszewski, D. Kodeboyina, A. Burcat, D. Leahy, D. Montoy, A.F. Wagner, Active thermochemical tables: thermochemistry for the 21st century, *J. Phys.* 16 (2005) 561-570.
- [52] B. Ruscic, R.E. Pinzon, M.L. Morton, G. von Laszewski, S.J. Bittner, S.G. Nijsure, K.A. Amin, M. Minkoff, A.F. Wagner, Introduction to active thermochemical tables: several "key" enthalpies of formation revisited, *J. Phys. Chem. A* 108 (2004) 9979-9997.
- [53] S.J. Klippenstein, L.B. Harding, B. Ruscic, Ab initio computations and active thermochemical tables hand in hand: heats of formation of core combustion species, *J. Phys. Chem. A* 121 (2017) 6580-6602.
- [54] A. Burcat, B. Ruscic, Third millenium ideal gas and condensed phase thermochemical database for combustion (with update from active thermochemical tables), Argonne National Lab.(ANL), Argonne, IL (United States), 2005.
- [55] J.M. Simmie, K.P. Somers, Benchmarking compound methods (CBS-QB3, CBS-APNO, G3, G4, W1BD) against the active thermochemical tables: a litmus test for cost-effective molecular formation enthalpies, *J. Phys. Chem. A* 119 (2015) 7235-7246.
- [56] K.P. Somers, J.M. Simmie, Benchmarking compound methods (CBS-QB3, CBS-APNO, G3, G4, W1BD) against the active thermochemical tables: formation enthalpies of radicals, *J. Phys. Chem. A* 119 (2015) 8922-8933.
- [57] J.M. Simmie, K.P. Somers, W.K. Metcalfe, H.J. Curran, Substituent effects in the thermochemistry of furans: A theoretical (CBS-QB3, CBS-APNO and G3) study, *J. Chem. Thermodyn.* 58 (2013) 117-128.
- [58] H.J. Curran, Rate constant estimation for C<sub>1</sub> to C<sub>4</sub> alkyl and alkoxy radical decomposition, *Int. J. Chem. Kinet.* 38 (2006) 250-275.

- [59] T. Kyogoku, T. Watanabe, S. Tsunashima, S. Sato, Arrhenius parameters for the reactions of hydrogen and deuterium atoms with four butenes, *Bulletin of the Chemical Society of Japan* 56 (1983) 19-21.
- [60] I.A. Awan, D.R. Burgess, Jr., J.A. Manion, Pressure dependence and branching ratios in the decomposition of 1-pentyl radicals: shock tube experiments and master equation modeling, *J. Phys Chem. A* 116 (2012) 2895-2910.
- [61] A. Comandini, I.A. Awan, J.A. Manion, Thermal decomposition of 1-pentyl radicals at high pressures and temperatures, *Chem. Phys. Lett.* 552 (2012) 20-26.
- [62] L.C. Jitariu, L.D. Jones, S.H. Robertson, M.J. Pilling, I.H. Hillier, Thermal rate coefficients via variational transition state theory for the unimolecular decomposition/isomerisation of 1-pentyl radical: ab initio and direct dynamics calculations, *J. Phys. Chem. A* 107 (2003) 8607-8617.
- [63] A.W. Jasper, N. Hansen, Hydrogen-assisted isomerizations of fulvene to benzene and of larger cyclic aromatic hydrocarbons, *Proc. Combust Inst.* 34 (2013) 279-287.



# Chapter 5 : A Theoretical Study of Cyclic Ether Formation Reactions

Published in: *Proc. Combust. Inst.* 36(1) (2017) 161–167

DOI: <https://doi.org/10.1016/j.proci.2016.05.006>

## Author Contributions

- (1) John Bugler: Collated numerical data, computed rate coefficients, analysed results, and wrote the manuscript.
- (2) Jennifer Power: Performed electronic structure calculations, and computed reaction barrier heights.
- (3) Henry J. Curran: Managed the project throughout, and reviewed manuscript prior to and post the review process.



## Abstract

Cyclisation reactions of hydroperoxyl-alkyl radicals forming cyclic ethers and hydroxyl radicals play an important role in low temperature oxidation chemistry. These reactions contribute to the competition between radical chain propagation and chain branching reaction pathways which dominate the reactivity of alkanes at temperatures where negative temperature coefficient (NTC) behaviour is often observed. This work is motivated by previous experimental and modelling evidences that current literature rate coefficients for these reactions are in need of refinement and/or re-determination. In light of this, the current study presents quantum-chemically-derived high-pressure limit rate coefficients for all cyclisation reactions leading to cyclic ether formation in alkanes ranging in size from C<sub>2</sub> to C<sub>5</sub>. Ro-vibrational properties of each stationary point were determined at the M06-2X/6-311++ G(d,p) level of theory. Coupled cluster (CCSD(T)) and Møller–Plesset perturbation theory (MP2) methods were employed with various basis sets and complete basis set extrapolation techniques to compute the energies of the resulting geometries. These methods, combined with canonical transition state theory, have been used to determine 43 rate coefficients, with enough structural diversity within the reactions to allow for their application to larger species for which the use of the levels of theory employed herein would be computationally prohibitive. The validity of an alternative, and computationally less expensive, technique to approximate the complete basis set limit energies is also discussed, together with implications of this work for combustion modelling.

## 1. Introduction

In recent years, there has been a proliferation of systematic theoretical studies concerning reaction pathways of importance in the low-temperature oxidation of alkanes [1–15]. The rapid increase in the number of studies of this kind is due, in part, to more readily available computational resources. This, coupled with the computationally inexpensive yet relatively accurate compound methods [16–22], as implemented in the Gaussian software packages [23] has aided the investigation of large arrays of reactions for which little or no experimental data are currently available. Several studies have determined high-pressure limit rate coefficients for large numbers of reactions within the important low-temperature reaction classes. Significant success has been achieved in chemical kinetic modelling of alkane oxidation systems by utilising these values [24–26]. Despite these successes, it has been highlighted that refinement of some important kinetic parameters is still necessary for further progress [24]. Particular disparity is seen amongst literature values for the title reactions. As is the case

with many of the important unimolecular reactions within the low-temperature oxidation pathways, most theoretical rate coefficients for the reactions of interest in this study have previously been derived using the CBS-QB3 compound method [16]. This is a popular method, particularly when studying large quantities of species and/or reactions, due to its relative speed and reliability [27]. Although relatively cost-effective, it has previously been highlighted as being potentially biased towards the under-prediction of reaction barrier in some instances [28]. For the reaction class of interest in this work, there may also be evidence of this based on investigations by Villano et al. [1], where an average difference of approximately  $2.4 \text{ kcal mol}^{-1}$  in 0 K barriers is observed between their values and those of DeSain et al. [29]. The barriers calculated by Villano et al. using the CBS-QB3 method are consistently lower than those calculated for the same reactions by DeSain et al., who used a combination of quadratic configuration interaction (QCISD(T)) and Møller-Plesset perturbation theory (MP2) methods with varying sized basis sets (see [29] for more details) to determine single point energies of stationary points characterised at the B3LYP/6-31G\* level of theory. In the instance of the cyclisation reaction of 4-hydroperoxyl-but-2-yl radical forming 2-methyloxetane and a hydroxyl radical, the 0 K barrier determined in both studies differs by  $13.1 \text{ kcal mol}^{-1}$ ! Further evidence of the under-prediction of reaction barriers for these reactions by the CBS-QB3 method is observed in the recent study of Zhang et al. on the oxidation of n-hexane [26]. It was found that without significant modifications to the rate rules proposed by Villano et al. [1] for this reaction class, model-predicted cyclic ether concentrations were too high when compared to those measured in a jet-stirred reactor. Although the determination of accurate thermochemistry is not the focus of this study, it is noteworthy that the CBS-QB3 method has recently been shown to lack both accuracy and precision when deriving enthalpies of formation via the atomisation method for a range of hydrocarbon and oxygenated species [27,30,31].

This study aims to provide high-fidelity rate coefficients for the reactions of interest through utilisation of high-level quantum chemical methods. A comprehensive set of reactions is chosen in order to allow application of the values derived in this work to similar reactions occurring in larger molecules, for which the use of computational methods such as those employed here is currently impractical.

## 2. Computational methods

### 2.1. Rate coefficient determination

All calculations have been performed using Gaussian 09 [23]. Geometries of minima and transition state (TS) structures have been optimised using the M06-2X functional [32] with the 6-311++G(d,p) basis set. Harmonic frequency analyses were employed at the same level of theory to verify the nature of the stationary points, with a single imaginary frequency indicative of a first-order saddle point on the potential energy surface (PES), corresponding to a TS structure. All frequencies were scaled by 0.98, with zero-point vibrational energies (ZPVEs) scaled by 0.97, as recommended for the M06-2X functional by Zhao and Truhlar [32]. Intrinsic reaction coordinate (IRC) calculations [33] were carried out with M06-2X/6-311++G(d,p) on each TS to ensure it was connected to the desired reactants and products. Single point energy (SPE) calculations have been carried out for all  $C_2H_5O_2$  and  $C_3H_7O_2$  reactants and TSs using the coupled cluster (CCSD(T)) method and employing relatively large basis sets (cc-pVTZ and cc-pVQZ [34]). The resulting energies were extrapolated to the complete basis set (CBS) limit using the following formula [35,36]:

$$E_{\text{CCSD(T)/CBS}} = E_{\text{CCSD(T)/QZ}} + (E_{\text{CCSD(T)/QZ}} - E_{\text{CCSD(T)/TZ}}) 4^4 / 5^4 - 4^4 \quad (1)$$

where TZ and QZ are abbreviations for cc-pVTZ and cc-pVQZ, respectively. For the  $C_4H_9O_2$  and  $C_5H_{11}O_2$  species, the CCSD(T)/cc-pVQZ calculations were computationally prohibitive. For these species, the CBS energies were estimated based on extrapolations of CCSD(T)/cc-pVDZ and CCSD(T)/cc-pVTZ energies. The MP2 method was then used to correct for the difference in cc-pVDZ and cc-pVTZ extrapolation energies. Here, cc-pVDZ and cc-pVTZ represent CBS extrapolations based on cc-pVDZ and cc-pVTZ, and cc-pVTZ and cc-pVQZ energies, respectively. The final energies were calculated using the following formula:

$$E_{\text{CCSD(T)/CBS}} = E_{\text{CCSD(T)/TZ}} + (E_{\text{CCSD(T)/TZ}} - E_{\text{CCSD(T)/DZ}}) 3^4 / 4^4 - 3^4 + E_{\text{MP2/QZ}} + (E_{\text{MP2/QZ}} - E_{\text{MP2/TZ}}) 4^4 / 5^4 - 4^4 - E_{\text{MP2/TZ}} - (E_{\text{MP2/TZ}} - E_{\text{MP2/DZ}}) 3^4 / 4^4 - 3^4 \quad (2)$$

Similar approaches have previously been used to approximate “higher-level” SPEs [6,37,38]. The validity of the approximation is investigated in this study by comparing the CCSD(T)/cc-pVTQZ energies of the  $C_2H_5O_2$  and  $C_3H_7O_2$  species with those determined using Eq. (2). This is further discussed in Section 3.1.

The  $T_1$  diagnostic [39] for all reactant species is  $\leq 0.013$ , indicating that the use of single-reference methods to describe the wave function is appropriate.  $T_1$  values for the TSs range from 0.031 to 0.040. While  $T_1$  values greater than 0.03 (for radicals) may be cause for

concern [40], none of the TSs have an unusually high value, with only six of the forty three complexes having a value greater than 0.035. Nevertheless, if lower uncertainties are required for the TS energies, multi-reference calculations are recommended. Relaxed PES scans were carried out for internal rotations corresponding to low frequency torsional modes in 10 degree increments as a function of dihedral angle with M06-2X/6-311++G(d,p). Rotational constants were computed as a function of dihedral angle using the Lamm module of the MultiWell program suite [41]. The resulting values were fitted to truncated Fourier series, and used as input for 1-D hindered internal rotation approximations. The Thermo application of MultiWell was used to compute high-pressure limit rate coefficients as a function of temperature (298.15 – 2000 K) from canonical transition state theory [42]. Quantum mechanical tunnelling has been accounted for via inclusion of 1-D tunnelling through an unsymmetrical Eckart energy barrier [43]. Although the Eckart formula depends on the heat of reaction, we have not computed this at the level at which the SPEs of the reactant and TS structures have been determined. In the present cases, where tunnelling contributions are quite small, any reasonable value of the heat of reaction input into the Eckart formula gives approximately the same value for the rate coefficient. Tests show that a 10 kcal mol<sup>-1</sup> variation in the heat of reaction results in a difference of ~1% in rate coefficient at 800 K. The resulting rate coefficients were fitted to the following modified Arrhenius expression:

$$k = A (T/T_{\text{ref}})^n \exp(-E/RT) \quad (3)$$

in which  $A$  is the A-factor,  $T$  is the temperature in units of Kelvin,  $T_{\text{ref}} = 1$  K,  $n$  is the temperature exponent, and  $E$  is related to the activation energy (by  $E_a = E + nRT$ ). This modified Arrhenius form was adequate to represent the numerical data, with a maximum deviation of 14% between computed and fitted rate coefficients. These expressions of the rate coefficients are listed in Table 5.1, Section 3.2.

## 2.2. Uncertainty

Zádor et al. [44] highlight an example of uncertainties in reaction barrier determinations for a benchmark set of twenty H-atom abstraction reactions compiled by Lynch et al. [45]. Senosiain et al. (J.P. Senosiain et al., unpublished data) tested a variety of methods against seventeen of these reactions in an attempt to quantify uncertainty in reaction barrier determination for each method. Geometries were optimised using either B3LYP [46] or MP2 [47] methods with the 6-311++G(d,p) basis set. SPE calculations were carried out using B3LYP, MP2, QCISD(T), and CCSD(T) methods with augmented and non-augmented cc-

pVTZ and cc-pVQZ basis sets extrapolated to the CBS limit. Absolute error values are lowest for the QCISD(T) and CCSD(T) methods, with > 50% of the calculated barriers within 1 kcal mol<sup>-1</sup> of the benchmark values. The absolute errors for these cases appear to be largely independent of the method used for geometry optimisation. The methods used here are quite similar to those used by Senosiain et al., so their results may be useful for estimation of uncertainties in the barrier heights presented here, although they are different from those compiled by Lynch et al. [45]. If it is assumed that the uncertainties in barrier heights calculated in this study are normally distributed, with 50% of the probability density function within 1 kcal mol<sup>-1</sup> of the calculated value, we arrive at a 2 $\sigma$  uncertainty of 3.0 kcal mol<sup>-1</sup>. Estimating uncertainties in frequency factors is more difficult. The assumption that individual contributions of hindered rotors are separable is likely to be adequate for the reactions of interest in this study due to the lack of long-range interactions within the molecules. Interactions such as hydrogen bonding tend to be more prevalent in molecules or complexes with multiple oxygenated moieties and leads to coupling of the internal rotors. This coupling, and the adequate treatment of rotors when it occurs, has been discussed previously by Sharma et al. [10], and suitable methods were applied to reactions of hydroperoxyl–alkyl–peroxyl radicals. Although the coupling of rotors is not likely to be significant in this study, neither is it likely that there is complete separability of rotors. On this basis, we estimate uncertainties in frequency factors to be approximately a factor of two per rotor “tied up” in the TS. A further factor of two may be assumed due to uncertainties in harmonic vibrational frequencies and the anharmonicities of these modes.

### 3. Results and Discussion

#### 3.1. Validity of CBS limit extrapolation approach

Barrier heights ( $E_{0K} + ZPVE$ ) calculated using both Eq. (1) and Eq. (2) for the reactions of C<sub>2</sub>H<sub>5</sub>O<sub>2</sub> and C<sub>3</sub>H<sub>7</sub>O<sub>2</sub> species are compared, and are tabulated in the Supplemental Material, Table S1. It is found that the barriers determined using coupled cluster and MP2 methods (denoted CC/MP2 hereafter) are consistently higher than those calculated using the coupled cluster (CC) method alone. The difference in values is quite consistent, with Eq. 2 giving barriers which are higher by an average of 0.46 kcal mol<sup>-1</sup>, with a 2 $\sigma$  dispersion of 0.09 kcal mol<sup>-1</sup>. The comparison set is small, but with such a consistent offset it seems reasonable to lower the barriers calculated using Eq. (2) for all of the reactions of C<sub>4</sub>H<sub>9</sub>O<sub>2</sub> and C<sub>5</sub>H<sub>11</sub>O<sub>2</sub> species by 0.46 kcal mol<sup>-1</sup> from their CC/MP2 values. This amount is within the uncertainty

of the calculated barrier heights, but the aim is that this offset will result in a more consistent set of values overall.

### 3.2. Comparisons with the literature

Computed rate coefficients are presented in Table 5.1. Due to spatial constraints we provide comparisons of these rate coefficients with literature values, as well as a detailed glossary of all species listed in Table 5.1, as Supplemental Material. However, an account of the results is also given here. As discussed in Section 1, Villano et al. [1] note that the barrier heights for these reactions calculated by DeSain et al. [29] are an average of 2.4 kcal mol<sup>-1</sup> higher than their own. The values calculated in this study fall between those calculated in the two studies, with barrier heights an average of 1.2 kcal mol<sup>-1</sup> higher than those determined by Villano et al. [1]. This may provide yet more evidence that CBS-QB3 tends to under-predict barrier heights. An example comparison of literature rate coefficients is shown in Fig. 5.1 for the cyclisation reaction of 3-hydroperoxyl-prop-2-yl radical forming methyloxirane and a hydroxyl radical. This comparison reflects the general trend seen when comparing literature rate coefficients with those calculated in this study, in that those computed here tend towards the lower end of values which currently exist. These lower rate coefficients may have been expected due to the findings of Zhang et al. [26], where some of the rate rules suggested by Villano et al. [1] had to be lowered by approximately a factor of 4 in the temperature region where these reactions are most important (~700 – 900 K) in order to improve model agreement with cyclic ether concentration profiles measured using a jet-stirred reactor. This was achieved by lowering the A-factor of the Arrhenius expressions by a factor of 2, and increasing the activation energy by 1 kcal mol<sup>-1</sup>.

**Table 5.1:** Rate Coefficients Calculated in This Study.

Reaction	$A$ (s <sup>-1</sup> )	$n$	$E$ (cal mol <sup>-1</sup> )
$\dot{C}_2H_4OOH1-2 \leftrightarrow C_2H_4O1-2 + \dot{O}H$	$1.68 \times 10^{07}$	1.40	10880.
$\dot{C}_3H_6OOH1-2 \leftrightarrow C_3H_6O1-2 + \dot{O}H$	$1.45 \times 10^{07}$	1.46	11850.
$\dot{C}_3H_6OOH1-3 \leftrightarrow C_3H_6O1-3 + \dot{O}H$	$7.56 \times 10^{05}$	1.56	18070.
$\dot{C}_3H_6OOH2-1 \leftrightarrow C_3H_6O1-2 + \dot{O}H$	$1.19 \times 10^{08}$	1.26	11630.
$\dot{C}_4H_8OOH1-2 \leftrightarrow C_4H_8O1-2 + \dot{O}H$	$3.06 \times 10^{07}$	1.41	11310.
$\dot{C}_4H_8OOH1-3 \leftrightarrow C_4H_8O1-3 + \dot{O}H$	$6.57 \times 10^{04}$	1.79	16150.
$\dot{C}_4H_8OOH1-4 \leftrightarrow C_4H_8O1-4 + \dot{O}H$	$1.38 \times 10^{05}$	1.44	9920.



$\dot{C}_4H_8OOH2-1 \leftrightarrow C_4H_8O1-2 + \dot{O}H$	$5.06 \times 10^{08}$	1.11	11030.
$\dot{C}_4H_8OOH2-3 \leftrightarrow C_4H_8O2-3_{anti} + \dot{O}H$	$8.98 \times 10^{07}$	1.22	10260.
$\dot{C}_4H_8OOH2-3 \leftrightarrow C_4H_8O2-3_{syn} + \dot{O}H$	$3.16 \times 10^{08}$	1.04	9930.
$\dot{C}_4H_8OOH2-4 \leftrightarrow C_4H_8O1-3 + \dot{O}H$	$3.57 \times 10^{06}$	1.36	16760.
$\dot{C}_4H_8OOHI-I \leftrightarrow C_4H_8OI-I + \dot{O}H$	$9.30 \times 10^{05}$	1.57	16670.
$\dot{C}_4H_8OOHI-T \leftrightarrow C_4H_8OI-T + \dot{O}H$	$2.64 \times 10^{07}$	1.35	10270.
$\dot{C}_4H_8OOHT-I \leftrightarrow C_4H_8OI-T + \dot{O}H$	$4.53 \times 10^{08}$	1.04	9930.
$\dot{C}_5H_{10}OOH1-2 \leftrightarrow C_5H_{10}O1-2 + \dot{O}H$	$4.67 \times 10^{12}$	0.25	12840.
$\dot{C}_5H_{10}OOH1-3 \leftrightarrow C_5H_{10}O1-3 + \dot{O}H$	$1.28 \times 10^{05}$	1.83	14460.
$\dot{C}_5H_{10}OOH1-4 \leftrightarrow C_5H_{10}O1-4 + \dot{O}H$	$4.73 \times 10^{05}$	1.24	8130.
$\dot{C}_5H_{10}OOH1-5 \leftrightarrow C_5H_{10}O1-5 + \dot{O}H$	$2.31 \times 10^{04}$	1.31	8550.
$\dot{C}_5H_{10}OOH2-1 \leftrightarrow C_5H_{10}O1-2 + \dot{O}H$	$2.57 \times 10^{09}$	1.04	11340.
$\dot{C}_5H_{10}OOH2-3 \leftrightarrow C_5H_{10}O2-3_{anti} + \dot{O}H$	$4.66 \times 10^{08}$	1.09	9850.
$\dot{C}_5H_{10}OOH2-3 \leftrightarrow C_5H_{10}O2-3_{syn} + \dot{O}H$	$7.46 \times 10^{08}$	0.70	9270.
$\dot{C}_5H_{10}OOH2-4 \leftrightarrow C_5H_{10}O2-4_{anti} + \dot{O}H$	$3.84 \times 10^{06}$	1.26	14970.
$\dot{C}_5H_{10}OOH2-4 \leftrightarrow C_5H_{10}O2-4_{syn} + \dot{O}H$	$1.39 \times 10^{06}$	1.49	15210.
$\dot{C}_5H_{10}OOH2-5 \leftrightarrow C_5H_{10}O1-4 + \dot{O}H$	$3.79 \times 10^{05}$	1.28	10220.
$\dot{C}_5H_{10}OOH3-1 \leftrightarrow C_5H_{10}O1-3 + \dot{O}H$	$2.40 \times 10^{06}$	1.52	17240.
$\dot{C}_5H_{10}OOH3-2 \leftrightarrow C_5H_{10}O2-3_{anti} + \dot{O}H$	$2.81 \times 10^{09}$	0.35	9860.
$\dot{C}_5H_{10}OOH3-2 \leftrightarrow C_5H_{10}O2-3_{syn} + \dot{O}H$	$4.20 \times 10^{09}$	0.71	10050.
$\dot{C}_5H_{10}OOHA-A \leftrightarrow C_5H_{10}OA-A + \dot{O}H$	$2.37 \times 10^{05}$	1.77	16610.
$\dot{C}_5H_{10}OOHA-B \leftrightarrow C_5H_{10}OA-B + \dot{O}H$	$2.44 \times 10^{08}$	1.22	10420.
$\dot{C}_5H_{10}OOHA-C \leftrightarrow C_5H_{10}OA-C_{anti} + \dot{O}H$	$1.16 \times 10^{04}$	1.96	16160.
$\dot{C}_5H_{10}OOHA-C \leftrightarrow C_5H_{10}OA-C_{syn} + \dot{O}H$	$4.25 \times 10^{04}$	1.78	14740.
$\dot{C}_5H_{10}OOHA-D \leftrightarrow C_5H_{10}OA-D + \dot{O}H$	$5.36 \times 10^{05}$	1.27	9350.
$\dot{C}_5H_{10}OOHB-A \leftrightarrow C_5H_{10}OA-B + \dot{O}H$	$1.59 \times 10^{09}$	0.85	9590.
$\dot{C}_5H_{10}OOHB-C \leftrightarrow C_5H_{10}OB-C + \dot{O}H$	$8.64 \times 10^{08}$	0.85	8780.
$\dot{C}_5H_{10}OOHB-D \leftrightarrow C_5H_{10}OB-D + \dot{O}H$	$1.21 \times 10^{07}$	1.22	16390.
$\dot{C}_5H_{10}OOHC-A \leftrightarrow C_5H_{10}OA-C_{anti} + \dot{O}H$	$3.79 \times 10^{03}$	2.69	14900.
$\dot{C}_5H_{10}OOHC-A \leftrightarrow C_5H_{10}OA-C_{syn} + \dot{O}H$	$2.21 \times 10^{05}$	1.67	16240.

$\dot{C}_5H_{10}OOHC-B \leftrightarrow C_5H_{10}OB-C + \dot{O}H$	$1.19 \times 10^{10}$	0.77	9420.
$\dot{C}_5H_{10}OOHC-D \leftrightarrow C_5H_{10}OC-D + \dot{O}H$	$1.23 \times 10^{09}$	1.01	10180.
$\dot{C}_5H_{10}OOHD-A \leftrightarrow C_5H_{10}OA-D + \dot{O}H$	$4.60 \times 10^{05}$	1.30	9360.
$\dot{C}_5H_{10}OOHD-B \leftrightarrow C_5H_{10}OB-D + \dot{O}H$	$1.14 \times 10^{05}$	1.65	13370.
$\dot{C}_5H_{10}OOHD-C \leftrightarrow C_5H_{10}OC-D + \dot{O}H$	$1.73 \times 10^{07}$	1.41	11350.
$neo\dot{C}_5H_{10}OOH \leftrightarrow neoC_5H_{10}O + \dot{O}H$	$5.88 \times 10^{06}$	1.55	15990.

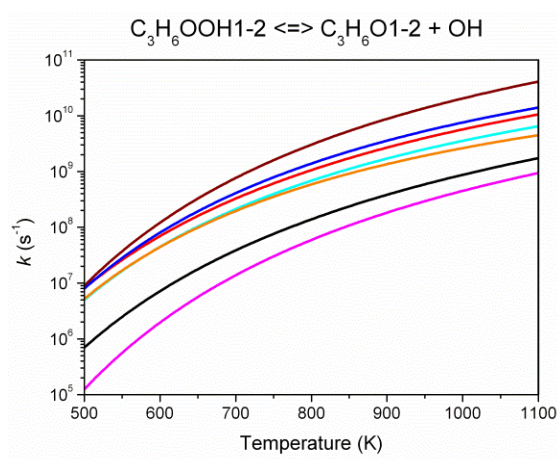


**Figure 5.1.** Comparison of literature values with this work for the cyclisation reaction of 3-hydroperoxyl-prop-2-yl radical forming methyloxirane and a hydroxyl radical. Black: This work, Red: Villano et al. [1], Blue: Miyoshi [2], Magenta: Wijaya et al. [3], Cyan: Cord et al. [4], Wine: Chan et al. [5], Orange: Goldsmith et al. [6].

### 3.3. Implications for combustion modelling

Figure 5.2 shows the effects of including the rate coefficients presented here for the reactions of  $C_5H_{11}\dot{O}_2$  to a recently published model describing oxidation of the pentane isomers [25]. Constant volume and perfectly-stirred reactor simulations were run under some representative conditions in which chemical kinetic models describing combustion processes are often validated. *n*-Pentane is chosen as the representative fuel, and CHEMKIN-PRO [48] was used for the simulations. The closed homogeneous batch reactor, and perfectly-stirred reactor modules within CHEMKIN-PRO were used to simulate the ignition delay times and species concentration profiles, respectively. Ignition delay simulations were run under stoichiometric fuel/‘air’ conditions (2.56% *n*-pentane, 20.46%  $O_2$ , 76.98%  $N_2$ ) at 10 and 20 atm, and from 650 – 1400 K. The perfectly-stirred reactor simulations were also run under stoichiometric conditions (1% *n*-pentane, 8%  $O_2$ , 91%  $N_2$ ) at 1 atm, and from 500–1100 K, at a residence time of 2 s. Also plotted are data presented in [25], Fig. 5.2 (a), as well

as jet-stirred reactor data yet to be published [49], Fig. 5.2 (b) and (c). The simulation results of two models (Model A and Model B) are shown. Model A is that presented in [25], with the rate coefficients for C<sub>5</sub> cyclic ether formation reactions taken from Villano et al. [1]. Model B is the same, but with the rate coefficients for the same reaction class replaced with those pertaining to n-pentane from Table 5.1 in this study. It is shown that there is an increase in reactivity in the NTC region in both sets of simulations, where the title reactions are known to be important, Fig. 5.2 (a) and (b). This reaction class is an important radical chain propagating one, and so this effect is as expected given that the newly computed rate coefficients are lower than those from Villano et al. [1]. The effects seen are not big in terms of overall reactivity, but in Fig. 5.2 (c) the perfectly-stirred reactor simulated concentration profiles of the two major cyclic ethers formed from n-pentane oxidation (2-methyltetrahydrofuran and 2,4-dimethyloxetane) are shown, and a significant effect is seen. Two peaks are observed in both concentration profiles at approximately 650 and 850 K, and factors of ~2–4 differences are seen in the simulated profiles at these temperatures. While model-predicted mole fractions of 2-methyltetrahydrofuran have gone from slightly over-predicting the experimental data to under-predicting it, those of 2,4-dimethyloxetane have improved considerably in terms of agreement with experiment. While the graphs in Fig. 5.2 are mainly for illustrative purposes, it is seen that the inclusion of the newly calculated rate coefficients into an existing model can bring about significant changes and overall improvement in predicting cyclic ether concentrations. Model B would require modifications in order to restore the accurate prediction of overall reactivity, but this test provides insights into the modelling implications of using the rate coefficients presented in Table 5.1.

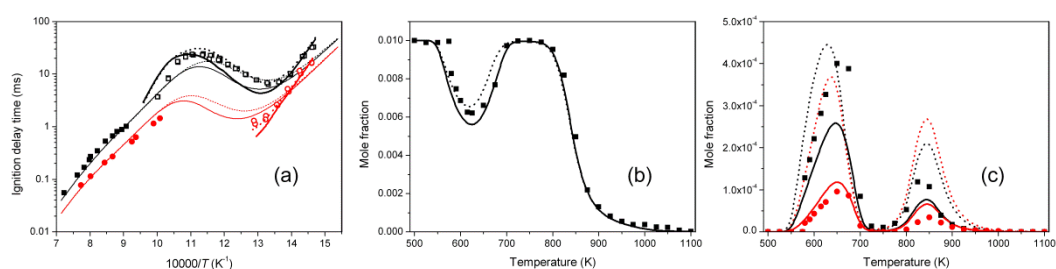


**Figure 5.2.** Model-simulated effects of rate coefficients presented in this study on n-pentane (a) ignition delay times at 10 (black) and 20 atm (red), and perfectly-stirred reactor profiles of (b) n-pentane, (c) 2-methyltetrahydrofuran (black), and 2,4-dimethyloxetane (red). Symbols represent experimental data, dashed lines represent Model A, and solid lines Model B (see Section 3.3 for details). The thicker lines in (a) represent simulations accounting for facility effects.

## 4. Conclusions

This paper presents a systematic and comprehensive study of the high-pressure limit kinetics of cyclic ether formation reactions from hydroperoxyl-alkyl radicals. The rate coefficients are presented and compared with those from the literature, and we find that those presented here are generally lower than the existing values. Two different approaches are compared for the determination of reaction barrier heights, and we validate a method which can approximate a “higher-level” answer at a lower computational cost. The implications that these new rate coefficients may have for combustion modelling are discussed, with results that are reasonably significant in terms of mechanism predictions.

While this study presents values which are determined at a higher level of theory than other studies for this reaction class, the modelling successes achieved by using values from these previous studies cannot be understated. Several recent studies emanating from this research group and collaborators have proven just how useful systematic studies of important reaction classes can be, even if the accuracy of those values are not state-of-the-art. It is likely that these successes were possible due to most of the rate coefficients for important reaction classes within low-temperature oxidation schemes being calculated at the same level of theory (CBS-QB3). While the absolute accuracies of the values are probably less than desirable, it may be the case that the relative values are more preferable, resulting in favourable model predictions.

A more accurate determination of uncertainties in rate coefficients derived using different theoretical methods would be extremely useful for chemical kinetic modellers. A benchmarking study of different model chemistries, for instance, would go a long way in this regard. However, obtaining suitable experimental data is likely difficult or currently impossible, so any such studies would have to rely on comparisons with state-of-the-art theoretical calculations. Computationally less accurate (and cheaper) methods with more accurate uncertainties may prove to be the most useful.

## Acknowledgements

The authors wish to acknowledge the support of the Irish Research Council in funding this project under project number EPSPG/2012/380, and also the provision of computational resources from the Irish Centre for High-End Computing, ICHEC, under project number ngche026c. We also thank Prof. John Simmie for helpful discussions and input on this work.

## References

- [1] S.M. Villano, L.K. Huynh, H.-H. Carstensen, A.M. Dean, *J. Phys. Chem. A* 116 (2012) 5068–5089.
- [2] A. Miyoshi, *J. Phys. Chem. A* 115 (2011) 3301–3325.
- [3] C.D. Wijaya, R. Sumathi, W.H. Green, *J. Phys. Chem. A* 107 (2003) 4908–4920.
- [4] M. Cord, B. Sirjean, R. Fournet, *J. Phys. Chem. A* 116 (2012) 6142–6158.
- [5] W.-T. Chan, H.O. Pritchard, I.P. Hamilton, *Phys. Chem. Chem. Phys.* 16 (1999) 3715–3719.
- [6] C.F. Goldsmith, W.H. Green, S.J. Klippenstein, *J. Phys. Chem. A* 116 (2012) 3325–3346.
- [7] C.-J. Chen, J.W. Bozzelli, *J. Phys. Chem. A* 103 (1999) 9731–9769.
- [8] H. Sun, J.W. Bozzelli, *J. Phys. Chem. A* 108 (2004) 1694–1711.
- [9] S. Snitsirawat, J.W. Bozzelli, *J. Phys. Chem. A* 118 (2014) 4631–4646.
- [10] S. Sharma, S. Raman, W.H. Green, *J. Phys. Chem. A* 114 (2010) 5689–5701.
- [11] F. Zhang, T.S. Dibble, *J. Phys. Chem. A* 115 (2011) 655–663.
- [12] J. Zádor, S.J. Klippenstein, J.A. Miller, *J. Phys. Chem. A* 115 (2011) 10218–10225.
- [13] S.M. Villano, L.K. Huynh, H.-H. Carstensen, A.M. Dean, *J. Phys. Chem. A* 115 (2011) 13425–13442.
- [14] A. Miyoshi, *Int. J. Chem. Kinet.* 44 (2012) 59–74.
- [15] S.M. Villano, H.-H. Carstensen, A.M. Dean, *J. Phys. Chem. A* 117 (2013) 6458–6473
- [16] J.A. Montgomery, M.J. Frisch, J.W. Ochterski, G.A. Petersson, *J. Chem. Phys.* 112 (2000) 6532–6542.
- [17] J.W. Ochterski, G.A. Petersson, J.A. Montgomery, *J. Chem. Phys.* 104 (1996) 2598–2619.
- [18] J.A. Pople, M. Head-Gordon, D.J. Fox, K. Raghavachari, L.A. Curtiss, *J. Chem. Phys.* 90 (1989) 5622–5629.
- [19] L.A. Curtiss, C. Jones, G.W. Trucks, K. Raghavachari, J.A. Pople, *J. Chem. Phys.* 93 (1990) 2537–2545.
- [20] L.A. Curtiss, K. Raghavachari, G.W. Trucks, J.A. Pople, *J. Chem. Phys.* 94 (1991) 7221–7230.
- [21] L.A. Curtiss, K. Raghavachari, P.C. Redfern, V. Rassolov, J.A. Pople, *J. Chem. Phys.* 109 (1998) 7764–7776.
- [22] L.A. Curtiss, P.C. Redfern, K. Raghavachari, *J. Chem. Phys.* 126 (2007) 084108.
- [23] M.J. Frisch, G.W. Trucks, H.B. Schlegel, et al., *Gaussian 09*, revision D.01, Gaussian, Inc., Wallingford, CT, 2009.
- [24] J. Bugler, K.P. Somers, E.J. Silke, H.J. Curran, *J. Phys. Chem. A* 119 (2015) 7510–7527.
- [25] J. Bugler, B. Marks, O. Mathieu, *Combust. Flame* 163 (2016) 138–156.
- [26] K. Zhang, C. Banyon, C. Togbé, P. Dagaut, J. Bugler, H.J. Curran, *Combust. Flame* 162 (2015) 4194–4207.
- [27] J.M. Simmie, K.P. Somers, *J. Phys. Chem. A* 119 (2015) 7235–7246.
- [28] J. Aguilera-Iparraguirre, H.J. Curran, W. Klopper, J.M. Simmie, *J. Phys. Chem. A* 112 (2008) 7047–7054.
- [29] J.D. DeSain, C.A. Taatjes, J.A. Miller, S.J. Klippenstein, D.K. Hahn, *Faraday Discuss.* 119 (2001) 101–120.
- [30] K.P. Somers, J.M. Simmie *J. Phys. Chem. A* 119 (2015) 8922–8933.
- [31] J.M. Simmie, *J. Phys. Chem. A* 119 (2015) 10511–10526.
- [32] Y. Zhao, D.G. Truhlar, *Theor. Chem. Acc.* 120 (2008) 215–241.
- [33] H.P. Hratchian, H.B. Schlegel, *J. Chem. Theory Comput.* 1 (2005) 61–69.
- [34] T.H. Dunning, *J. Chem. Phys.* 90 (1989) 1007–1023.

- [35] J.M.L. Martin, Chem. Phys. Lett. 259 (1996) 669–678.
- [36] D. Feller, D.A. Dixon, J. Chem. Phys. 115 (2001) 3484–3496.
- [37] J.A. Miller, S.J. Klippenstein, J. Phys. Chem. A 107 (2003) 7783–7799.
- [38] C.F. Goldsmith, G.R. Magoon, W.H. Green, J. Phys. Chem. A 116 (2012) 9033–9057
- [39] T.J. Lee, P.R. Taylor, Int. J. Quantum Chem. Quantum Chem. Symp. 23 (1989) 199–207.
- [40] S.J. Klippenstein, L.B. Harding, Proc. Combust. Inst. 32 (2009) 149–155.
- [41] MultiWell-2014.1 Software, 2014, designed and maintained by J. R. Barker with contributors N. F. Ortiz, J. M. Preses, L. L. Lohr, A. Maranzana, P. J. Stimac, T. L. Nguyen, and T. J. D. Kumar, University of Michigan, Ann Arbor, MI, <http://aoss.engin.umich.edu/multiwell/>.
- [42] H. Eyring, J. Chem. Phys. 3 (1935) 107–115.
- [43] C. Eckart, Phys. Rev. 35 (1930) 1303–1309.
- [44] J. Zádor, C.A. Taatjes, R.X. Fernandes, Prog. Energy Combust. Sci. 37 (2011) 371–421.
- [45] B.J. Lynch, P.L. Fast, M. Harris, D.G. Truhlar, J. Phys. Chem. A 104 (2000) 4811–4815.
- [46] C. Lee, W. Yang, R.G. Parr, Phys. Rev. B 37 (1988) 785–789.
- [47] C. Møller, M.S. Plesset, Phys. Rev. 46 (1934) 618–622.
- [48] CHEMKIN-PRO 15101, Reaction Design, San Diego, 2010.
- [49] J. Bugler, A. Rodriguez, O. Herbinet, et al., Proc. Combust. Inst 36 (2017) 441–448

# Chapter 6 : A single pulse shock tube study of pentene isomer pyrolysis

Published in: *Proc. Combust. Inst.*38(1) (2021) 881–889

DOI: <https://doi.org/10.1016/j.proci.2020.06.069>

## Author Contributions

- (1) Shashank S. Nagaraja: Design of the facility, experiments and manuscript preparation
- (2) Jennifer Power: Ab-initio calculations
- (3) Goutham Kukkadapu: Chemical kinetic modelling and manuscript preparation
- (4) Shijun Dong: Chemical kinetic modelling
- (5) Scott W. Wagnon: Chemical kinetic modelling
- (6) William J.Pitz: Project management and manuscript review
- (7) Henry J.Curran: Project management and manuscript review





## Abstract

A single-pulse shock tube study of the four pentene isomers is carried out at  $2 \pm 0.16$  bar and 900 – 1600 K. C<sub>1</sub> to C<sub>6</sub> species profiles were recorded using gas chromatography mass spectrometry analyses. The species are identified using mass spectrometry and quantified by flame ionisation detection. High-pressure limiting and pressure-dependent rate constants for 2M1B, 2M2B and 3M1B + H were calculated using RRKM theory with a Master Equation (ME) analysis using the Master Equation System Solver, MESS. A mechanism was formulated based on rate rules and theoretical calculations. Comparisons between experimental results and model simulations are provided for all of the five pentene isomers investigated with satisfactory agreement. Furthermore, an insight is provided into the influence of molecular structure on the reactivity of pyrolysis chemistry. Interestingly, it is found that the HACA mechanism is much less prominent for benzene formation compared to the role of cyclopentadienyl radical recombination with methyl radicals and also the recombination of propargyl radicals.

## 1. Introduction

Alkenes are one of the major components of commercial fuels and understanding their consumption reactions is important in producing more accurate predictions of their pyrolysis and oxidation in combustors. The oxidation of alkenes has been widely studied due to their importance as intermediates during ignition of alkanes and they are also known to impart higher octane sensitivity (RON – MON) in commercial fuels [1]. In addition, olefins are precursors to allene, propyne and isomers of butadiene which are known to be important intermediates to the formation of benzene and polycyclic aromatic hydrocarbons (PAHs) [2,3]. Furthermore, recent studies have shown the importance of C<sub>5</sub> species i.e. pentadiene isomers and cyclopentadiene [4–6] in the formation of benzene and naphthalene, among others. This explains our interest in studying the pyrolysis of C<sub>5</sub> species.

Although there have been a few studies related to the oxidation of 1-pentene [7–10], pyrolysis studies providing species profiles for reactants, intermediates and products are scarce. Tsang [11] performed a few 1-pentene pyrolysis experiments at 1000–1200 K during his study of cyclopentane but no further pyrolysis experiments are available. Manion and Awan [12] performed experiments of 2-pentene pyrolysis with hydrogen radical precursors in their study of the decomposition of pentyl radicals. Westbrook et al. [13] carried out an experimental and modelling study on 2-methyl-2-butene (2M2B) in a shock tube and in a jet-stirred reactor. Ruwe et al. [14] studied the consumption and hydrocarbon growth processes

in a 2M2B flame. Furthermore, in a different study, Ruwe et al. [15] studied and demonstrated the effect of molecular structure on sooting tendencies of *n*-pentane, 1-pentene and 2M2B. From our literature review it is clear that the pyrolysis of the C<sub>5</sub> olefins is not well studied and structural effects influencing the formation of aromatics are not clearly understood. Therefore we have studied the pyrolysis of the five pentene isomers in a single pulse shock-tube and carried out gas chromatography/mass spectrometry (GC-MS) analysis. Several important C<sub>1</sub>–C<sub>6</sub> intermediates were quantified which demonstrate the effect of fuel molecular structure on pyrolysis. Numerical simulations were conducted using a detailed kinetic model from NUIG, and the differences in the pyrolysis chemistry of the isomers, and the formation of benzene is discussed.

## 2. Experiments

Experiments were performed using the NUIG single pulse shock tube (SPST), Figure 6.1. The facility is described in detail in the Supplementary material (SM). 2M2B ( $\geq 95\%$ ) was obtained from Sigma Aldrich. Trans-2-pentene (*t*-2-C<sub>5</sub>H<sub>10</sub>,  $\geq 99\%$ ) was obtained from Fisher Scientific. 2M1B ( $\geq 98\%$ ) and 3M1B ( $\geq 95\%$ ) were obtained from TCI UK. Pure-shield argon (Ar) supplied by BOC Ireland was used as the bath gas. 99.99% pure krypton (Kr) obtained from Sigma Aldrich was used as an internal standard. 99.9% pure helium supplied by BOC Ireland was used as the driver gas for all experiments. For all experiments, mixtures containing the 2% fuel, 0.5% Kr and 97.5% Ar were prepared based on partial pressures in a 40 L mixing vessel. KJLC capacitance manometers were used to monitor pressure levels.

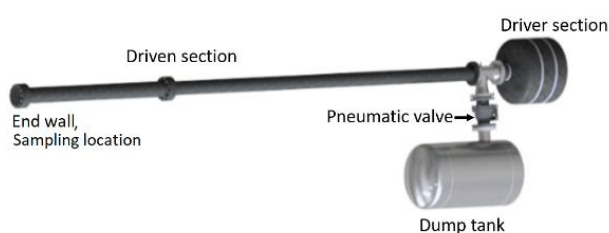


**Figure 6.1.** Schematic of the NUIG SPST.

The uncertainties in reflected temperatures are calculated based on the uncertainties in shock velocities and are approximately  $\pm 2\%$  based on calculations suggested by Petersen et al. [16]. Uncertainties in calibrated species concentration are approximately 10% and in estimated species concentrations, calculated using effective carbon number method [17], are approximately 20% respectively. The uncertainty in reactant mole fractions is  $\pm 0.02\%$ . The uncertainty in the residence time is  $\pm 2\%$ . The  $2\sigma$  variation in the calculated reflected

pressures is approximately 8%. The MS system is used to identify and quantify Kr and an FID is used for all other organic species. The sample is introduced into a GS-Gaspro column through a split/split-less inlet which is maintained at 200 °C. Helium is used as the carrier gas and a constant flow rate of 0.9 ml min<sup>-1</sup> is maintained through the column for all the experiments. The temperature programming of the GC was optimized for every fuel and the system was calibrated using a 23 gas GC standard obtained from BOC Ireland.

### 3. Kinetic Modelling

Simulations were performed using Chemkin-Pro [18] assuming a closed homogeneous batch reactor at constant volume. We used the residence time approach for all our simulations in the range 3–4 ms, with details provided as SM [19]. The mechanism used to simulate the data is provided as SM. Reaction rates for  $\dot{H}$ -atom abstraction by methyl ( $\dot{C}H_3$ ) radicals from the fuel were obtained using rate rule analogy as shown by Cai et al. [20]. Rates for  $\dot{H}$ -atom abstraction from primary, secondary and tertiary allylic sites were obtained from a theoretical study by Wang et al. [21].

#### 3.1. Computational Methods

The methods are similar to the ones in our previous studies of 1- and 2-pentene +  $\dot{H}$  [22] and 1,3-pentadiene +  $\dot{H}$  [23] and were adopted for all electronic structure calculations for the 2M1B, 2M2B and 3M1B +  $\dot{H}$  potential energy surfaces (PES), which is a current work-in-progress. Geometries of each minimum and transition state were optimised at the  $\omega$ B97XD/aug-cc-pVTZ level of theory. Single point energies for minima and transition states were calculated at the CCSD(T)/cc-pVXZ and MP2/cc-pVXZ, where X= D, T and Q, levels of theory, which were then extrapolated to the complete basis set limit using equation (1) [2]:

$$E_{\text{CCSD(T)/CBS}} = E_{\text{CCSD(T)/cc-pVTZ}} + (E_{\text{CCSD(T)/cc-pVTZ}} - E_{\text{CCSD(T)/cc-pVDZ}}) (3^4 / 4^4 - 3^4) + E_{\text{MP2/cc-pVQZ}} + (E_{\text{MP2/cc-pVQZ}} - E_{\text{MP2/cc-pVTZ}}) (4^4 / 5^4 - 4^4) - E_{\text{MP2/cc-pVTZ}} - (E_{\text{MP2/cc-pVTZ}} - E_{\text{MP2/cc-pVDZ}}) (3^4 / 4^4 - 3^4).$$

High-pressure limiting and pressure dependent rate constants were calculated using RRKM theory with Master Equation (ME) analysis using the Master Equation System Solver, MESS, [24] which are available in the mechanism file provided as SM.

Thermochemical values for the C<sub>5</sub> species were calculated as a function of temperature (298–2000 K), with enthalpies of formation determined using a series of isodesmic reactions as described in our previous work [22]. Temperature-dependent enthalpies, entropies and heat capacities were then calculated using traditional statistical thermodynamics methods as

implemented in MESSPF [24], with NASA polynomials fitted using PAC99 [25], which are provided as SM.

## 4. Results and discussions

In this section, we first present comparisons of the experimental and simulated mole fractions of the fuel and intermediates for the five pentene isomers. Thereafter, by comparing the mole fractions of the intermediates produced during the pyrolysis of the five isomers, we analyze the effect of molecular structure on the pyrolysis chemistry.

### 4.1. 1-Pentene

Experimental data for 1-pentene ( $1-C_5H_{10}$ ) is taken from our article on the pyrolysis of 1-alkenes [26]. The current mechanism's predictions are shown in Figure 6.2. A reaction flux diagram (RFD) for 1-pentene pyrolysis at 1243 K is provided in Figure 6.3.

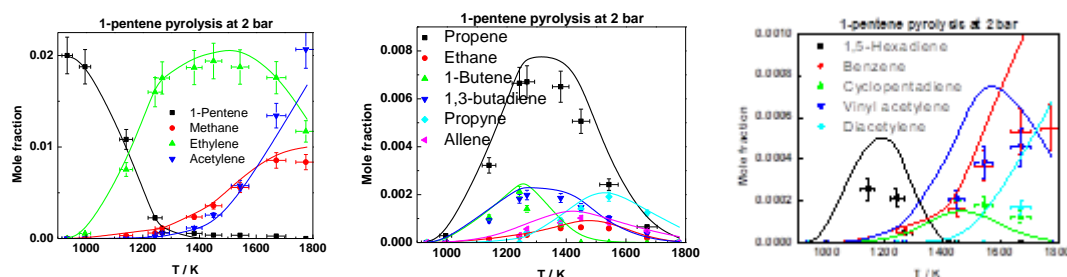


**Figure 6.2.** Species profiles for 1-pentene pyrolysis. Solid lines: model simulations.

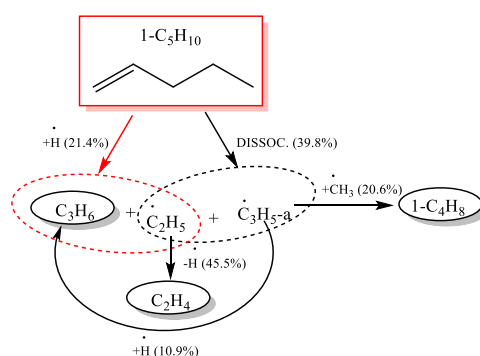


**Figure 6.3.** RFD for 1-pentene pyrolysis at ~50% fuel consumption, 2.13 bar, 1243 K.

Based on kinetic simulations, 1-pentene decomposes to form either allyl and an ethyl radical or undergoes a retro-ene reaction to produce ethylene and propene. Bimolecular reactions of 1-pentene with  $\dot{H}$  atoms can produce propene ( $C_3H_6$ ) and ethyl radicals ( $\dot{C}_2H_5$ ) or ethylene ( $C_2H_4$ ) and *n*-propyl ( $n-\dot{C}_3H_7$ ) radicals. H-atom abstraction from 1-pentene produces

1-penten-3-yl ( $\dot{C}_5H_9$ 1-3) radicals which dissociate into 1,3-butadiene (1,3- $C_4H_6$ ) and methyl radicals. Allyl radicals ( $\dot{C}_3H_5$ -a) decompose to form allene ( $C_3H_4$ -a) and  $\dot{H}$  atoms and/or their self-disproportionation reaction produces allene and propene. They can also undergo radical-recombination reaction with  $\dot{C}H_3$  radicals to form 1-butene (1- $C_4H_8$ ). The self-recombination of methyl radicals and the allyl + ethyl disproportionation reaction are the main sources of ethane ( $C_2H_6$ ). Propyne ( $C_3H_4$ -p) is produced via the isomerisation of allene. Methane ( $CH_4$ ) is produced via H-atom abstraction by  $\dot{C}H_3$  radicals from the fuel and other stable intermediate species. Acetylene ( $C_2H_2$ ) is produced from the dissociation of vinyl radicals and the bimolecular reactions of allene and propyne with  $\dot{H}$  atoms.

## 4.2. Trans-2-pentene

Pyrolysis experiments of t-2- $C_5H_{10}$  were carried out at 2 bar in the range of 900–1500 K. The major products are methane, ethane, ethylene, acetylene, propene, 1-butene, 1,3-butadiene, allene and propyne. The species profiles are illustrated in Figure 6.4. We found two  $C_5H_8$  species but could not distinguish them as the mass spectra of pentadienes are similar. However, from studies by Manion and Awan [12], one species can be assigned 1,3-pentadiene and the other could be cyclopentene. We also observe the formation of cis-2-pentene (c-2- $C_5H_{10}$ ). We believe this could be similar to the cis-trans isomerisation of 2-butene as discussed by Lifshitz et al. [27]. An earlier ignition delay time study on 2-butenes [28] had shown that the reactivities were similar for the cis and trans isomers and therefore, the current mechanism includes one species to represent both.

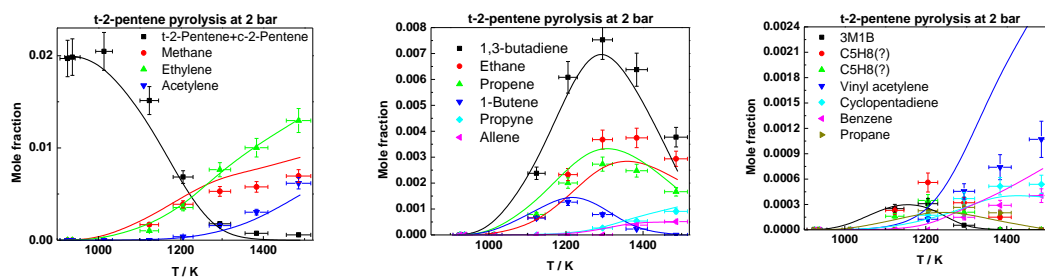


**Figure 6.4.** Species profiles for t-2-pentene pyrolysis. Solid lines: model simulations.

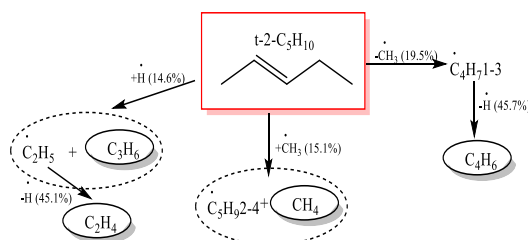


**Figure 6.5.** RFD for t-2-pentene pyrolysis at ~50% fuel consumption, 2.01 bar, 1205.4 K.

A reaction pathway analysis diagram for t-2-pentene pyrolysis is provided in Figure 6.5. Trans-2-pentene can decompose into  $\dot{\text{C}}\text{H}_3$  and 1-buten-3-yl ( $\dot{\text{C}}_4\text{H}_7\text{1-3}$ ) radicals,  $\dot{\text{C}}_4\text{H}_7\text{1-3}$  subsequently produces 1,3-butadiene via H-atom elimination. The fuel and intermediates can undergo  $\dot{\text{H}}$ -atom abstraction by  $\dot{\text{C}}\text{H}_3$  radicals to form methane. The reaction of 2-pentene with  $\dot{\text{H}}$  atoms produces propene and ethyl radicals. Ethyl radicals undergo  $\beta$ -scission to produce ethylene and  $\dot{\text{H}}$  atoms. Ethane is produced via  $\dot{\text{C}}\text{H}_3$  radical self-recombination. Acetylene formation channels are similar to those for 1-pentene as discussed earlier.

### 4.3. 2-methyl-1-butene

2-methyl-1-butene pyrolysis study was carried out at 2 bar in the range of 900 – 1600 K. The major products are methane, ethane, ethylene, acetylene, propene, allene, propyne, iso-butene (i-C<sub>4</sub>H<sub>8</sub>), 1,3-butadiene and isoprene (2M13BDE). Species profiles are shown in Figure 6.6.

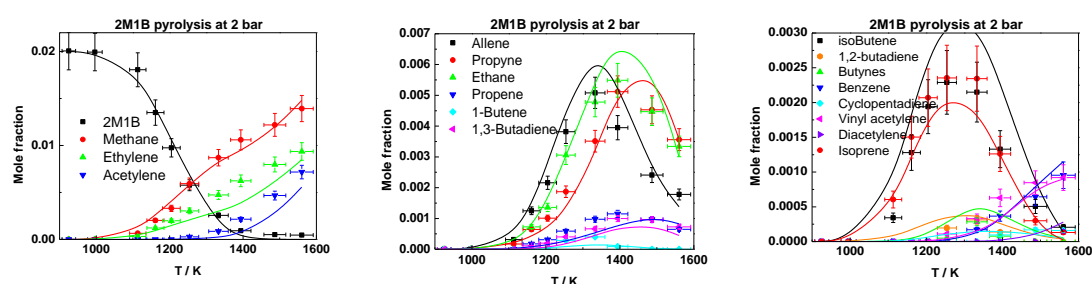


**Figure 6.6.** Species profiles for 2M1B pyrolysis. Solid lines: model simulations.

2M1B can dissociate into 2-methyl-allyl (i- $\dot{\text{C}}_4\text{H}_7$ ) and methyl radicals or can react with  $\dot{\text{H}}$  atoms to form isobutene. It can also undergo H-atom abstraction by  $\dot{\text{C}}\text{H}_3$  radicals or  $\dot{\text{H}}$  atoms from the primary and secondary allylic site to form 2-methyl-1-butenyl ( $\text{a}\dot{\text{C}}_5\text{H}_9\text{-a2}$ ) and 2-methyl-1-buten-3-yl ( $\text{a}\dot{\text{C}}_5\text{H}_9\text{-c}$ ) radicals, respectively.  $\text{a}\dot{\text{C}}_5\text{H}_9\text{-c}$  radicals dissociate to form isoprene and  $\text{a}\dot{\text{C}}_5\text{H}_9\text{-a2}$  radicals dissociate to form allene and ethyl radicals. Also, 2-methyl-allyl radicals decompose to form allene and  $\dot{\text{C}}\text{H}_3$  radicals.  $\text{a}\dot{\text{C}}_5\text{H}_9\text{-a2}$  radicals can isomerise to form 2-methyl-1-buten-4-yl ( $\text{a}\dot{\text{C}}_5\text{H}_9\text{-d}$ ) radicals. These dissociate to form ethylene and propen-2-yl ( $\dot{\text{C}}_3\text{H}_5\text{-t}$ ) radicals which in turn dissociate to form propyne and  $\dot{\text{H}}$  atoms. Propyne is also formed by isomerisation of allene. Methane, ethane, ethylene and acetylene formation reactions are similar to those for the linear pentenes. The RFD for 2M1B pyrolysis is shown in Figure 6.7.

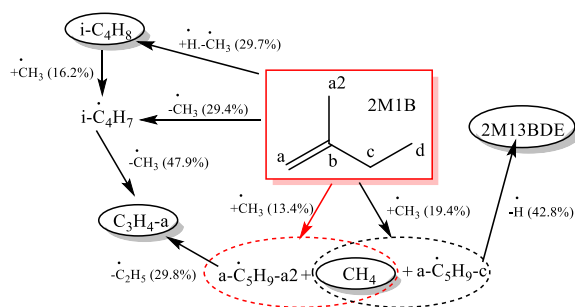


**Figure 6.7.** RFD for 2M1B pyrolysis at  $\sim 50\%$  fuel consumption, 2.01 bar, 1254.2 K.

#### 4.4. 2-methyl-2-butene

A pyrolysis study was carried out at 2 bar and in the temperature range of 900–1750 K and the major species are identical to 2M1B pyrolysis, Figure 6.8. 2M2B and isoprene co-elute in the GC capillary column used in this study and could not be separated, so for comparison we show the sum of the two molecules in both experiments and simulations.

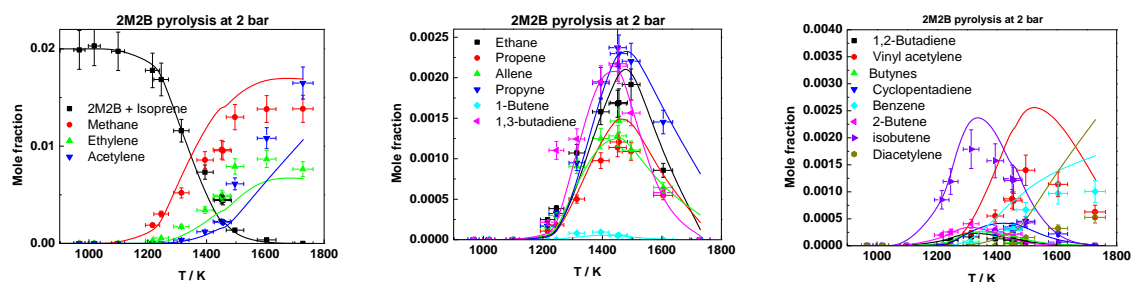


**Figure 6.8.** Species profile for 2M2B pyrolysis. Solid lines: model simulations.

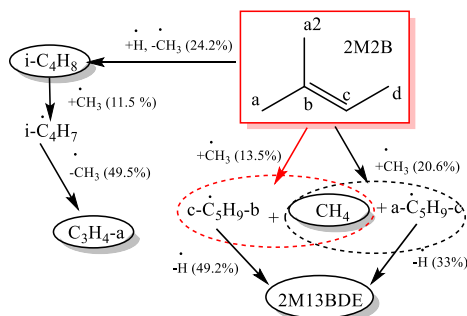


**Figure 6.9.** RFD for 2M2B pyrolysis at  $\sim 50\%$  fuel consumption, 2.13 bar, 1451.2 K.

2M2B ( $\text{b-C}_5\text{H}_{10}$ ) can undergo H-atom abstraction by  $\dot{\text{H}}$  atoms and  $\dot{\text{C}}\text{H}_3$  radicals from three primary allylic sites to form isopentenyl radicals. These radicals form isoprene via H-elimination. 2M2B can also react with  $\dot{\text{H}}$  atoms to produce isobutene and methyl radicals. Isobutene dissociates to methyl-allyl ( $\dot{\text{C}}_4\text{H}_7$ ) radicals which further dissociate to form allene and  $\dot{\text{C}}\text{H}_3$  radicals. The current mechanism under-predicts the formation of 1,3-C<sub>4</sub>H<sub>6</sub> by a factor of two. Propene is formed from isopentenyl radicals and isobutene. Ethane, ethylene,

methane and acetylene formation pathways for 2M1B and 2M2B are the same. An RFD for 2M2B pyrolysis is illustrated in Figure 6.9.

#### 4.5. 3-methyl-1-butene

3M1B has a tertiary-allylic hydrogen and it enabled the study of the rate law for such H-atom abstractions. 3M1B pyrolysis study was carried out at 2 bar and 800 – 1450 K. Methane, ethane, ethylene, acetylene, propene, 2-butene, 1,3-butadiene, 2-pentene and isoprene are major products. Species profiles with respect to temperature are illustrated in Figure 6.10.

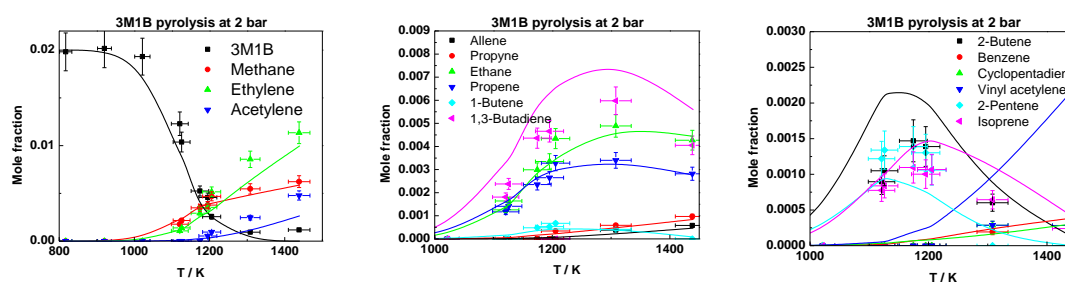


**Figure 6.10.** Species profile for 3M1B pyrolysis. Solid lines: model simulations.

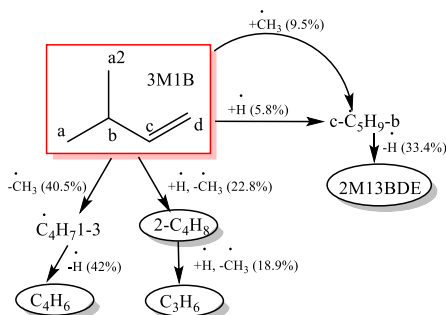


**Figure 6.11.** RFD for 3M1B pyrolysis at ~50% fuel consumption, 2.01 bar, 1205 K.

3M1B ( $c\text{-C}_5\text{H}_{10}$ ) can either decompose to 1-buten-3-yl ( $\dot{\text{C}}_4\text{H}_7\text{1-3}$ ) radicals or react with  $\dot{\text{H}}$  atoms to form 2-butene ( $2\text{-C}_4\text{H}_8$ ). 3M1B can also undergo H-atom abstraction by  $\dot{\text{H}}$  atoms or  $\dot{\text{C}}\text{H}_3$  radicals from the tertiary allylic site to form isopentenyl radicals which dissociate to isoprene.  $\dot{\text{C}}_4\text{H}_7\text{1-3}$  radicals dissociate to 1,3-butadiene via  $\beta$ -scission. 2-butene reacts with  $\dot{\text{H}}$  atoms to form propene and methyl radicals. Ethylene is formed from  $c\text{-C}_5\text{H}_{10} + \dot{\text{H}}$ ,  $1,3\text{-C}_4\text{H}_6 + \dot{\text{H}}$  and ethyl radical decomposition reactions. Ethane, methane and acetylene formation reactions are similar to all of the other pentenes. An RFD at 1205 K is provided as Figure 6.11.

## 5. Discussion

### 5.1. Fuel reactivities and ethylene formation

From our experimental measurements, we were able to determine that the predicted reactivities of all of the pentenes are sufficiently accurate, Figure 6.12. The reactivities appear



to decrease with increasing number of allylic hydrogen atoms. 3M1B, with only tertiary allylic hydrogen has the highest reactivity and 2M2B with nine primary allylic hydrogen atoms has the lowest reactivity, while linear pentenes with secondary allylic hydrogen atoms show intermediate reactivity.

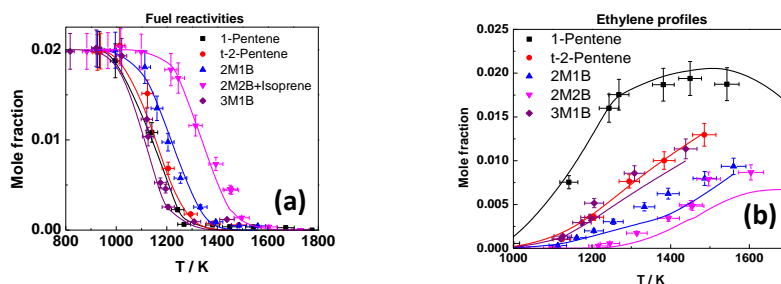


**Figure 6.12.** (a) Fuel reactivities for pentenes, (b) Ethylene formation. Solid lines: model simulations.

Ethylene is one of the initial stable products, with its concentrations and shape being significantly higher and different for 1-pentene corroborating the presence of the retro-ene reaction. For the other isomers, 3M1B and t-2-pentene show similar concentrations due to their initial unimolecular decomposition reactions producing  $\dot{\text{C}}\text{H}_3 + \dot{\text{C}}_4\text{H}_7\text{-1-3} \rightarrow 1,3\text{-C}_4\text{H}_6 + \dot{\text{H}} \rightarrow \text{C}_2\text{H}_4 + \dot{\text{C}}_2\text{H}_3$  and  $\dot{\text{C}}\text{H}_3 + \dot{\text{C}}\text{H}_3 \rightarrow \text{C}_2\text{H}_6 \rightarrow \text{CH}_4/\text{H}_2 + \dot{\text{C}}_2\text{H}_5 \rightarrow \text{C}_2\text{H}_4 + \dot{\text{H}}$ .

## 5.2. Formation of benzene and aromatic precursors

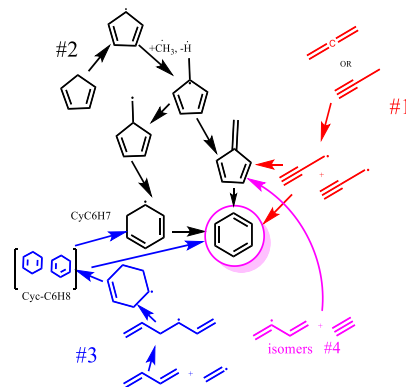


**Figure 6.13.** Benzene formation pathways.

The reactions illustrated in Figure 6.13 show some of the important reactions of the C<sub>3</sub>–C<sub>5</sub> intermediates forming benzene. We compared the concentrations of these intermediates and conducted flux analyses to illustrate how the important pathways for benzene changes with isomer molecular structure. Trans-2-pentene and 3M1B produce higher concentrations of 1,3-butadiene due to their initial unimolecular decomposition into 1-buten-3-yl radical, Figure 6.14(a). At > 90% fuel consumption, the amount of

cyclopentadiene produced is higher for 2M2B and t-2-pentene compared to the other isomers, Figure 6.14(b). This appears to show the significance of the location of the double bond on the formation of cyclopentadiene.

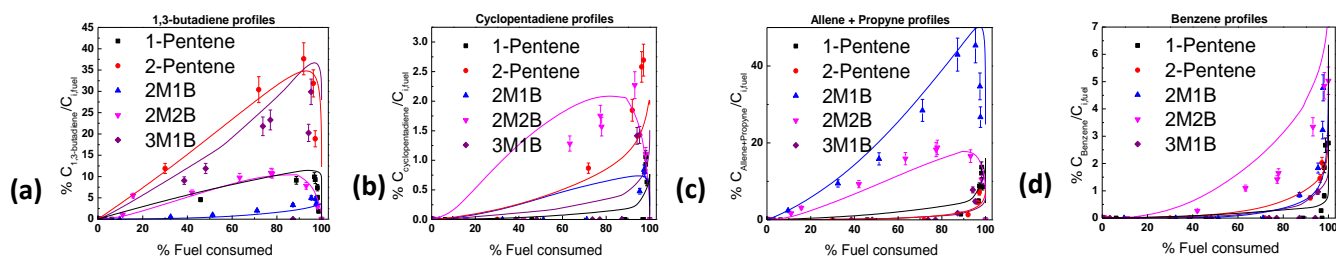


**Figure 6.14.** Experiment results for (a) 1,3-butadiene concentration; (b) Cyclopentadiene concentration; (c) Allene and propyne total concentration; (d) Benzene concentration. Fuel consumed is calculated as (initial fuel concentration – final fuel concentration)/initial fuel concentration at a given temperature. This aids in offsetting the effect of fuel reactivity.

The concentrations of allene and propyne is higher in the pyrolysis of 2M1B, Figure 6.6 , owing to the unimolecular decomposition of the fuel to 2-methyl-allyl radicals and abstraction from the primary allylic site, both of which undergo  $\beta$ -scission to produce allene, Figure 6.14(c). 2M2B also produces lower amounts of allene and propyne compared to 2M1B due to the absence of a direct route to the formation of 2-methyl-allyl radical, Figure 6.8. An efficient way to allene and propyne is through abstractions from isobutene, produced from  $2M2B + \dot{H} = \text{isobutene} + \dot{C}H_3$ , to produce 2-methyl-allyl radicals and subsequent decomposition of these to allene +  $\dot{C}H_3$ . The absence of a direct pathway to the formation of 2-methyl-allyl radicals explains the difference in concentrations of the C<sub>3</sub>H<sub>4</sub> isomers produced during the pyrolysis of 2M1B and 2M2B. Interestingly, the concentrations of benzene presented in Figure 6.14(d) shows that 2M2B produces more benzene than all of the other isomers. Also, the predictions from the mechanism are satisfactory.

To gain insights into the effect of molecular structure on pyrolysis chemistry, we conducted an integrated reaction path analysis of the different pathways to identify differences in the chemistry producing benzene, Figure 6.15. It can be seen that propargyl recombination is important for benzene formation. Moreover, the  $\dot{C}_5H_5 + \dot{C}H_3$  reaction pathway is crucial for benzene formation irrespective of the geometry of the molecule. Furthermore, vinyl addition to 1,3-butadiene seems important for linear pentenes and for 3M1B. Interestingly, the HACA mechanism is relatively less important than the propargyl

pathway [29] as the bimolecular reaction of 1,3-butadiene with  $\dot{\text{H}}$  atoms to produce ethylene and vinyl radicals dominates over H-atom abstraction by  $\dot{\text{H}}$  atoms [30].

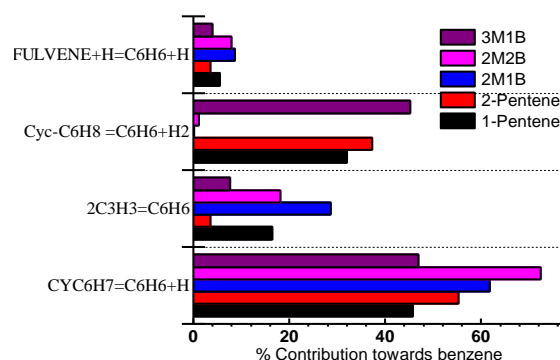


**Figure 6.15.** Relative ROP of Benzene at 1400 K and 2 bar.

## 6. Conclusions

A SPST pyrolysis study was carried out on t-2-pentene, 2M1B, 2M2B and 3M1B at 2 bar. Species were identified using GC-MS and were quantified using an FID. High-pressure limiting and pressure dependent rate constants for 2M1B, 2M2B and 3M1B +  $\dot{\text{H}}$  were calculated using RRKM theory with Master Equation (ME) analysis. A mechanism was formulated based on rate rules and the theoretical calculations. Comparisons between experimental and simulated results show that the predictions for all of the major species are satisfactory. Furthermore, reactivities of the fuels studied clearly show the influence of molecular geometry on unimolecular dissociation and H-atom abstractions from different allylic sites. Also, the molecular geometry impacts the benzene formation pathways and this study shows that 2M2B produces more benzene than other pentenes. In addition, the HACA mechanism has a relatively lower prominence for benzene formation compared to other pathways.

## Acknowledgements

The authors would like to acknowledge Science Foundation Ireland for funding via project numbers 15/IA/3177 and 16/SP/3829. The work at LLNL was performed under the auspices of the U.S. Department of Energy (DOE), Contract DE-AC52-07NA27344, and was supported by the U.S. Department of Energy, Vehicle Technologies Office, program managers, Mike Weismiller and Gurpreet Singh.

## References

- [1] M. Mehl, T. Faravelli, F. Giavazzi, et al., *Energy Fuels*. 20 (2006) 2391–2398. doi:10.1021/ef060339s.
- [2] J.A. Miller, S.J. Klippenstein, *J. Phys. Chem. A*. 107 (2003) 7783–7799. doi:10.1021/jp030375h.
- [3] H. Wang, M. Frenklach, *Combust. Flame*. 110 (1997) 173–221. doi:10.1016/S0010-2180(97)00068-0.
- [4] S. Sharma, W.H. Green, *J. Phys. Chem. A*. 113 (2009) 8871–8882. doi:10.1021/jp900679t.
- [5] C. Cavallotti, D. Polino, A. Frassoldati, E. Ranzi, *J. Phys. Chem. A*. 116 (2012) 3313–3324. doi:10.1021/jp212151p.
- [6] L. Ruwe, L. Cai, K. Moshhammer, N. Hansen, H. Pitsch, K. Kohse-Höinghaus, *Combust. Flame*. (2019) 411–423. doi:10.1016/j.combustflame.2019.05.013.
- [7] G. González Alatorre, H. Böhm, B. Atakan, K. Kohse-Höinghaus, *Z. Phys. Chem.* 215 (2001) 981–995. doi:10.1524/zpch.2001.215.8.981.
- [8] R. Minetti, A. Roubaud, E. Therssen, M. Ribaucour, L. Sochet, *Combust. Flame*. 118 (1999) 213–220. doi:10.1016/S0010-2180(98)00151-5.
- [9] Y. Cheng, E. Hu, X. Lu, X. Li, J. Gong, Q. Li, Z. Huang, *Proc. Combust. Inst.* 36 (2017) 1279–1286. doi:10.1016/J.PROCI.2016.08.026.
- [10] S. Touchard, F. Buda, G. Dayma, P.A. Glaude, R. Fournet, F. Battin-Leclerc, *Int. J. Chem. Kinet.* 37 (2005) 451–463. doi:10.1002/kin.20096.
- [11] W. Tsang, *Int. J. Chem. Kinet.* 10 (1978) 599–617. doi:10.1002/kin.550100607.
- [12] J.A. Manion, I.A. Awan, *Proc. Combust. Inst.* 34 (2013) 537–545. doi:10.1016/j.proci.2012.05.078.
- [13] C.K. Westbrook, W.J. Pitz, et al., *J. Phys. Chem. A*. 119 (2015) 7462–7480. doi:10.1021/acs.jpca.5b00687.
- [14] L. Ruwe, K. Moshhammer, N. Hansen, K. Kohse-Höinghaus, *Combust. Flame*. 175 (2017) 34–46. doi:10.1016/j.combustflame.2016.06.032.
- [15] L. Ruwe, K. Moshhammer, N. Hansen, K. Kohse-Höinghaus, *Phys. Chem. Chem. Phys.* 20 (2018) 10780–10795. doi:10.1039/C7CP07743B.
- [16] E.L. Petersen, M.J.A. Rickard, M.W. Crofton, E.D. Abbey, M.J. Traum, D.M. Kalitan, *Meas. Sci. Technol.* 16 (2005) 1716–1729. doi:10.1088/0957-0233/16/9/003.
- [17] J.T. Scanlon, D.E. Willis, *J. Chromatogr. Sci.* 23 (1985) 333–340. doi:10.1093/chromsci/23.8.333.
- [18] R. CHEMKIN-PRO, 15112, Reaction Design, Inc., San Diego, CA. (2011).
- [19] X. Han, J.M. Mehta, K. Brezinsky, *Combust. Flame*. 209 (2019) 1–12. doi:10.1016/j.combustflame.2019.07.022.
- [20] L. Cai, H. Pitsch, S.Y. Mohamed, V. Raman, J. Bugler, H. Curran, S.M. Sarathy, *Combust. Flame*. 173 (2016) 468–482. doi:10.1016/j.combustflame.2016.04.022.
- [21] K. Wang, S.M. Villano, A.M. Dean, *Phys. Chem. Chem. Phys.* 17 (2015) 6255–6273. doi:10.1039/c4cp05308g.
- [22] J. Power, K.P. Somers, C.-W. Zhou, S. Peukert, H.J. Curran, *J. Phys. Chem. A*. (2019). doi:10.1021/acs.jpca.9b06378.
- [23] Y. Sun, C.-W. Zhou, K.P. Somers, H.J. Curran, *J. Phys. Chem. A*. (2019). doi:10.1021/acs.jpca.9b06628.
- [24] Y. Georgievskii, J.A. Miller, M.P. Burke, S.J. Klippenstein, *J. Phys. Chem. A*. 117 (2013) 12146–12154. doi:10.1021/jp4060704.
- [25] B.J. McBride, S. Gordon, Computer program for calculating and fitting thermodynamic functions, (1992).

- [26] S.S. Nagaraja, J. Liang, S. Dong, S. Panigrahy, A.B. Sahu, G.Kukkadapu, W.J. Pitz, H.J. Curran, *Combust. Flame* 219 (2020) 456–466.
- [27] A. Lifshitz, S.H. Bauer, E.L. Resler, *J. Chem. Phys.* 38 (1963) 2056–2063. doi:10.1063/1.1733933.
- [28] Y. Li, C.W. Zhou, K.P. Somers, K. Zhang, H.J. Curran, *Proc. Combust. Inst.* 36 (2017) 403–411. doi:10.1016/j.proci.2016.05.052.
- [29] J.A. Miller, C.F. Melius, *Combust. Flame.* 91 (1992) 21–39. doi:10.1016/0010-2180(92)90124-8.
- [30] Y. Li, S.J. Klippenstein, C.-W. Zhou, H.J. Curran, *J. Phys. Chem. A.* 121 (2017) 7433–7445. doi:10.1021/acs.jpca.7b05996.



# Chapter 7 : General conclusions and future work

## 1. Conclusions

*This thesis* mainly focuses on the ab-initio and modelling studies of the reactions of  $\dot{\text{H}}$  atom addition to and H-atom abstraction by  $\dot{\text{H}}$  atoms from  $\text{C}_2$ – $\text{C}_5$  unsaturated alkenes. These include ethylene, propene, 1-butene, 2-butene, isobutene, 1-pentene, 2-pentene, 2-methyl-1-butene, 2-methyl-2-butene, and 3-methyl-1-butene. Another work involved the study of cyclisation reactions of hydroperoxyl-alkyl radicals forming cyclic ethers and hydroxyl radicals, (Chapter 5). Chapter 6 entitled “A single pulse shock-tube study of pentene isomer pyrolysis” includes results from Chapter 3, “ A Theoretical Study of the Reaction of Hydrogen Atoms with Three Pentene Isomers; 1-Methyl-1-Butene, 2-Methyl-2-Butene, and 3-methyl-1-Butene”.

For the reactions of  $\dot{\text{H}}$  atoms with  $\text{C}_2$  –  $\text{C}_5$  unsaturated alkenes, the associated thermochemical values of the species involved were calculated as a function of temperature (298 – 2000 K), with the enthalpies of formation determined using a network of isodesmic reactions. The density functional theory (DFT)  $\omega\text{B97XD}$  method coupled with the aug-cc-pVTZ basis set was used for geometry optimisations and frequency analyses. Low-frequency torsional modes were treated via relaxed PES scans in 10-degree increments using the  $\omega\text{B97XD}/6\text{-}311\text{++G(d,p)}$  method, with the potential energies as a function of dihedral angle used as input for a one-dimensional (1-D) hindered rotor approximation as implemented in the Master Equation System Solver (MESS). To compute barrier heights, single point energies for minima and transition states were calculated at the coupled cluster level, specifically (CCSD(T)) and Møller-Plesset perturbation theory (MP2), with cc-pVTZ basis sets, where X = D, T and Q levels of theory. High-pressure limiting and pressure-dependent rate constants were calculated using Rice-Ramsperger-Kassel-Marcus (RRKM) theory coupled with a one-dimensional (1-D) master equation (ME).

As a validation of the theoretical results calculated in *this thesis*, the results were implemented into chemical kinetic models (AramcoMech3.0, NUIGMech1.0 and NUIGMech1.2) and simulations were compared to new hydrogen atomic resonance absorption spectrometry ( $\dot{\text{H}}$ -ARAS) experimental measurements taken as part of a collaboration with Dr. Sebastian Peukert at Duisburg-Essen University. These experiments serve as direct validation targets for our calculation results, with good agreement being observed. Moreover, pyrolysis experiments of linear and branched 1-alkenes using the single

pulse shock tube at NUIG were performed, and serve as in-direct validation targets. It was found that both H-atom abstraction reactions and chemical activation pathways are important in capturing the species mole fractions of the products of pyrolysis.

In Chapter 5, rate constants for the low-temperature reaction class: cyclisation of hydroperoxyl-alkyl ( $\dot{Q}OOH$ ) radicals to form cyclic ethers and hydroxyl radicals ( $\dot{Q}OOH \leftrightarrow$  cyclic ether +  $\dot{O}H$ ) were calculated, involving species ranging in size from  $C_2H_5\dot{O}_2$  to  $C_5H_{11}\dot{O}_2$ . The rate constants were determined using density functional theory (DFT) and ab initio approaches. The use of these rate coefficients in the NUIG pentane oxidation model produces favourable agreement with  $C_5$  cyclic ether concentration measurements in JSRs at Nancy and Orléans. These had previously been over-predicted by the model utilising literature rate constant values.

## 2. Future Work

- (1) *This thesis* mainly focused on the reactions of  $\dot{H}$ -atoms with  $C_2$ – $C_5$  alkenes. Studies including  $\dot{O}H$  and  $H\dot{O}_2$  radical addition and abstraction from larger alkenes such as the branched pentene isomers would be useful in exploring the oxidation chemistry of larger branched alkenes, particularly at practical combustor conditions.
- (2) Chapter 3 presents the work on the reactions of  $\dot{H}$  atoms with three branched pentene isomers. Test calculations implied that variational effects were effectively negligible for isomerisation and H-atom abstraction reactions. However, for  $\dot{H}$  atom addition reactions our calculations are over-estimated by a factor of 2–3. Therefore, although good agreement is observed between our model predictions and experiment, future works should include variational transition-state theory, treatment of multi-dimensional torsions, and an-harmonic effects in order to develop a more comprehensive RRKM/ME model for combustion.
- (3) Direct experimental validation targets for the reactions of  $\dot{H}$  atoms with the branched butene and pentene isomers such as  $\dot{H}$ -ARAS experiments like those presented in Chapter 2 would be useful as additional validation targets.



## Appendix A

### Supplementary Material: A Theoretical, Experimental and Modelling Study of the Reaction of Hydrogen Atoms with 1- and 2-Pentene

#### A.1 Experimental Conditions

**Table AS1:** Experimental Mixture Compositions for  $\dot{H}$ -ARAS Experiments. Argon was used as the Diluent Gas. Reactant Mole Fractions are Expressed as ppm.

Mixture	C <sub>2</sub> H <sub>5</sub> I	C <sub>5</sub> H <sub>10</sub> -1	C <sub>5</sub> H <sub>10</sub> -2	<i>p</i> (atm)	<i>T</i> / K
A	0.34	0.00	8.49	1.48	980
				1.56	1032
				1.50	1044
				1.56	1055
B	0.35	8.90	0.00	1.45	985
				1.50	1031
				1.47	1046

**Table AS2:** Mixtures Compositions from Literature Studies [1-3]: the Remaining Balance is Argon

Author	Mixture	Components in mixtures ( $\mu\text{L/L}$ )					
		1-C <sub>5</sub> H <sub>11</sub> I	CCP	13DMB	135TMB	HME	(E)-2-C <sub>5</sub> H <sub>10</sub>
Awan [1]	A	290	150	10800	–	–	–
	B	190	100	–	8500	–	–
	C	200	100	–	4000	–	–
	D	50	100	–	4200	–	–
	E	50	100	–	4600	–	–
Comandini [2] (UIC)	A	45.7	–	–	–	–	–
	B	49.8	–	–	–	–	–
	C	95.2	–	–	–	–	–
	D	98.3	–	–	–	–	–
Comandini [2] (NIST)	A	40	–	–	–	–	–
Manion [3]	A	–	75	–	5896	46	4083
	B	–	75	–	3937	45	6230

1-C<sub>5</sub>H<sub>11</sub>I = 1-iodopentane, CCP = chlorocyclopentane, 13DMB = 1,3-dimethylbenzene, 135TMB = 1,3,5-trimethylbenzene, HME = hexamethylethane.

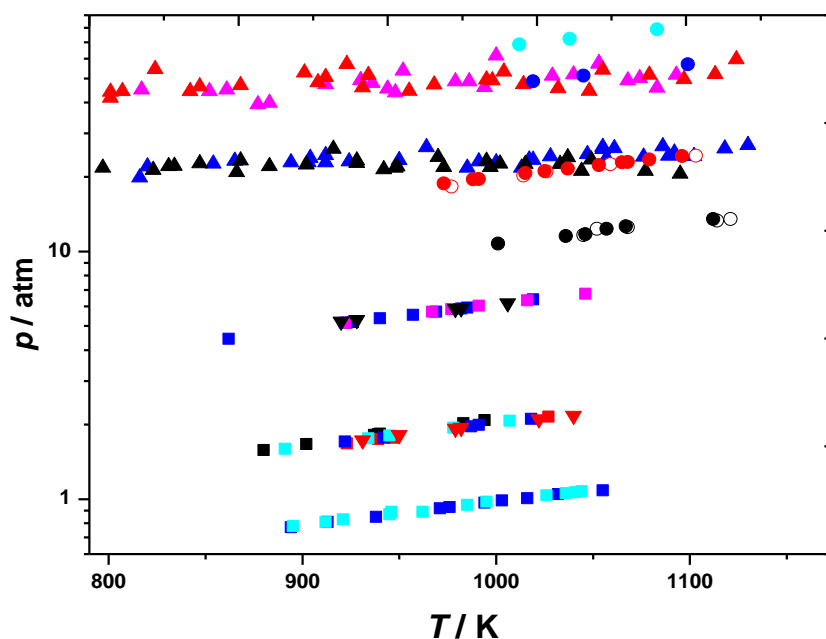


**Figure AS1.** Temperature and pressure ranges of the experiments carried out by Awan [1] (■), Comandini [2] – UIC (▲), Comandini [2] – NIST (▼) and Manion [3] (●). Manion [3] closed ● represents mixture A, while open ● represents mixture B. Mixture A (black), mixture B (red), mixture C (blue), mixture D (magenta), mixture E (cyan). Where there are more than one composition for a mixture: mixture A1 (black), A2 (red), A3 (blue), A4 (cyan). B1 (black), B2 (red).

## A.2 Theoretical Energies

**Table AS3:** Formation Enthalpies. Zero-point energy corrected 0 K Enthalpies and ZPE's (kJ/mol) for Species on  $C_5H_{11}$  PES based on the CBS extrapolations reported in the main text. \*RO-aug-cc-pVXZ energies. <sup>a</sup> equatorial conformer, <sup>b</sup> axial conformer, <sup>c</sup> syn conformer, <sup>d</sup> anti conformer.

Species	*Enthalpy / kJ mol <sup>-1</sup>	Enthalpy / kJ mol <sup>-1</sup>	ZPE/kJ/mol
H	216.03	216.03	0.0
H <sub>2</sub>	-0.96	-1.51	26.52
CH <sub>3</sub>	149.63	150.49	78.24
C <sub>2</sub> H <sub>4</sub>	63.40	65.86	134.66
C <sub>2</sub> H <sub>5</sub>	132.74	134.94	156.16
C <sub>3</sub> H <sub>6</sub>	39.06	42.44	210.19
C <sub>3</sub> H <sub>7</sub> -1	121.82	125.01	233.14
C <sub>4</sub> H <sub>8</sub> -1	27.05	31.33	286.12
C <sub>5</sub> H <sub>9</sub> -11	–	263.29	324.59
C <sub>5</sub> H <sub>9</sub> -12	–	248.58	324.95
C <sub>5</sub> H <sub>9</sub> -13	146.76	154.85	324.69
C <sub>5</sub> H <sub>9</sub> -14	–	210.16	322.00
C <sub>5</sub> H <sub>9</sub> -15	–	220.33	321.90
C <sub>5</sub> H <sub>9</sub> -22	–	241.40	324.36
C <sub>5</sub> H <sub>9</sub> -23	–	242.22	325.32
C <sub>5</sub> H <sub>9</sub> -24	134.66	142.97	322.88
C <sub>5</sub> H <sub>9</sub> -25	–	210.81	320.32
C <sub>5</sub> H <sub>10</sub> -1	13.34	18.50	361.64
C <sub>5</sub> H <sub>10</sub> -2	3.01	8.16	360.42
C <sub>5</sub> H <sub>11</sub> -1	92.39	97.41	382.30
C <sub>5</sub> H <sub>11</sub> -2	81.21	86.40	382.26
C <sub>5</sub> H <sub>11</sub> -3	82.31	87.57	382.46
C <sub>5</sub> H <sub>10</sub> -1+H⇌C <sub>5</sub> H <sub>9</sub> -11+H <sub>2</sub>	–	299.04	354.70
C <sub>5</sub> H <sub>10</sub> -1+H⇌C <sub>5</sub> H <sub>9</sub> -12+H <sub>2</sub>	–	286.43	354.02
C <sub>5</sub> H <sub>10</sub> -1+H⇌C <sub>5</sub> H <sub>9</sub> -13+H <sub>2</sub>	251.27	256.84	354.77
C <sub>5</sub> H <sub>10</sub> -1+H⇌C <sub>5</sub> H <sub>9</sub> -14+H <sub>2</sub>	–	265.61	353.94
C <sub>5</sub> H <sub>10</sub> -1+H⇌C <sub>5</sub> H <sub>9</sub> -15+H <sub>2</sub>	–	275.40	354.48
C <sub>5</sub> H <sub>10</sub> -2+H⇌C <sub>5</sub> H <sub>9</sub> -13+H <sub>2</sub>	247.98	253.94	353.93
C <sub>5</sub> H <sub>10</sub> -2+H⇌C <sub>5</sub> H <sub>9</sub> -22+H <sub>2</sub>	–	277.92	353.39
C <sub>5</sub> H <sub>10</sub> -2+H⇌C <sub>5</sub> H <sub>9</sub> -23+H <sub>2</sub>	–	277.69	353.61
C <sub>5</sub> H <sub>10</sub> -2+H⇌C <sub>5</sub> H <sub>9</sub> -24+H <sub>2</sub>	240.00	245.60	353.66
C <sub>5</sub> H <sub>10</sub> -2+H⇌C <sub>5</sub> H <sub>9</sub> -25+H <sub>2</sub>	–	266.40	353.11
C <sub>5</sub> H <sub>11</sub> -1⇌C <sub>5</sub> H <sub>11</sub> -2 (3MR)	–	258.46	373.45
C <sub>5</sub> H <sub>11</sub> -1⇌C <sub>5</sub> H <sub>11</sub> -2 (5MR) <sup>a</sup>	188.91	194.59	374.76
C <sub>5</sub> H <sub>11</sub> -1⇌C <sub>5</sub> H <sub>11</sub> -2 (5MR) <sup>b</sup>	189.75	195.42	375.22
C <sub>5</sub> H <sub>11</sub> -1⇌C <sub>5</sub> H <sub>11</sub> -3	253.76	259.68	372.48
C <sub>5</sub> H <sub>11</sub> -2⇌C <sub>5</sub> H <sub>11</sub> -3 <sup>c</sup>	253.59	259.01	374.07
C <sub>5</sub> H <sub>11</sub> -2⇌C <sub>5</sub> H <sub>11</sub> -3 <sup>d</sup>	247.20	252.61	373.76
C <sub>2</sub> H <sub>4</sub> +C <sub>3</sub> H <sub>7</sub> -1⇌C <sub>5</sub> H <sub>11</sub> -1	215.66	222.41	375.74
C <sub>3</sub> H <sub>6</sub> +C <sub>2</sub> H <sub>5</sub> ⇌C <sub>5</sub> H <sub>11</sub> -2	204.16	211.02	373.91
C <sub>4</sub> H <sub>8</sub> -1+CH <sub>3</sub> ⇌C <sub>5</sub> H <sub>11</sub> -3	210.62	217.31	372.66
C <sub>5</sub> H <sub>10</sub> -1+H⇌C <sub>5</sub> H <sub>11</sub> -1	244.58	250.97	365.71
C <sub>5</sub> H <sub>10</sub> -1+H⇌C <sub>5</sub> H <sub>11</sub> -2	237.17	243.46	364.92
C <sub>5</sub> H <sub>10</sub> -2+H⇌C <sub>5</sub> H <sub>11</sub> -2	229.97	236.22	364.16
C <sub>5</sub> H <sub>10</sub> -2+H⇌C <sub>5</sub> H <sub>11</sub> -3	230.44	236.78	364.50

**Table AS4:** Restricted open-shell 0 K electronic energies in hartrees for minima and transition states. <sup>a</sup>equatorial conformer, <sup>b</sup>axial conformer, <sup>c</sup>syn conformer, <sup>d</sup>anti conformer.

Species	ROMP2/AUG-CC-PVDZ	ROMP2/AUG-CC-PVTZ	ROMP2/AUG-CC-PVQZ	ROCCSD(T)/AUG-CC-PVDZ	ROCCSD(T)/AUG-CC-PVTZ
C <sub>2</sub> H <sub>4</sub>	-78.32774	-78.40438	-78.42759	-78.36788	-78.44347
C <sub>2</sub> H <sub>5</sub>	-78.88563	-78.96460	-78.98775	-78.93046	-79.00790
C <sub>3</sub> H <sub>6</sub>	-117.51886	-117.63382	-117.66842	-117.57656	-117.69003
C <sub>3</sub> H <sub>7</sub> -1	-118.07232	-118.18888	-118.22338	-118.13539	-118.24995
C <sub>4</sub> H <sub>8</sub> -1	-156.70624	-156.85865	-156.90450	-156.78186	-156.93228
C <sub>5</sub> H <sub>10</sub> -1	-195.89429	-196.08409	-196.14116	-195.98777	-196.17508
C <sub>5</sub> H <sub>10</sub> -2	-195.89719	-196.08754	-196.14473	-195.99043	-196.17832
C <sub>5</sub> H <sub>11</sub> -1	-196.44736	-196.63893	-196.69604	-196.54667	-196.73529
C <sub>5</sub> H <sub>11</sub> -2	-196.45041	-196.64258	-196.69985	-196.55001	-196.73925
C <sub>5</sub> H <sub>11</sub> -3	-196.45011	-196.64211	-196.69940	-196.54980	-196.73888
C <sub>5</sub> H <sub>9</sub> -13	-195.25796	-195.44294	-195.49914	-195.34631	-195.52916
C <sub>5</sub> H <sub>9</sub> -24	-195.26197	-195.44769	-195.50407	-195.34923	-195.53279
CH <sub>3</sub>	-39.69825	-39.73876	-39.75033	-39.72425	-39.76365
H	-0.99867	-0.49982	-0.49995	-0.49928	-0.49982
H <sub>2</sub>	-1.15612	-1.16500	-1.16671	-1.16467	-1.17264
C <sub>2</sub> H <sub>4</sub> +C <sub>3</sub> H <sub>7</sub> -1⇌C <sub>5</sub> H <sub>11</sub> -1	-196.39367	-196.58561	-196.64251	-196.49765	-196.68634
C <sub>3</sub> H <sub>6</sub> +C <sub>2</sub> H <sub>5</sub> ⇌C <sub>5</sub> H <sub>11</sub> -2	-196.39749	-196.58977	-196.64675	-196.50081	-196.68987
C <sub>4</sub> H <sub>8</sub> -1+CH <sub>3</sub> ⇌C <sub>5</sub> H <sub>11</sub> -3	-196.39502	-196.58725	-196.64416	-196.49812	-196.68707
C <sub>5</sub> H <sub>10</sub> -1+H⇌C <sub>5</sub> H <sub>11</sub> -1	-196.38635	-196.57681	-196.63398	-196.48289	-196.67074

$C_5H_{10-1}+H\rightleftharpoons C_5H_{11-2}$	-196.38912	-196.57979	-196.63703	-196.48496	-196.67311
$C_5H_{10-1}+H\rightleftharpoons C_5H_9-13+H_2$	-196.37770	-196.56836	-196.62566	-196.47586	-196.66385
$C_5H_{10-2}+H\rightleftharpoons C_5H_{11-2}$	-196.39104	-196.58204	-196.63936	-196.48704	-196.67546
$C_5H_{10-2}+H\rightleftharpoons C_5H_{11-3}$	-196.39059	-196.58168	-196.63903	-196.48684	-196.67536
$C_5H_{10-2}+H\rightleftharpoons C_5H_9-13+H_2$	-196.37850	-196.56957	-196.62697	-196.47628	-196.66462
$C_5H_{10-2}+H\rightleftharpoons C_5H_9-24+H_2$	-196.38150	-196.57262	-196.63000	-196.47910	-196.66757
$C_5H_{11-1}\rightleftharpoons C_5H_{11-2}$ (5MR) <sup>a</sup>	-196.41291	-196.60418	-196.66130	-196.50757	-196.69572
$C_5H_{11-1}\rightleftharpoons C_5H_{11-2}$ (5MR) <sup>b</sup>	-196.41281	-196.60413	-196.66123	-196.50741	-196.69561
$C_5H_{11-1}\rightleftharpoons C_5H_{11-3}$	-196.38631	-196.57766	-196.63492	-196.48175	-196.66993
$C_5H_{11-2}\rightleftharpoons C_5H_{11-3}$ <sup>c</sup>	-196.38545	-196.57847	-196.63595	-196.48016	-196.67017
$C_5H_{11-2}\rightleftharpoons C_5H_{11-3}$ <sup>d</sup>	-196.38783	-196.58081	-196.63833	-196.48243	-196.67242

**Table AS5: 0 K** electronic energies in hartrees for minima and transition states. a equatorial conformer, b axial conformer, c syn conformer, d anti conformer.

Species	MP2/CC-PVDZ	MP2/CC-PVQZ	MP2/CC-PVTZ	CCSD(T)/CC-PVDZ	CCSD(T)/CC-PVTZ
$C_2H_4$	-78.31422	-78.42519	-78.39918	-78.35399	-78.43855
$C_2H_5$	-78.87159	-78.98464	-78.95856	-78.91544	-79.00244
$C_3H_6$	-117.49906	-117.66482	-117.62574	-117.55590	-117.68220
$C_3H_7-1$	-118.05131	-118.21899	-118.17991	-118.11299	-118.24161
$C_4H_8-1$	-156.67943	-156.89966	-156.84762	-156.75372	-156.92152
$C_5H_{10-1}$	-195.86040	-196.13506	-196.07006	-195.95206	-196.16132

$C_5H_{10-2}$	-195.86404	-196.13875	-196.07372	-195.95548	-196.16475
$C_5H_{11-1}$	-196.41240	-196.68915	-196.62402	-196.50942	-196.72105
$C_5H_{11-2}$	-196.41594	-196.69281	-196.62759	-196.51341	-196.72507
$C_5H_{11-3}$	-196.41541	-196.69233	-196.62715	-196.51302	-196.72476
$C_5H_9-11$	-195.17285	-195.43851	-195.37535	-195.27115	-195.47428
$C_5H_9-12$	-195.17835	-195.44473	-195.38141	-195.27616	-195.47979
$C_5H_9-13$	-195.21279	-195.47933	-195.41592	-195.31121	-195.51513
$C_5H_9-14$	-195.19785	-195.46515	-195.40154	-195.28895	-195.49293
$C_5H_9-15$	-195.19463	-195.46181	-195.39829	-195.28521	-195.48917
$C_5H_9-22$	-195.18166	-195.44761	-195.38433	-195.27910	-195.48237
$C_5H_9-23$	-195.18129	-195.44756	-195.38426	-195.27885	-195.48239
$C_5H_9-24$	-195.21653	-195.48303	-195.41960	-195.31502	-195.51890
$C_5H_9-25$	-195.19766	-195.46485	-195.40130	-195.28823	-195.49216
$CH_3$	-39.69037	-39.74864	-39.73566	-39.71578	-39.76098
$H$	-0.49928	-0.49995	-0.49981	-0.49928	-0.49981
$H_2$	-1.15513	-1.16655	-1.16462	-1.16346	-1.17234
$C_2H_4+C_3H_7-1\rightleftharpoons C_5H_{11-1}$	-196.34741	-196.62627	-196.56130	-196.45713	-196.67115
$C_3H_6+C_2H_5\rightleftharpoons C_5H_{11-2}$	-196.35151	-196.63009	-196.56515	-196.46103	-196.67484
$C_4H_8-1+CH_3\rightleftharpoons C_5H_{11-3}$	-196.34875	-196.62765	-196.56267	-196.45791	-196.67192
$C_5H_{10-1}+H\rightleftharpoons C_5H_{11-1}$	-196.34257	-196.61907	-196.55376	-196.44417	-196.65576
$C_5H_{10-1}+H\rightleftharpoons C_5H_{11-2}$	-196.34674	-196.62339	-196.55797	-196.44663	-196.65817
$C_5H_{10-1}+H\rightleftharpoons C_5H_9-11+H_2$	-196.31533	-196.59181	-196.52650	-196.42188	-196.63331

$C_5H_{10-1}+H \rightleftharpoons C_5H_9-12+H_2$	-196.32129	-196.59778	-196.53243	-196.42649	-196.63782
$C_5H_{10-1}+H \rightleftharpoons C_5H_9-13+H_2$	-196.33611	-196.61306	-196.54745	-196.43762	-196.64900
$C_5H_{10-1}+H \rightleftharpoons C_5H_9-14+H_2$	-196.33611	-196.61305	-196.54752	-196.43406	-196.64550
$C_5H_{10-1}+H \rightleftharpoons C_5H_9-15+H_2$	-196.33189	-196.60894	-196.54342	-196.43044	-196.64199
$C_5H_{10-2}+H \rightleftharpoons C_5H_{11-2}$	-196.34840	-196.62508	-196.55970	-196.44900	-196.66067
$C_5H_{10-2}+H \rightleftharpoons C_5H_{11-3}$	-196.34778	-196.62466	-196.55923	-196.44867	-196.66050
$C_5H_{10-2}+H \rightleftharpoons C_5H_9-13+H_2$	-196.33693	-196.61335	-196.54790	-196.43889	-196.65002
$C_5H_{10-2}+H \rightleftharpoons C_5H_9-22+H_2$	-196.32416	-196.60082	-196.53537	-196.42929	-196.64068
$C_5H_{10-2}+H \rightleftharpoons C_5H_9-23+H_2$	-196.32421	-196.60097	-196.53552	-196.42938	-196.64084
$C_5H_{10-2}+H \rightleftharpoons C_5H_9-24+H_2$	-196.34151	-196.61814	-196.55262	-196.44177	-196.65298
$C_5H_{10-2}+H \rightleftharpoons C_5H_9-25+H_2$	-196.33484	-196.61184	-196.54631	-196.43341	-196.64488
$C_5H_{11-1} \rightleftharpoons C_5H_{11-2}$ (3MR)	-196.34406	-196.62408	-196.55818	-196.44089	-196.65503
$C_5H_{11-1} \rightleftharpoons C_5H_{11-2}$ (5MR) <sup>a</sup>	-196.37168	-196.64808	-196.58296	-196.46969	-196.68111
$C_5H_{11-1} \rightleftharpoons C_5H_{11-2}$ (5MR) <sup>b</sup>	-196.37125	-196.64806	-196.58289	-196.46915	-196.68091
$C_5H_{11-1} \rightleftharpoons C_5H_{11-3}$	-196.34373	-196.62114	-196.55581	-196.44292	-196.65511
$C_5H_{11-2} \rightleftharpoons C_5H_{11-3}$ <sup>c</sup>	-196.34387	-196.62386	-196.55798	-196.44098	-196.65510
$C_5H_{11-2} \rightleftharpoons C_5H_{11-3}$ <sup>d</sup>	-196.34632	-196.62629	-196.56034	-196.44333	-196.65732

**Table AS6:** 0 K electronic energies in hartrees for compound methods used to construct isodesmic reaction network.

Species	CBS-QB3	CBS-APNO	G3	G4
C <sub>2</sub> H <sub>4</sub>	-78.41664	-78.53221	-78.50742	-78.52188
C <sub>2</sub> H <sub>5</sub>	-78.97155	-79.08864	-79.06398	-79.07909
C <sub>2</sub> H <sub>6</sub>	-79.63057	-79.74798	-79.72339	-79.73811
C <sub>3</sub> H <sub>5</sub> -11	-116.97143	-117.14475	-117.10669	-117.12912
C <sub>3</sub> H <sub>5</sub> -12	-116.97759	-117.15075	-117.11241	-117.13498
C <sub>3</sub> H <sub>5</sub> -13	-117.00951	-117.18315	-117.14490	-117.16578
C <sub>3</sub> H <sub>6</sub>	-117.64623	-117.82051	-117.78219	-117.80388
C <sub>3</sub> H <sub>7</sub> -1	-118.19633	-118.37181	-118.33391	-118.35668
C <sub>3</sub> H <sub>7</sub> -2	-118.20141	-118.37676	-118.33814	-118.36138
C <sub>3</sub> H <sub>8</sub>	-118.85586	-119.03178	-118.99390	-119.01578
C <sub>4</sub> H <sub>10</sub>	-158.08156	-158.31591	-158.26482	-158.29393
C <sub>4</sub> H <sub>7</sub> -11	-156.19674	-156.42853	-156.37718	-156.40729
C <sub>4</sub> H <sub>7</sub> -12	-156.20257	-156.43432	-156.38265	-156.41278
C <sub>4</sub> H <sub>7</sub> -13	-156.23982	-156.47191	-156.41992	-156.44863
C <sub>4</sub> H <sub>7</sub> -14	-156.21132	-156.44368	-156.39227	-156.42286
C <sub>4</sub> H <sub>8</sub> -1	-156.87127	-157.10402	-157.05249	-157.08132
C <sub>4</sub> H <sub>8</sub> -2	-156.87579	-157.10862	-157.05687	-157.08576
C <sub>4</sub> H <sub>9</sub> -1	-157.42207	-157.65602	-157.60488	-157.63539
C <sub>4</sub> H <sub>9</sub> -2	-157.42663	-157.66037	-157.60859	-157.63948
C <sub>5</sub> H <sub>10</sub> -1	-196.09699	-196.38824	-196.32352	-196.35951
C <sub>5</sub> H <sub>10</sub> -2	-196.10103	-196.39239	-196.32739	-196.36345
C <sub>5</sub> H <sub>11</sub> -1	-196.64779	-196.94017	-196.87582	-196.91411
C <sub>5</sub> H <sub>11</sub> -2	-196.65239	-196.94460	-196.87958	-196.91821
C <sub>5</sub> H <sub>11</sub> -3	-196.65188	-196.94404	-196.87911	-196.91761
C <sub>5</sub> H <sub>9</sub> -11	-195.42249	-195.71276	-195.64822	-195.68612
C <sub>5</sub> H <sub>9</sub> -12	-195.42851	-195.71868	-195.65377	-195.69169
C <sub>5</sub> H <sub>9</sub> -13	-195.46494	-195.75551	-195.69030	-195.72669
C <sub>5</sub> H <sub>9</sub> -14	-195.44172	-195.73257	NaN	-195.70529
C <sub>5</sub> H <sub>9</sub> -15	-195.43758	-195.72850	-195.66368	-195.70157
C <sub>5</sub> H <sub>9</sub> -22	-195.43137	-195.72165	-195.65652	-195.69457
C <sub>5</sub> H <sub>9</sub> -23	-195.43104	-195.72142	-195.65621	-195.69414
C <sub>5</sub> H <sub>9</sub> -24	-195.46974	-195.76028	-195.69451	-195.73108



C <sub>5</sub> H <sub>9</sub> -25	-195.44120	-195.73215	NaN	-195.70533
CH <sub>3</sub>	-39.74480	-39.80368	-39.79329	-39.79995
CH <sub>4</sub>	-40.41001	-40.46893	-40.45762	-40.46531
IC <sub>4</sub> H <sub>10</sub>	-158.08456	-158.31891	-158.26780	-158.29704

### A.3 Comparison of Energies and Rate Constants Computed in This Work with Literature Data

While comparing our high pressure limiting rate constants with those from the literature, a large discrepancy for the reaction  $\dot{C}_5H_{11-1} \rightleftharpoons \dot{C}_5H_{11-3}$  was observed between this work and Awan et al.. Their rate constant was a factor of ~400 times larger at 500 K. This prompted us to re-calculate the rate constant using their ChemRate supplementary input files. Their reported rate constant was  $3.39 \times 10^5 (T/298)^{6.837} \exp(-9444/T)$ , which was then corrected to  $2.38 \times 10^9 T^{0.977} \exp(-17144.8/T)$ . By doing so, the rate constant for the reaction  $\dot{C}_5H_{11-1} \rightleftharpoons \dot{C}_5H_{11-3}$  is in better agreement with both this work and with the literature data, as shown below.

Reaction barriers were also calculated using their ChemRate input files and compared to those reported in their supplementary material. Differences were observed for two reactions,  $\dot{C}_5H_{11-1} \rightleftharpoons \dot{C}_5H_{11-2}$  and  $\dot{C}_5H_{11-1} \rightleftharpoons \dot{C}_5H_{11-3}$ . Respective forward reaction barriers of 92.60 and 142.90 kJ mol<sup>-1</sup> were obtained based on the ChemRate input files, and these are the values compared with throughout. Corrected energy barriers at 0 K and 298 K are shown in Table AS7.

**Table AS7:** Corrected Energy Barriers at 0 K and 298 K from Awan et al. [1] Supplementary Material

Reaction	Best-fit					A priori			
	$E_{298}^a$	$E_{298}^b$	ChemRate	$E_0^a$	$E_0^b$	$E_{298}^a$	$E_{298}^b$	$E_0^a$	$E_0^b$
$\dot{C}_5H_{11-1} \rightleftharpoons \dot{C}_5H_{11-2}$	105.00	92.60	92.60	108.00	94.60	105.30	94.48	108.60	96.80
$\dot{C}_5H_{11-2} \rightleftharpoons \dot{C}_5H_{11-1}$	117.40			121.40		116.12		120.40	
$\dot{C}_5H_{11-1} \rightleftharpoons \dot{C}_5H_{11-3}$	155.60	142.90	142.90	157.80	144.50	170.00	160.40	172.20	161.00
$\dot{C}_5H_{11-3} \rightleftharpoons \dot{C}_5H_{11-1}$	168.30			171.10		179.60		183.40	

<sup>a</sup>Values reported in supplementary material <sup>b</sup>Corrected values \*Units kJ mol<sup>-1</sup>

**Table AS8:** Differences Between Literature 0 K Reaction Barriers to Those Calculated in This Study

Reaction	Reaction	[a]	[b]	[c]	[d]	[e]
$\dot{C}_5H_{11-2} \rightleftharpoons C_5H_{10-2} + \dot{H}$	R13	-9.55	-7.65	-	-	-
$\dot{C}_5H_{11-1} \rightleftharpoons C_2H_4 + n-\dot{C}_3H_7$	R15	-2.16	-7.76	-	7.70	-
$\dot{C}_5H_{11-2} \rightleftharpoons C_3H_6 + \dot{C}_2H_5$	R16	-3.14	-5.24	-	4.25	-
$\dot{C}_5H_{11-3} \rightleftharpoons \dot{C}_4H_8-1 + \dot{C}H_3$	R17	-5.31	-4.11	-	-	-
$\dot{C}_5H_{11-1} \rightleftharpoons \dot{C}_5H_{11-2}$	R18	0.29	-1.91	1.99	-16.59	-3.21
$\dot{C}_5H_{11-2} \rightleftharpoons \dot{C}_5H_{11-3}$	R19	-0.36	-16.86	1.74	-15.36	-
$\dot{C}_5H_{11-2} \rightleftharpoons \dot{C}_5H_{11-3}$	R20	-	-	-0.19	-	-

Units: (kJ mol<sup>-1</sup>) [a] Awan “*a priori*”[1], [b] Awan “best fit model” [1], [c] Hayes et al. G3MP2B3 [4], [d] Jitariu (PUMP-SAC2/6-311G\*\*) [5], [e] Sirjean CBS-QB3 [6].

Differences in 0 K reaction barriers between this study and other literature sources are shown in Table AS8, with differences defined as  $\Delta^\ddagger H_{0K} \text{ Literature} - \Delta^\ddagger H_{0K} \text{ ThisWork}$ , and the lowest energy barrier calculated in this work is employed. Hayes et al. [4] calculated the reaction barriers for H-atom transfer reactions in alkyl, allylic and oxoallylic radicals using the G3MP2B3 composite method. Their [4] G3MP2B3 barriers are in very good agreement with those calculated in this work, with a mean absolute error and 2 $\sigma$  variation of  $1.31 \pm 1.59$  kJ mol<sup>-1</sup> computed, with the reaction barrier of (R18) showing the largest difference of +1.99 kJ mol<sup>-1</sup>. The corresponding barrier computed by Sirjean et al. [6] at the CBS-QB3 level of theory is 3.21 kJ mol<sup>-1</sup> lower than this work, although it is known that CBS-QB3 tends to under-predict barrier heights [7-8]. The largest discrepancies between this work and literature are found when we compare the results of Jitariu et al. [5], with deviations of  $9.82 \pm 9.07$  kJ mol<sup>-1</sup> are observed. Overall the agreement with Hayes and Sirjean is quite reasonable, and some of the Jitariu results appear to be outliers. What is surprising are the deviations between the Awan and Hayes results, since G3MP2B3 was used in both studies.

Figure AS2 compares high-pressure limiting rate constants, bearing in mind these variations in the computed barriers, although differences in computed ro-vibrational properties also influence these comparisons. Differences will be summarised based on an absolute percentage error ( $\epsilon$ ), where  $\bar{\epsilon}$  is the mean absolute percentage error and  $\epsilon_{\max}$  = maximum absolute percentage error (%). We have compared our computed high-pressure limiting rate constants with eight studies in the literature; Awan [1], Comandini [2], Jitariu [5], Davis [9], Sirjean [6], Miyoshi [10], Yamauchi [11], and Yu [12].

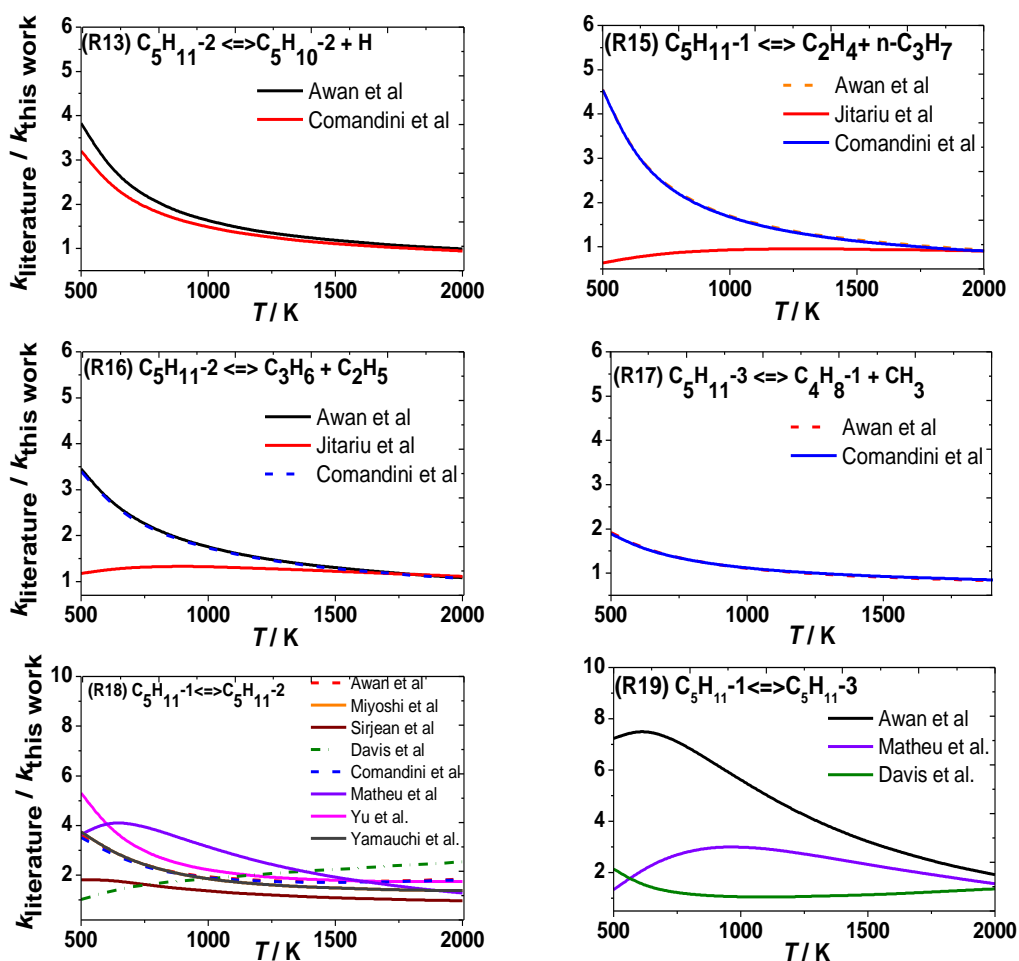


**Figure AS2.** Ratio of the literature [1-2, 5-6, 9-10, 13] rate constants to those computed in this work as a function of temperature.

In terms of general trends, the rate constants in the present work appear to be consistently lower than the literature data, particularly at low temperatures, where differences in computed energies, tunnelling corrections, and torsional barriers tend to be most important. At temperatures above 1000 K, where most of the available combustion relevant data are, high-pressure limiting rate constants tend to agree to within a factor of two or less.

Awan and Comandini's [1-2], reported high-pressure limit rate constants are fitted from 400–1900 K but as stated, their rate constants have been reported so as to allow for accurate reproduction of their model results. They estimate that the uncertainty in the absolute rate constants is about a factor of two at 100 K at the 90% confidence interval. For R13, R15, R16, R17 and R18, our calculated rate constants at 1000 K are within a factor  $\sim 2$  of those reported by Awan and Comandini.

For R19, Awan et al. [1] are a factor of ~6 faster at 1000 K. Their 0K best fit reaction barrier for this reaction, corrected in this work as described in Section 2, is 144.5 kJ mol<sup>-1</sup>, 16.86 kJ mol<sup>-1</sup> lower than our computed reaction barrier. At 1000 K, a barrier difference of 16.86 kJ mol<sup>-1</sup> justifies this difference. Although, G3MP2B3 was used by both Awan and Hayes, Hayes'[4] barrier for this reaction is in excellent agreement with this work. Our rate constant for this reaction shows excellent agreement with Davis et al. [9] over the temperature range 500–2000. The largest discrepancy observed between Matheu et al. [13] and this work for R19 is approximately a factor of three at 1000 K.

This study also shows excellent agreement with Jitariu et al. [5] for R15 and R16 over the temperature range 500–2000 K. However, there is quite a discrepancy across different literature sources and this work for R18. The rate constants in this study are in good agreement with those from Sirjean et al. [6] in the temperature range 500–2000 K with results being within a factor ~2. For Miyoshi et al. and Yamauchi et al. [10-11], our rate constants are within a factor ~3 above 700 K. Figure AS3 illustrates experimental rate constants by Miyoshi with theoretically derived rate constants from this work. It can be observed by the dashed lines that a 1.5 kcal mol<sup>-1</sup> reduction in all three barriers for the reaction  $\dot{C}_5H_{11-1} \rightleftharpoons \dot{C}_5H_{11-2}$  bring the results to closer agreement. Agreement with Yu et al. [12] for R18 is within a factor ~3 above 700 K. At lower temperature, differences are larger, and reasons accounting for these differences are discussed within the main text.

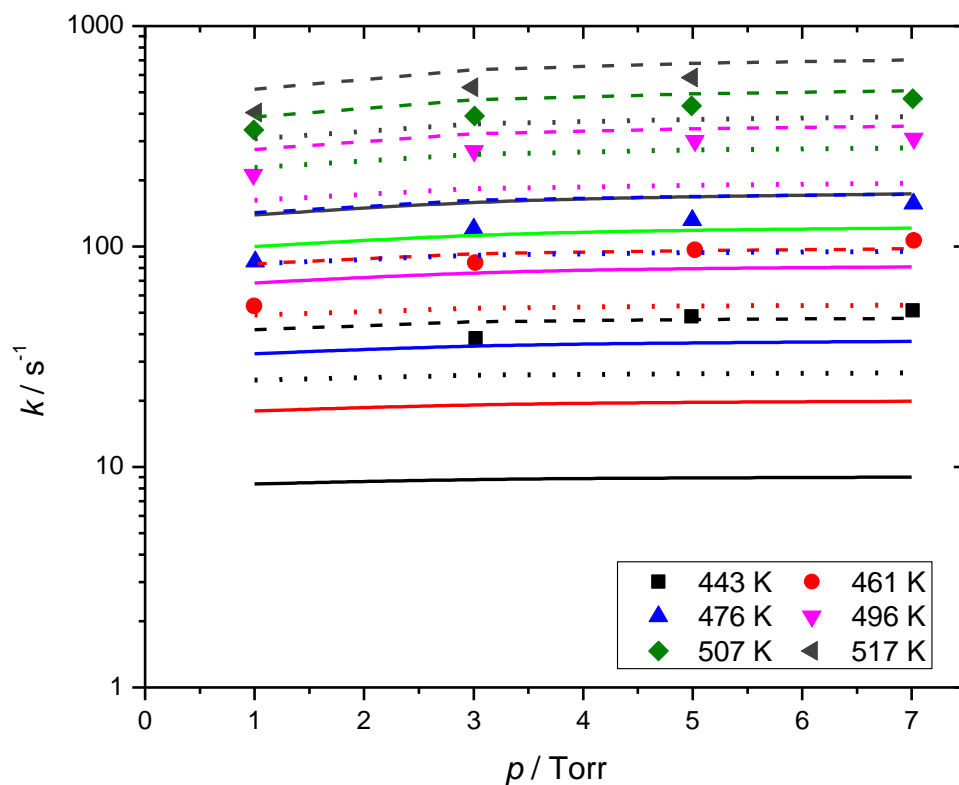


**Figure AS3.** Experimental rate constants (symbols) from Miyoshi et al. [10] for the isomerisation of  $\dot{\text{C}}_5\text{H}_{11-1} \rightleftharpoons \dot{\text{C}}_5\text{H}_{11-2}$  with theoretically-derived rate constants from *this work* (lines). Solid lines represent unmodified RRKM/ME results, dashed lines represent the result of a 1.5 kcal mol<sup>-1</sup> reduction in all three barriers for the reaction  $\dot{\text{C}}_5\text{H}_{11-1} \rightleftharpoons \dot{\text{C}}_5\text{H}_{11-2}$ , and dotted lines represent the result of a 0.5 kcal mol<sup>-1</sup> reduction in these barriers with a corresponding 10% increase in the imaginary frequencies. Lennard-Jones parameters of 7.098 cm<sup>-1</sup> and 2.576 Å were used for the He bath gas, with energy transfer parameters the same as used for Ar (see main text).

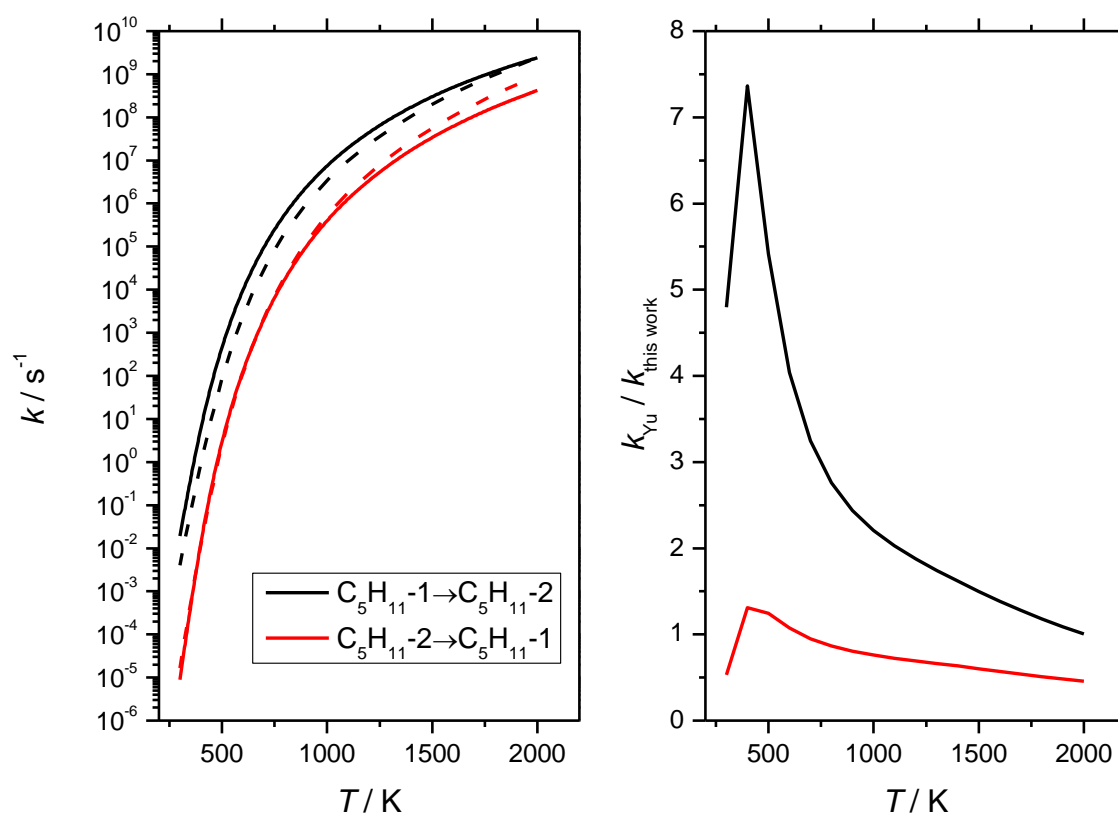


**Figure AS4.** Comparison of absolute high-pressure limiting rate constants (left) and ratios of rate constants for the reaction  $\dot{\text{C}}_5\text{H}_{11}\text{-1} \rightleftharpoons \dot{\text{C}}_5\text{H}_{11}\text{-2}$  from Yu et al. [12] (solid) and *this work* (dashed).

## A.4 Thermochemical Data

### Isodesmic Reactions

#### C<sub>5</sub>H<sub>10-2</sub>

(1)	C <sub>5</sub> H <sub>10-2</sub>	+	CH <sub>4</sub>	=	C <sub>2</sub> H <sub>4</sub>	+	C <sub>4</sub> H <sub>10</sub>	Δ <sub>r</sub> H
Δ <sub>r</sub> H	<b>-5.17</b>		-66.56		60.91		-98.65	33.99
±	<b>0.91</b>		0.06		0.12		0.26	0.86
(2)	C <sub>5</sub> H <sub>10-2</sub>	+	CH <sub>4</sub>	=	C <sub>3</sub> H <sub>6</sub>	+	C <sub>3</sub> H <sub>8</sub>	Δ <sub>r</sub> H
Δ <sub>r</sub> H	<b>-4.85</b>		-66.56		34.98		-82.74	23.63
±	<b>0.46</b>		0.06		0.21		0.19	0.37
(3)	C <sub>5</sub> H <sub>10-2</sub>	+	CH <sub>4</sub>	=	C <sub>4</sub> H <sub>8-2</sub>	+	C <sub>2</sub> H <sub>6</sub>	Δ <sub>r</sub> H
Δ <sub>r</sub> H	<b>-5.04</b>		-66.56		9.24		-68.33	12.51
±	<b>0.61</b>		0.06		0.41		0.13	0.43
(4)	C <sub>5</sub> H <sub>10-2</sub>	+	C <sub>2</sub> H <sub>6</sub>	=	C <sub>3</sub> H <sub>6</sub>	+	C <sub>4</sub> H <sub>10</sub>	Δ <sub>r</sub> H
Δ <sub>r</sub> H	<b>-5.37</b>		-68.33		34.98		-98.65	10.03
±	<b>0.55</b>		0.13		0.21		0.26	0.42
(5)	C <sub>5</sub> H <sub>10-2</sub>	+	C <sub>2</sub> H <sub>6</sub>	=	C <sub>4</sub> H <sub>8-2</sub>	+	C <sub>3</sub> H <sub>8</sub>	Δ <sub>r</sub> H
Δ <sub>r</sub> H	<b>-5.14</b>		-68.33		9.24		-82.74	-0.04
±	<b>0.49</b>		0.13		0.41		0.19	0.16
<b>Δ<sub>r</sub>H<sub>0K</sub> = -5.07 ± 0.29 kJ mol<sup>-1</sup></b>								

#### C<sub>5</sub>H<sub>11-1</sub>

(1)	C <sub>5</sub> H <sub>11-1</sub>	+	CH <sub>4</sub>	=	C <sub>4</sub> H <sub>9-1</sub>	+	C <sub>2</sub> H <sub>6</sub>	Δ <sub>r</sub> H
Δ <sub>r</sub> H	<b>86.73</b>		-66.56		102.52		-68.33	14.02
±	<b>1.92</b>		0.06		0.72		0.13	1.78
(2)	C <sub>5</sub> H <sub>11-1</sub>	+	C <sub>2</sub> H <sub>6</sub>	=	C <sub>4</sub> H <sub>9-1</sub>	+	C <sub>3</sub> H <sub>8</sub>	Δ <sub>r</sub> H
Δ <sub>r</sub> H	<b>86.63</b>		-68.33		102.52		-82.74	1.47
±	<b>1.65</b>		0.13		0.72		0.19	1.47
(3)	C <sub>5</sub> H <sub>11-1</sub>	+	C <sub>3</sub> H <sub>8</sub>	=	C <sub>4</sub> H <sub>9-1</sub>	+	C <sub>4</sub> H <sub>10</sub>	Δ <sub>r</sub> H
Δ <sub>r</sub> H	<b>86.21</b>		-82.74		102.52		-98.65	0.41
±	<b>1.49</b>		0.19		0.72		0.26	1.26
(4)	C <sub>5</sub> H <sub>11-1</sub>	+	C <sub>2</sub> H <sub>4</sub>	=	C <sub>4</sub> H <sub>9-1</sub>	+	C <sub>3</sub> H <sub>6</sub>	Δ <sub>r</sub> H
Δ <sub>r</sub> H	<b>86.53</b>		60.91		102.52		34.98	-9.94
±	<b>1.81</b>		0.12		0.72		0.21	1.64
(5)	C <sub>5</sub> H <sub>11-1</sub>	+	C <sub>3</sub> H <sub>6</sub>	=	C <sub>4</sub> H <sub>9-1</sub>	+	C <sub>4</sub> H <sub>8-1</sub>	Δ <sub>r</sub> H
Δ <sub>r</sub> H	<b>86.28</b>		34.98		102.52		20.86	2.12
±	<b>1.68</b>		0.21		0.72		0.38	1.45
<b>Δ<sub>r</sub>H<sub>0K</sub> = 86.45 ± 0.76 kJ mol<sup>-1</sup></b>								

C<sub>5</sub>H<sub>11-2</sub>

(1)	C <sub>5</sub> H <sub>11-2</sub>	+	CH <sub>4</sub>	=	C <sub>4</sub> H <sub>9-2</sub>	+	C <sub>2</sub> H <sub>6</sub>	Δ <sub>r</sub> H
Δ <sub>r</sub> H	<b>74.27</b>		-66.56		90.19		-68.33	14.14
±	<b>1.94</b>		0.06		0.98		0.13	1.66
(2)	C <sub>5</sub> H <sub>11-2</sub>	+	C <sub>2</sub> H <sub>6</sub>	=	C <sub>4</sub> H <sub>9-2</sub>	+	C <sub>3</sub> H <sub>8</sub>	Δ <sub>r</sub> H
Δ <sub>r</sub> H	<b>74.17</b>		-68.33		90.19		-82.74	1.60
±	<b>1.68</b>		0.13		0.98		0.19	1.35
(3)	C <sub>5</sub> H <sub>11-2</sub>	+	C <sub>3</sub> H <sub>8</sub>	=	C <sub>4</sub> H <sub>9-2</sub>	+	C <sub>4</sub> H <sub>10</sub>	Δ <sub>r</sub> H
Δ <sub>r</sub> H	<b>73.75</b>		-82.74		90.19		-98.65	0.54
±	<b>1.55</b>		0.19		0.98		0.26	1.15
(4)	C <sub>5</sub> H <sub>11-2</sub>	+	C <sub>2</sub> H <sub>4</sub>	=	C <sub>4</sub> H <sub>9-2</sub>	+	C <sub>3</sub> H <sub>6</sub>	Δ <sub>r</sub> H
Δ <sub>r</sub> H	<b>74.07</b>		60.91		90.19		34.98	-9.81
±	<b>1.82</b>		0.12		0.98		0.21	1.52
(5)	C <sub>5</sub> H <sub>11-2</sub>	+	C <sub>3</sub> H <sub>6</sub>	=	C <sub>4</sub> H <sub>9-2</sub>	+	C <sub>4</sub> H <sub>8-1</sub>	Δ <sub>r</sub> H
Δ <sub>r</sub> H	<b>73.82</b>		34.98		90.19		20.86	2.25
±	<b>1.71</b>		0.21		0.98		0.38	1.34
<b>Δ<sub>r</sub>H<sub>0K</sub> = 73.99 ± 0.77 kJ mol<sup>-1</sup></b>								

C<sub>5</sub>H<sub>11-3</sub>

(1)	C <sub>5</sub> H <sub>11-3</sub>	+	CH <sub>4</sub>	=	C <sub>4</sub> H <sub>9-2</sub>	+	C <sub>2</sub> H <sub>6</sub>	Δ <sub>r</sub> H
Δ <sub>r</sub> H	<b>75.68</b>		-66.56		90.19		-68.33	12.73
±	<b>1.78</b>		0.06		0.98		0.13	1.48
(2)	C <sub>5</sub> H <sub>11-3</sub>	+	C <sub>2</sub> H <sub>6</sub>	=	C <sub>4</sub> H <sub>9-2</sub>	+	C <sub>3</sub> H <sub>8</sub>	Δ <sub>r</sub> H
Δ <sub>r</sub> H	<b>75.58</b>		-68.33		90.19		-82.74	0.19
±	<b>1.54</b>		0.13		0.98		0.19	1.17
(3)	C <sub>5</sub> H <sub>11-3</sub>	+	C <sub>3</sub> H <sub>8</sub>	=	C <sub>4</sub> H <sub>9-2</sub>	+	C <sub>4</sub> H <sub>10</sub>	Δ <sub>r</sub> H
Δ <sub>r</sub> H	<b>75.16</b>		-82.74		90.19		-98.65	-0.87
±	<b>1.40</b>		0.19		0.98		0.26	0.95
(4)	C <sub>5</sub> H <sub>11-3</sub>	+	C <sub>2</sub> H <sub>4</sub>	=	C <sub>4</sub> H <sub>9-2</sub>	+	C <sub>3</sub> H <sub>6</sub>	Δ <sub>r</sub> H
Δ <sub>r</sub> H	<b>75.49</b>		60.91		90.19		34.98	-11.23
±	<b>1.73</b>		0.12		0.98		0.21	1.40
(5)	C <sub>5</sub> H <sub>11-3</sub>	+	C <sub>3</sub> H <sub>6</sub>	=	C <sub>4</sub> H <sub>9-2</sub>	+	C <sub>4</sub> H <sub>8-1</sub>	Δ <sub>r</sub> H
Δ <sub>r</sub> H	<b>75.236</b>		34.98		90.19		20.86	0.84
±	<b>1.56</b>		0.21		0.98		0.38	1.14
<b>Δ<sub>r</sub>H<sub>0K</sub> = 75.40 ± 0.71 kJ mol<sup>-1</sup></b>								



C<sub>5</sub>H<sub>9</sub>1-1

(1)	C <sub>5</sub> H <sub>9</sub> 1-1	+	CH <sub>4</sub>	=	C <sub>4</sub> H <sub>7</sub> 1-1	+	C <sub>2</sub> H <sub>6</sub>	Δ <sub>r</sub> H
Δ <sub>r</sub> H	<b>247.3</b>		-66.56		263.30		-68.33	14.23
±	<b>2.08</b>		0.06		0.90		0.13	1.87
(2)	C <sub>5</sub> H <sub>9</sub> 1-1	+	C <sub>2</sub> H <sub>6</sub>	=	C <sub>4</sub> H <sub>7</sub> 1-1	+	C <sub>3</sub> H <sub>8</sub>	Δ <sub>r</sub> H
Δ <sub>r</sub> H	<b>247.19</b>		-68.33		263.30		-82.74	1.69
±	<b>1.82</b>		0.13		0.90		0.19	1.56
(3)	C <sub>5</sub> H <sub>9</sub> 1-1	+	C <sub>2</sub> H <sub>3</sub>	=	C <sub>4</sub> H <sub>7</sub> 1-1	+	C <sub>3</sub> H <sub>5</sub> -1	Δ <sub>r</sub> H
Δ <sub>r</sub> H	<b>247.25</b>		301.14		263.30		277.99	-7.10
±	<b>1.45</b>		0.34		0.90		0.79	0.75
(4)	C <sub>5</sub> H <sub>9</sub> 1-1	+	C <sub>2</sub> H <sub>4</sub>	=	C <sub>4</sub> H <sub>7</sub> 1-1	+	C <sub>3</sub> H <sub>6</sub>	Δ <sub>r</sub> H
Δ <sub>r</sub> H	<b>248.00</b>		60.91		263.30		34.98	-9.73
±	<b>1.75</b>		0.12		0.90		0.21	1.73
(5)	C <sub>5</sub> H <sub>9</sub> 1-1	+	C <sub>3</sub> H <sub>6</sub>	=	C <sub>4</sub> H <sub>7</sub> 1-1	+	C <sub>4</sub> H <sub>8</sub> -1	Δ <sub>r</sub> H
Δ <sub>r</sub> H	<b>248.02</b>		34.98		263.30		20.86	2.34
±	<b>1.56</b>		0.21		0.90		0.38	1.53
<b>Δ<sub>r</sub>H<sub>0K</sub> = 247.50 ± 0.76 kJ mol<sup>-1</sup></b>								

C<sub>5</sub>H<sub>9</sub>1-2

(1)	C <sub>5</sub> H <sub>9</sub> 1-2	+	CH <sub>4</sub>	=	C <sub>4</sub> H <sub>7</sub> 1-2	+	C <sub>2</sub> H <sub>6</sub>	Δ <sub>r</sub> H
Δ <sub>r</sub> H	<b>232.07</b>		-66.56		248.39		-68.33	14.55
±	<b>1.99</b>		0.06		0.94		0.13	1.75
(2)	C <sub>5</sub> H <sub>9</sub> 1-2	+	C <sub>2</sub> H <sub>6</sub>	=	C <sub>4</sub> H <sub>7</sub> 1-2	+	C <sub>3</sub> H <sub>8</sub>	Δ <sub>r</sub> H
Δ <sub>r</sub> H	<b>231.96</b>		-68.33		248.39		-82.74	2.01
±	<b>1.73</b>		0.13		0.94		0.19	1.44
(3)	C <sub>5</sub> H <sub>9</sub> 1-2	+	C <sub>2</sub> H <sub>3</sub>	=	C <sub>4</sub> H <sub>7</sub> 1-2	+	C <sub>3</sub> H <sub>5</sub> -1	Δ <sub>r</sub> H
Δ <sub>r</sub> H	<b>232.02</b>		301.14		248.39		277.99	-6.78
±	<b>1.44</b>		0.34		0.94		0.79	0.68
(4)	C <sub>5</sub> H <sub>9</sub> 1-2	+	C <sub>2</sub> H <sub>4</sub>	=	C <sub>4</sub> H <sub>7</sub> 1-2	+	C <sub>3</sub> H <sub>6</sub>	Δ <sub>r</sub> H
Δ <sub>r</sub> H	<b>231.87</b>		60.91		248.39		34.98	-9.41
±	<b>1.88</b>		0.12		0.94		0.21	1.61
(5)	C <sub>5</sub> H <sub>9</sub> 1-2	+	C <sub>3</sub> H <sub>6</sub>	=	C <sub>4</sub> H <sub>7</sub> 1-2	+	C <sub>4</sub> H <sub>8</sub> -1	Δ <sub>r</sub> H
Δ <sub>r</sub> H	<b>231.89</b>		34.98		248.39		20.86	2.66
±	<b>1.73</b>		0.21		0.94		0.38	1.43
<b>Δ<sub>r</sub>H<sub>0K</sub> = 231.91 ± 0.77 kJ mol<sup>-1</sup></b>								

C<sub>5</sub>H<sub>9</sub>1-3

(1)	C <sub>5</sub> H <sub>9</sub> 1-3	+	CH <sub>4</sub>	=	C <sub>4</sub> H <sub>7</sub> 1-3	+	C <sub>2</sub> H <sub>6</sub>	Δ <sub>r</sub> H
Δ <sub>f</sub> H	<b>142.97</b>		-66.56		<b>152.21</b>		-68.33	12.47
±	<b>1.77</b>		0.06		<b>0.82</b>		0.13	1.56
(2)	C <sub>5</sub> H <sub>9</sub> 1-3	+	C <sub>2</sub> H <sub>6</sub>	=	C <sub>4</sub> H <sub>7</sub> 1-3	+	C <sub>3</sub> H <sub>8</sub>	Δ <sub>r</sub> H
Δ <sub>f</sub> H	<b>142.86</b>		-68.33		<b>152.21</b>		-82.74	-0.07
±	<b>1.51</b>		0.13		<b>0.82</b>		0.19	1.25
(3)	C <sub>5</sub> H <sub>9</sub> 1-3	+	C <sub>2</sub> H <sub>4</sub>	=	C <sub>4</sub> H <sub>7</sub> 1-3	+	C <sub>3</sub> H <sub>6</sub>	Δ <sub>r</sub> H
Δ <sub>f</sub> H	<b>142.77</b>		60.91		<b>152.21</b>		34.98	-11.49
±	<b>1.67</b>		0.12		<b>0.82</b>		0.21	1.43
(4)	C <sub>5</sub> H <sub>9</sub> 1-3	+	C <sub>3</sub> H <sub>6</sub>	=	C <sub>4</sub> H <sub>7</sub> 1-3	+	C <sub>4</sub> H <sub>8</sub> -1	Δ <sub>r</sub> H
Δ <sub>f</sub> H	<b>142.79</b>		34.98		<b>152.21</b>		20.86	0.58
±	<b>1.50</b>		0.21		<b>0.82</b>		0.38	1.23
<b>Δ<sub>f</sub>H<sub>0K</sub> = 137.77 ± 0.81 kJ mol<sup>-1</sup></b>								

C<sub>5</sub>H<sub>9</sub>1-4

(1)	C <sub>5</sub> H <sub>9</sub> 1-4	+	CH <sub>4</sub>	=	C <sub>4</sub> H <sub>7</sub> 1-4	+	C <sub>2</sub> H <sub>6</sub>	Δ <sub>r</sub> H
Δ <sub>f</sub> H	<b>195.24</b>		-66.56		222.68		-68.33	25.66
±	<b>0.95</b>		0.06		0.78		0.13	0.52
(2)	C <sub>5</sub> H <sub>9</sub> 1-4	+	C <sub>2</sub> H <sub>6</sub>	=	C <sub>4</sub> H <sub>7</sub> 1-4	+	C <sub>3</sub> H <sub>8</sub>	Δ <sub>r</sub> H
Δ <sub>f</sub> H	<b>195.17</b>		-68.33		222.68		-82.74	13.09
±	<b>1.18</b>		0.13		0.78		0.19	0.86
(3)	C <sub>5</sub> H <sub>9</sub> 1-4	+	C <sub>2</sub> H <sub>4</sub>	=	C <sub>4</sub> H <sub>7</sub> 1-4	+	C <sub>3</sub> H <sub>6</sub>	Δ <sub>r</sub> H
Δ <sub>f</sub> H	<b>195.15</b>		60.91		222.68		34.98	1.60
±	<b>0.82</b>		0.12		0.78		0.21	0.83
(4)	C <sub>5</sub> H <sub>9</sub> 1-4	+	C <sub>3</sub> H <sub>6</sub>	=	C <sub>4</sub> H <sub>7</sub> 1-4	+	C <sub>4</sub> H <sub>8</sub> -1	Δ <sub>r</sub> H
Δ <sub>f</sub> H	<b>194.79</b>		34.98		222.68		20.86	13.77
±	<b>0.89</b>		0.21		0.78		0.38	0.93
<b>Δ<sub>f</sub>H<sub>0K</sub> = 195.08 ± 0.47 kJ mol<sup>-1</sup></b>								

C<sub>5</sub>H<sub>9</sub>1-5

(1)	C <sub>5</sub> H <sub>9</sub> 1-5	+	CH <sub>4</sub>	=	C <sub>4</sub> H <sub>8</sub> -1	+	C <sub>2</sub> H <sub>5</sub>	Δ <sub>r</sub> H
Δ <sub>r</sub> H	<b>204.96</b>		-66.56		20.86		130.94	13.67
±	<b>3.85</b>		0.06		0.38		0.28	3.83
(2)	C <sub>5</sub> H <sub>9</sub> 1-5	+	CH <sub>4</sub>	=	C <sub>3</sub> H <sub>6</sub>	+	C <sub>3</sub> H <sub>7</sub> -1	Δ <sub>r</sub> H
Δ <sub>r</sub> H	<b>205.60</b>		-66.56		34.98		118.27	14.21
±	<b>2.81</b>		0.06		0.21		0.60	2.74
(3)	C <sub>5</sub> H <sub>9</sub> 1-5	+	C <sub>2</sub> H <sub>6</sub>	=	C <sub>4</sub> H <sub>8</sub> -1	+	C <sub>3</sub> H <sub>7</sub> -1	Δ <sub>r</sub> H
Δ <sub>r</sub> H	<b>205.43</b>		-68.33		20.86		118.27	2.31
±	<b>2.49</b>		0.13		0.38		0.60	2.40
(4)	C <sub>5</sub> H <sub>9</sub> 1-5	+	C <sub>2</sub> H <sub>6</sub>	=	C <sub>3</sub> H <sub>6</sub>	+	C <sub>4</sub> H <sub>9</sub> -1	Δ <sub>r</sub> H
Δ <sub>r</sub> H	<b>205.71</b>		-68.33		34.98		102.52	0.12
±	<b>1.35</b>		0.13		0.21		0.72	1.11
(5)	C <sub>5</sub> H <sub>9</sub> 1-5	+	C <sub>3</sub> H <sub>8</sub>	=	C <sub>4</sub> H <sub>8</sub> -1	+	C <sub>4</sub> H <sub>9</sub> -1	Δ <sub>r</sub> H
Δ <sub>r</sub> H	<b>205.64</b>		-82.75		20.86		102.52	0.77
±	<b>1.33</b>		0.18		0.38		0.72	1.08
<b>Δ<sub>r</sub>H<sub>0K</sub> = 205.46 ± 0.83 kJ mol<sup>-1</sup></b>								

C<sub>5</sub>H<sub>9</sub>2-1

(1)	C <sub>5</sub> H <sub>9</sub> 2-1	+	CH <sub>4</sub>	=	C <sub>3</sub> H <sub>5</sub> -13	+	C <sub>3</sub> H <sub>8</sub>	Δ <sub>r</sub> H
Δ <sub>r</sub> H	<b>137.98</b>		-66.56		179.54		-82.74	25.37
±	<b>2.58</b>		0.06		0.55		0.19	2.52
(2)	C <sub>5</sub> H <sub>9</sub> 2-1	+	C <sub>2</sub> H <sub>6</sub>	=	C <sub>3</sub> H <sub>5</sub> -13	+	C <sub>4</sub> H <sub>10</sub>	Δ <sub>r</sub> H
Δ <sub>r</sub> H	<b>137.46</b>		-68.33		179.54		-98.65	11.76
±	<b>2.17</b>		0.13		0.55		0.26	2.08
(3)	C <sub>5</sub> H <sub>9</sub> 2-1	+	C <sub>2</sub> H <sub>4</sub>	=	C <sub>3</sub> H <sub>5</sub> -13	+	C <sub>4</sub> H <sub>8</sub> -1	Δ <sub>r</sub> H
Δ <sub>r</sub> H	<b>137.43</b>		60.91		179.54		20.86	2.06
±	<b>2.36</b>		0.12		0.55		0.38	2.26
(4)	C <sub>5</sub> H <sub>9</sub> 2-1	+	C <sub>3</sub> H <sub>6</sub>	=	C <sub>3</sub> H <sub>5</sub> -13	+	C <sub>5</sub> H <sub>10</sub> -1	Δ <sub>r</sub> H
Δ <sub>r</sub> H	<b>137.61</b>		34.98		179.54		<b>5.29</b>	12.24
±	<b>2.34</b>		0.21		0.55		<b>0.25</b>	2.25
<b>Δ<sub>r</sub>H<sub>0K</sub> = 137.60 ± 1.18 kJ mol<sup>-1</sup></b>								

C<sub>5</sub>H<sub>9</sub>2-2

(1)	C <sub>5</sub> H <sub>9</sub> -22	+	CH <sub>4</sub>	=	C <sub>3</sub> H <sub>5</sub> 1-2	+	C <sub>3</sub> H <sub>8</sub>	Δ <sub>r</sub> H
Δ <sub>f</sub> H	<b>225.00</b>		-66.56		262.81		-82.74	21.61
±	<b>2.84</b>		0.06		0.78		0.19	2.72
(2)	C <sub>5</sub> H <sub>9</sub> -22	+	C <sub>2</sub> H <sub>6</sub>	=	C <sub>3</sub> H <sub>5</sub> 1-2	+	C <sub>4</sub> H <sub>10</sub>	Δ <sub>r</sub> H
Δ <sub>f</sub> H	<b>224.48</b>		-68.33		262.81		-98.65	8.01
±	<b>2.39</b>		0.13		0.78		0.26	2.24
(3)	C <sub>5</sub> H <sub>9</sub> -22	+	C <sub>2</sub> H <sub>4</sub>	=	C <sub>3</sub> H <sub>5</sub> 1-2	+	C <sub>4</sub> H <sub>8</sub> -1	Δ <sub>r</sub> H
Δ <sub>f</sub> H	<b>224.46</b>		60.91		262.81		20.86	-1.70
±	<b>2.58</b>		0.12		0.78		0.38	2.43
(4)	C <sub>5</sub> H <sub>9</sub> -22	+	C <sub>3</sub> H <sub>6</sub>	=	C <sub>3</sub> H <sub>5</sub> 1-2	+	C <sub>5</sub> H <sub>10</sub> -1	Δ <sub>r</sub> H
Δ <sub>f</sub> H	<b>224.63</b>		34.98		262.81		<b>5.29</b>	8.49
±	<b>2.48</b>		0.21		0.78		<b>0.25</b>	2.33
<b>Δ<sub>f</sub>H<sub>0K</sub> = 224.62 ± 1.28 kJ mol<sup>-1</sup></b>								

C<sub>5</sub>H<sub>9</sub>2-3

(1)	C <sub>5</sub> H <sub>9</sub> 2-3	+	CH <sub>4</sub>	=	C <sub>3</sub> H <sub>5</sub> -1	+	C <sub>3</sub> H <sub>8</sub>	Δ <sub>r</sub> H
Δ <sub>f</sub> H	<b>225.54</b>		-66.56		280.00		-82.74	38.27
±	<b>2.91</b>		0.06		0.81		0.19	2.79
(2)	C <sub>5</sub> H <sub>9</sub> 2-3	+	C <sub>2</sub> H <sub>6</sub>	=	C <sub>3</sub> H <sub>5</sub> -1	+	C <sub>4</sub> H <sub>10</sub>	Δ <sub>r</sub> H
Δ <sub>f</sub> H	<b>225.02</b>		-68.33		280.00		-98.65	24.66
±	<b>2.53</b>		0.13		0.81		0.26	2.38
(3)	C <sub>5</sub> H <sub>9</sub> 2-3	+	C <sub>2</sub> H <sub>4</sub>	=	C <sub>3</sub> H <sub>5</sub> -1	+	C <sub>4</sub> H <sub>8</sub> -1	Δ <sub>r</sub> H
Δ <sub>f</sub> H	<b>224.99</b>		60.91		280.00		20.86	14.96
±	<b>2.65</b>		0.12		0.81		0.38	2.49
(4)	C <sub>5</sub> H <sub>9</sub> 2-3	+	C <sub>3</sub> H <sub>6</sub>	=	C <sub>3</sub> H <sub>5</sub> -1	+	C <sub>5</sub> H <sub>10</sub> -1	Δ <sub>r</sub> H
Δ <sub>f</sub> H	<b>225.17</b>		34.98		280.00		5.29	25.14
±	<b>2.69</b>		0.21		0.81		0.25	2.54
<b>Δ<sub>f</sub>H<sub>0K</sub> = 225.18 ± 1.33 kJ mol<sup>-1</sup></b>								

C<sub>5</sub>H<sub>9</sub>2-4

(1)	C <sub>3</sub> H <sub>9</sub> 2-4	+	CH <sub>4</sub>	=	C <sub>4</sub> H <sub>7</sub> 1-3	+	C <sub>2</sub> H <sub>6</sub>	Δ <sub>r</sub> H
Δ <sub>r</sub> H	<b>126.04</b>		-66.56		152.21		-68.33	24.40
±	<b>1.77</b>		0.06		0.82		0.13	1.56
(2)	C <sub>3</sub> H <sub>9</sub> 2-4	+	C <sub>2</sub> H <sub>6</sub>	=	C <sub>4</sub> H <sub>7</sub> 1-3	+	C <sub>3</sub> H <sub>8</sub>	Δ <sub>r</sub> H
Δ <sub>r</sub> H	<b>125.95</b>		-68.33		152.21		-82.74	11.85
±	<b>1.61</b>		0.13		0.82		0.19	1.37
(3)	C <sub>3</sub> H <sub>9</sub> 2-4	+	C <sub>2</sub> H <sub>4</sub>	=	C <sub>4</sub> H <sub>7</sub> 1-3	+	C <sub>3</sub> H <sub>6</sub>	Δ <sub>r</sub> H
Δ <sub>r</sub> H	<b>125.84</b>		60.91		152.21		34.98	0.44
±	<b>1.53</b>		0.12		0.82		0.21	1.27
(4)	C <sub>3</sub> H <sub>9</sub> 2-4	+	C <sub>3</sub> H <sub>6</sub>	=	C <sub>4</sub> H <sub>7</sub> 1-3	+	C <sub>4</sub> H <sub>8</sub> -1	Δ <sub>r</sub> H
Δ <sub>r</sub> H	<b>125.59</b>		34.98		152.21		20.86	12.50
±	<b>1.74</b>		0.21		0.82		0.38	1.47
<b>Δ<sub>r</sub>H<sub>0K</sub> = 125.86 ± 0.83 kJ mol<sup>-1</sup></b>								

C<sub>5</sub>H<sub>9</sub>2-5

(1)	C <sub>3</sub> H <sub>9</sub> 2-5	+	CH <sub>4</sub>	=	C <sub>3</sub> H <sub>6</sub>	+	C <sub>3</sub> H <sub>7</sub> -1	Δ <sub>r</sub> H
Δ <sub>r</sub> H	<b>195.74</b>		-66.56		34.98		118.27	24.06
±	<b>3.44</b>		0.06		0.21		0.60	3.38
(2)	C <sub>3</sub> H <sub>9</sub> 2-5	+	CH <sub>4</sub>	=	C <sub>4</sub> H <sub>8</sub> -1	+	C <sub>2</sub> H <sub>5</sub>	Δ <sub>r</sub> H
Δ <sub>r</sub> H	<b>194.68</b>		-66.56		20.86		13.94	23.68
±	<b>4.55</b>		0.06		0.38		0.28	4.52
(3)	C <sub>3</sub> H <sub>9</sub> 2-5	+	C <sub>2</sub> H <sub>6</sub>	=	C <sub>3</sub> H <sub>6</sub>	+	C <sub>4</sub> H <sub>9</sub> -1	Δ <sub>r</sub> H
Δ <sub>r</sub> H	<b>195.99</b>		-68.33		34.98		102.52	9.84
±	<b>1.75</b>		0.13		0.21		0.72	1.58
(4)	C <sub>3</sub> H <sub>9</sub> 2-5	+	C <sub>2</sub> H <sub>6</sub>	=	C <sub>4</sub> H <sub>8</sub> -1	+	C <sub>3</sub> H <sub>7</sub> -1	Δ <sub>r</sub> H
Δ <sub>r</sub> H	<b>195.28</b>		-68.33		20.86		118.27	12.18
±	<b>3.06</b>		0.13		0.38		0.60	2.98
<b>Δ<sub>r</sub>H<sub>0K</sub> = 195.72 ± 1.32 kJ mol<sup>-1</sup></b>								

C<sub>4</sub>H<sub>7</sub>1-1

(1)	C <sub>4</sub> H <sub>7</sub> 1-1	+	CH <sub>4</sub>	=	C <sub>3</sub> H <sub>5</sub> 1-1	+	C <sub>2</sub> H <sub>6</sub>	Δ <sub>r</sub> H
Δ <sub>f</sub> H	<b>263.35</b>		-66.56		277.98		-68.33	12.86
±	<b>1.84</b>		0.06		1.12		0.13	1.46
(2)	C <sub>4</sub> H <sub>7</sub> 1-1	+	CH <sub>4</sub>	=	C <sub>2</sub> H <sub>3</sub>	+	C <sub>3</sub> H <sub>8</sub>	Δ <sub>r</sub> H
Δ <sub>f</sub> H	<b>263.31</b>		-66.56		301.14		-82.74	21.64
±	<b>2.83</b>		0.06		0.34		0.19	2.80
(3)	C <sub>4</sub> H <sub>7</sub> 1-1	+	C <sub>2</sub> H <sub>6</sub>	=	C <sub>3</sub> H <sub>5</sub> 1-1	+	C <sub>3</sub> H <sub>8</sub>	Δ <sub>r</sub> H
Δ <sub>f</sub> H	<b>263.26</b>		-68.33		277.98		-82.74	0.31
±	<b>1.62</b>		0.13		1.12		0.19	1.14
(4)	C <sub>4</sub> H <sub>7</sub> 1-1	+	C <sub>2</sub> H <sub>3</sub>	=	C <sub>3</sub> H <sub>5</sub> 1-1	+	C <sub>3</sub> H <sub>5</sub> 1-1	Δ <sub>r</sub> H
Δ <sub>f</sub> H	<b>263.30</b>		301.14		277.98		277.98	-8.47
±	<b>1.53</b>		0.34		1.12		1.12	0.58
<b>Δ<sub>f</sub>H<sub>0K</sub> = 263.30 ± 0.94 kJ mol<sup>-1</sup></b>								

C<sub>4</sub>H<sub>7</sub>1-2

(1)	C <sub>4</sub> H <sub>7</sub> 1-2	+	CH <sub>4</sub>	=	C <sub>3</sub> H <sub>5</sub> 1-2	+	C <sub>2</sub> H <sub>6</sub>	Δ <sub>r</sub> H
Δ <sub>f</sub> H	<b>248.54</b>		-66.56		262.40		-68.33	12.09
±	<b>1.72</b>		0.06		1.20		0.13	1.23
(2)	C <sub>4</sub> H <sub>7</sub> 1-2	+	CH <sub>4</sub>	=	C <sub>2</sub> H <sub>3</sub>	+	C <sub>3</sub> H <sub>8</sub>	Δ <sub>r</sub> H
Δ <sub>f</sub> H	<b>248.49</b>		-66.56		301.14		-82.74	36.46
±	<b>2.57</b>		0.06		0.34		0.19	2.54
(3)	C <sub>4</sub> H <sub>7</sub> 1-2	+	C <sub>2</sub> H <sub>6</sub>	=	C <sub>2</sub> H <sub>3</sub>	+	C <sub>4</sub> H <sub>10</sub>	Δ <sub>r</sub> H
Δ <sub>f</sub> H	<b>247.96</b>		-68.33		301.14		-98.65	22.86
±	<b>2.20</b>		0.13		0.34		0.26	2.16
(4)	C <sub>4</sub> H <sub>7</sub> 1-2	+	C <sub>2</sub> H <sub>6</sub>	=	C <sub>3</sub> H <sub>5</sub> 1-2	+	C <sub>3</sub> H <sub>8</sub>	Δ <sub>r</sub> H
Δ <sub>f</sub> H	<b>248.44</b>		-68.33		262.40		-82.74	-0.45
±	<b>1.53</b>		0.13		1.20		0.19	0.91
<b>Δ<sub>f</sub>H<sub>0K</sub> = 248.39 ± 0.94 kJ mol<sup>-1</sup></b>								

C<sub>4</sub>H<sub>7</sub>1-3

(1)	C <sub>4</sub> H <sub>7</sub> 1-3	+	CH <sub>4</sub>	=	C <sub>3</sub> H <sub>5</sub> 1-3	+	C <sub>2</sub> H <sub>6</sub>	Δ <sub>r</sub> H
Δ <sub>r</sub> H	<b>152.39</b>		-66.56		179.60		-68.33	25.44
±	<b>1.59</b>		0.06		0.50		0.13	1.50
(2)	C <sub>4</sub> H <sub>7</sub> 1-3	+	CH <sub>4</sub>	=	C <sub>2</sub> H <sub>4</sub>	+	C <sub>3</sub> H <sub>7</sub> -1	Δ <sub>r</sub> H
Δ <sub>r</sub> H	<b>150.38</b>		-66.56		60.91		118.27	95.35
±	<b>3.22</b>		0.06		0.12		0.60	3.16
(3)	C <sub>4</sub> H <sub>7</sub> 1-3	+	C <sub>2</sub> H <sub>6</sub>	=	C <sub>3</sub> H <sub>5</sub> 1-3	+	C <sub>3</sub> H <sub>8</sub>	Δ <sub>r</sub> H
Δ <sub>r</sub> H	<b>152.29</b>		-68.33		179.60		-82.74	12.90
±	<b>1.40</b>		0.13		0.50		0.19	1.29
(4)	C <sub>4</sub> H <sub>7</sub> 1-3	+	C <sub>2</sub> H <sub>3</sub>	=	C <sub>3</sub> H <sub>5</sub> 1-3	+	C <sub>3</sub> H <sub>5</sub> 1-1	Δ <sub>r</sub> H
Δ <sub>r</sub> H	<b>152.34</b>		301.14		179.60		277.99	4.11
±	<b>1.41</b>		0.34		0.50		0.79	1.00
<b>Δ<sub>r</sub>H<sub>0K</sub> = 152.21 ± 0.82 kJ mol<sup>-1</sup></b>								

C<sub>4</sub>H<sub>7</sub>1-4

(1)	C <sub>4</sub> H <sub>7</sub> 1-4	+	CH <sub>4</sub>	=	C <sub>3</sub> H <sub>6</sub>	+	C <sub>2</sub> H <sub>5</sub>	Δ <sub>r</sub> H
Δ <sub>r</sub> H	<b>222.02</b>		-66.56		34.98		130.94	10.46
±	<b>3.74</b>		0.06		0.21		0.28	3.73
(2)	C <sub>4</sub> H <sub>7</sub> 1-4	+	CH <sub>4</sub>	=	C <sub>2</sub> H <sub>4</sub>	+	C <sub>3</sub> H <sub>7</sub> -1	Δ <sub>r</sub> H
Δ <sub>r</sub> H	<b>222.68</b>		-66.56		60.91		118.27	23.06
±	<b>2.63</b>		0.06		0.12		0.60	2.56
(3)	C <sub>4</sub> H <sub>7</sub> 1-4	+	C <sub>2</sub> H <sub>6</sub>	=	C <sub>3</sub> H <sub>6</sub>	+	C <sub>3</sub> H <sub>7</sub> -1	Δ <sub>r</sub> H
Δ <sub>r</sub> H	<b>222.48</b>		-68.33		34.98		118.27	-0.90
±	<b>2.40</b>		0.13		0.21		0.60	2.31
(4)	C <sub>4</sub> H <sub>7</sub> 1-4	+	C <sub>2</sub> H <sub>6</sub>	=	C <sub>2</sub> H <sub>4</sub>	+	C <sub>4</sub> H <sub>9</sub> -1	Δ <sub>r</sub> H
Δ <sub>r</sub> H	<b>222.79</b>		-68.33		60.91		102.52	8.97
±	<b>1.24</b>		0.13		0.12		0.72	1.00
(5)	C <sub>4</sub> H <sub>7</sub> 1-4	+	C <sub>3</sub> H <sub>8</sub>	=	C <sub>3</sub> H <sub>6</sub>	+	C <sub>4</sub> H <sub>9</sub> -1	Δ <sub>r</sub> H
Δ <sub>r</sub> H	<b>222.69</b>		-82.74		34.98		102.52	-2.40
±	<b>1.27</b>		0.19		0.21		0.72	1.00
<b>Δ<sub>r</sub>H<sub>0K</sub> = 222.68 ± 0.78 kJ mol<sup>-1</sup></b>								

### A.5 Comparison Entropies and Heat Capacities from This Work and Literature Data

For the common species presented in the main text, the mean absolute errors (MAEs) between the rotational constants for each rotor calculated in this work, and by Awan et al. [1], are on the order of  $0.1 \pm 0.24 \text{ cm}^{-1}$ , which leads to MAEs of  $0.2 \pm 0.5 \text{ J K}^{-1} \text{ mol}^{-1}$  in the computed entropies averaged over all rotors. The differences in the computed entropies can therefore not be rationalised by differences in the computed rotational constants, which are generally in good agreement. The treatment of the potential energy appears more sensitive however, and we find that the symmetric  $n$ -fold potential treatment of the potential energy

employed by Awan et al. [1] leads to a systematic underprediction of the entropies of each rotor, and hence, each species. In the following paragraphs, the differences refer to those derived from test calculations where the rotational constant employed by Awan et al. is adopted for each rotor, and the differences in the entropy are entirely due to differences in the treatment of potential energy as a function of angle, with a negative difference implying an underprediction of the Awan et al. [1] entropy relative to ours.

In the case of the 1-pentyl radical, differences in entropy arising from different treatments of the potential energy amount to approximately  $-0.1$  ( $\dot{\text{C}}\text{H}_2\text{-CH}_2\text{CH}_2\text{CH}_2\text{CH}_3$ ),  $-2.5$  ( $\dot{\text{C}}\text{H}_2\text{CH}_2\text{-CH}_2\text{CH}_2\text{CH}_3$ ),  $-2.4$  ( $\text{CH}_2\text{CH}_2\text{CH}_2\text{-CH}_2\text{CH}_3$ ) and  $-1.2$  ( $\dot{\text{C}}\text{H}_2\text{CH}_2\text{CH}_2\text{CH}_2\text{-CH}_3$ )  $\text{J K}^{-1} \text{mol}^{-1}$ . One would therefore expect the Awan et al. entropy for 1-pentyl to underestimate ours by  $-6 \text{ J K}^{-1} \text{mol}^{-1}$ , but this difference is reduced to  $-3.4 \text{ J K}^{-1} \text{mol}^{-1}$  due to their subsequent over-prediction of the vibrational entropy relative to us by approximately  $+2.5 \text{ J K}^{-1} \text{mol}^{-1}$ .

For the 2-pentyl radical, no such difference in the vibrational entropy is observed, and the differences between the Awan et al. [1] computed entropies and our calculations of  $-0.8$  ( $\text{CH}_3\text{-}\dot{\text{C}}\text{HCH}_2\text{CH}_2\text{CH}_3$ ),  $-0.6$  ( $\text{CH}_3\dot{\text{C}}\text{H-CH}_2\text{CH}_2\text{CH}_3$ ),  $-2.2$  ( $\text{CH}_3\dot{\text{C}}\text{HCH}_2\text{-CH}_2\text{CH}_3$ ) and  $-1.2$  ( $\text{CH}_3\dot{\text{C}}\text{HCH}_2\text{CH}_2\text{-CH}_3$ )  $\text{J K}^{-1} \text{mol}^{-1}$ , account almost entirely for the  $-4.8 \text{ J K}^{-1} \text{mol}^{-1}$  reduction in their entropy values relative to ours.

For the 3-pentyl radical, the differences in the rotor contributions to the entropy are  $-1.3$  ( $\text{CH}_3\text{-CH}_2\dot{\text{C}}\text{HCH}_2\text{CH}_3$ ),  $-0.4$  ( $\text{CH}_3\text{CH}_2\text{-}\dot{\text{C}}\text{HCH}_2\text{CH}_3$ ),  $-0.4$  ( $\text{CH}_3\text{CH}_2\dot{\text{C}}\text{H-CH}_2\text{CH}_3$ ), and  $-1.3$  ( $\text{CH}_3\text{CH}_2\dot{\text{C}}\text{HCH}_2\text{-CH}_3$ )  $\text{J K}^{-1} \text{mol}^{-1}$ , leading to a combined difference of  $-3.3 \text{ J K}^{-1} \text{mol}^{-1}$ , but this difference accounts for less than half of the total observed difference of  $-8.6 \text{ J K}^{-1} \text{mol}^{-1}$ . Further tests prove that their vibrational and external rotational entropies are effectively the same as ours (within  $< 0.5 \text{ J K}^{-1} \text{mol}^{-1}$ ), and we can only account for the remaining  $-5.3 \text{ J K}^{-1} \text{mol}^{-1}$  difference in entropies by applying an external symmetry correction of  $R \times \ln(2)$  ( $-5.8 \text{ J mol}^{-1} \text{K}^{-1}$ ) for 3-pentyl – a correction which we do not apply in our work, but one which would explain entirely the remaining differences between our calculations and those by Awan et al.

The differences in our results versus Burcat's [14] can be explained with a similar rationale to the above, given the similarity of their approach to that of Awan et al. For 1-pentyl and 2-pentyl radicals we note that Burcat treated only 3 of the 4 internal rotations, which likely leads to their further under-prediction of the entropy relative to our values and those from Awan et al. For 2-penten-5-yl radical ( $\dot{\text{C}}_5\text{H}_9\text{2-5}$ ), Burcat's under-prediction of the entropy relative to our calculation is consistent with the trends described above, whereby



a Pitzer-Gwinn-like treatment [15] tends to under-predict the entropy contribution of internal rotations, in particular, asymmetric rotors such as the ethyl rotors common to all  $C_5$  species in this work. For the 2-penten-1-yl radical ( $\dot{C}_5H_9-1$ ), our under-prediction of the entropy relative to Burcat [14] is likely due to the fact that we do not treat the allylic  $\dot{C}H_2-CH=CHCH_2CH_3$  moiety as a hindered rotor, whereas Burcat does.

In the clearly outlying case of *E*-2-pentene, we have re-computed the thermochemistry using the rotational constants, vibrational frequencies, internal rotation properties, etc., provided by Burcat and we arrive at a result of  $\approx 346 \text{ J K}^{-1} \text{ mol}^{-1}$ , which is in excellent agreement with this work and Awan et al, thus implying that their reported value of  $\approx 370 \text{ J K}^{-1} \text{ mol}^{-1}$  may be due to an error in their polynomial fitting, rather than their fundamental statistical thermodynamics calculations.

## A.6 Comparison of Gibbs Free Energies and Boltzmann Factors computed in This work with Literature Data

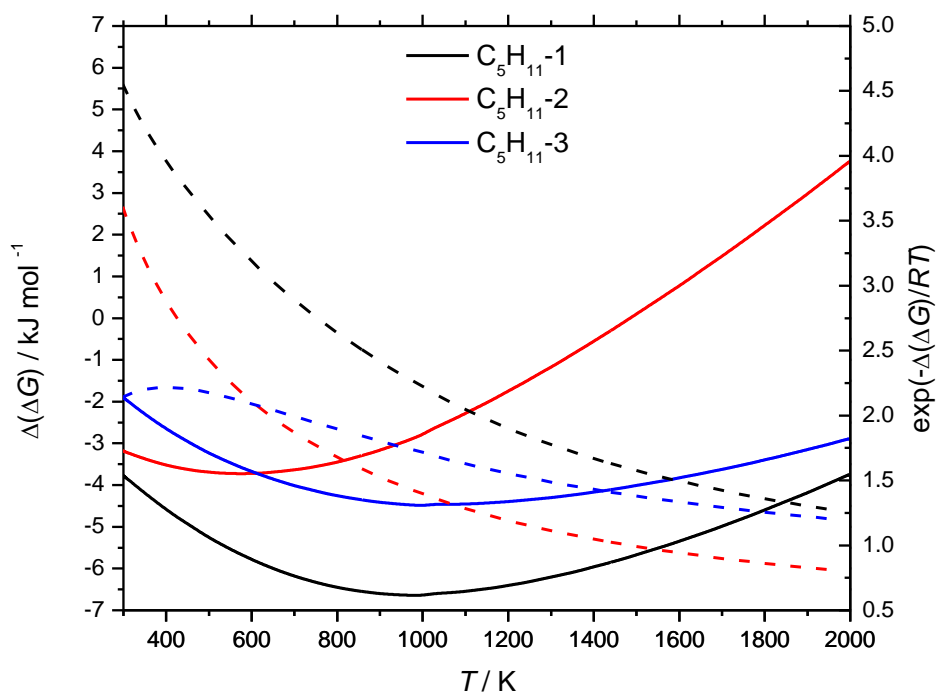


**Figure AS5.** Gibbs Free Energies computed in this work for the pentyl radicals minus those of Awan et al. ( $\Delta\Delta G$ , left y-axis) and corresponding Boltzmann functions (right y-axis, dashed lines).

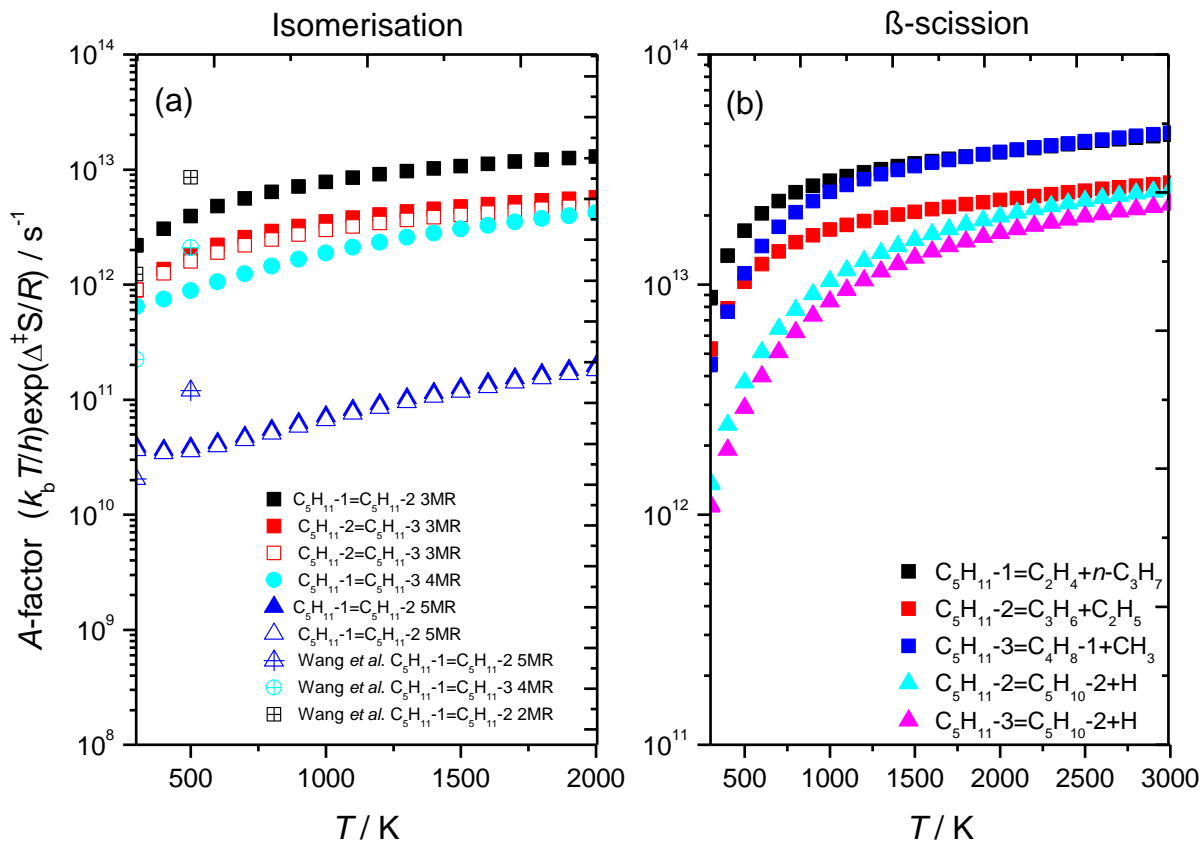


**Figure AS6.** Tunnelling-less pre-exponential factors computed versus temperature for (a) isomerisation and (b)  $\beta$ -scission reactions with corresponding results from Wang *et al.* [16]

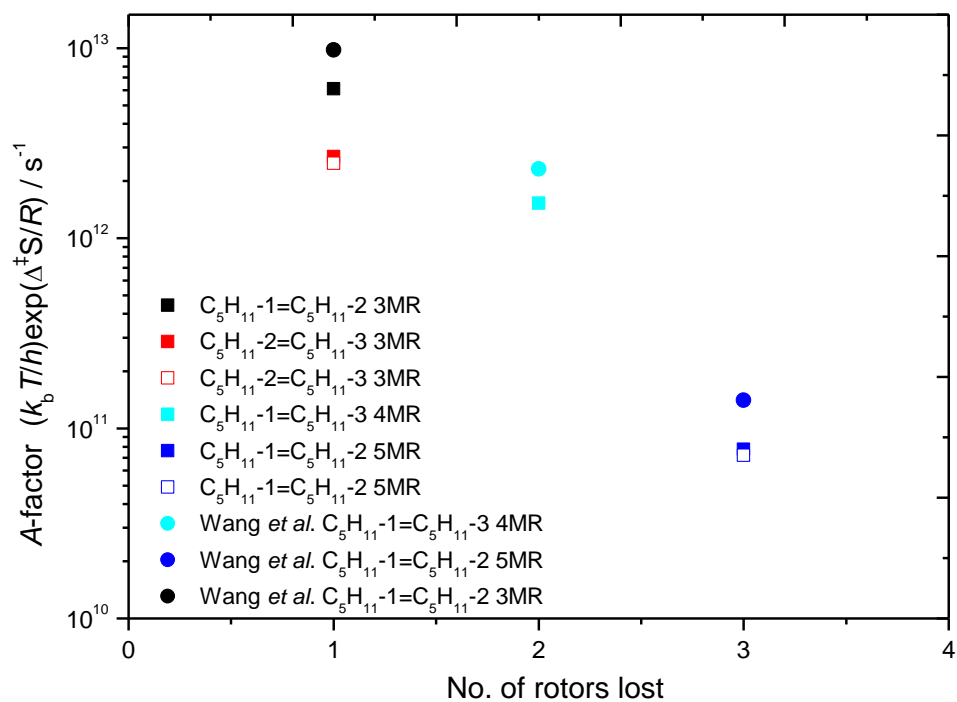


**Figure AS7.** Tunnelling-less pre-exponential factors versus number of rotors lost in transition. Square symbols represent this work, while circles represent rate rules for corresponding reactions from Wang et al. [16]

## A.7 Kinetic Modelling of $\dot{\text{H}}$ -ARAS Experiments

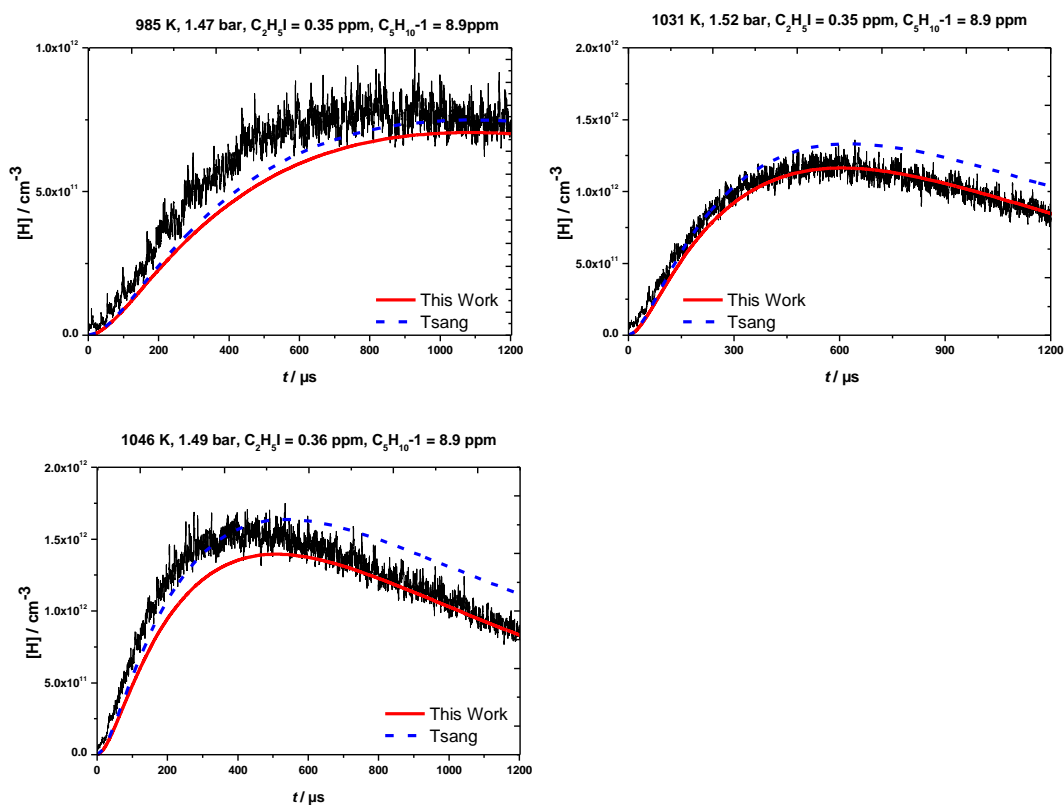


**Figure AS8.** Effect of the inclusion the recommended rate constants of Tsang [17] for 1-pentene unimolecular decomposition on the predictions of H-atom time profiles measured for 1-pentene/ $\text{C}_2\text{H}_5\text{I}$ /Ar mixtures.

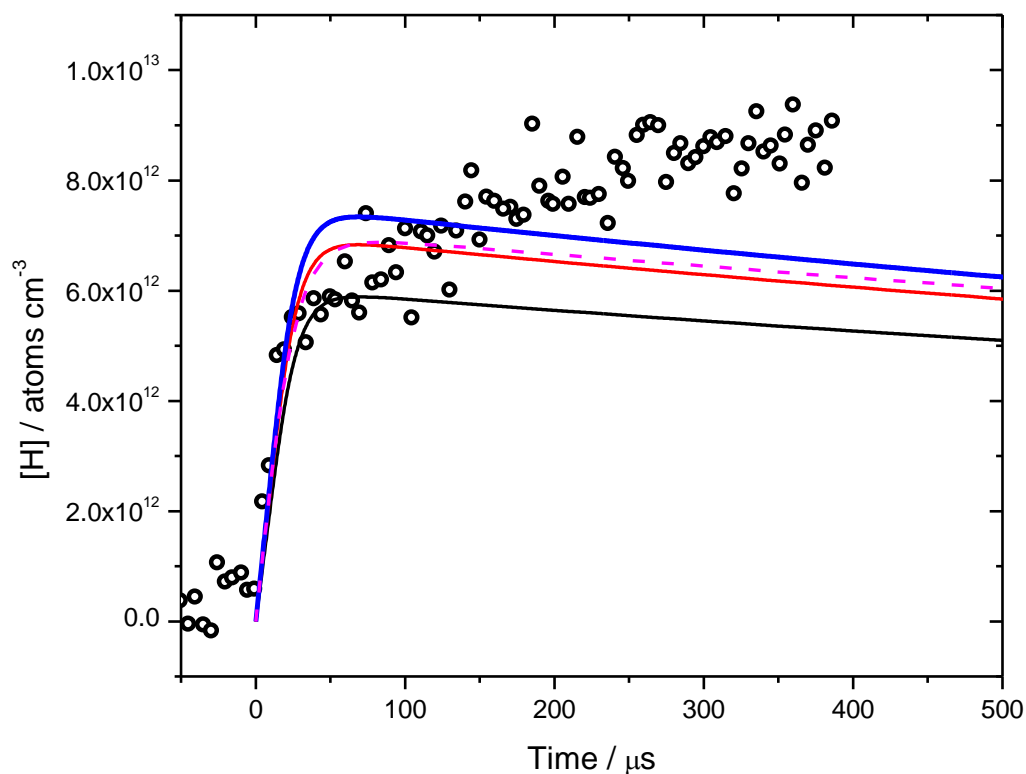


**Figure AS9.** Model predictions of measured hydrogen atom profiles [11]. Solid black line are nominal predictions from this work. The solid red and solid blue line show the influence of a  $0.5 \text{ kcal mol}^{-1}$  and  $1.0 \text{ kcal mol}^{-1}$  reduction in the barriers for  $\dot{\text{C}}_5\text{H}_{11-1} \rightleftharpoons \dot{\text{C}}_5\text{H}_{11-2}$  and re-computation of the RRKM/ME results. The dashed magenta line represents predictions of the model from *this work* with the temperature- and pressure-dependent rate constants from Manion et al. [3] employed.

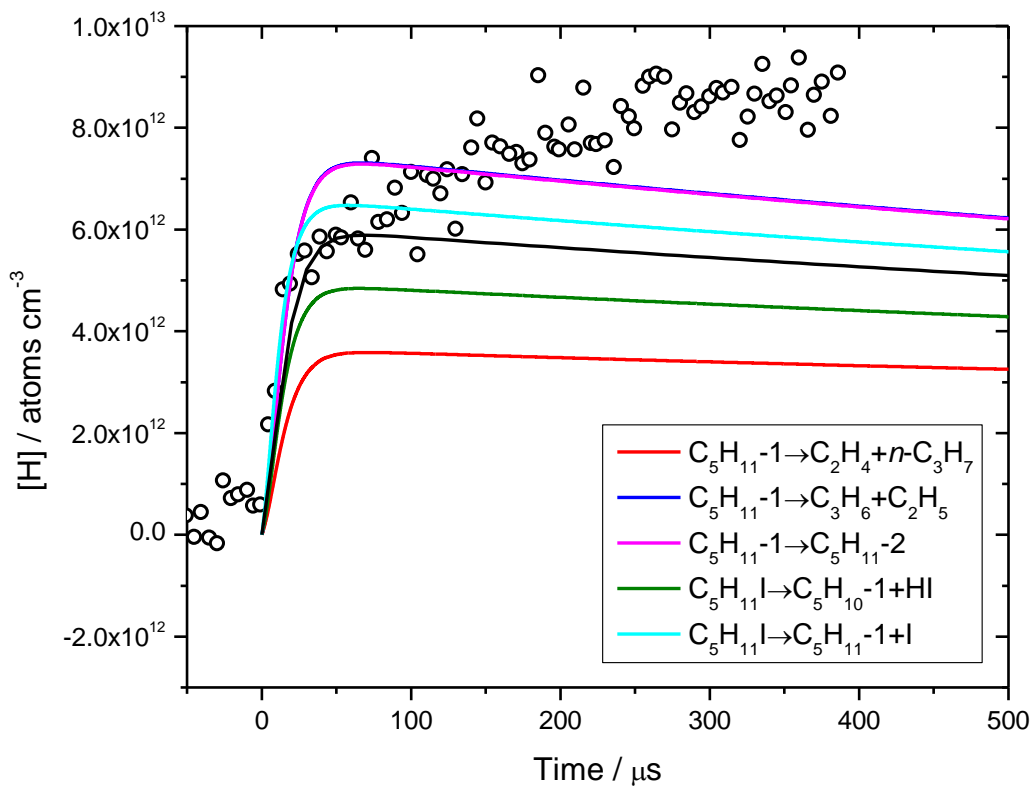


**Figure AS10.** Model predictions of measured hydrogen atom profiles with the most sensitive rate constants for hydrogen atom production increased by factors of two.

## Appendix B

### Supplementary Material: A Theoretical Study of the Reaction of Hydrogen Atoms with Three Pentene Isomers; 2-Methyl-1-Butene, 2-Methyl-2-Butene, and 3-Methyl-1-Butene.

**Table BS1:** Glossary of C<sub>5</sub> species considered in this work, including IUPAC name.

Name in mechanism	Structure	IUPAC
$aC_5H_{10}$		2-methyl-1-butene
$bC_5H_{10}$		2-methyl-2-butene
$cC_5H_{10}$		3-methyl-1-butene
$a\dot{C}_5H_{11}$		2-methyl-1-butanyl
$b\dot{C}_5H_{11}$		2-methyl-2-butanyl
$c\dot{C}_5H_{11}$		3-methyl-2-butanyl
$d\dot{C}_5H_{11}$		3-methyl-1-butanyl
$a\dot{C}_5H_9-a1$		2-methyl-1-buten-1-yl
$a\dot{C}_5H_9-a2$		2-methylene-but-1-yl



$a\dot{C}_5H_9-c$		2-methyl-2-buten-1-yl
$a\dot{C}_5H_9-d$		3-methyl-3-buten-1-yl
$b\dot{C}_5H_9-c$		3-methyl-2-buten-2-yl
$c\dot{C}_5H_9-a$		2-methyl-3-buten-1-yl
$c\dot{C}_5H_9-b$		3-methyl-2-buten-1-yl
$c\dot{C}_5H_9-c$		3-methyl-1-buten-2-yl
$c\dot{C}_5H_9-d$		3-methyl-1-buten-1-yl

**Table BS2.** Heat capacity comparisons of  $C_5$  species with literature data.

Species	Study	$C_p$							
		298	300	400	500	600	800	1000	1500
$aC_5H_{10}$	This Work	105.97	106.47	133.66	159.29	181.94	216.73	243.31	285.03
	NIST	109.96							
	Leon	105.64	138.22	161.17	182.02	200.92	233.36	259.46	302.84
	Burcat		103.27	129.83	156.01	179.71	216.51	244.44	285.43
	AramcoMech 3.0		108.65	137.54	162.74	184.66	220.12	246.58	286.98
	Cheng		108.65	137.54	162.74	184.66	220.12	246.58	286.98
	Westbrook		108.70	137.66	162.81	184.64	220.00	246.62	286.98
$bC_5H_{10}$	This Work	102.59	103.05	128.57	153.73	176.57	212.44	240.03	283.38
	NIST								
	Leon	105.02	132.94	157.27	179.30	199.16	233.00	259.86	302.98
	Burcat		104.08	128.22	152.72	175.38	211.48	239.32	281.67
	AramcoMech 3.0		110.37	138.06	162.54	184.08	219.41	246.09	286.72
	Cheng		110.37	138.06	162.54	184.08	219.41	246.09	286.72
	Westbrook		110.42	138.18	162.61	184.06	219.30	246.13	286.72

cC <sub>5</sub> H <sub>10</sub>	This Work	108.16	108.67	136.18	161.76	184.14	218.18	244.29	285.44
	NIST	115.00							
	Leon	105.62	137.16	160.31	181.34	200.38	233.04	259.28	302.69
	Burcat		105.64	131.39	156.59	179.27	214.31	241.28	282.02
	AramcoMech 3.0		109.00	138.48	164.05	186.16	221.69	248.06	288.34
	Cheng		109.00	138.48	164.05	186.16	221.69	248.06	288.34
	Westbrook		109.06	138.62	164.13	186.13	221.55	248.11	288.34
aC <sub>5</sub> H <sub>11</sub>	This Work	116.11	116.66	145.85	172.86	196.41	232.21	259.64	302.97
	NIST								
	Leon	113.80	147.61	172.38	194.86	215.21	250.08	278.04	324.14
	Burcat								
	AramcoMech 3.0		117.57	148.86	175.68	198.63	235.14	262.18	304.58
	Cheng		117.33	148.61	175.52	198.62	235.57	262.92	305.26
	Westbrook		117.65	149.04	175.77	198.59	234.97	262.23	304.58
bC <sub>5</sub> H <sub>11</sub>	This Work	107.96	108.43	135.03	162.10	186.82	224.88	254.38	300.42
	NIST								
	Leon	113.62	141.3	167.4	191.03	212.34	248.65	277.49	323.84
	Burcat		110.62	139.80	167.25	191.45	228.56	257.01	300.36
	AramcoMech 3.0		115.29	143.34	168.65	191.32	229.29	258.46	302.67
	Cheng		110.03	138.78	164.73	187.98	226.91	256.74	301.76
	Westbrook		115.34	143.44	168.70	191.30	229.20	258.49	302.67
cC <sub>5</sub> H <sub>11</sub>	This Work	113.79	114.29	142.00	168.71	192.50	229.00	257.30	301.75
	NIST								
	Leon	114.30	144.03	169.58	192.74	213.65	249.35	277.81	323.97
	Burcat								
	AramcoMech 3.0		114.65	144.17	204.80	218.44	242.73	263.39	301.68
	Cheng		113.84	144.01	170.53	193.75	231.53	259.78	302.60
	Westbrook		114.69	144.27	170.24	193.00	230.25	258.50	301.68
dC <sub>5</sub> H <sub>11</sub>	This Work	118.13	118.67	147.63	174.59	198.10	233.58	260.78	303.66
	NIST								
	Leon	114.00	148.18	172.84	195.24	215.51	250.26	278.16	324.21
	Burcat		121.58	151.75	178.75	201.79	236.25	262.67	303.36
	AramcoMech 3.0		117.57	148.86	175.68	198.63	235.14	262.18	304.58
	Cheng		117.36	148.61	175.52	198.65	235.57	262.92	305.26
	Westbrook		117.65	149.04	175.77	198.59	234.97	262.23	304.58
aC <sub>5</sub> H <sub>9</sub> -a1	This Work	107.21	107.65	131.48	153.81	173.60	204.51	228.23	265.86
	NIST								
	Leon								
	Burcat								
	AramcoMech 3.0								
	Cheng								
	Westbrook		111.11	137.42	159.98	179.36	210.48	233.89	269.73
aC <sub>5</sub> H <sub>9</sub> -a2	This Work	103.01	103.54	130.94	155.72	176.91	208.36	232.27	269.75
	NIST								
	Leon	104.07	140.25	159.91	177.84	194.13	222.24	245.06	283.83
	Burcat								
	AramcoMech 3.0		104.99	133.24	157.61	178.56	211.81	235.97	271.63
	Cheng		104.99	133.24	157.61	178.56	211.81	235.97	271.63
	Westbrook		105.03	133.34	157.67	178.54	211.71	236.01	271.63

aĈ <sub>5</sub> H <sub>9</sub> -c	This Work	100.41	100.90	127.13	151.60	173.02	205.55	230.26	268.84
	NIST								
	Leon	105.98	135.84	156.61	175.47	192.55	221.79	245.24	283.88
	Burcat								
	AramcoMech 3.0		102.19	129.92	154.04	174.95	208.56	233.42	270.88
	Cheng		102.19	129.92	154.04	174.95	208.56	233.42	270.88
Westbrook		105.58	133.12	156.94	177.52	210.73	235.61	272.25	
aĈ <sub>5</sub> H <sub>9</sub> -d	This Work	105.99	106.45	130.93	153.80	173.88	204.69	228.38	265.82
	NIST								
	Leon	106.04	137.12	157.49	176.02	192.82	221.67	244.92	283.66
	Burcat								
	AramcoMech 3.0		103.92	130.58	153.76	173.86	206.26	230.39	267.36
	Cheng		103.92	130.58	153.76	173.86	206.26	230.39	267.36
Westbrook		107.59	134.10	156.81	176.27	207.33	230.49	266.04	
bĈ <sub>5</sub> H <sub>9</sub> -c	This Work	104.37	104.77	127.05	149.01	169.10	201.20	225.90	264.78
	NIST								
	Leon								
	Burcat								
	AramcoMech 3.0								
	Cheng								
Westbrook									
cĈ <sub>5</sub> H <sub>9</sub> -a	This Work	109.36	109.81	133.98	156.68	176.54	206.52	229.76	266.27
	NIST								
	Leon	105.79	135.79	156.41	175.15	192.12	221.24	244.65	283.47
	Burcat	108.45	108.99	137.37	162.49	183.69	214.73	237.30	270.06
	AramcoMech 3.0		104.15	131.49	155.09	175.41	207.88	231.90	268.65
	Cheng		104.15	131.49	155.09	175.41	207.88	231.90	268.65
Westbrook		104.21	131.64	155.17	175.38	207.74	231.94	268.65	
cĈ <sub>5</sub> H <sub>9</sub> -b	This Work	100.39	100.87	126.59	150.89	172.37	205.21	230.05	268.80
	NIST								
	Leon	105.56	133.77	154.96	174.17	191.54	221.23	244.97	283.73
	Burcat	106.54	107.05	134.74	159.69	181.08	212.94	236.15	270.10
	AramcoMech 3.0		104.15	131.49	155.09	175.41	207.88	231.90	268.65
	Cheng		101.02	128.58	152.71	173.78	207.92	233.36	271.51
Westbrook		101.05	128.97	153.25	174.34	208.41	233.80	270.67	
cĈ <sub>5</sub> H <sub>9</sub> -c	This Work	106.57	107.04	132.27	155.54	175.80	206.46	229.93	266.82
	NIST								
	Leon								
	Burcat								
	AramcoMech 3.0								
	Cheng								
Westbrook									
cĈ <sub>5</sub> H <sub>9</sub> -d	This Work	107.52	108.01	133.68	156.93	176.97	207.35	230.55	267.15
	NIST								
	Leon								
	Burcat	105.82	106.34	134.18	159.35	180.92	212.88	236.21	270.23
	AramcoMech 3.0								
	Cheng								
Westbrook									

Units: heat capacities (J K<sup>-1</sup> mol<sup>-1</sup>).

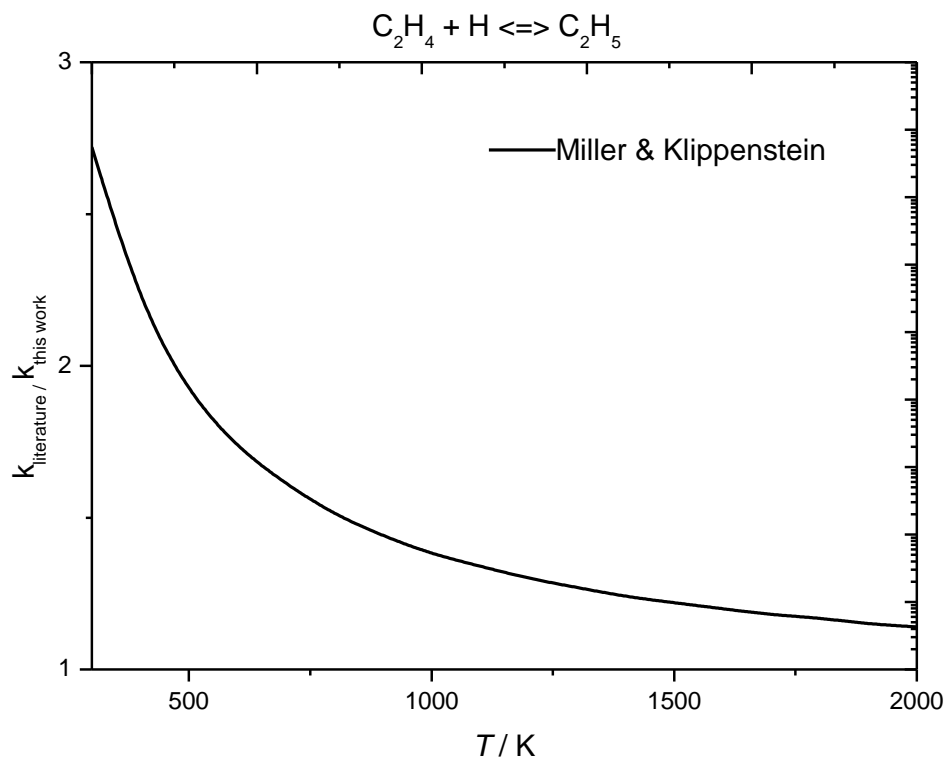


**Figure BS1.** Rate constant comparison between methods adopted in the current work and Miller and Klippenstein for the reaction  $H + C_2H_4$ .

**Table BS3:** 0 K electronic energies in hartrees for compound methods used to construct isodesmic reaction networks.

Species	CBS-QB3	CBS-APNO	G3	G4
aC <sub>5</sub> H <sub>10</sub>	-196.10273	-196.39397	-196.32904	-196.36516
bC <sub>5</sub> H <sub>10</sub>	-196.10515	-196.39646	-196.33123	-196.36746
cC <sub>5</sub> H <sub>10</sub>	-196.09983	-196.39100	-196.32636	-196.36251
aĈ <sub>5</sub> H <sub>11</sub>	-196.64951	-196.94191	-196.87749	-196.91578
bĈ <sub>5</sub> H <sub>11</sub>	-196.65758	-196.94995	-196.88454	-196.92329
cĈ <sub>5</sub> H <sub>11</sub>	-196.65441	-196.94667	-196.88174	-196.92030
dĈ <sub>5</sub> H <sub>11</sub>	-196.65064	-196.94302	-196.87868	-196.91701
aĈ <sub>5</sub> H <sub>9</sub> -a1	-195.46432	-195.75482	-195.69005	-195.72637
aĈ <sub>5</sub> H <sub>9</sub> -a2	-195.42718	-195.71748	-195.65270	-195.69063
aĈ <sub>5</sub> H <sub>9</sub> -c	-195.46836	-195.75895	-195.69350	-195.72995
aĈ <sub>5</sub> H <sub>9</sub> -d	-195.44305	-195.73382	-195.66868	-195.70741
bĈ <sub>5</sub> H <sub>9</sub> -c	-195.43562	-195.72597	-195.66054	-195.69857
cĈ <sub>5</sub> H <sub>9</sub> -a	-195.43961	-195.73032	NaN	-195.70405
cĈ <sub>5</sub> H <sub>9</sub> -b	-195.47112	-195.76164	-195.69612	-195.73265
cĈ <sub>5</sub> H <sub>9</sub> -c	-195.43057	-195.72071	-195.65587	-195.69382
cĈ <sub>5</sub> H <sub>9</sub> -d	-195.42525	-195.71548	-195.65102	-195.68902

**Table BS4:** T1 Diagnostic Values for C<sub>5</sub> species and Transition States.

Species	T1
aC <sub>5</sub> H <sub>10</sub>	0.009
bC <sub>5</sub> H <sub>10</sub>	0.009
cC <sub>5</sub> H <sub>10</sub>	0.009
aĊ <sub>5</sub> H <sub>11</sub>	0.010
bĊ <sub>5</sub> H <sub>11</sub>	0.011
cĊ <sub>5</sub> H <sub>11</sub>	0.010
dĊ <sub>5</sub> H <sub>11</sub>	0.010
aĊ <sub>5</sub> H <sub>9</sub> -a1	0.022
aĊ <sub>5</sub> H <sub>9</sub> -a2	0.025
aĊ <sub>5</sub> H <sub>9</sub> -c	0.023
aĊ <sub>5</sub> H <sub>9</sub> -d	0.013
bĊ <sub>5</sub> H <sub>9</sub> -c	0.024
cĊ <sub>5</sub> H <sub>9</sub> -a	0.014
cĊ <sub>5</sub> H <sub>9</sub> -b	0.023
cĊ <sub>5</sub> H <sub>9</sub> -c	0.024
cĊ <sub>5</sub> H <sub>9</sub> -d	0.025
aC <sub>5</sub> H <sub>10</sub> + Ĥ ⇌ aĊ <sub>5</sub> H <sub>9</sub> -a1 + H <sub>2</sub>	0.024
aC <sub>5</sub> H <sub>10</sub> + Ĥ ⇌ aĊ <sub>5</sub> H <sub>9</sub> -a2 + H <sub>2</sub>	0.022
aC <sub>5</sub> H <sub>10</sub> + Ĥ ⇌ aĊ <sub>5</sub> H <sub>9</sub> -c + H <sub>2</sub>	0.020
aC <sub>5</sub> H <sub>10</sub> + Ĥ ⇌ aĊ <sub>5</sub> H <sub>9</sub> -d + H <sub>2</sub>	0.013
bC <sub>5</sub> H <sub>10</sub> + Ĥ ⇌ aĊ <sub>5</sub> H <sub>9</sub> -c + H <sub>2</sub>	0.022
bC <sub>5</sub> H <sub>10</sub> + Ĥ ⇌ bĊ <sub>5</sub> H <sub>9</sub> -c + H <sub>2</sub>	0.024
bC <sub>5</sub> H <sub>10</sub> + Ĥ ⇌ cĊ <sub>5</sub> H <sub>9</sub> -b + H <sub>2</sub>	0.022
cC <sub>5</sub> H <sub>10</sub> + Ĥ ⇌ cĊ <sub>5</sub> H <sub>9</sub> -a + H <sub>2</sub>	0.015
cC <sub>5</sub> H <sub>10</sub> + Ĥ ⇌ cĊ <sub>5</sub> H <sub>9</sub> -b + H <sub>2</sub>	0.019
cC <sub>5</sub> H <sub>10</sub> + Ĥ ⇌ cĊ <sub>5</sub> H <sub>9</sub> -c + H <sub>2</sub>	0.024
cC <sub>5</sub> H <sub>10</sub> + Ĥ ⇌ cĊ <sub>5</sub> H <sub>9</sub> -d + H <sub>2</sub>	0.025
aC <sub>5</sub> H <sub>10</sub> + Ĥ ⇌ aĊ <sub>5</sub> H <sub>11</sub>	0.021
aC <sub>5</sub> H <sub>10</sub> + Ĥ ⇌ bĊ <sub>5</sub> H <sub>11</sub>	0.024
bC <sub>5</sub> H <sub>10</sub> + Ĥ ⇌ bĊ <sub>5</sub> H <sub>11</sub>	0.022
bC <sub>5</sub> H <sub>10</sub> + Ĥ ⇌ cĊ <sub>5</sub> H <sub>11</sub>	0.024
cC <sub>5</sub> H <sub>10</sub> + Ĥ ⇌ cĊ <sub>5</sub> H <sub>11</sub>	0.023
cC <sub>5</sub> H <sub>10</sub> + Ĥ ⇌ dĊ <sub>5</sub> H <sub>11</sub>	0.023
aĊ <sub>5</sub> H <sub>11</sub> ⇌ C <sub>3</sub> H <sub>6</sub> + Ċ <sub>2</sub> H <sub>5</sub>	0.025
aĊ <sub>5</sub> H <sub>11</sub> ⇌ C <sub>4</sub> H <sub>8</sub> -1 + ĊH <sub>3</sub>	0.025
bĊ <sub>5</sub> H <sub>11</sub> ⇌ iC <sub>4</sub> H <sub>8</sub> + ĊH <sub>3</sub>	0.024
cĊ <sub>5</sub> H <sub>11</sub> ⇌ C <sub>4</sub> H <sub>8</sub> -2 + ĊH <sub>3</sub>	0.025
dĊ <sub>5</sub> H <sub>11</sub> ⇌ C <sub>2</sub> H <sub>4</sub> + iĊ <sub>3</sub> H <sub>7</sub>	0.025
aĊ <sub>5</sub> H <sub>11</sub> ⇌ bĊ <sub>5</sub> H <sub>11</sub>	0.013
aĊ <sub>5</sub> H <sub>11</sub> ⇌ cĊ <sub>5</sub> H <sub>11</sub>	0.014
aĊ <sub>5</sub> H <sub>11</sub> ⇌ dĊ <sub>5</sub> H <sub>11</sub>	0.012
bĊ <sub>5</sub> H <sub>11</sub> ⇌ cĊ <sub>5</sub> H <sub>11</sub>	0.013
bĊ <sub>5</sub> H <sub>11</sub> ⇌ dĊ <sub>5</sub> H <sub>11</sub>	0.014
cĊ <sub>5</sub> H <sub>11</sub> ⇌ dĊ <sub>5</sub> H <sub>11</sub>	0.012

## B.1 Approximate Variational Transition State Theory

A systematic treatment of variational effects for all pathways is not possible given the computational cost it would incur, and it is also unnecessary since not all pathways will be equally influenced. We have therefore focused on three prototypical systems which are representative of the reactions on our PES, an abstraction reaction, an isomerisation reaction and a H atom addition reaction. In all cases the reactions with the lowest barriers from these classes have been studied as variational effects are expected to be strongest in these instances (external  $\dot{\text{H}}$  atom addition, tertiary allylic  $\dot{\text{H}}$ -atom abstraction and a 5 membered ring transition state isomerisation). These reactions were as follows:

- $2\text{M1B} + \dot{\text{H}} \leftrightarrow \text{b}\dot{\text{C}}_5\text{H}_{11}$
- $3\text{M1B} + \dot{\text{H}} \leftrightarrow \text{c}\dot{\text{C}}_5\text{H}_9\text{-b} + \text{H}_2$
- $\text{d}\dot{\text{C}}_5\text{H}_{11} \leftrightarrow \text{a}\dot{\text{C}}_5\text{H}_{11}$

For each of the above transition states IRC calculations was carried out using the WB97XD/aug-cc-pvtz model chemistry to obtain molecular coordinates along the minimum energy reaction path. For each geometry along the reaction coordinate, a harmonic frequency analysis was carried out using the same level of theory and the zero-point-corrected electronic energy was computed, with imaginary modes omitted from the computation of the ZPE. For each geometry we then computed the rate constants as a function of temperature via conventional transition state theory using MESS. At a given temperature, the structure that gave the minimum rate constant was assumed to be the bottleneck/transition state. This variationally optimised rate constant was then compared with the high-pressure-limit rate constant computed for the saddle point that is currently used to estimate  $k(\text{TST})$ , with the ratio of the two being the approximate variational correction at a given temperature. For simplicity, hindered rotor treatment and tunneling corrections were not included. It was assumed that the change in hindered rotor partition functions vary modestly as a function of distance along the IRC, and that this effect is captured to some extent in the variation in the harmonic frequencies. The variational rate constants therefore account for changes in reaction barrier, vibrational partition function, and rotational partition function. It was found that for the isomerisation reaction that there is no effect and that our saddle point is the transition state, as expected given the large barrier. For the  $\dot{\text{H}}$ -atom abstraction, the effect amounts to ~15 % over the temperature range 300 to 2000 K. For the  $\dot{\text{H}}$  atom addition reaction, it is about a factor of 2–3 above 1000 K and a factor of 2.1–2.5 in the shock-tube regime. The  $\dot{\text{H}}$ -atom addition reactions are most strongly influenced, as expected given their low barriers.

Inspection of variations in energy barriers and partition functions shows that this factor of 2–3 decrease stems from the multiplicative effect of decreases in the vibrational partition function by factors of 1.5, 1.2, 1.2 and 1.2 for low frequency modes 4–7 (this information can be found in the Supporting Information), rather than changes in barriers or external rotational constants.

## B.2 Anharmonic Frequencies

We have carried out isolated test calculations on  $\dot{\text{H}}$  atom abstraction and  $\dot{\text{H}}$  atom addition reactions to see the effect of including anharmonic over harmonic frequencies, which are provided as Supplementary material. For H-atom abstraction by  $\dot{\text{H}}$  atoms from the tertiary allylic carbon site of 3M1B ( $\text{cC}_5\text{H}_{10}$ ) forming the  $\text{c}\dot{\text{C}}_5\text{H}_9\text{-b}$  radical +  $\text{H}_2$ , we observe very little difference. Using anharmonic frequencies reduces the high-pressure limiting rate constant by

2 – 3% in the temperature range 298 – 2000 K. On the other hand, for  $\dot{\text{H}}$  atom addition to 3M1B forming the  $\text{c}\dot{\text{C}}_5\text{H}_{11}$  radical, the use of anharmonic frequencies increases the rate constant by 3 – 5%. A comparison of our computed rate constant for  $\dot{\text{H}}$  atom addition to  $\text{C}_2\text{H}_4$  (calculated using the same approach as the current work) to that calculated by Miller and Klippenstein [18] is presented in the Supplementary material. Miller and Klippenstein investigated the  $\dot{\text{H}} + \text{C}_2\text{H}_2$  and  $\text{C}_2\text{H}_4$  reactions, as well as their reverse dissociations using high level electronic structure calculations, employing a 2-D master equation and variational transition state theory (VTST). The largest difference observed is at 300 K, where Miller and Klippenstein are a factor of 2.72 times faster than the current work. From 800 K, our calculated rate constant is within a factor of  $\sim 1.5$  of theirs. Whilst not including effects such as VTST, multi-dimensional hindered rotor treatment and anharmonic effects, our target predictability against experimental data such as  $\dot{\text{H}}$ -ARAS and pyrolysis experiments is quite satisfactory. However, these could possibly be improved with future studies employing such methods.

## References

- [1] Awan, I. A.; Burgess, D. R., Jr.; Manion, J. A., Pressure dependence and branching ratios in the decomposition of 1-pentyl radicals: shock tube experiments and master equation modeling. *J. Phys. Chem. A* 2012, 116 (11), 2895-910.
- [2] Comandini, A.; Awan, I. A.; Manion, J. A., Thermal decomposition of 1-pentyl radicals at high pressures and temperatures. *Chem. Phys. Lett.* 2012, 552, 20-26.
- [3] Manion, J. A.; Awan, I. A., The decomposition of 2-pentyl and 3-pentyl radicals. *Proc. Combust. Inst.* 2013, 34 (1), 537-545.
- [4] Hayes, C. J.; Burgess, D. R., Kinetic Barriers of H-Atom Transfer Reactions in Alkyl, Allylic, and Oxoallylic Radicals as Calculated by Composite Ab Initio Methods. *J. Phys. Chem. A* 2009, 113 (11), 2473-2482.
- [5] Jitariu, L. C.; Jones, L. D.; Robertson, S. H.; Pilling, M. J.; Hillier, I. H., Thermal rate coefficients via variational transition state theory for the unimolecular decomposition/isomerization of 1-pentyl radical: Ab initio and direct dynamics calculations. *J. Phys. Chem. A* 2003, 107 (41), 8607-8617.
- [6] Sirjean, B.; Dames, E.; Wang, H.; Tsang, W., Tunneling in Hydrogen-Transfer Isomerization of n-Alkyl Radicals. *J. Phys. Chem. A* 2012, 116 (1), 319-332.
- [7] Aguilera-Iparraguirre, J.; Curran, H. J.; Klopper, W.; Simmie, J. M., Accurate Benchmark Calculation of the Reaction Barrier Height for Hydrogen Abstraction by the Hydroperoxyl Radical from Methane. Implications for  $C_nH_{2n+2}$  where  $n = 2 \rightarrow 4$ . *J. Phys. Chem. A* 2008, 112 (30), 7047-7054.
- [8] Bugler, J.; Power, J.; Curran, H. J., A theoretical study of cyclic ether formation reactions. *Proc. Combust. Inst.* 2017, 36 (1), 161-167.
- [9] Davis, A. C.; Francisco, J. S., Ab Initio Study of Hydrogen Migration across n-Alkyl Radicals. *J. Phys. Chem. A* 2011, 115 (14), 2966-2977.
- [10] Miyoshi, A.; Widjaja, J.; Yamauchi, N.; Koshi, M.; Matsui, H., Direct investigations on the thermal unimolecular isomerization reaction of 1-pentyl radicals. *Proc. Combust. Inst.* 2002, 29, 1285-1293.
- [11] Yamauchi, N.; Miyoshi, A.; Kosaka, K.; Koshi, M.; Matsui, H., Thermal Decomposition and Isomerization Processes of Alkyl Radicals. *J. Phys. Chem. A* 1999, 103 (15), 2723-2733.
- [12] Yu, T.; Zheng, J.; Truhlar, D., Multi-structural variational transition state theory. Kinetics of the 1,4-hydrogen shift isomerization of the pentyl radical with torsional anharmonicity. *Chem. Sci.* 2011, 2, 2199-2213.
- [13] Matheu, D. M.; Green, W. H.; Grenda, J. M., Capturing pressure-dependence in automated mechanism generation: Reactions through cycloalkyl intermediates. *Int. J. Chem. Kinet.* 2003, 35 (3), 95-119.
- [14] Burcat, A.; Ruscic, B. Third millennium ideal gas and condensed phase thermochemical database for combustion (with update from active thermochemical tables); Argonne National Lab.(ANL), Argonne, IL (United States): 2005.
- [15] Pitzer, K. S.; Gwinn, W. D., Energy Levels and Thermodynamic Functions for Molecules with Internal Rotation : I. Rigid Frame with Attached Tops. In *Molecular Structure and Statistical Thermodynamics*, pp 33-46.
- [16] Wang, K.; Villano, S. M.; Dean, A. M., Reactivity-Structure-Based Rate Estimation Rules for Alkyl Radical H Atom Shift and Alkenyl Radical Cycloaddition Reactions. *J. Phys. Chem. A* 2015, 119 (28), 7205-7221.
- [17] Tsang, W., Thermal decomposition of cyclopentane and related compounds. *Int. J. Chem. Kinet.* 1978, 10 (6), 599-617.
- [18] Miller, J. A.; Klippenstein, S. J., The  $H + C_2H_2 (+ M) \rightleftharpoons C_2H_3 (+ M)$  and  $H + C_2H_2 (+ M) \rightleftharpoons C_2H_5 (+ M)$  reactions: Electronic structure, variational transition-state theory, and



solutions to a two-dimensional master equation. *Phy. Chem. Chem. Phys* 2004, 6 (6), 1192-1202.